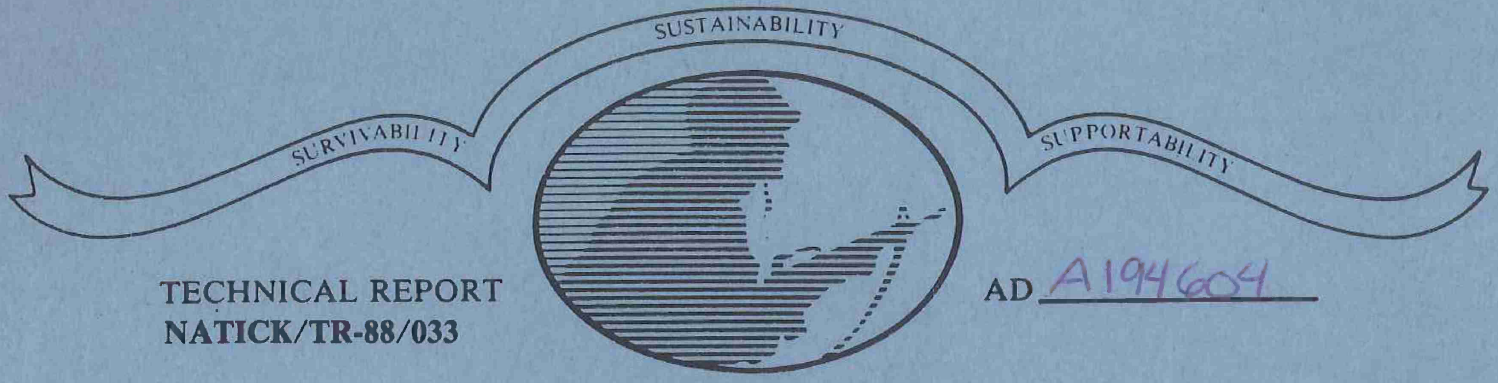

TECHNICAL REPORT
NATICK/TR-88/033

AD A194604

MATERIALS BIOTECHNOLOGY SYMPOSIUM PROCEEDINGS

23 - 24 JUNE 1987

DAVID L. KAPLAN
EDITOR

UNITED STATES ARMY NATICK
RESEARCH, DEVELOPMENT AND ENGINEERING CENTER
NATICK, MASSACHUSETTS 01760-5000

SCIENCE AND ADVANCED TECHNOLOGY DIRECTORATE

DISCLAIMERS

The findings contained in this report are not to be construed as an official Department of the Army position unless so designated by other authorized documents.

Citation of trade names in this report does not constitute an official endorsement or approval of the use of such items.

DESTRUCTION NOTICE

For Classified Documents:

Follow the procedures in DoD 5200.22-M, Industrial Security Manual, Section II-19 or DoD 5200.1-R, Information Security Program Regulation, Chapter IX.

For Unclassified/Limited Distribution Documents:

Destroy by any method that prevents disclosure of contents or reconstruction of the document.

Unclassified
SECURITY CLASSIFICATION OF THIS PAGE

AD-A194 604

REPORT DOCUMENTATION PAGE

DTIC ELECTE MAY 05 1988 S H D

Form Approved
OMB No 0704-0188
Exp Date Jun 30 1986

1a REPORT SECURITY CLASSIFICATION: Unclassified	1b RESTRICTIVE MARKINGS
2a SECURITY CLASSIFICATION AUTHORITY	3 DISTRIBUTION/AVAILABILITY OF REPORT: Approved for public release, distribution unlimited
2b DECLASSIFICATION/DOWNGRADING SCHEDULE	
4 PERFORMING ORGANIZATION REPORT NUMBER(S): NATICK/TR-88/033	5 MONITORING ORGANIZATION REPORT NUMBER(S)
6a NAME OF PERFORMING ORGANIZATION: US Army Natick RD&E Center; 6b OFFICE SYMBOL (If applicable): STRNC-YEP	7a NAME OF MONITORING ORGANIZATION
6c ADDRESS (City, State, and ZIP Code): Natick, MA 01760-5020	7b ADDRESS (City, State, and ZIP Code)
8a NAME OF FUNDING/SPONSORING ORGANIZATION; 8b OFFICE SYMBOL (If applicable)	9 PROCUREMENT INSTRUMENT IDENTIFICATION NUMBER
8c ADDRESS (City, State, and ZIP Code)	10 SOURCE OF FUNDING NUMBERS

PROGRAM ELEMENT NO.	PROJECT NO	TASK NO	WORK UNIT ACCESSION NO.
1L162723	AH98CH-001		

11 TITLE (Include Security Classification)

Materials Biotechnology Symposium Proceedings, 23-24 June 1987

12 PERSONAL AUTHOR(S)
David L. Kaplan, Editor

13a TYPE OF REPORT	13b TIME COVERED	14 DATE OF REPORT (Year, Month, Day)	15 PAGE COUNT
Final	FROM 87/6/23 TO 87/6/24	87/11/5	294

16 SUPPLEMENTARY NOTATION

17 COSATI CODES		
FIELD	GROUP	SUB-GROUP

18 SUBJECT TERMS (Continue on reverse if necessary and identify by block number)
Biotechnology, Proteins, Computations, Materials, Molecules, Polymers, Polypeptides, Symposium

19 ABSTRACT (Continue on reverse if necessary and identify by block number)

The Materials Biotechnology Symposium was held at the U.S. Army Natick Research, Development and Engineering Center, Natick, Massachusettes, on June 23 and 24, 1987. The meeting was jointly sponsored by Natick and the U.S. Army Research Office, Triangle Park, North Carolina. The Symposium was attended by government, university and corporate researchers. Sessions included ~~in the meeting~~ were: structure/function relationships for proteins, polysaccharides, and lipids; protein engineering; recombinant DNA; production, processing and analysis of biopolymers; and polymers, pigments and other bio-products.

— cont'd pg v

20 DISTRIBUTION/AVAILABILITY OF ABSTRACT	21 ABSTRACT SECURITY CLASSIFICATION
☒ UNCLASSIFIED/UNLIMITED ☐ SAME AS RPT. ☐ DTIC USERS	UNCLASSIFIED

22a NAME OF RESPONSIBLE INDIVIDUAL	22b TELEPHONE (Include Area Code)	22c OFFICE SYMBOL
David L. Kaplan	617-651-4983	STRNC-YEP

DD FORM 1473, 84 MAR — 83 APR edition may be used until exhausted. All other editions are obsolete.

SECURITY CLASSIFICATION OF THIS PAGE
Unclassified

PREFACE

The Symposium was co-sponsored by the U.S. Army Natick RD&E Center (Natick) and the U.S. Army Research Office. The meeting was held at Natick during June 23-24, 1987.

The Materials Biotechnology Symposium was organized in an attempt to focus a meeting on scientific research in biotechnology related to materials. The application of biotechnology to materials science is necessarily broad in scope, as is reflected in the diversity of topics presented at the symposium. In addition, the participation of government, university and corporate research activities was sought in order to provide a more complete picture of current interests and research approaches.

Natick's responsibility is to provide protection for the individual soldier, including clothing, shelter, air drop and food support areas. Materials needs and applications are critical in all of these systems and therefore biotechnology related to materials is of significant importance.

Focusing the research tools of biotechnology on materials science offers new and unique opportunities for scientists. A great deal can be learned from the architectures and structure/function relationships which have evolved in natural systems. This knowledge can serve as a guide for the design and development of new and novel materials. By combining the tools of biotechnology with materials science, natural systems can be manipulated to derive the functional characteristics desirable for materials and their applications.

The basic understanding of natural polymers, including structure and function, is one of the most critical areas to address rather than relying on trial and error approaches which will be less efficient and slower in reaping potential benefits down the road. We must understand how these natural products function in their native environments, whether fibrous or globular proteins, carbohydrates, lipids, or other nontraditional biopolymers. The diversity of structures and associated functions for these polymers is incredible, and we are only at the beginning of this knowledge base with the necessary modeling tools and analytical techniques.

The editor wishes to extend his appreciation to Dr. Shirley Tove, U.S. Army Research Office, for her support and assistance; to the Conveners for their efforts, to the personnel in the Materials Protection and Biotechnology Division of the Science and Advanced Technology Directorate (Natick) for their hard work, to Eileen Collins of the Library staff (Natick) for her support, and Lucy Morana and Kim Weiss (Natick) for typing of this report.

David L. Kaplan, Ph.D.
Editor

TABLE OF CONTENTS

† No manuscript provided

6. Poster Sessions

CONFORMATIONAL ANALYSIS OF POLYPEPTIDES AND PROTEINS FOR THE STUDY OF PROTEIN FOLDING, MOLECULAR RECOGNITION, AND MOLECULAR DESIGN*

Harold A. Scheraga
Baker Laboratory of Chemistry
Cornell University
Ithaca, New York 14853-1301

ABSTRACT

Conformational energy calculations provide an understanding as to how interatomic interactions lead to the three-dimensional structures of polypeptides and proteins, and how these molecules interact with other molecules. Illustrative results of such calculations pertain to model systems (α-helices and β-sheets, and interactions between them), to various open-chain and cyclic peptides, to fibrous proteins, to globular proteins, and to enzyme-substrate complexes. In most cases, the validity of the computations is established by experimental tests of the predicted structures.

INTRODUCTION

Twenty-five years ago, we began to develop computational methods[1] for the conformational analysis of polypeptides and proteins to study protein folding, protein structure, and interactions between proteins and other molecules (molecular recognition), and to suggest loci for site-specific mutations in natural proteins to modify their structure and reactivity (molecular design). The motivation for this development derived from our early experimental work on the structure of bovine pancreatic ribonuclease.[2] Before the X-ray structure of ribonuclease was known, we used solution physical chemical methods to identify three noncovalent tyrosyl...aspartate interactions,[2] whose locations were confirmed by the subsequently determined X-ray structure[3] (Fig. 1). These, together with the known locations of the four disulfide bonds, and the proximity of His 12, Lys 41 and His 119 in the active site of this enzyme, provided distance information that could serve as useful constraints to determine the three-dimensional structures of proteins by means of conformational energy calculations.

* This paper first appeared in the Israel Journal of Chemistry, Vol. 27, 1986.

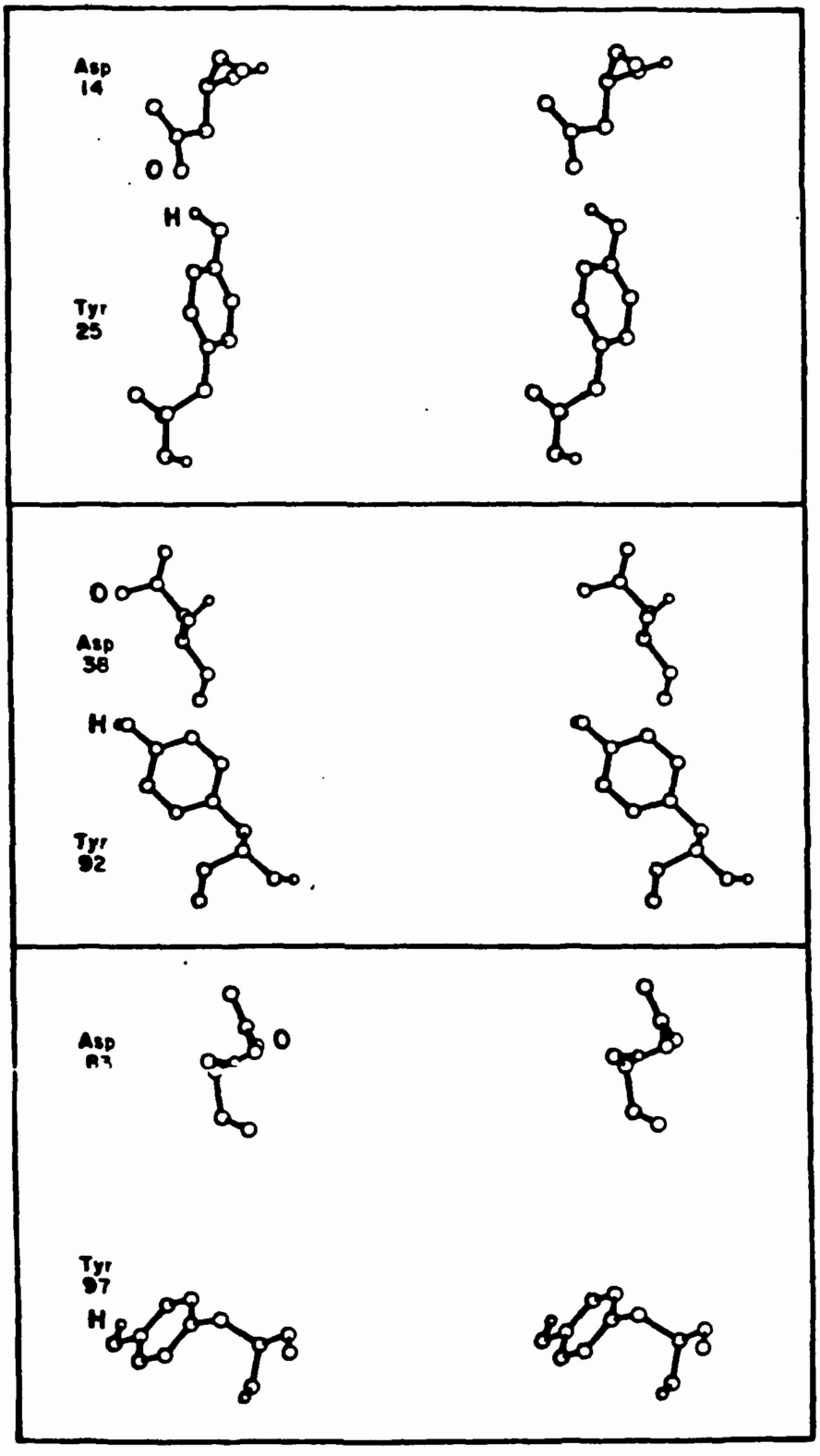

FIGURE 1. Three tyr..asp interactions deduced from solution physical chemical experiments.[2] The drawing is based on the subsequently determined X-ray coordinates of Wlodawer et al.[3]

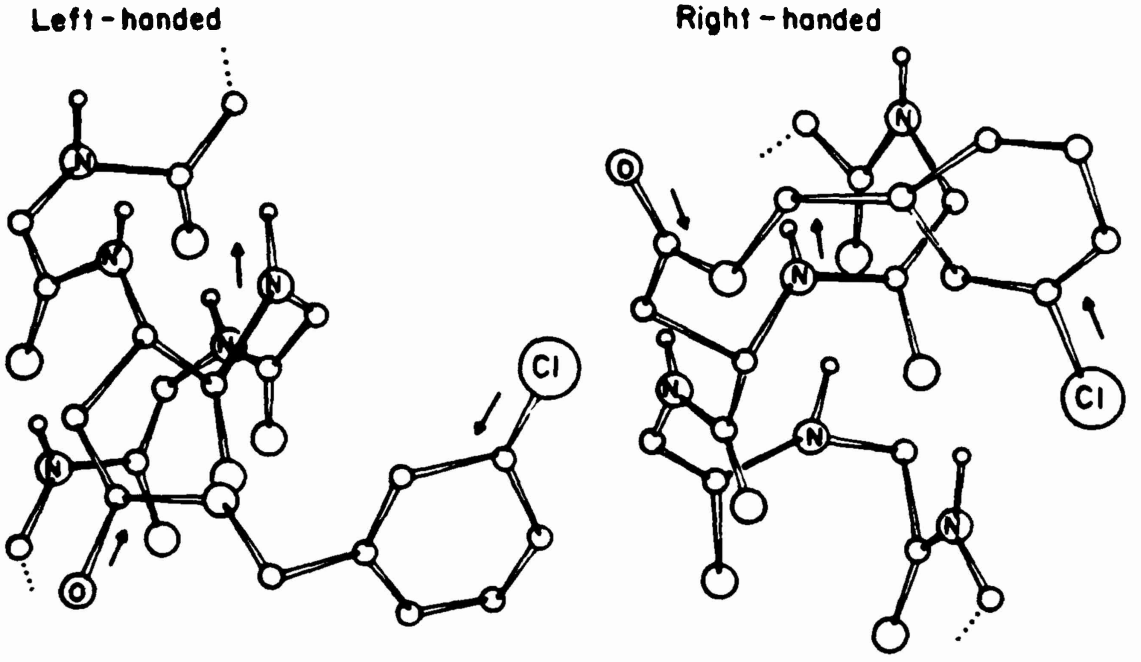

FIGURE 2. Orientation of the side chains of the lowest-energy left- and right-handed α-helices of poly (m-Cl-benzyl-L-aspartate).[22] The arrows represent the directions of the C-Cl, ester, and amide dipoles, respectively. The dipole-dipole interactions are more favorable in the left handed form.

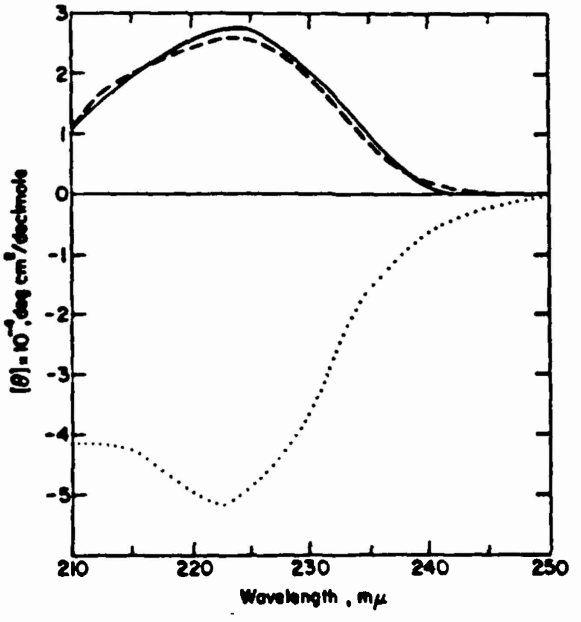

FIGURE 3. Circular dichroism spectra[32] of poly (-benzyl-L-aspartates) in dioxane at 25°C. The symbols (___), (---), and (...) correspond to o-, m-, and p-Cl-benzyl derivatives, respectively.

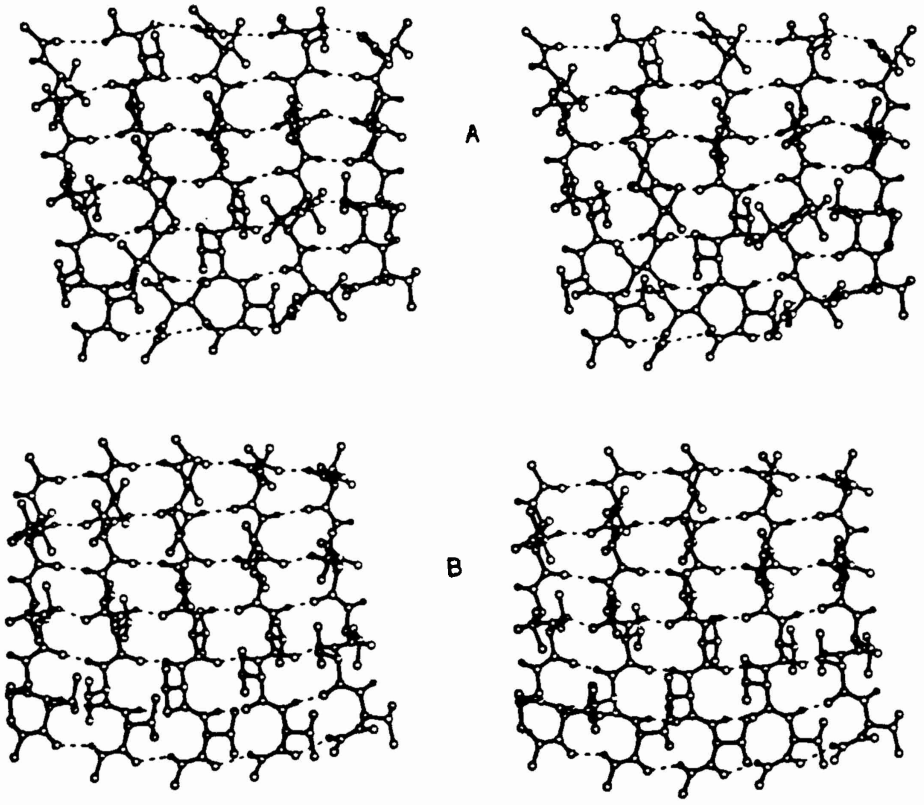

FIGURE 4. Stereo drawings of the minimum-energy β-sheets with five $CH_3CO-(L-Val)_6-NHCH_3$ chains.[24] (A) Antiparallel structure. (B) Parallel structure.

Initially,[1,4,5] only hard-sphere potentials were used in the computations, but subsequently more complete empirical energy functions were developed both in our laboratory[6-10] and elsewhere.[11-14] Our current main program is ECEPP/2, Empirical Conformational Energy Program for Peptides.[9,10] Procedures have also been introduced to take hydration and entropy effects into account, and to carry out energy minimization, Monte Carlo and molecular dynamics computations in a multi-dimensional space: these procedures have been reviewed on numerous occasions.[8,15-21]

While improvements in potential functions can be expected, the present ones are sufficiently accurate to provide agreement between various computational and experimental results, as will be shown here. The main obstacle to further progress is the multiple-minima problem, and much effort is being devoted to surmount this difficulty. In fact, this problem has already been solved for small open-chain and cyclic peptides and for fibrous proteins such as collagen, and progress is being made in the area of globular proteins.

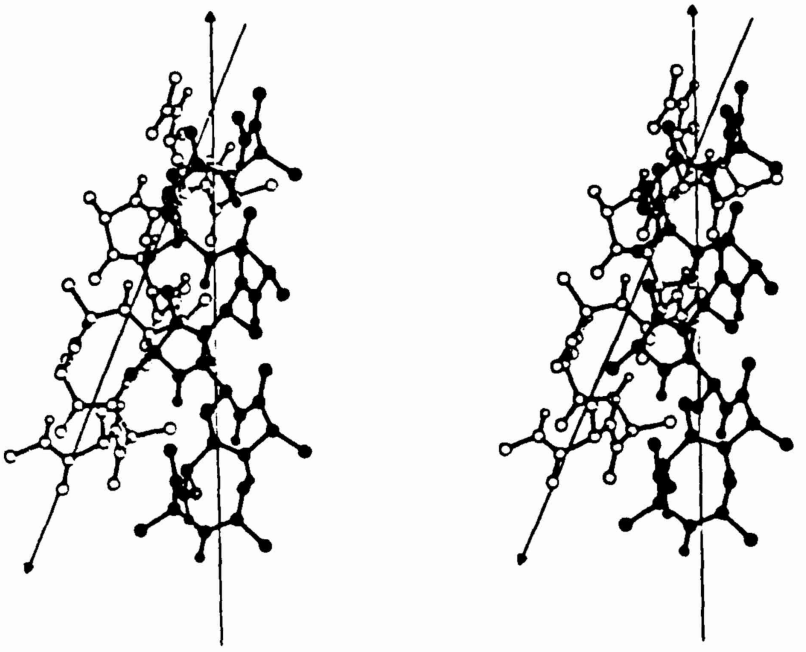

FIGURE 5. Stereo drawing of two CH_3CO-(L-Ala)$_{10}$-$NHCH_3$ α-helices in the lowest-energy packing arrangement.[27] The helix axes are indicated by arrows, with the head of the arrow pointing in the direction of the C-terminals of each helix.

This article will describe some of the conformational problems that have been elucidated by this computational methodology, and will summarize some of the current efforts being made to overcome the multi-minima problem for globular proteins. We shall describe first the results of computations on model systems of increasing complexity, and then consider the conformations of small open-chain and cyclic peptides, fibrous proteins, and globular proteins. Further details can be found in several recent reviews.[18-21]

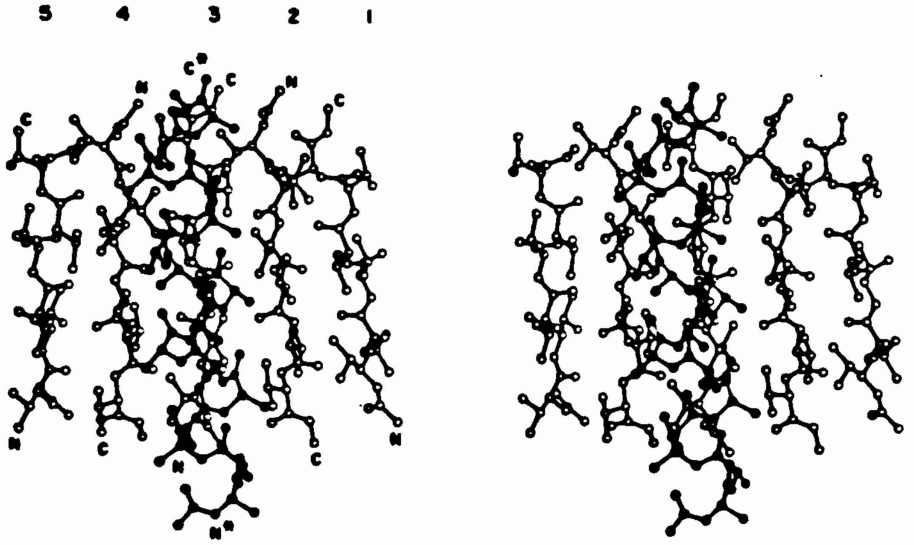

FIGURE 6. Stereo drawing of the lowest-energy packing arrangement of a CH_3CO-(L-Ala)$_{16}$-$NHCH_3$ α-helix and an antiparallel CH_3CO-(L-Val)$_6$-$NHCH_3$ β-sheet.[29]

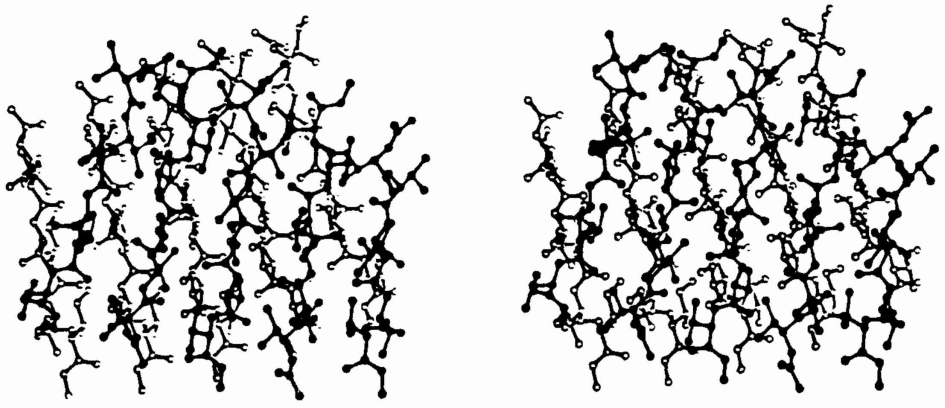

FIGURE 7. Stereo drawing of the lowest-energy packing arrangement of a CH_3CO-(L-Ile)$_6$-$NHCH_3$ parallel-chain β-sheet (open atoms) and a CH_3CO-(L-Val)$_6$-$NHCH_3$ antiparallel-chain β-sheet (filled atoms).[30]

MODEL SYSTEMS

Conformational energy calculations have demonstrated how interatomic interactions lead to the preferred twists of α-helices[7,22] and β-sheets,[23-26] and to the preferred modes of packing of α-helices with α-helices,[25,27,28] α-helices with β-sheets,[29] β-sheets with β-sheets,[30] and pairs of triple helices of collagen with each other.[31] Some examples are provided in Figs. 2-8. Figure 2 illustrates how side chain-backbone dipole-dipole interactions play a dominant role in leading to a left-handed helix in poly(m-Cl-benzyl-L-aspartate).[22] The predicted[22] left-handedness of the o- and m-derivatives, and the right-handedness of the p-derivative, where subsequently verified by circular dichroism measurements,[32] as indicated in Fig. 3. Figure 4 shows the computed right-handed twist of poly-L-valine β-sheets.[24] The lowest-energy packing arrangements for α...α, α...β, β...β pairs, and pairs of triple-helical collagen structures are illustrated in Figs. 5-8, respectively.

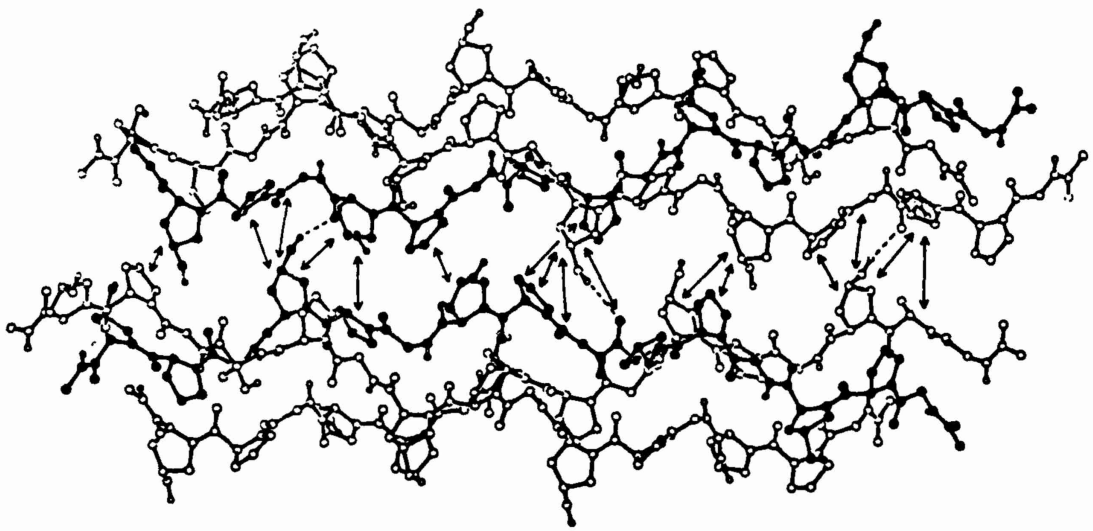

FIGURE 8. Computed lowest-energy packing arrangement[31] of two $[CH_3CO-(Gly-Pro-Hyp)_5-NHCH_3]_3$ triple helices, showing the near-parallel alignment of the two triple helices and O-H...O=C hydrogen bonds (dashed lines) between the triple helices. The arrows indicate residues that are in contact between the two triple helices.

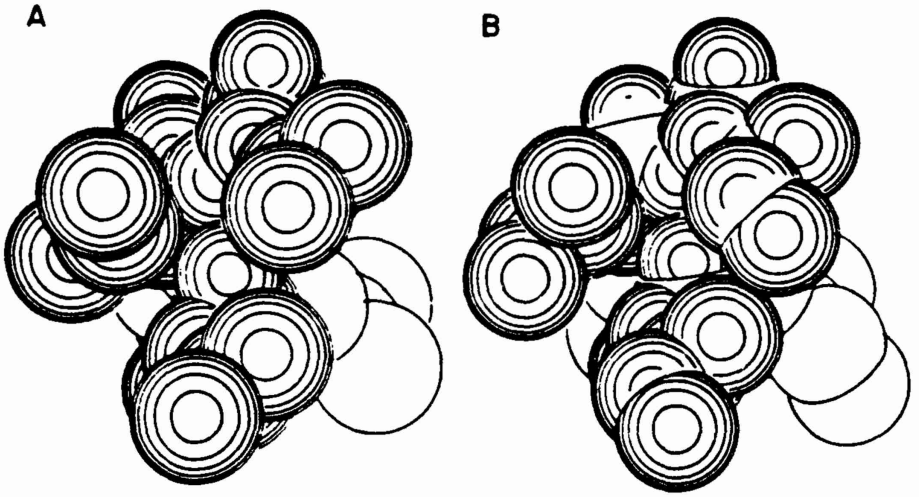

FIGURE 9. Space-filling models[36] of α-helical poly(L-valine) (A) and poly(L-isoleucine) (B).

TABLE I. Comparison of Lowest-energy Structures Obtained by Two Different Methods[a]

	SMAPPS	Build-up plus Energy Minimization
	Backbone Dihedral Angles (DEG)	
Tyr φ	-86	-87
ψ	154	155
Gly φ	-155	-157
ψ	95	96
Gly φ	71	71
ψ	-90	-91
Phe φ	-90	-91
ψ	-40	-38
Met φ	-165	-165
ψ	-50	-48
Energy(kcal/mol)	-10.64	-10.66

[a] In this computation, the side chains were constrained to have the conformations of Fig.12. More recently, this constraint has been eliminated (G.H. Paine and H. A. Scheraga, unpublished results).

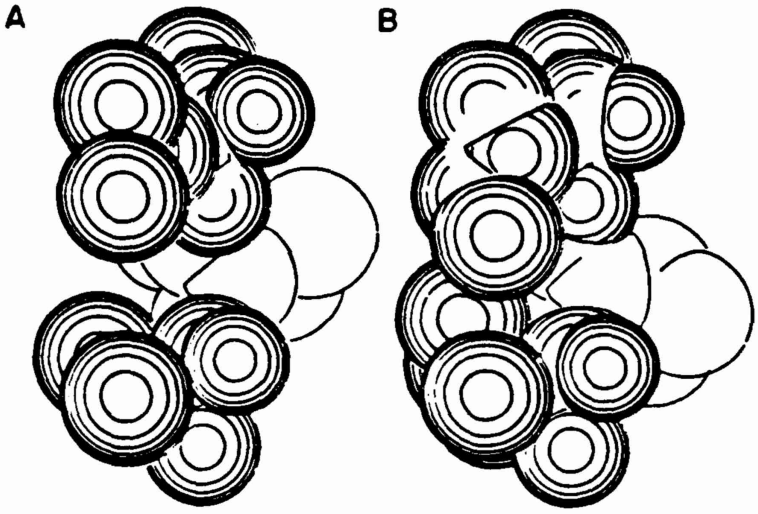

FIGURE 10. Space-filling models[36] of the β-conformation (the dominant species in the coil form) of poly(L-valine) (A) and poly(L-isoleucine) (B).

Conformational transitions have also been treated by this methodology, e.g.[33] the interconversion of the cis and trans forms of poly(L-proline),[34] of the α- and ω-helical forms of a crystalline homopolyamino acid,[35-37] and the α-helical and coils forms of various homopolyamino acids. For example, the helix-coil transition curves for poly(L-valine) and poly(L-isoleucine) in water differ markedly from each other, primarily because of the different degrees of hydration of the side chains in the helical and coil forms of the two polymers;[36] the different effects of hydration arise from the difference in side chain-side chain separation, because of the extra methyl group in isoleucine, as illustrated in Figs. 9 and 10.

A model poly(L-alanine) chain has recently been used to test a new procedure for overcoming the multiple-minima problem.[38] This procedure is based on the assumption that each residue must have optimal electrostatic energy; i.e., the dipole moment of each residue must be optimally aligned in the electrostatic field created by the whole molecule. If it is not, the orientation of the dipole moment (of each residue, in turn) is changed to improve the electrostatic energy. Since this involves a local movement (in the field of the whole molecule), it is computationally very fast. Then the energy of the whole molecule [taking all (ECEPP) interactions, not only electrostatic, into account] is minimized, and the whole procedure is repeated iteratively.

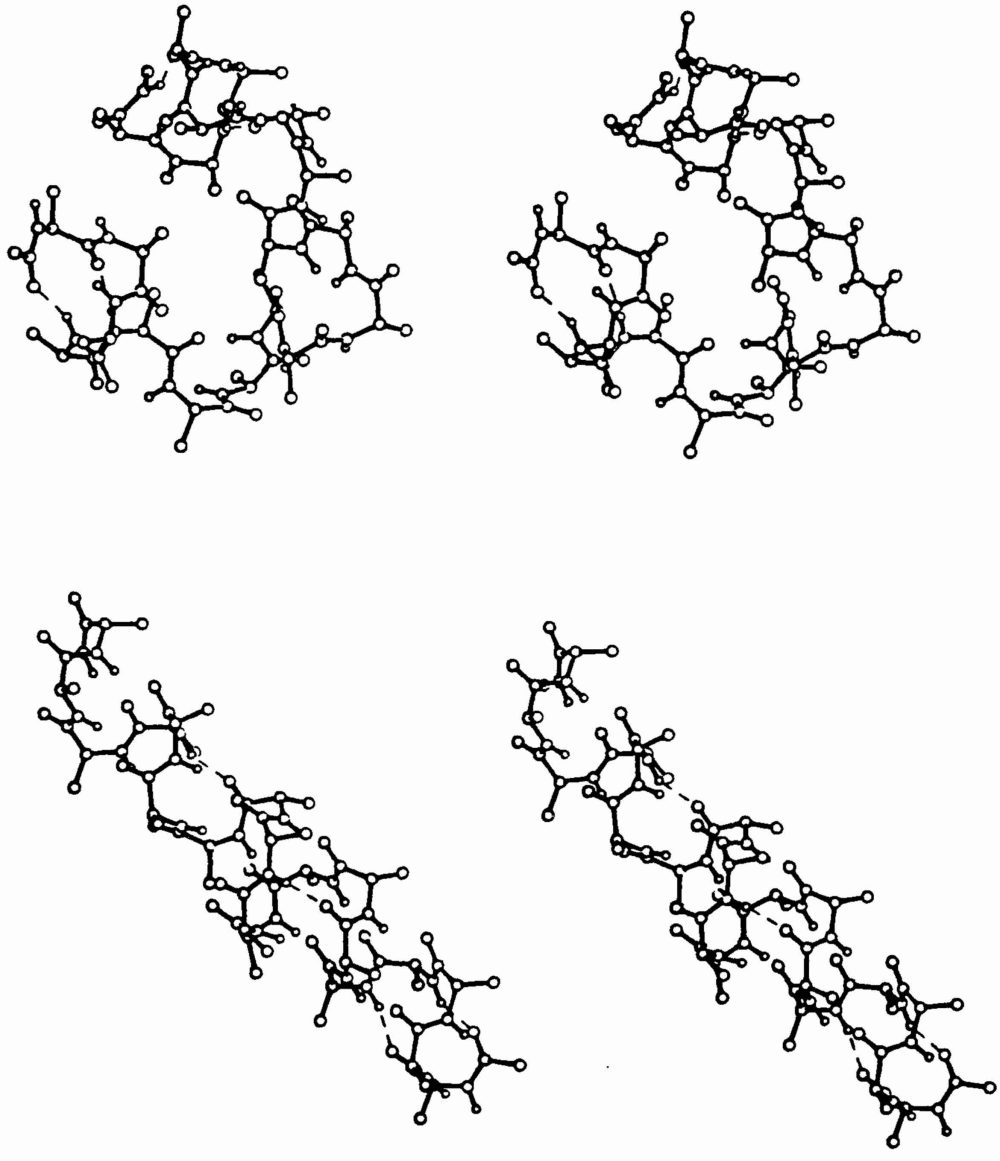

FIGURE 11. Test of procedure to surmount the multiple-minima problem.[38] Stereo-diagrams illustrating (top) a compact conformation of CH_3CO-$(Ala)_{19}$-$NHCH_3$ after complete ECEPP energy minimization to reach this particular local minimum, and (bottom) the global-minimum (α-helix) structure attained by first optimizing the local electrostatic interactions and then carrying out a complete (ECEPP) energy minimization.

Thus far, this procedure has been tested on a 19-residue poly-(L-alanine) chain with acetyl- and N-methyl amide terminal blocking groups. The global minimum of this structure (in the absence of water) is an α-helix. The starting conformations were very far from the helical conformation and, in trivially short computation time, the global minimum was achieved.[38] The top stereo diagram of Fig. 11 illustrates one of the starting conformations (optimized by conventional energy minimization), which is very far from a helical one; i.e., the minimization procedure was trapped in this high-energy local minimum. After application of the electrostatic-optimization procedure (and subsequent energy minimization with the complete ECEPP function), the global-minimum (α-helix) structure at the bottom of Fig. 11 was obtained. Unlike the usual minimization procedures, which make small changes in the dihedral angles, this new procedure can make very large changes (even 100° - 200°) in these independent variables, as illustrated in Fig. 11. Whereas conventional energy minimization gave the structure at the top of Fig. 11, the new procedure surmounted local barriers and attained the global minimum. This method is now being tested on other structures for which the global minimum is not an α-helix.

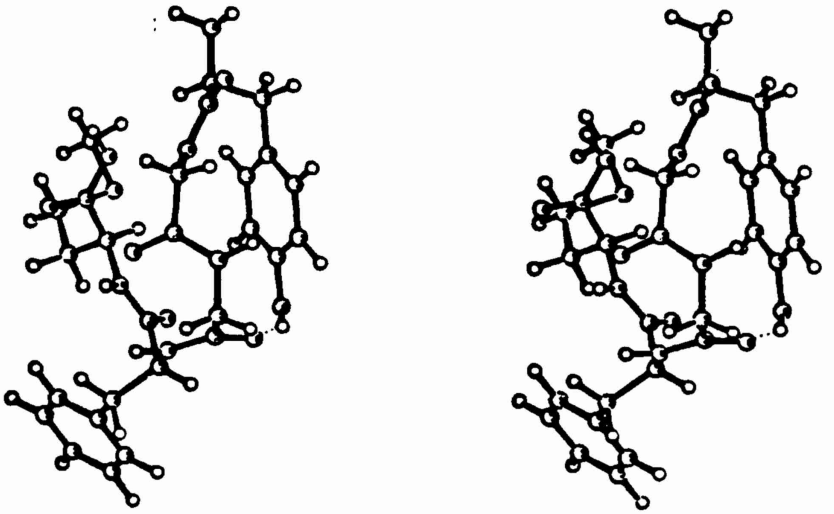

FIGURE 12. Stereo drawing of lowest-energy conformation of Met-enkephalin.[39]

OPEN-CHAIN AND CYCLIC PEPTIDES

A "build-up" procedure[18,19] has been used to surmount the multiple-minima problem for small open-chain and cyclic peptides. In this method, longer peptides are built up from all possible combinations of low-energy conformations of shorter-peptides. This assures an adequate coverage of conformational space. Energy minimization is carried out at each stage of the build-up procedure. The problem of storage of numerous conformations is alleviated by (legitimately) eliminating inconsistent conformations. For example, in building up the pentapeptide A-B-C-D-E from the tetrapeptides A-B-C-D and B-C-D-E, all tetrapeptides in which the conformations of the common tripeptide fragment B-C-D are not similar can be eliminated. When this procedure was applied to the pentapeptide Met-enkephalin,[39] with the sequence Tyr-Gly-Gly-Phe-Met, the hairpin-bend structure of Fig. 12 was obtained; a more recent improvement of the build-up procedure[40] led to a slightly altered conformation with a somewhat lower energy. Simultaneously, a new procedure, based on statistical mechanics and designed to surmount the multiple-minima problem by an adaptive importance sampling Monte Carlo method,[41] was applied to this same pentapeptide. This procedure (SMAPPS, Statisical mechanical algorithm for predicting protein structure) gave identifical results to those obtained by the build-up method, as can be seen in Table I.

The results of Table I obtained by two very different computational procedures, using the same potential functions, demonstrate the validity of both procedures. Work is currently in progress to pack this molecule into a crystal to determine the possible influence of intermolecular interactions on the conformation of this short linear peptide. (Parenthetically, it may be pointed out that SMAPPS evaluates the partition function directly. Hence, it may possibly provide a solution to the problem of computing free energies directly by a Monte Carlo procedure; tests of this possibility are in progress.)

A larger oligopeptide, the 20-residue membrane-bound portion of melittin has also yielded to the build-up procedure. The lowest-energy, largely -helical structure[42] is shown in Fig. 13. X-ray[43] and NMR[44] structural information is available for melittin as a tetramer in a crystal or as a monomer bound to micelles, respectively; considering possible environmental effects in either of these forms, the general agreement with experiment is satisfactory.

Gramicidin S, a cyclic decapeptide, serves as an example of the application of the computational (build-up) methodology to a cyclic molecule. The requirement to close the ring constitutes an additional constraint during the energy minimization. Figure 14a shows the computed structure,[45,46] and Fig. 14b provides a diagram of the subsequently determined X-ray structure[47] which agrees[46,48] with the predicted one. When the structure was computed[45] in 1975, it was stated that "the ornithine side chain may be free to occupy more than one rotational state...(and there is) a hydrogen bond between a $-NH_2$ proton of Orn and the backbone CO of Phe. There is no experimental evidence indicating the existence of this interaction." When the X-ray structure was reported[47]

SCHERAGA

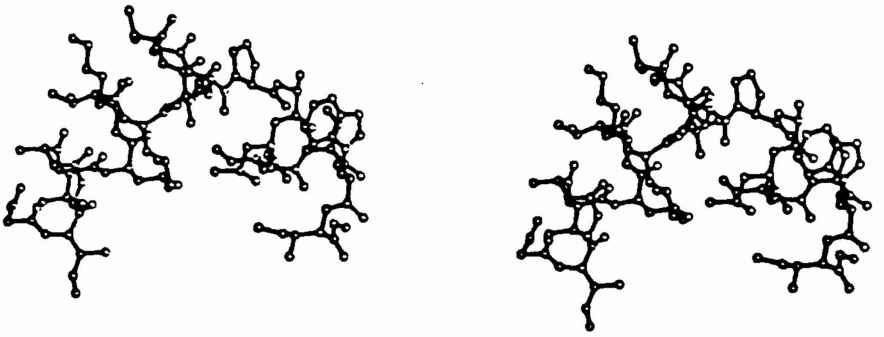

FIGURE 13. Stereo view of the lowest-energy structure calculated for residues 1-20 of melittin.[42]

in 1978, it was stated that "there is an intra-molecular hydrogen bond... between...the ornithine side-chain nitrogen atom and the D-phenylalanine carbonyl oxygen atom which has not been predicted." Figure 14a, which has a computed rotational variant[46] of the previously computed[45] side-chain conformation of ornithine, clearly shows the predicted hydrogen bond (the original computed rotational variant[45] had the Orn and Phe partners interchanged). The distortion of the X-ray structure in the lower right-hand corner of Fig. 14b (not seen in the symmetrical computed one of Fig. 14a) probably arises from the presence of a urea molecule in the crystal.

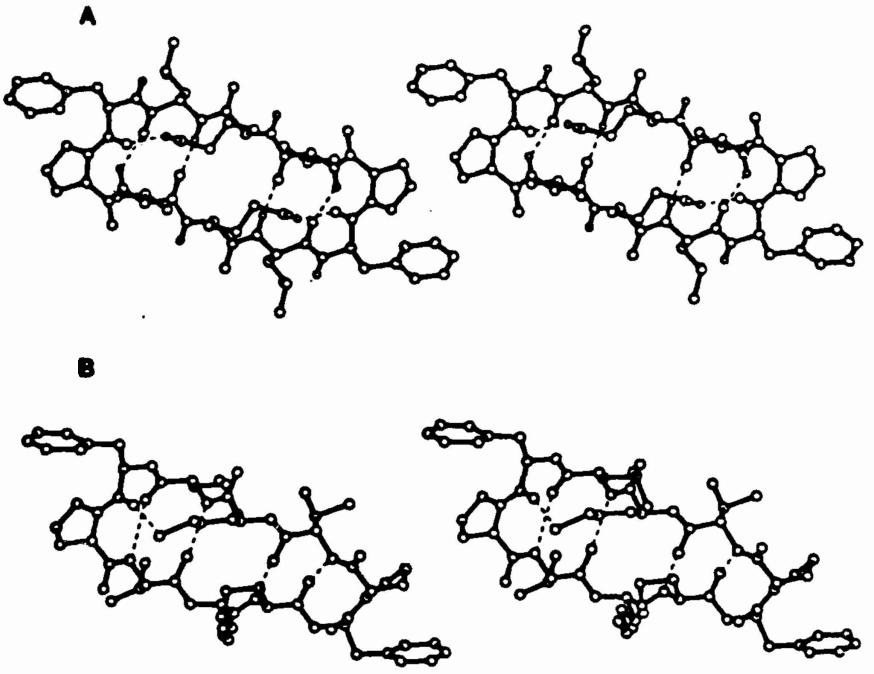

FIGURE 14. Computed[45,46] (A) and X-ray[47] (B) structures of gramicidin S showing (among other things) a hydrogen bond between the ornithine side chain and the phenylalanine backbone carbonyl group.

FIBROUS PROTEINS

Collagen is an example of a fibrous protein which involves interchain association to form a triple-stranded coiled-coil structure. Conformational energy calculations have been carried out on several synthetic poly(tripeptide) analogs, poly(Gly-X-Y), of collagen.[49-52] Because of the regularity conditions imposed on each tripeptide in the computations, the number of degrees of freedom was small, so that, again, the multiple-minima problem was surmounted by an adequate coverage of conformational space, using the build-up procedure. The computations indicated that poly(Gly-Pro-Pro), poly(Gly-Pro-Hyp), and poly(Gly-Pro-Ala) form stable triple-stranded coiled-coil collagen-like structures, whereas poly(Gly-Ala-Pro) does not, all in agreement with experiment. Figure 8 illustrates two calculated low-energy (collagen-like) structures in favorable contact with each other.

The computations also provided an explanation for the association of the chains [in contrast to the single-chain structures of α-helical forms of, e.g., poly(γ-benzyl-L-glutamate)]; viz., the resulting interchain interactions among the three chains of collagen lower the energy of a tripeptide unit below that in the nonassociated single chain. Furthermore, the inter-chain interactions induce a slight conformational change in going from the low-energy form of the single chain to the lower-energy form of the triple-stranded complex.

After completion of the calculations[49] on poly(Gly-Pro-Pro), it was learned that Okuyama et al.[53] had carried out a single-crystal X-ray structure analysis of $(Pro\text{-}Pro\text{-}Gly)_{10}$. Our structure is in agreement with theirs, with an rms deviation of 0.3Å for all (nonhydrogen) atoms, based on a comparison between the X-ray coordinates (kindly provided to us by Professor M. Kakudo) and our computed ones.

Similar methodology, already referred to in Section 2, is being used to investigate the formation of fibrils in collagen. The packing of two triple-stranded structures is shown in Fig. 8. Computations with assemblies of more than two triple-stranded structures are in progress.

GLOBULAR PROTEINS

As an introduction to the applicability of our computational methodology to globular proteins, we consider first two types of problems, refinement of X-ray structures of proteins and calculation of structures of homologous proteins, where the multiple-minima problem is not so serious, because one starts the computations with structures that are close to the global-minimum ones.

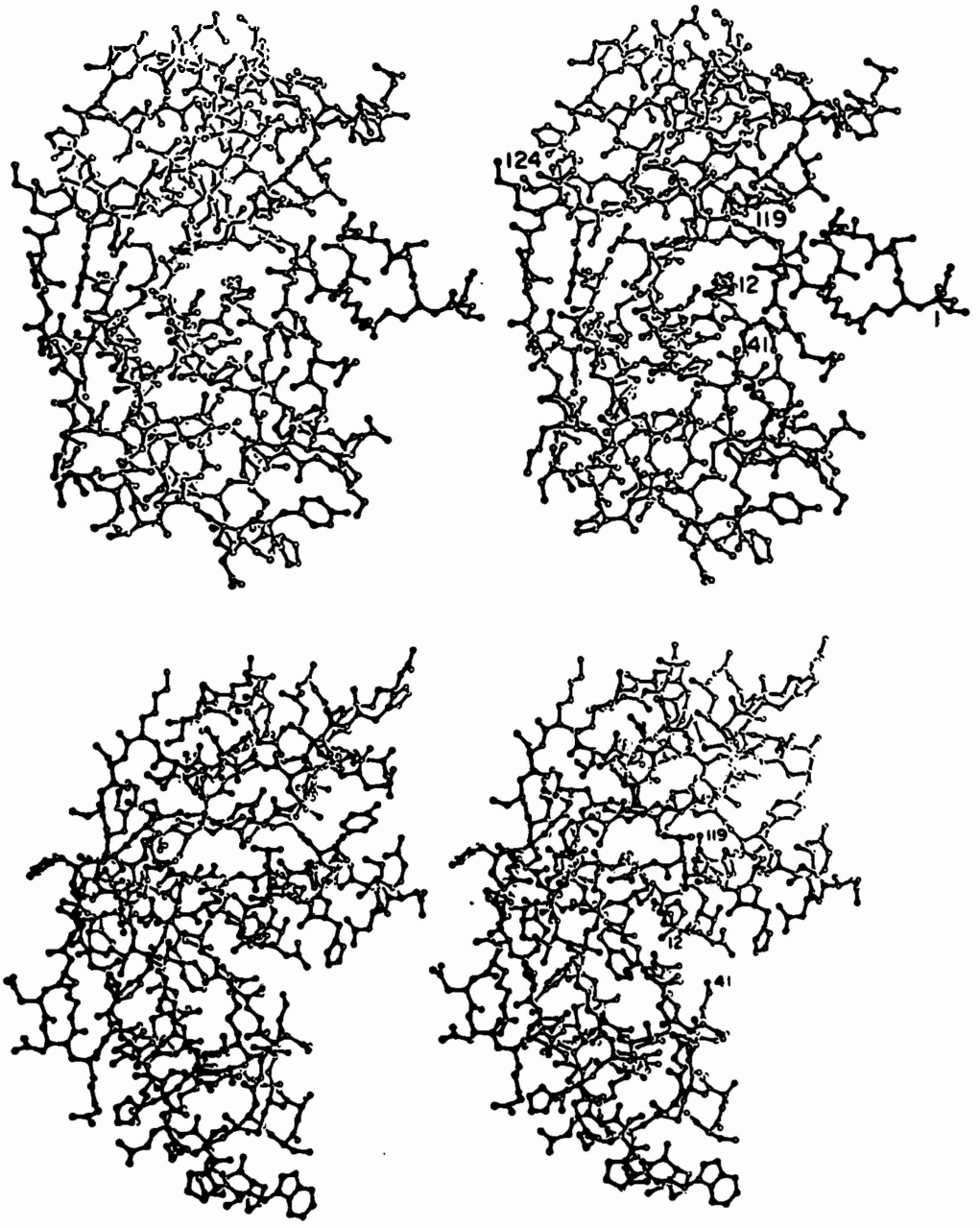

FIGURE 15. Stereo ORTEP diagrams of the full (heavy)-atom structures of ribonuclease (top) and angiogenin (bottom).[63] The active-site residues His-12, Lys-41, and His-119 (Bovine pancreatic ribonuclease numbering) are labeled in each structure.

Refinement of X-ray Structures of Proteins

We have used energy minimization to refine X-ray data by eliminating steric overlaps and providing low-energy structures. This procedure has been applied to several proteins, as summarized in Ref. 20.

FIGURE 16. Stereo views of space-filling models[76] of (top) the active site of native hen egg with lysozyme; (middle) energy-minimized model-built hexamer [$(GlcNAc)_6$] bound to the active site (right-sided mode); and (bottom) lowest-energy hexamer bond to the active site (left-sided mode).

We have also combined energy minimization with re-computation of electron density maps at each stage of refinement to make optimal use of low-resolution X-ray data.[54,55] The procedure was applied[55] to 2.5 Å-resolution data[56] for bovine pancreatic trypsin inhibitor to obtain a structure that was a satisfactory approximation to the one that had been obtained by use of 1.5 Å-resolution data.[57]

Calculation of Structures of Homologous Proteins

If the X-ray structure of a protein is known, the structure of a homologous protein can be obtained by "inserting" the amino acid sequence of the protein of unknown structure into the known structure of the other homologous protein. The energy of the structure obtained in this manner will be very high, expecially because of overlaps in regions where the sequences of the homologous proteins differ. However, these overlaps can be relieved, and the energy reduced, by minimization.

We have applied this procedure to obtain a structure of α-lactalbumin from that of lysozyme[58] and those of several snake venom inhibitors from that of bovine pancreatic trypsin inhibitor.[59] Subsequently, Berliner and Kaptein[60] obtained evidence that is compatible with our predicted conclusions about tryptophan residues of α-lactalbumin, and Gerkin[61] reported to a high pK_a for the N-terminal amino group, which "supports its interaction in an ion pair as proposed by Warme et al." Just recently, Koga and Berliner,[62] in further NMR studies, reported that "the experimental results were consistent with a putative three-dimensional α-lactalbumin model,[58] which predicted the close proximity of Ile-95, Tyr-103, Trp-60, and Trp-104." We recently applied this procedure to obtain a preliminary structure of angiogenin[63] (a protein that induces in vivo formation of blood vessels) by taking advantage of its homology to pancreatic ribonuclease A (see Fig. 15).

Strategies to Overcome Multiple-Minima Problem

In the absence of the structure of a homologous protein, other strategies must be used to obtain a starting conformation that can reach the global minimum by direct energy minimization. These strategies include the build-up and electrostatic-optimization procedures (mentioned in Sections 3 and 2, respectively), the use of distance constraints,[64,65] empirical data on short-, medium-, and long-range interactions,[64-68] and a factor analysis* of amino acid properties,[69,70] to limit the area of

* Using a factor analysis, it was possible to express the physical properties of the 20[69] naturally occurring amino acids in terms of 10 orthogonal factors.[69] These factors are then used[70] to search the protein data bank for amino acid sequences that have similar properties as the corresponding sequences of an unknown protein. Presumably, such sequences would then have similar three-dimensional structures. However, we have shown[70] that the sequences (whose properties are being compared) must be rather long ($\geq$ 15 residues) before the comparisons become meaningful.

conformational space searched, and other methods of searching, e.g., SMAPPS[41] and relaxation of dimensionality.[71] These procedures are used separately, and in various combinations with each other, to locate the approximate native conformation of a globular protein. They are all intended as the initial approaches in the computations. In the final stages, the results from all of these procedures are collated into an approximate three-dimensional structure whose energy should lie in the potential well containing the global minimum (i.e., this structure should be a good approximation of the native structure). Then, the conformational energy of this structure is minimized, taking all pair interactions (over the whole molecule) into account. These methods are being tested on a protein of known structure (bovine pancreatic trypsin inhibitor) and are currently being applied to one of unknown structure (human leukocyte interferon[72]).

This same methodology can also be used in protein design. By substituting one or more amino acids in specific parts of the sequence, and then minimizing the energy of the resulting structure, it is possible to assess the effect of the mutation(s) on the stability of the protein. One can therefore determine the effect of removing or adding a disulfide bond, or, say, substituting an alanine for a proline residue that might be postulated to play a rate-limiting role in protein folding.

ENZYME-SUBSTRATE COMPLEXES

The same computational methodology is also applicable to enzyme-substrate complexes, thereby providing information about the structures and energetics involved in molecular recognition and specificity.[73] Molecular details of such enzyme-substrate complexes are required in order to understand the mechanism of enzyme action. The computation pertains essentially to a docking process in which a flexible substrate approaches a flexible enzyme as the energy is minimized. Such calculations have been carried out for complexes of α-chymotrypsin with oligopeptides[74,75] and of hen egg white lysozyme with oligosaccharides.[75,76] Figure 16 illustrates two computed binding modes[76] for hexasaccharide substrates of hen egg white lysozyme, a "left-sided" and a "right-sided" binding mode. The former was predicted to predominate for $(GlcNAc)_6$. This prediction was subsequently verified[77] by experiments involving competition between oligosaccharides and monoclonal antibodies for binding to hen egg white lysozyme and by measurements of the Michaelis-Menten constant K_M for hen egg white lysozyme and for a homologous lysozyme from ringed neck pheasant, the latter having several different amino acids in the "right-sided" binding site.

CONCLUSIONS

The methodology underlying the results described herein has provided an understanding of the behavior of model systems, i.e., as to how interatomic interactions lead to the experimental observations. Similar understanding has been gained about the conformational properties of small open-chain and cyclic structures and fibrous proteins. Several strategies are currently being explored to try to surmount the multiple-minima problem for globular proteins. If successful, they should lead to predictable protein structures and to predictable effects of site-specific mutagenesis. They have already led to testable predictions about enzyme-substrate interactions, and offer the hope of understanding the fundamental processes in molecular recognition.

ACKNOWLEDGMENTS

This work was supported by the National Science Foundation (DMB84-01811), the National Institutes of Health (GM-14312), and the National Foundation for Cancer Research.

REFERENCES

1. G. Némethy and H.A. Scheraga, Biopolymers, 3, 155 (1965).

2. H.A. Scheraga, Fed. Proc., 26, 1380 (1967).

3. A. Wlodawer, R. Bott and L. Sjolin, J. Biol. Chem., 257, 1325 (1982).

4. G.N. Ramachandran, C. Ramakrishnan and V. Sasisekharan, J. Mol. Biol., 7, 95 (1963).

5. H.A. Scheraga, S.J. Leach, R.A. Scott and G. Némethy, Disc. Faraday Soc., 40, 268 (1965).

6. R.A. Scott and H.A. Scheraga, J. Chem. Phys., 45, 2091 (1966).

7. T. Ooi, R.A. Scott, G. Vanderkooi and H.A. Scheraga, J. Chem. Phys., 46, 4410 (1967).

8. H.A. Scheraga, Adv. Phys. Org. Chem., 6, 103 (1968).

9. F.A. Momany, R.F. McGuire, A.W. Burgess and H.A. Scheraga, J. Phys. Chem., 79, 2361 (1975).

10. G. Némethy, M.S. Pottle and H.A. Scheraga, J. Phys. Chem., 87, 1883 (1983).

11. P. DeSantis, E. Giglio, A.M. Liquori and A. Ripamonti, Nature, 206, 456 (1965).

12. D.A. Brant and P.J. Flory, J. Am. Chem. Soc., 87, 2791 (1965).

13. A.T. Hagler, E. Huler and S. Lifson, J. Am. Chem. Soc., 96, 5319 (1974).

14. J. Hermans, D.R. Ferro, J.E. McQueen and S.C. Wei, Jerusalem Symp. Quantum Chem. Biochem., 8, 459 (1975).

15. H.A. Scheraga, Chem. Revs., 71, 195 (1971).

16. C.B. Anfinsen and H.A. Scheraga, Adv. Protein Chem., 29, 205 (1975).

17. G. Némethy and H.A. Scheraga, Quart. Rev. Biophys., 10, 239 (1977).

18. H.A. Scheraga, Biopolymers, 20 1877 (1981).

19. H.A. Scheraga, Biopolymers, 22, 1 (1983).

20. H.A. Scheraga, Carlsberg Research Commun., 49, 1 (1984).

21. H.A. Scheraga, Annals N.Y. Acad. Sci., 439, 170 (1985).

22. J.F. Yan, F.A. Momany and H.A. Scheraga, J. Am. Chem. Soc., 92, 1109 (1970).

23. K.C. Chou, M. Pottle, G. Némethy, Y. Ueda and H.A. Scheraga, J. Mol. Biol., 162, 89 (1982).

24. K.C. Chou and H.A. Scheraga, Proc. Natl. Acad. Sci., U.S., 79, 7047 (1982).

25. H.A. Scheraga, K.C. Chou and G. Némethy, in "Conformation in Biology," Ed. R. Srinivasan and R.H. Sarma, Adenine Press, pp. 1-10 (1983).

26. K.C. Chou, G. Némethy, M.S. Pottle and H.A. Scheraga, Biochemistry, 24, 7948 (1985).

27. K.C. Chou, G. Némethy and H.A. Scheraga, J. Phys. Chem., 87, 2869 (1983). Erratum: ibid., 87, 4772 (1983).

28. K.C. Chou, G. Némethy and H.A. Scheraga, J. Am. Chem. Soc., 106, 3161 (1984). Erratum: ibid., 107, 2199 (1985).

29. K.C. Chou, G. Némethy, S. Rumsey, R.W. Tuttle and H.A. Scheraga, J. Mol. Biol., 186, 591 (1985).

30. K.C. Chou, G. Némethy, S. Rumsey, R.W. Tuttle and H.A. Scheraga, J. Mol. Biol., 188, 641 (1986).

31. G. Némethy and H.A. Scheraga, Biochemistry, 25, 3184 (1986).

32. E.H. Erenrich, R.H. Andreatta and H.A. Scheraga, J. Am. Chem. Soc., 92, 1116 (1970).

33. S. Tanaka and H.A. Scheraga, Macromolecules, 8, 516 (1975).

34. Y.C. Fu, R.F. McGuire and H.A. Scheraga, Macromolecules, 7, 468 (1974).

35. N. Gō, M. Gō and H.A. Scheraga, Proc. Natl. Acad. Sci., U.S., 59, 1030 (1968).

36. M. Gō and H.A. Scheraga, Biopolymers, 23, 1961 (1984).

37. F.T. Hesselink, T. Ooi and H.A. Scheraga, Macromolecules, 6, 541 (1973).

38. L. Peila and H.A. Scheraga, Biopolymers, in press.

39. Y. Isogai, G. Nemethy and H.A. Scheraga, Proc. Natl. Acad. Sci., U.S., 74, 414 (1977).

40. M. Vásquez and H.A. Scheraga, Biopolymers, 24, 1437 (1985).

41. G.H. Paine and H.A. Scheraga, Biopolymers, 24, 1391 (1985).

42. M.R. Pincus, R.D. Klausner and H.A. Scheraga, Proc. Natl. Acad. Sci., U.S., 79, 5107 (1982).

43. T.C. Terwilliger, L. Weissman and D. Eisenberg, Biophys. J., 37, 353 (1982).

44. L.R. Brown, W. Braun, A. Kumar and K. Wüthrich, Biophys. J., 37, 319 (1982).

45. M. Dygert, M. Gō and H.A. Scheraga, Macromolecules, 8, 750 (1975).

46. G. Némethy and H.A. Scheraga, Biochem. Biophys. Res. Commun., 118, 643 (1984).

47. S.E. Hull, R. Karlsson, P. Main, M.M. Woolfson and E.J. Dodson, Nature, 275, 206 (1978).

48. S. Rackovsky and H.A. Scheraga, Proc. Natl. Acad. Sci., U.S., 77, 6965 (1980).

49. M.H. Miller and H.A. Scheraga, J. Polymer Sci.: Polymer Symposia, No. 54, pp. 171-200 (1976).

50. M.H. Miller, G. Némethy and H.A. Scheraga, Macromolecules, 13, 470 (1980).

51. M.H. Miller, G. Némethy and H.A. Scheraga, Macromolecules, 13, 910 (1980).

52. G. Némethy, M.H. Miller and H.A. Scheraga, Macromolecules, 13, 914 (1980).

53. K. Okuyama, N. Tanaka, T. Ashida and M. Kakudo, Bull. Chem. Soc. Japan, 49, 1805 (1976).

54. S. Fitzwater and H.A. Scheraga, Acta Cryst., A36, 211 (1980).

55. S. Fitzwater and H.A. Scheraga, Proc. Natl. Acad. Sci., U.S., 79, 2133 (1982).

56. R. Huber, D. Kukla, A. Rühlmann, O. Epp and H. Formanek, Naturwissenschaften, 57, 389 (1970).

57. J. Deisenhofer and W. Steigemann, Acta Cryst., B31, 238 (1975).

58. P.K. Warme, F.A. Momany, S.V. Rumball, R.W. Tuttle and H.A. Scheraga, Biochemistry, 13, 768 (1974).

59. M.K. Swenson, A.W. Burgess and H.A. Scheraga, in "Frontiers in Physicochemical Biology," ed. B. Pullman, Academic Press, pp. 115-142 (1978).

60. L.J. Berliner and R. Kaptein, Biochemistry, 20, 799 (1981).

61. T.A. Gerken, Fed. Proc., 42, 2001 (1983).

62. K. Koga and L.J. Berliner, Biochemistry, 24, 7257 (1985).

63. K.A. Palmer, H.A. Scheraga, J.F. Riordan and B.L. Vallee, Proc. Natl. Acad. Sci., U.S., 83, 1965 (1986).

64. H. Wako and H.A. Scheraga, J. Protein Chem., 1, 5 (1982).

65. H. Wako and H.A. Scheraga, J. Protein Chem., 1, 85 (1982).

66. H. Meirovitch and H.A. Scheraga, Proc. Natl. Acad. Sci., U.S., 78, 6584 (1981).

67. T. Kikuchi, G. Némethy and H.A. Scheraga, J. Comput. Chem., 7, 67 (1986).

68. H. Wako, N. Saitô and H.A. Scheraga, J. Protein Chem., 2, 221 (1983).

69. A. Kidera, Y. Konishi, M. Oka, T. Ooi and H.A. Scheraga, J. Protein Chem., 4, 23 (1985).

70. A. Kidera, Y. Konishi, T. Ooi and H.A. Scheraga, J. Protein Chem., 4, 265 (1985).

71. E.O. Purisima and H.A. Scheraga, Proc. Natl. Acad. Sci., U.S., 83, 2782 (1986).

72. K.D. Gibson, S. Chin, M.R. Pincus, E. Clementi and H.A. Scheraga, Symp. on "Supercomputer Simulations in Chemistry," Montreal, Aug. 27, 1985, in press.

73. H.A. Scheraga, Pont. Acad. Sci. Scr. Var., 55, 21 (1984). Also, in Proceedings of the XVIIIth International Solvay Conference on Chemistry, in press.

74. K.E.B. Platzer, F.A. Momany and H.A. Scheraga, Intl. J. Peptide and Protein Research, 4, 201 (1972).

75. H.A. Scheraga, M.R. Pincus and K.E. Burke, in "Structure of Complexes Between Biopolymers and Low Molecular Weight Molecules," eds. W. Bartmann and G. Snatzke, John Wiley, Chichester, pp. 53-76 (1982).

76. M.R. Pincus and H.A. Scheraga, Macromolecules, 12, 633 (1979).

77. S.J. Smith-Gill, J.A. Rupley, M.R. Pincus, R.P. Carty and H.A. Scheraga, Biochemistry, 23, 993 (1984).

ELASTIC MOLECULAR MACHINES AND A NEW MOTIVE FORCE IN PROTEIN MECHANISMS

Dan W. Urry

Laboratory of Molecular Biophysics
The University of Alabama at Birmingham
P. O. Box 311/University Station
Birmingham, Alabama 35294

Abstract

It is demonstrated that the polypentapeptide, $(Val^1\text{-}Pro^2\text{-}Gly^3\text{-}Val^4\text{-}Gly^5)n$ when γ-irradiation cross-linked, can perform work on raising the temperature from 20° to $40^{\circ}C$. This is due to an inverse temperature transition leading to a regular helical structure called a dynamic β-spiral, which exhibits entropic elastomeric force. Processes which alter the hydrophobicity of a peptide segment can shift the temperature of an inverse temperature transition. When the hydrophobicity is changed reversibly as is possible with 20% Glu^4-poly-pentapeptide, the temperature for the onset of the inverse temperature transition can be reversibly shifted from being initiated at $37^{\circ}C$ at pH 2 ($COOH$) to being initiated at $50^{\circ}C$ at pH 7 (COO^-). Presumably therefore once a synthetic elastomeric matrix is formed from 20% Glu^4-polypentapeptide, it should be possible at $50^{\circ}C$ to turn "on" elastomeric force by changing the pH from 7 to 2 and to turn "off" elastomeric force by returning the pH to 7. This is called mechanochemical coupling of the first kind, and, in addition to ionization and deionization, it should be possible similarly to turn off and on elastomeric force by phosphorylation and dephosphorylation, respectively.

When the elastomeric state is arrived at by means of a regular transition from a more ordered state (e.g., α-helix) to a less ordered state (e.g., a spiral) on raising the temperature and a chemical process can change the temperature of the transition, this is referred to as mechanochemical coupling of the second kind. Mechanochemical coupling ongoing from an ordered state to a disordered state has often been considered. The studies on the polypentapeptide bring consideration of an inverse temperature transition for mechanochemical coupling of the first kind and of a less-ordered but nonrandom state for mechanochemical coupling of the second kind. It is proposed that these new considerations are relevant to mechanisms for the turning on and off of elastic forces in protein mechanisms as varied as those of enzymes and muscle contraction.

The Polypentapeptide of Elastin as an Elastic Molecular Machine

By definition a machine is a device for doing work and work is performed when a force acts against resistance to produce motion in a body. Consider as a specific example a weight suspended from the synthetic elastomeric polypentapeptide band at $20^{\circ}C$ in water (see Figure 1A). The band is formed on γ-irradiation of $(Val^1\text{-}Pro^2\text{-}Gly^3\text{-}Val^4\text{-}Gly^5)n$ where n is greater than 100, and the composition is approximately 40% peptide, 60% water by weight (1,2). On raising the temperature to

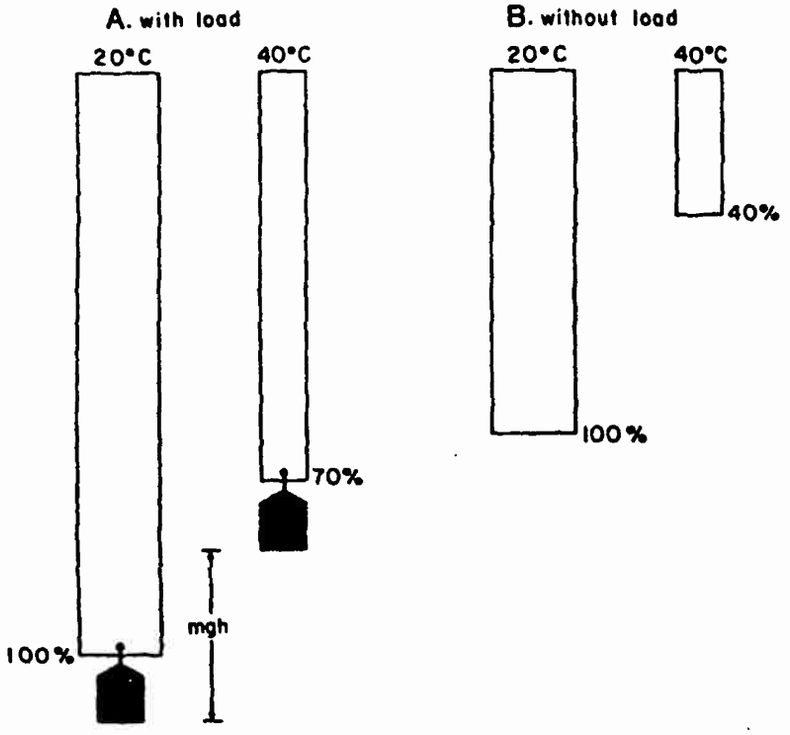

Figure 1: The polypentapeptide of elastin as an elastic molecular machine. High molecular weight $(Val\text{-}Pro\text{-}Gly\text{-}Val\text{-}Gly)_n$ with n greater than 100 is γ-irradiation cross-linked when in a viscoelastic state of 40% peptide, 60% water by weight to form an insoluble band of material.

A. A weight of 300 gms/cm^2 of band cross-sectional area measured at 40°C is applied. At 20°C in water, the length is taken as 100%. On raising the temperature to 40°C, the band shortens to 70% lifting the weight. The work performed is mgh. B. A band of cross-linked polypentapeptide is depicted at 20°C in water in the absence of any load. On raising the temperature to 40°C, the sample contracts to approximately 40% of its original length. The heat absorbed during this inverse temperature transition is approximately 1 cal/gm polypentapeptide. This shortening of the sample is due to the winding up of the polypentapeptide chain into a helical structure, termed a β-spiral, as shown in Figure 2.

40°C, the weight (300 grams/cm^2 elastomer cross-section) is raised against gravity as the synthetic elastomeric band shortens to 70% of its 20°C length (3). For a band 10 cm long, the weight would be raised 3 cm against the pull of gravity. The same qualitative result is obtained with the entropic elastomer, latex rubber, but for this classical rubber the length change is much less, only about 5% instead of 30% (3). Both elastomers are molecular machines but the polypentapeptide elastomer is a more effective machine for moving an object when changing the temperature from 20° to 40°C. What occurs as the result of this temperature change in the polypentapeptide is an enhanced effect due to an inverse temperature transition wherein the polypentapeptide wraps up into a helical structure, i.e., a β-spiral, on raising the temperature from 20°C to 40°C (4). The helical structure is the result of optimizing intramolecular hydrophobic interactions. The heat absorbed during this inverse temperature transition occurring between 20° to 40°C is approximately 1 cal/gram of the polypentapeptide in water. The class of β-spirals to which the elastomeric polypentapeptide belongs is shown in Figure 2 (5-8) and the length change under zero load is from 100% to 40% on going from 20°C to 40°C (see Figure 1B). At fixed length, development of elastomeric force (f) correlates with structure development (4) and as shown in Figure 3, the structure so formed exhibits entropic elastomeric force (9). As will be further discussed below, the polypentapeptide forms an entropic anisotropic elastomer.

Entropic Elastomeric Force Resulting From an Inverse Temperature Transition

Previously entropic elastomeric force has been taken to require that the polymeric system be a network of random chains in adherence to the classical theory of rubber elasticity (10). When elastin fibers were shown to give a result like that in Figure 3 for the polypentapeptide of elastin in the temperature range above 40°C, the conclusion was "A network of random chains within elastin fibers, like that in a typical rubber, is clearly indicated" (11). In a typical rubber, the decrease in entropy on deformation is taken to be due to the displacement from a random distribution to end-to-end chain lengths (12,13). But a random distribution of end-to-end chain lengths is not the product of an inverse temperature transition. An inverse temperature transition involves an increase in polymer order on increasing the temperature. For the polypentapeptide of elastin, it is demonstrated in Figure 3 that entropic elastomeric force occurs above 40°C on completion of the inverse temperature transition, that is, once the increase in order has occurred. This is because the elastomeric force, f, is the sum of two components: f_e, an internal energy component and f_s, the entropic component. When ln[elastomeric force/T(°K)] is plotted versus temperature, a zero slope is taken to mean that $f_e/f = 0$, that is, the elastomer exhibits dominantly entropic elastomeric force (14). As shown in Figure 3 (solid curve), the cross-linked polypentapeptide exhibits a dominantly entropic elastomeric force above 40°C (15, 16).

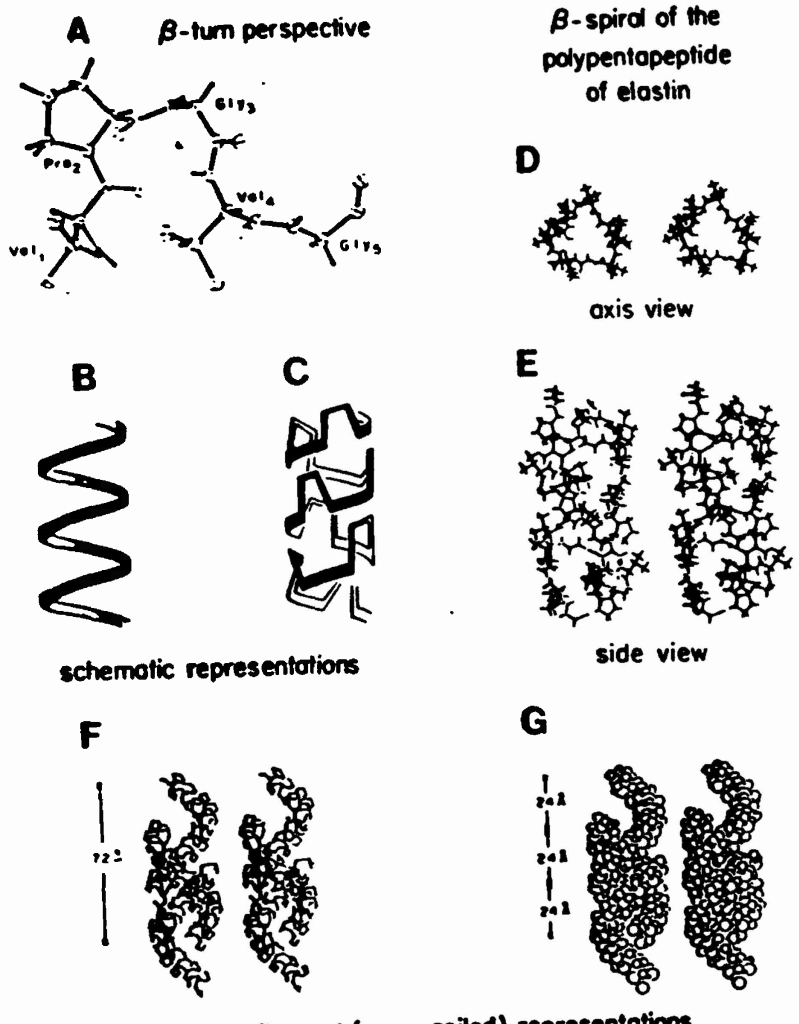

Figure 2:

Molecular conformation of the 40°C state of the polypentapeptide of elastin in water.

A. The β_1-turn perspective of the pentamer, showing the Val^1 C-O_2... HN Val^4 ten atom hydrogen bonded ring with Pro^2-Gly^3 at the corners. Adapted with permission from reference 5. Raman studies indicate that the β-turn is present before and after the transition observed in Figure 1B on going from 20° to 40°C (6). B. On raising the temperature, the largely extended series of β-turns wrap up into a helix in which the β_1-turns function as spacers between turns of the helix as shown in C. The helix with β-turns spacers is called a β-spiral and it is the wrapping up into a β-spiral that is responsible for the dramatic contraction of size seen in Figure 1B. The length change for the depicted β-spiral to become an extended series of β-turns is close to a factor of 3; interestingly, not a unreasonable factor of 2.5 is observed (see Figure 1B). (B., C. and D. reproduced with permission from reference 7.) D. and E. are stereo pair perspectives of the detailed β-spiral seen in axis view (d) and side view (E). The interturn contacts are hydrophobic and result from the optimization of intramolecular hydrophobic contacts developed during the inverse temperature transition. Between the β_1-turns are suspended segments running from the Val^4 α-carbon to the Val^1 α-carbon in which the peptide moieties can undergo large amplitude, low frequency librational motions. On stretching these librational motions become damped which is a decrease in entropy that provides the resistance to and the restoring force from deformation. This is called the librational entropy mechanism of elasticity (7). E. is reproduced with permission from reference 8.

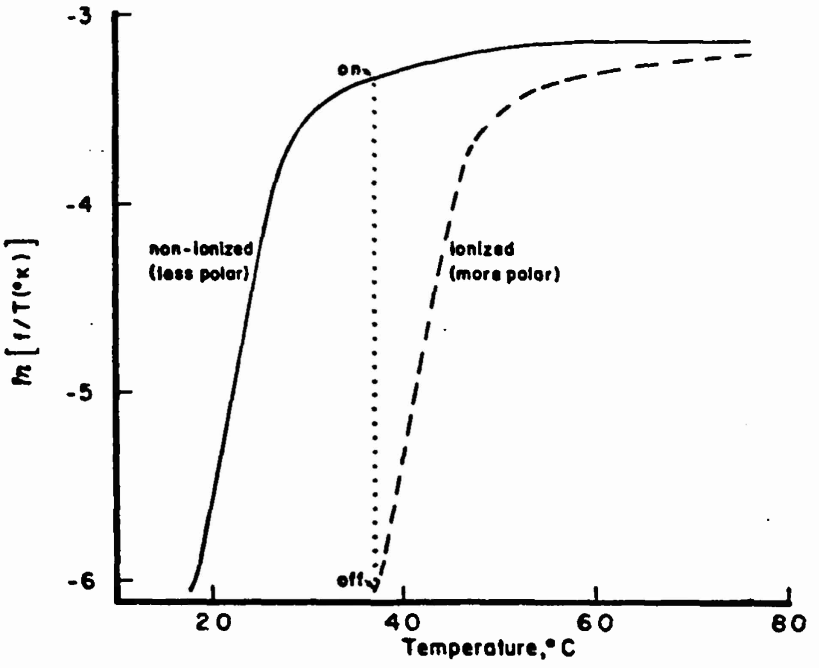

Figure 3: Thermoelasticity data on the γ-irradiation cross-linked polypentapeptide of elastin (solid curve). The observation that the slope of the ln[f/T°K)] versus temperature curve at fixed extension is near zero above 40°C is the basis for arguing that the elastomeric force is dominantly entropic. The data (9) is used in the present context to demonstrate the effect of decreasing the hydrophobicity, i.e., increasing the hydrophilicity, as for example by ionization of a residue within the polypentapeptide such as an occasional glutamic acid residue or by a phosphorylation of a serine or threonine residue. The effect of making this polymer more polar would be to raise the temperature midpoint of the inverse temperature transition that is responsible for the observed development of elastomeric force. The expected result is the dashed curve. The perspective is, therefore, that the elastomeric force is turned on at 37°C when the polypeptide is neutral and is turned off when the polypeptide is more polar or charged.

Numerous physical characterizations of the polypentapeptide of elastin in water have shown that on raising the temperature from 20° to 40°C, there is an increase in molecular order. Those physical characterizations include: i. light and electron microscopy demonstrating on increasing the temperature a self-assembly into fibers, comprised of parallel aligned fibrils, which in turn are comprised of parallel aligned filaments (7,17,18); ii. light scattering following the aggregation with increase in temperature (2); iii. circular dichroism showing an increase in intramolecular order with occurrence of regularly recurring β-turns (19); iv. the nuclear Overhauser effect demonstrating the intramolecular hydrophobic interactions attending the inverse temperature transition (20); v. composition studies showing the phase transition to a unique composition of polypentapeptide plus water (2); vi. nuclear magnetic resonance relaxation studies showing a decrease in backbone mobility on raising the temperature through the inverse temperature transition (21,22); vii. dielectric relaxation studies showing the development of an intense, low frequency, high amplitude, localized, Debye-type relaxation on raising the temperature through the inverse temperature transition (23,24); viii. and the above noted temperature dependence of elastomer length (3). Having demonstrated an increase in order on arriving at 40°C, thermal denaturation can be demonstrated on raising the temperature above 60° to 80°C (2) and by circular dichroism showing the decrease in intramolecular order on standing at 80°C (2); and thermal denaturation has been demonstrated directly in the loss of elastomeric force and elastic modulus on heating at 80°C (25). These are not the properties of random chain networks. Accordingly a new understanding is required for the decrease in entropy on deformation and it is one of a damping of internal chain dynamics on deformation called the librational entropy mechanism of elasticity (9,26,27). A new understanding of entropic elastomeric force has emerged from which interesting new possibilities arise.

Effect of Changing Hydrophobicity of Polypeptide Elastomers

The fact that the elastomeric force development occurs with shortening by means of an inverse temperature transition (3,4) gives interesting new potential to the polypentapeptide and like elastomers as molecular machines. It has been shown (28,29) that changing the hydrophobicity of the repeating unit in the elastomeric polypeptide changes the temperature range of the inverse temperature transition, which gives rise to regular structure; that changing the hydrophobicity changes the temperature range over which elastomeric force develops, and that changing the hydrophobicity changes the range over which the elastomer shortens. For example, increasing the hydrophobicity of the polypentapeptide (VPGVG)n as in the Ile^1-polypentapeptide, (IPGVG)n, analog (28) lowers the temperature range over which the transition occurs by some 20°C from a midpoint of near 30°C for (VPGVG)n to near 10°C for (IPGVG)n. Furthermore when the hydrophobicity is decreased as when the Val^4 residue is removed as in the polytetrapeptide (VPGG)n, the product is an elastomer but the

development of elastomeric force is now shifted to 50°C (29). Thus by changing the hydrophobicity, the midpoint temperature of the inverse temperature transition for the development of elastomeric force has been shifted over the temperature range from 10°C to 50°C. Increase the hydrophobicity and the inverse temperature transition occurs at a lower temperature; decrease the hydrophobicity and the inverse temperature transition occurs at a higher temperature. Even the magnitudes of the shifts are calculable from the change in hydrophobicity (29,30,31).

When temperature is limited as a variable, therefore, as an example in the case of living organisms, varying the hydrophobicity would be a useful way to perform work. Decreasing hydrophobicity which, of course, is equivalent to increasing hydrophilicity can be achieved by hydroxylation. Accordingly, it has been shown, by chemically introducing hydroxyproline in place of proline and by direct hydroxylation of (VPGVG)n using the enzyme prolyl hydroxylase, that the temperature range of the inverse temperature transition can be raised in proportion to the amount of replacement or conversion of proline to hydroxyproline (32). When the ratio of (Val-Pro-Gly-Val-Gly) to (Val-Hyp-Gly-Val-Gly) was 9:1 in the polymerizing mixture, the resulting polymer exhibited a transition midpoint that was shifted 7°C to higher temperature; for (Val-Hyp-Gly-Val-Gly)n itself the transition midpoint was above 65°C (32). What would be of particular interest would be to shift reversibly the temperature of the inverse temperature transition and thereby to turn "on" and "off" the elastomeric force. One means would be protonation or deprotonation of a functional side chain; another might be enzymatic reactions wherein there is an interconversion between charged and uncharged states of a side chain; and yet another could be the phosphorylation and dephosphorylation, for example, of a serine or threonine side chain. The use of pH is briefly considered below.

Reversibly Changing Hydrophobicity of the Polypentapeptide as a Means of Turning Elastomeric Force "On" and "Off"

As shown in Figure 4, the inverse temperature transition can be followed by means of the temperature profiles for aggregation for the polypentapeptide and its 20% Glu^4 analog. Changing one in five Val^4 residues to a Glu^4 residue, when the pH is 2 where the side chain is the carboxyl, changes the onset of the inverse temperature transition from 25°C to 37°C. On ionization of the side chain to form the carboxylate anion at pH 6, the onset of the inverse temperature shifts further to 49°C. Once the 20% Glu^4-polypentapeptide is cross-linked to form the elastomeric matrix, it is expected that the elastomer can most effectively at 50°C be turned "on" at pH 2 and "off" by changing the pH to 7. This would be a chemomechanical transducer. If 50°C were not the desired temperature, for example, if lower temperature were desired, then more hydrophobic residues could be used in place of Val^1 and Val^4.

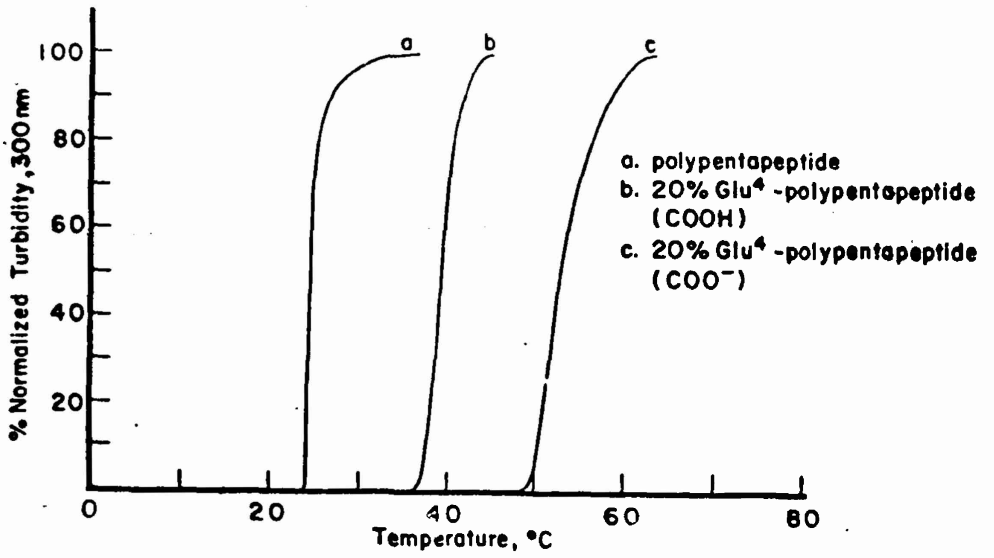

Figure 4: Temperature profiles of aggregation showing the temperature dependence of the intermolecular aspect of the inverse temperature transition. This also coincides with the intramolecular component of the inverse temperature transition. Curve a: the polypentapeptide of elastin; curve b: 20% Glu^4-polypentapeptide at pH 2 where the polar side chain is the COOH moiety; and curve c: 20% Glu^4-polypentapeptide where the side chain is ionized (COO-) at pH 6. The solid curve in Figure 3 showing the development of force with temperature corresponds to curve a. On the basis of this, it is expected that the 20% Glu^4-polypentapeptide cross-linked matrix would develop elastomeric force with a midpoint temperature near 40°C when at pH 2 and that force development would shift to a midpoint temperature of near 55°C when at pH 7. Therefore at 50°C, changing the pH from 2 to 7 should turn off elastomeric force and the reverse should turn on elastomeric force.

Starting with Ile^1-polypentapeptide, which has a transition midpoint of about 10°C (28), inclusion of a more polar residue, such as Glu, Asp, His, Lys, or Tyr, for example in every third pentamer at position four would raise the temperature of the transition toward 30°C for the nonionized state. The appropriate mix of Ile^1 and Val^1 and of Val^4 and the more polar side chain at position four would allow the midpoint of the transition to be selected over a temperature of 10°C to above 30°C. On ionization the transition would shift to a higher temperature yet. Suppose that the non-ionized analog exhibited a transition midpoint near 30°C and that the β-spiral structure were formed and the development of elastomeric force were essentially complete by 37°C, as in the solid curve of Figure 3, then on ionization (e.g., on raising the pH above the pK of the ionizable function) the transition midpoint would shift to a higher temperature; the structure would unwind and the elastomeric force would be turned off as in the dashed curve of Figure 3. Lowering the pH to below the pK would cause the elastomeric force to turn back on. A change in the activity of the hydrogen ion becomes the switch. A number of other switches could be devised.

Mechanochemical Coupling

Previously, developments of elastomeric force with increase in temperature have been conformed to considerations of the classical theory of rubber elasticity with consideration of an order to disorder transition. In one proposed mechanism for the power stroke of muscle contraction in the S-2 fragment of myosin, an α-helix to random coil transition provides an interesting possibility to consider (33,34). The polypentapeptide data, in which the elastomeric state is a nonrandom β-spiral structure, indicate that random coil is not a necessary consideration and even suggests that it could be incorrect since the elastic modulus on thermal randomization of the polypentapeptide of elastin and of elastin itself becomes so low as to be of little relevance to the elastic forces of muscle contraction (16,25). Accordingly, analysis in terms of an α-helix to spiral transition seems warranted. Thus the situation could be one as shown in Figure 5 in which an α-helix with 1.5Å/residue converts to a spiral with about half the translation per residue, e.g., 0.7Å/residue as in the β-spiral of Figure 2. This would be consistent with the pitch estimated for the β-spirals of the polypentapeptide with about 15 residues per turn of spiral (8), of the polytetrapeptide with about 16 residues/turn (35), of the polyhexapeptide with about 12 residues/turn (36) and of the polynonapeptide with about 18 residues per turn (Chang, Trapane and Urry, in preparation). With heptamer repeats in myosin grouped as 28mers (37) some fourteen residues per turn would be reasonable for a spiral structure. Whatever the details of the situation, one looks for a chemical process to shift the temperature of the transition such that at a given temperature the elastic contraction could occur as the result of a chemical process.

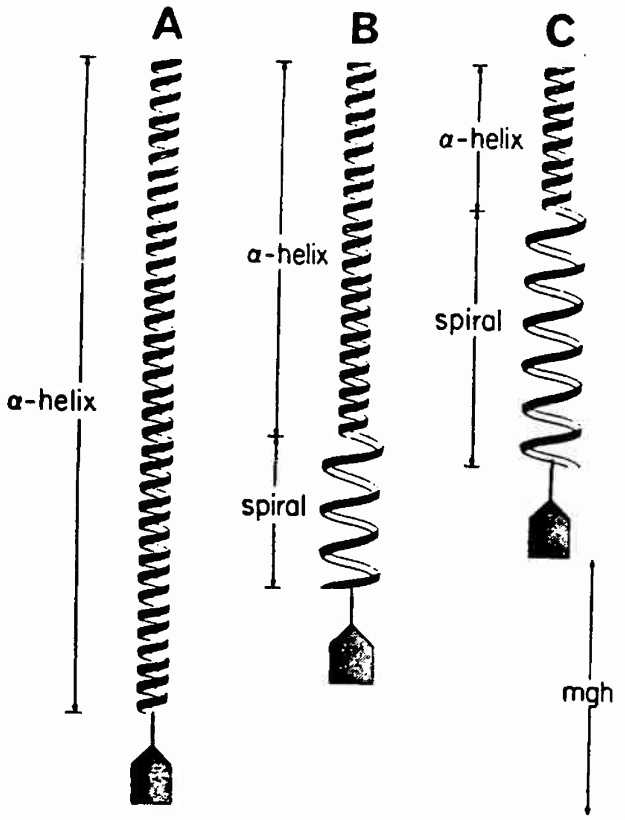

Figure 5: Proposed α-helix to spiral structural transition for the turning on of elastomeric force with the result of lifting a weight. The α-helix is shown with a graded instability such that the lower end would first convert to spiral on raising the temperature as in B and then as the temperature increased further, the conversion would continue on up the chain as shown in C. The graded instability with respect to temperature would facilitate reversibility in a condensed matrix.

There have now been discussed two kinds of mechanochemical coupling. Mechanochemical coupling of the first kind in which an inverse temperature transition from a higher to a lower entropy structure is the transition for the development of elastomeric force, and mechanochemical coupling of the second kind, which utilizes a standard transition from a lower entropy state to a higher entropy state. The structural transitions for these two kinds of coupling are shown schematically in Figure 6. A key element of these considerations is that there exist structures intermediate in entropy between the α-helix, β-sheet and collagen triple stranded (ordered and relatively rigid) structures on the one hand the random chain networks or random coil structures on the other hand. That such regular structures of intermediate entropy exist has been shown with the sequential elastomeric polypeptides of elastin as well as in the series of helical structures that can exist for the polydipeptide gramicidin A (9).

Entropic Motive Force in Protein Mechanisms

Having demonstrated entropic elastomeric force to be due to internal chain dynamics in nonrandom polypeptide systems, it seems appropriate to note situations in which protein elastic processes may be viewed in terms of this new perspective. Several examples will be briefly noted below.

Elastin: The most striking primary structural feature of porcine and bovine elastin is the polypentapeptide considered above. It is not suprising therefore that similar physical characterizations of elastin have shown it to be an entropic elastomer which forms its elastic structure by means of an inverse temperature transition (15,16,38). Accordingly, it is expected that increased hydrophilicity such as prolyl hydroxylation would raise the temperature of the inverse temperature transition and limit fiber formation. This process has been observed in cell culture (39) and has been proposed to be the reason for the near absence of elastic fibers in the scar tissue of wound repair (40). Of further medical significance is that by the foregoing reasoning, any oxidative process should shift the inverse temperature transition, that gaves rise to elastin fibers, to higher temperature and cause an unwinding of the spiral structures in elastin. A loss of elastic recoil and elongation has been looked for and observed using a superoxide generating system with bovine ligamentum nuchae elastin (38). Elastin fiber oxidation has been proposed in the initiation of pulmonary emphysema (38), which is characterized by disrupted elastic fibers and loss of elastic recoil of the lung (41). Oxidation loss of elastic recoil can also be considered in the sagging and wrinkling of skin with age.

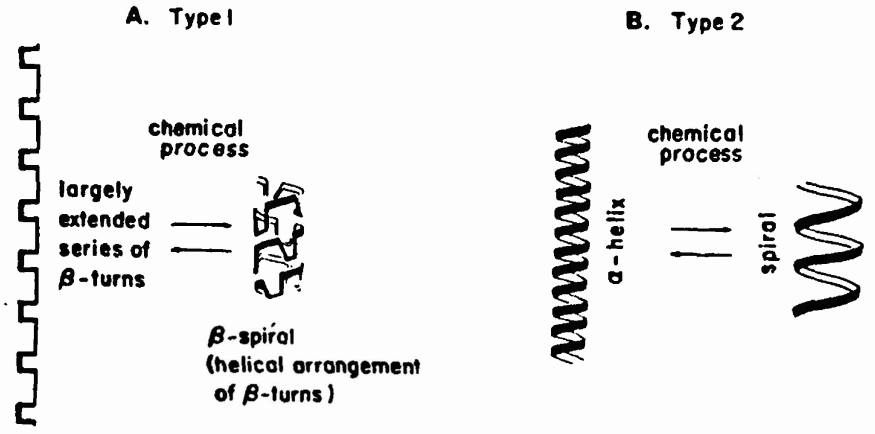

Figure 6: Structural Transitions for Mechanochemical Coupling

A. Type 1. The structural transition is from a higher entropy to a lower entropy state with increase in temperature, that is, it is an inverse temperature transition. The example involves a largely extended high entropy series of β-turns that wrap up to form an elastic β-spiral. A β-spiral is defined as a helical arrangement of β-turns. The result of the inverse temperature transition is the optimization of intramolecular, interturn hydrophobic interactions. Increasing hydrophobicity lowers the temperature of the transition and decreasing hydrophobicity increases the temperature of the transition. The development of elastomeric force at fixed extension occurs as the result of the inverse temperature transition and therefore by this analysis, elastomeric force can be turned on and off by varying the temperature of the transition, that is, by reversibly changing the hydrophobicity of the polarity of the polymer, for example by ionization of a side chain; the result is that the temperature for the transition is raised above the fixed temperature and elastomeric force is turned off. Deionization would lower the temperature of the transition to below the fixed temperature and would turn elastomeric force back on. Enzymatic phosphorylation and dephosphorylation at constant temperature and constant pH would be another means of reversibly shifting the temperature of the transition by reversibly changing the hydrophobicity of the polypeptide. B. Type 2. The structural transition is from a lower entropy state to a higher entropy state with increase in temperature, that is, this is a standard transition. The example is the conversion of an α-helix to an elastic spiral wherein changes in internal chain dynamics give rise to an entropic elastomeric force. The relaxed state of the spiral has a lower axis translation per residue (0.5Å/residue) than the α-helix (1.5Å/residue) such that the structural conversion results in a contraction. Any chemical process which shifted the temperature of the transition by changing the relative free energies of the structure could turn on or off the elastomeric force of the spiral structure. Possible chemical processes would be changes in pH, changes in calcium ion concentration or phosphorylation/dephosphorylation. The mechanism, Type 2, has been generally considered to be mechanochemical coupling. The element introduced by the work on polypeptide elastomeric biomaterials is the consideration of a spiral structure instead of a random coil.

Summarizing Comments

The general implications of the foregoing considerations are several: i. Elastic processes in polypeptides and proteins need not be described in terms of networks of random chains or random coil structure; indeed it may be incorrect to do so. ii. Entropic elastomeric force can be exhibited by a short anisotropic peptide segment due to internal chain dynamics (the librational entropy mechanism of elasticity). Random chain networks are not required. iii. Whether in a short peptide segment of a globular protein or in a fibrillar protein, it is expected that elastomeric force can be turned "on" and "off" by reversibly changing the hydrophobicity of the polypeptide. A most obvious means of doing so would be phosphorylation and dephosphorylation. And iv. It should be possible to design a wide range of polypeptide elastomeric biomaterials that could function in thermomechanical, chemomechanical and electromechanical transduction.

Acknowledgement

This work was supported in part by Department of the Navy, Office of Naval Research contract N00014-86-K-0402.

References

1. D. W. Urry and K. U. Prasad, "Syntheses, Characterizations and Medical Uses of the Polypentapeptide of Elastin and Its Analogs," In Biocompatibility of Tissue Analogues, (D. F. Williams, ed.), CRC Press, Inc., Boca Raton, Florida, 89-116, 1985.

2. D. W. Urry, T. L. Trapane and K. U. Prasad, "Phase-Structure Transitions of the Elastin Polypentapeptide-Water System Within the Framework of Composition-Temperature Studies," Biopolymers, 24, 2345-2356, 1985.

3. D. W. Urry, B. Haynes and R. D. Harris, "Temperature Dependence of Length of Elastin and Its Polypentapeptide," Biochem. and Biophys. Res. Commun. 141(2), 749-755, 1986.

4. D. W. Urry. "Elasticity of the Polypentapeptide of Elastin Due to a Regular, Non-random, Dynamic Conformation: Review of Temperature Studies," In Biomolecular Stereodynamics III, (R. H. Sarma and M. H. Sarma, Eds.) Adenine Press, Guilderland, New York, 173-196, 1985.

5. W. J. Cook, H. M. Einspahr, T. L. Trapane, D. W. Urry and C. E. Bugg, "The Crystal Structure and Conformation of the Cyclic Trimer of a Repeat Pentapeptide of Elastin, Cyclo-(L-Valyl-L-Prolyl-Glycyl-L-Valyl-Glycyl)$_3$," J. Am. Chem. Soc., 102, 5502-5505, 1980.

6. G. J. Thomas, Jr., Betty Prescott and D. W. Urry, "Raman Amide Bands of Type-II β-turns in Cyclo-(VPGVG)$_3$ and Poly(VPGVG), and Implications for Protein Secondary Structure Analysis," Biopolymers (in press).

7. D. W. Urry, "What is Elastin; What is Not," Ultrastruct. Pathol., 4 227-251, 1983.

8. C. M. Venkatachalam and D. W. Urry, "Development of a Linear Helical Conformation From Its Cyclic Correlate. β-Spiral Model of the Elastin Poly(pentapeptide), (VPGVG)$_n$," Macromolecules, 14, 1225-1229, 1981.

9. D. W. Urry, C. M. Venkatachalam, S. A. Wood and K. U. Prasad, "Molecular Structures and Librational Processes in Sequential Polypeptides: From Ion Channel Mechanisms to Bioelastomers," In Structure and Motion: Membranes, Nucleic Acids and Proteins, (E. Clementi, G. Corongiu, M. H. Sarma and R. H. Sarma Eds.), Adenine Press, Guilderland, New York, 185-203, 1985.

10. C. A. J. Hoeve, and P. J. Flory, "The Elastic Properties of Elastin," J. Am. Chem. Soc., 80, 6523-6526, 1958.

11. C. A. J. Hoeve, and P. J. Flory, "The Elastic Properties of Elastin," Biopolymers 13, 677-686, 1974.

12. P. J. Flory, "Principles of Polymer Chemistry," Cornell University Press, Ithaca, 1953.

13. L. Mandelkern, "An Introduction to Macromolecules," 2nd Edition, Springer-Verlag, Inc., New York, 1983.

14. K. L. Dorrington and N. G. McCrum, "Elastin as a Rubber," Biolpolymers, 403-436, 1984.

15. D. W. Urry, "Protein Elasticity Based on Conformations of Sequential Polypeptides: The Biological Elastic Fiber," J. Protein Chem., 3, 403-436, 1984.

16. D. W. Urry, "Entropic Elastic Processes in Protein Mechanisms. Part 1. Elastic Structure Due to an Inverse Temperature Transition and Elasticity Due to Internal Chain Dynamics," J. Protein Chem. (in press).

17. D. W. Urry, K. Okamoto, R. D. Harris, C. F. Hendrix and M. M. Long, "Synthetic, Cross-Linked Polypentapeptide of Tropoelastin: An Anisotropic, Fibrillar Elastomer," Biochemistry, 15, 4083-4089, 1976.

18. D. Volpin, D. W. Urry, I. Pasquali-Ronchetti and L. Gotte, "Studies by Electron Microscopy on the Structure of Coacervates of Synthetic Polypeptides of Tropoelastin," Micron, 7, 193-198, 1976.

19. D. W. Urry, R. G. Shaw and K. U. Prasad, "Polypentapeptide of Elastin: Temperature Dependence of Ellipticity and Correlation with Elastomeric Force." Biochem. Biophys. Res. Commun., 130, 50-57, 1985.

20. D. W. Urry, M. A. Khaled, R. S. Rapaka and K. Okamoto, "Nuclear Overhauser Enhancement Evidence for Inverse Temperature Dependence of Hydrophobic Side Chain Proximity in the Polytetrapeptide of Tropoelastin," Biochem. Biophys. Res. Commun., 79(3), 700-706, 1977.

21. D. W. Urry, T. L. Trapane, M. Iqbal, C. M. Venkatachalam, and K. U. Prasad, "Carbon-13 NMR Relaxation Studies Demonstrate an Inverse Temperature Transition in the Elastin Polypentapeptide," Biochemistry, 24, 5182-5189, 1985.

22. D. W. Urry, T. L. Trapane, R. B. McMichens, M. Iqbal, R. D. Harris and K. U. Prasad, "Nitrogen-15 NMR Relaxation Study of Inverse Temperature Transitions in Elastin Polypentapeptide and its Cross-linked Elastomer," Biopolymers, 25, S209-S228, 1986.

23. R. Henze and D. W. Urry, "Dielectric Relaxation Studies Demonstrate a Peptide Librational Mode in the Polypentapeptide of Elastin," J. Am. Chem. Soc., 107, 2991-2993, 1985.

24. D. W. Urry, Rolf Henze, Roland D. Harris, Kari U. Prasad, "Polypentapeptide of Elastin: Temperature Dependence Correlation of Elastomeric Force and Dielectric Permittivity." Biochem. Biophys. Res. Commun., 125(3), 1082-1088, 1984.

25. D. W. Urry, "Physiocochemical Properties of Elastin and Constituent Sequences," in Elastin and Elastases, (Ladislas Robert and William Hornebeck, eds.), CRC Press, Boca Raton (in press).

26. D. W. Urry, C. M. Venkatachalam, M. M. Long and K. U. Prasad, "Dynamic β-spirals and a Librational Entropy Mechanism of Elasticity," In Conformation in Biology (R. Srinivasan and R. H. Sarma, eds.) G. N. Ramachandran Festschrift Volume, Adenine Press, USA, 11-27, 1982.

27. D. W. Urry and C. M. Venkatachalam, "A Librational Entropy Mechanism for Elastomers with Repeating Peptide Sequences in Helical Array," Int. J. Quantum Chem.: Quantum Biol. Symp. No. 10, 81-93, 1983.

28. D. W. Urry, M. M. Long, R. D. Harris, and K. U. Prasad, "Temperature Correlated Force and Structure Development in Elastomeric Polypeptides: The Ile^{1} Analog of the Polypentapeptide of Elastin," Biopolymers, 25, 1939-1953, 1986.

29. D. W. Urry, R. D. Harris, M. M. Long and K. U. Prasad, "Polytetrapeptide of Elastin: Temperature Correlated Elastomeric Force and Structure Development," Int. J. Pept. and Protein Res., 28(6), 649-660, 1986.

30. Y. Nozaki, and C. Tanford, "The Solubility of Amino Acids and Two Glycine Peptides in Aqueous Ethanol and Dioxane Solutions," J. Biol. Chem., 246, 2211-2217, 1971.

31. H. B. Bull and K. Breese, "Surface Tension of Amino Acid Solutions: A Hydrophobicity Scale of the Amino Acid Residues," Arch. Biochem. Biophys. 161, 655-670, 1974.

32. D. W. Urry, H. Sugano, K. U. Prasad, M. M. Long and R. S. Bhatnagar, "Prolyl Hydroxylation of the Polypentapeptide Model of Elastin Impairs Fiber Formation," Biochem. Biophys. Res. Commun., 90(1), 194-198, 1979.

33. W. F. Harrington, "On the Origin of the Contractile Force in Skeletal Muscle," Proc. Natl. Acad. Sci., 76, 5066-5070, 1979.

34. J. Skolnick, "Possible Role of Helix-Coil Transitions in the Microscopic Mechanism of Muscle Contraction," Biophys. J., 51, 227-243, 1987.

35. M. A. Khaled, K. U. Prasad, C. M. Venkatachalam and D. W. Urry, "Nuclear Magnetic Resonance and Conformational Energy Characterization of Repeat Peptides of Elastin: The cyclohexadecapeptide, cyclo (L Val_1-L Pro_2-Gly_3-Gly_4)$_4$," J. Am. Chem. Soc., 107, 7139-7145, 1985.

36. D. W. Urry and M. M. Long, "Conformations of the Repeat Peptides of Elastin in Solution: An Application of Proton and Carbon-13 Magnetic Resonance to the Determination of Polypeptide Secondary Structure," CRC Crit. Rev. Biochem., 4, 1-45, 1976.

37. A. D. McLachlan, "Structural Implications of the Myosin Amino Acid Sequence," Ann. Rev. Biophys. Bioeng., 13, 167-189, 1984.

38. D. W. Urry, "Entropic Elastic Processes in Protein Mechanisms. Part 2. Simple (Passive) and Coupled (Active) Developments of Elastic Forces," J. Protein Chem, (in press).

39. L. M. Barone, B. Faris, S. D. Chipman, P. Toselli, B. W. Oakes and C. Franzblau, "Alteration of the Extracellular Matrix of Smooth Muscle Cells by Ascorbate Treatment," Biochim. Biophys. Acta., 840, 245-254, 1985.

40. D. W. Urry, R. S. Bhatnagar, H. Sugano, K. U. Prasad and R. S. Rapaka, "A Molecular Basis for Defective Elastic Tissue in Environmentally Induced Lung Disease," In Molecular Basis of Environmental Toxicity (R. S. Bhatnagar, Ed.) Ann Arbor Science Publishers, Inc., Ann Arbor, Michigan, p. 515-530, 1980.

41. J. G. Clark, C. Kuhn and R. P. Mecham, "Lung Connective Tissue," In. Rev. Connect. Tissue Res, 10, 249-331. 1983.

42. K. Wang, "Sarcomere-Associated Cytoskeletal Lattices in Striated Muscle," In Cell and Muscle Motility, (J. W. Shay, Ed.) Plenum Publishing Corporation, 6, 315-369, 1985.

43. K. Maruyama, I. Mabuchi, S. Matsubara and K. Ohashi, "An Elastin Protein from the Cortical Layer of the Sea Urchin Egg," Biochem. Biophys. Acta., 446, 321-324, 1976.

44. K. Maruyama, S. Matsubara, Reiji Natori, Y. Nonomura, S. Kimura, K. Ohashi, F. Murakami, S. Handa and G. Eguchi, "Connectin, an Elastic Protein of Muscle," J. Biochem, 82, 317-337, 1977.

45. A. Magid, H. P. Ting-Beall, Melanie Carvell, T. Kontis and C. Lucaveche, "Connecting Filaments, Core Filaments, and Side-Struts: A Proposal to Add Three New Load-Bearing Structures to the Sliding Filament Model," In Contractile Mechanisms in Muscle, (G. H. Pollack and H. Sugi, Eds.), Plenum Publishers, New York, New York, 307-328, 1984.

46. R. Lumry and H. Eyring, "Conformation Changes of Proteins," J. Phys. Chem. 58, 110-120, 1954.

47. R. Lumry and R. G. Gregory, in The Fluctuating Enzyme (R. G. Welch, Ed.), J. Wiley and Sons, New York, 1-190, 1986.

48. B. Gavish, "Molecular Dynamics and the Transient Strain Model of Enzyme Catalysis," In: The Fluctuating Enzyme, J. Wiley & Sons, New York, 263-339, 1986.

49. D. E. Koshland, "The Role of Flexibility in Enzyme Action," Cold Spring Harbor Symp. Quant. Biol., 28, 473-482, 1963.

50. M. N. Liebman, C. A. Venanzi and H. Weinstein, "Structural Analysis of Carboxypeptidase A and its Complexes with Inhibitors as a Basis for Modeling Enzyme Recognition and Specificity," Biopolymers, 24, 1721-1758, 1985.

51. K. A. Rubinson, "Closed Channel-Open Channel Equilibrium of the Sodium Channel of Nerve: Simple Models of Macromolecular Equilibria," Biophysical Chemistry, 25, 57-72, 1986.

52. Review of Transduction in Biological Systems, Science, 234, 286-287, 1986.

53. M. G. Hibberd and D. R. Trentham, "Relationships Between Chemical and Mechanical Events During Muscular Contraction," Ann. Rev. Biophys. Chem., 15, 119-161, 1986.

54. E. W. Taylor, "Cell Motility," J. Cell Sci. Suppl., 4, 89-102, 1986.

55. F. Solomon, "What Myosin Might Do," Science, 236, 1043-1044, 1987.

56. D. A. Knecht and W. F. Loomis, "Antisense RNA Inactivation of Myosin Heavy Chain Gene Expression in Dictyostelium discoideum," Science, 236, 1081, 1987.

57. A. De Lozanne and J. A. Spudich, "Disruption of the Dicryosrelium Myosin Heavy Chain Gene by Homologous Recombination," Science, 236, 1086, 1987.

COLLAGEN AND HIERARCHICAL STRUCTURE

A. Hiltner, J. J. Cassidy and E. Baer

Department of Macromolecular Science
Case Western Reserve University
Cleveland, Ohio 44106

Abstract

In bridging the gap between detail at a molecular level and macroscopic properties it is highly instructive to consider a hierarchical organization of structure, and to examine how interactions at and between these various levels of structure exert important, often specific, influence. We discuss examples of remarkably effective structural hierarchies in bio-composite systems, particularly in soft connective tissue including tendon, intestine and intervertebral disc. The lessons to be learned from these highly specific natural polymeric systems may now begin to provide guidelines for designing synthetic macromolecular materials with structural hierarchies uniquely suited for specific applications or to serve directly in device functions.

Introduction

Soft connective tissues are designed to serve unique functions in the mammalian kingdom. Each such tissue possesses a complex architecture made from a few components organized into a macromolecular multicomposite structure. In general, these complex morphologies consist of collagen fibrils embedded in a gel-like matrix.

In this review paper, the biological role of soft connective tissues is emphasized by using three selected examples. Tendon functions mainly in uniaxial tension and serves as the primary connecting linkage between muscle and bone. Intestine is an example of a structure that is required to function in more complex deformation modes comprising multiaxial tension. This system which functions as tube-like conduit is anisotropic in the hoop and longitudinal directions. A soft tissue that functions primarily in compression is the intervertebral disc. The disc serves in compression and shear as a pad between rigid bone structures.

All of these soft connective tissues contain high modulus fibrils composed of types I, II, or III collagen. The collagen fibril, which is a basic building block in all connective tissues, is itself an oriented composite structure (Figure 1) (1). Collagen is a fibrous protein with glycine, proline and hydroxyproline as the basic chemical constituents with a number of other amino acids present in variable proportions. The chains, which are uniformly 290 nm long, form a triple helical structure called tropocollagen. It is generally believed that five tropocollagen molecules are staggered longitudinally about one quarter of the molecular length to form a fibrous entity termed the microfibril which is 3.6 nm in diameter. This stagger, combined with a gap between the ends of

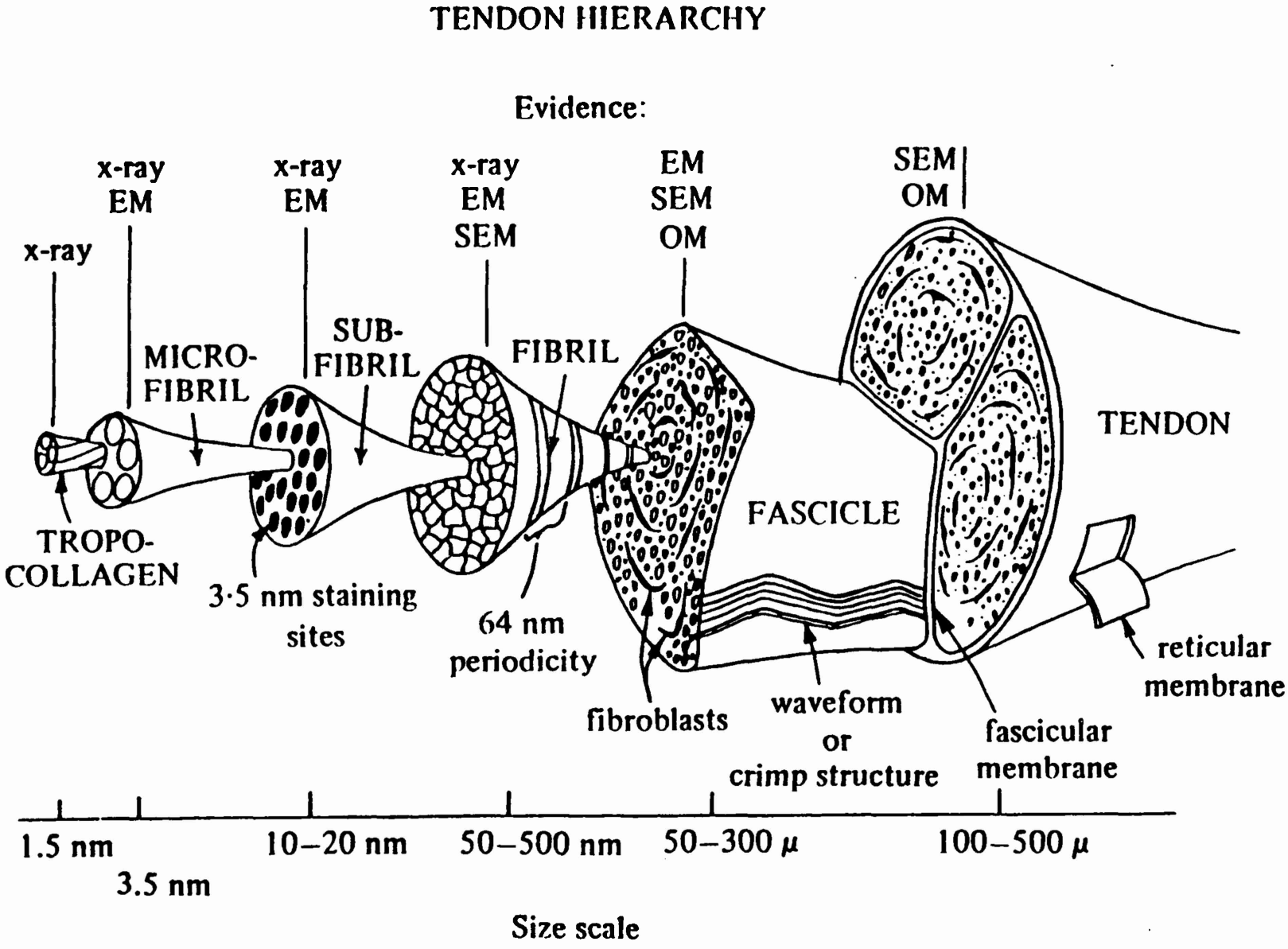

Figure 1. The hierarchical composite structure of the collagen fibril. (Baer, et al., see Ref. 1).

consecutive tropocollagen molecules, is responsible for the characteristic 64 nm periodicity which can be seen by both electron microscopy and x-ray diffraction methods. It follows that such microfibrils have both polar and nonpolar segments which are readily accessible to specific inter- and intra-fibrillar interactions. There is speculation that the microfibrils are packed in a tetragonal lattice into subfibrils about 30 nm in diameter. These subfibrils are then assembled into the collagen fibril which varies in diameter between 50-500 nm from tissue to tissue and in the maturing animal.

Fibrils are subsequently surrounded by the extrafibrillar matrix and are oriented in a hierarchical architecture to form specific soft tissues. The mechanical properties that are required for the specific function are derived from this hierarchical design. The primary macromolecular component of the matrix is a highly branched aggregate of subunits. The proteoglycan subunits consist of a core protein with numerous pendant mucopolysaccharide molecules. The subunits in turn are attached as branches to high molecular weight hyaluronic acid. The relative amounts of the mucopolysaccharides, specifically chondroitin sulfates 4 and 6 and keratan sulfate, vary from one tissue to another, from one part of the tissue to another, and with the age of the tissue. When swollen with water, this ultra-high molecular weight proteoglycan aggregate forms an extremely efficient network structure which connects and maintains the hierarchical architecture of collagen fibrils. The properties of this matrix material are strongly dependent on and regulated by the large quantities of bound and free water.

All of the soft tissues that are described in this paper must function reversibly under numerous repeated loadings during the entire lifetime of the system. In addition, these structures exhibit rate dependent viscoelastic behavior which accommodates the need for energy absorption, the need to resist the accumulation of damage and subsequently ultimate fracture. Since each tissue serves in prescribed stress fields anisotropic composite structures insure the ultimate in structural efficiency. Subsequently, the tissue properties in the direction of maximum stress are directionally reinforced to serve in the required mechanical environment.

Tendon

Tendon is a uniaxial structure with parallel assembly of type I collagen fibrils to form larger fibers. These fibers have a wavy configuration on the level of the light microscopy (Figure 2) which is important for the mechanical function of the tissue (2-4). The initial response of the tendon to stress is the gradual straightening of the wavy fibers. This corresponds, in the stress-strain relationship, to a region of small but gradually increasing slope. Stresses experienced by the tendon in normal physiological function generally fall within this range.

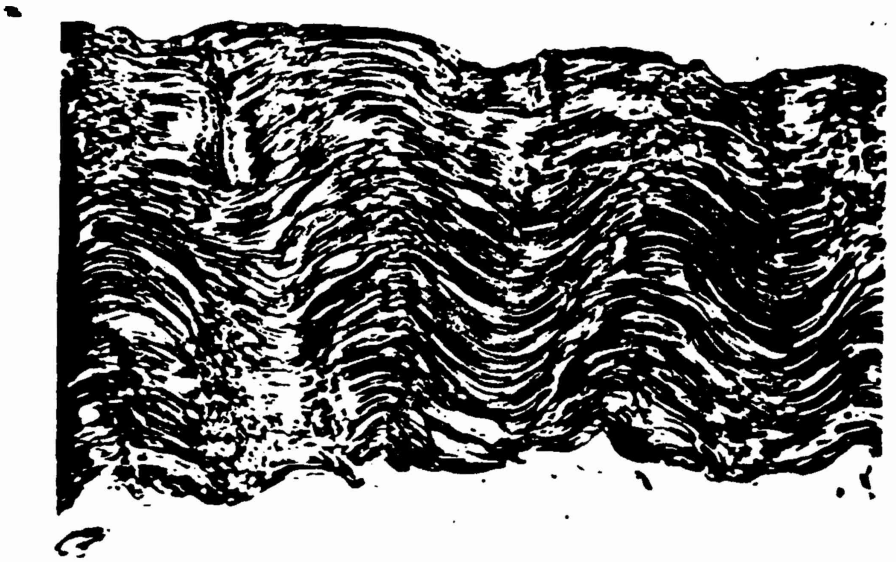

Figure 2. Histological longitudinal section of the rat tail tendon fascicle showing the planar waveform. (Niven, et al., see Ref. 11).

When viewed in the polarizing optical microscope, the wavy fibers produce a characteristic banding pattern of bright and dark extinction bands (5). Detailed analysis of the banding pattern has revealed that the waveform is a planar zig-zag rather than a helix (2). The planar nature of the waveform has subsequently been confirmed by other methods (6-8). Nevertheless, the origin of the waviness has not been explained. Buckling of the collagen fibers in response to compressive forces exerted by a network of elastin fibers may occur in some tissues, such as skin and aorta, but is not the mechanism in tendon which is essentially free of elastin fibers. Alternative mechanisms include structurally distinct "crimp sites", "bimetallic strip" internal tensions and fiber-matrix interactions (9). The planar waveform has been induced in synthetic polymer fibers by differential shrinkage of a surrounding matrix (10). By analogy, the collagen waveform may be caused by a change in the relative volumes of collagen fibrils and the hydrated proteoglycan matrix during development and aging.

Arrays of crimped fibers, which are much like ribbons, are organized into fascicles which are roughly triangular in cross-section and 150 to 300 microns in diameter (11). These fascicles constitute the basic tendon unit. A number of approaches have been used to model the mechanical behavior of the tendon fascicle. Some models consider only the elastic behavior at low strains (12-14). Models for the visco-elastic behavior are generally phenomenological and employ combinations of non-linear springs and dashpots (14-17). While these models very accurately reproduce the mechanical behavior of tendon, they do not consider actual tendon morphology and therefore have little structural significance. The experimental data have also been accurately fit by models which are based on the actual morphology and treat the tendon as a composite of wavy elastic fibers in a viscoelastic matrix (12). This approach additionally reproduces the effects of maturation and aging on the mechanical properties of tendon by considering changes which are observed in the shape of the waveform (2). A gradually decreasing angle of the waveform correlates quantitatively with shortening of the initial low modulus region of the stress-strain relationship (Figure 3). Surprisingly, the modulus of the extended collagen fibers does not change during aging (2, 18).

While the elastic properties of tendon in the physiological range are determined at the size level of the waveform, the damage processes which determine the ultimate strength of tendon involve the fibril structure. Fibril size distribution of rat tail tendon changes considerably during maturation and aging (19). For newborn, the fibrils are uniformly about 30 nm in diameter. During maturation and aging the size increases to a maximum of about 450 nm. The distribution in the mature tendon is very broad so that small fibrils fill the voids between larger ones to produce a packing arrangement with a very high volume fraction of fibrils. Proteoglycan makes up less than 1 percent of the dry weight of the tendon. Hydrated, it forms a continuous matrix between the

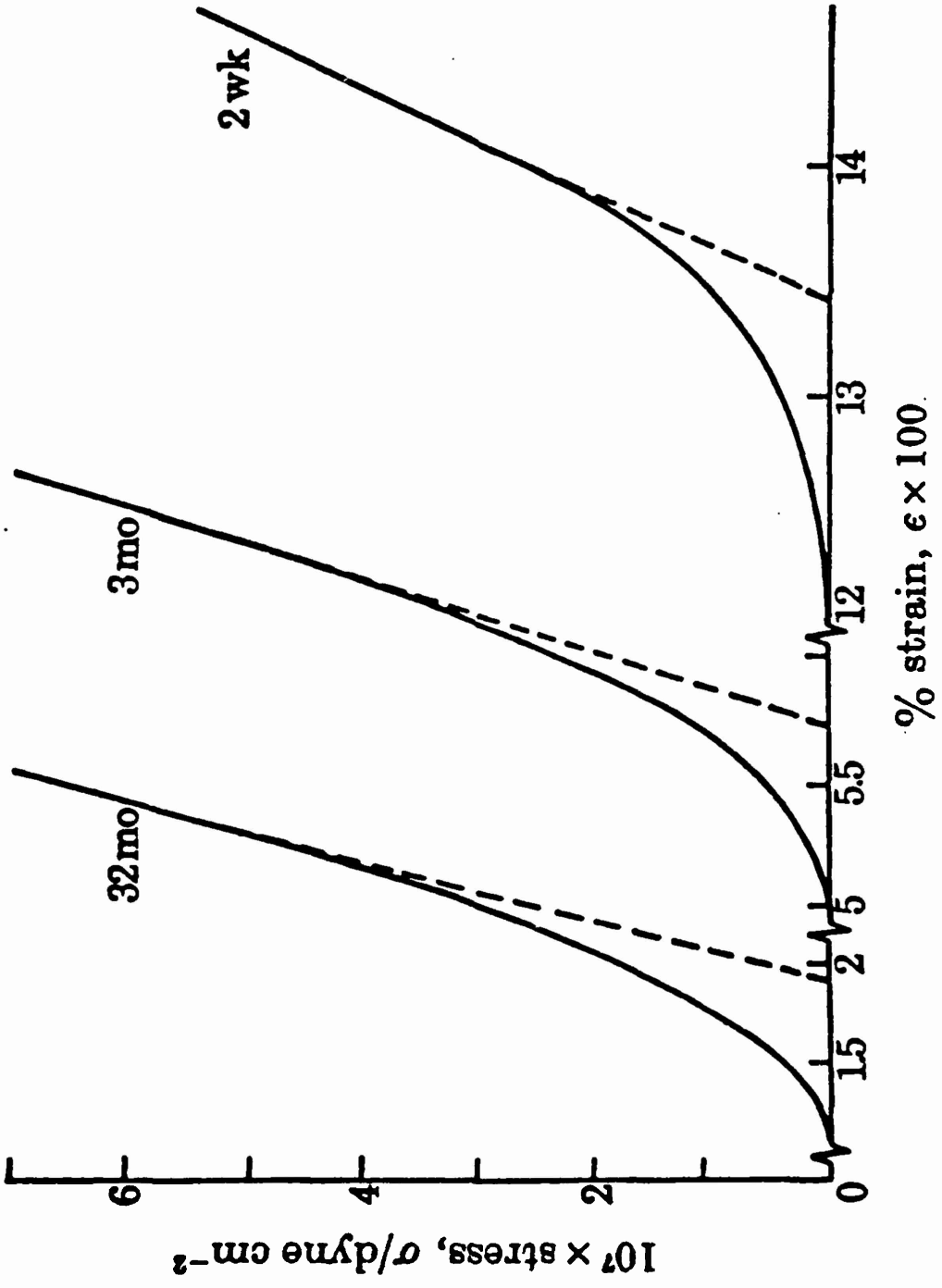

Figure 3. Stress strain curves in the toe region from young, mature and old rat tail tendons. (Diamant, et al., see Ref. 2).

fibrils and provides the adhesion that gives the tendon lateral integrity. Dissociation of the fibril into microfibrils and subfibrils, and slippage of collagen molecules within these entities are the primary damage mechanisms when rat tail tendon is deformed beyond the elastic limit (18). The fibril becomes more resistant to these damage processes with aging (Figure 4). Stronger intrafibrillar interactions produced by crosslinking mechanisms are manifested in the stress-strain relationship as a continuous increase in ultimate strength during aging.

Intestine

The intestinal tissues are rich in collagen. The small intestine (bovine) contains 28 percent collagen based on dry, fat-free weight and the large intestine 38 percent collagen (20). Histological (21) and chemical (22) analyses have shown that elastin is an insignificant component compared to collagen. Human and mouse intestine contain two major types of collagen, types I and III (23). Type I represents the major component and appears to be about 60-70 percent of total collagen whereas type III is 30-40 percent. The collagen of intestine has little, if any, turnover during rapid growth and maturation, and thus appears to be metabolically inert (24).

Collagen in intestine is found in four layers: the submucosa, circular and longtudinal layers of smooth muscle, and the serosa. The major contribution of collagen is made by the submucosa (25). Histological methods have shown that the collagen of the submucosa and serosa is primarily type I and the collagen in the muscularis is primarily reticulin or glycosylated type III (J.M. Anderson, M.B. Yaffe, and A. Hiltner, submitted for publication).

In the transmission electron microscope, type I collagen fibrils of the submucosa exhibit the typical 64 nm periodicity (26) and appear fairly uniform in diameter (27). The fibril diameter for rat intestine increases gradually from 50 nm at 3 weeks of age to 80 nm at 12 months of age (28).

Morphologically type I and type III collagen form separate fibrous networks. Type III collagen fibers, possibly about 0.2 m in diameter (29), form a loosely woven network throughout the muscularis (Figure 5). The orientation of the network changes between the longitudinal and circular muscle layers in such a way that the spaces in the meshwork have the same size and orientation as the smooth muscle cells (Anderson, et al.). Functionally, this network of type III collagen maintains the spacial arrangement of the muscle cells and connects them so that forces generated by individual myocytes are linked and the muscle layer functions as a unit.

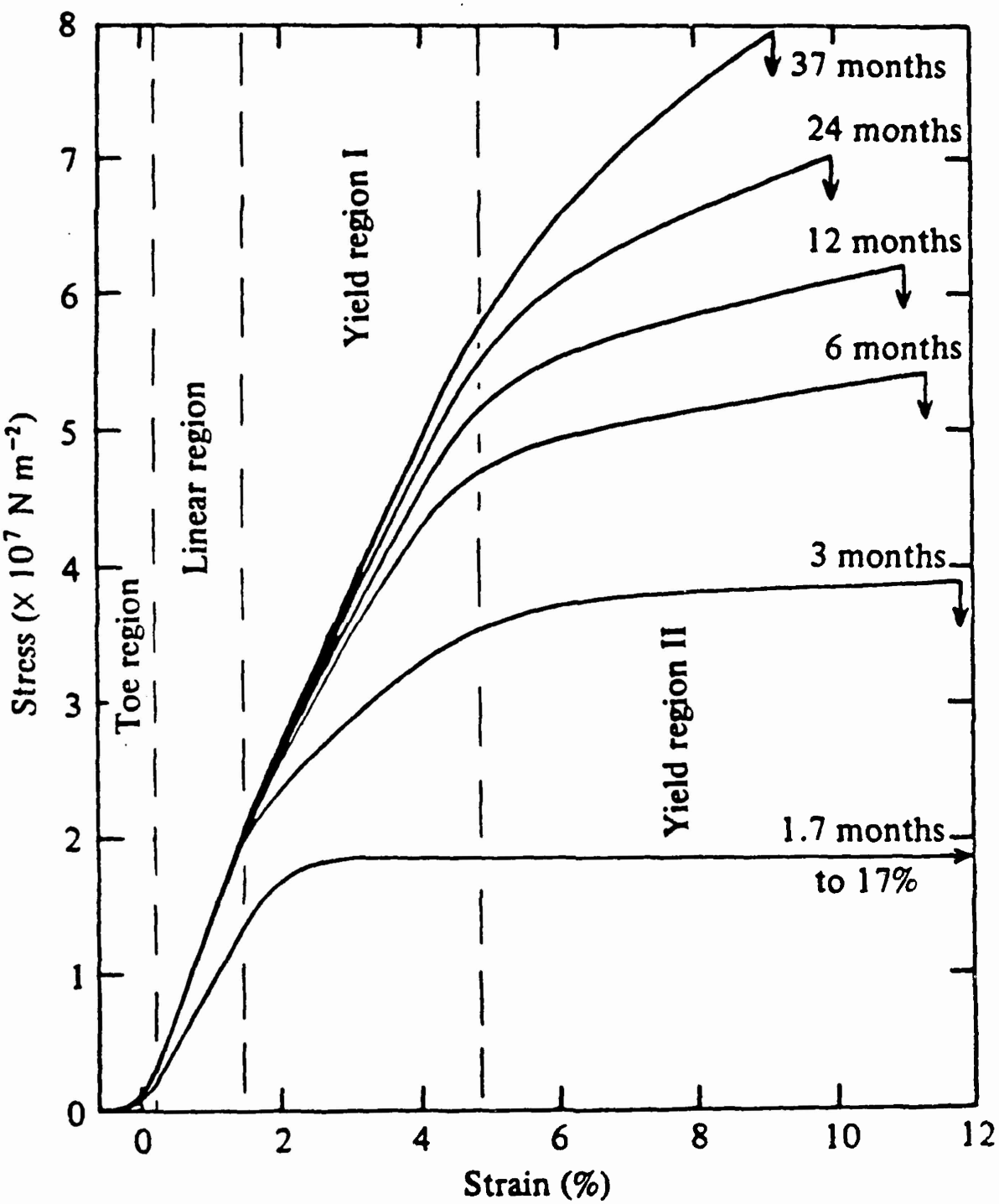

Figure 4. Stress-strain behavior of rat tail tendon in the linear and yield regions. (Kastelic and Baer, See Ref. 18).

Figure 5. Circular section of the rat intestine stained for reticulin. The serosa is barely visible at the top, the other three layers from top to bottom are the longitudinal and circular muscle layers and the submucosa. The mucosal layer is out of the photograph. (Anderson et al., submitted).

Type I collagen is located primarily in the submucosa as a relatively dense layer of fibers 4-6 m in diameter (29,30). The unusually high tensile strength of the intestine, as demonstrated by its commercial use in surgical sutures and tennis racket strings, is produced by the unique organization of these fibrous entities. Polarizing optical microscopy (31) and scanning electron microscopy (29) have demonstrated that the collagen fibers are arranged in layers with the fibers in each layer densely packed in parallel undulating arrays. The fiber direction in the one layer is approximately 60° to the fiber orientation in the adjacent layer which produces an overall biaxial orientation (Figure 6). With the wavy fibers at $+30^{\circ}$ and -30° to the long axis of the intestine, they form helices of opposite sense as they wind around the lumen.

The initial response of the tissue to tensile stress is straightening of the undulating fibers and perhaps some angular change in the biaxial orientation (31). This results in a gradually increasing modulus. When straightened, the relatively inextensible fibers ultimately provide the intestine with sufficient strength to protect against bursting. In addition, the biaxial organization produces highly anisotropic mechanical behavior. Measurements on bovine intestine (30) have shown that the tissue is considerably more elastic in the transverse direction than the longitudinal direction. From the biomechanics point of view this feature uniquely suits the physiological function of the tissue which necessitates changes in diameter rather than length. The diagonal orientation of the fibers has the additional advantage that it reduces the tendency of the intestine to buckle where it bends.

Distinct and separate networks of type I and type III collagen fibers have previously been observed in artery (32) and the peripheral nervous system (33). Comparison of the observations on artery and peripheral nerves with the findings on intestine reveals certain similarities in collagen function. In each of these tissues, thin type III collagen fibers form a network which encases a vital cellular component - muscle cells in the intestinal muscularis and arterial media, nerve fibers in the peripheral nerve endoneurium. This suggests that the function of the type III collagen network is to physically interconnect individual cells and maintain their spacial arrangement.

In each tissue, thicker type I collagen fibers are found in a separate relatively dense layer which surrounds and protects the delicate cellular component and gives mechanical strength to the tissue. In these examples, type I collagen is found predominantly in the submucosa and serosa of intestine, the adventitia of artery and the epineurium (and perhaps the perineurium) of peripheral nerves. Furthermore, the observation that thick type I collagen fibers, but not type III collagen, are present in tissues such as tendon, dura and fibrous cartilage which serve only a mechanical function is consistent with the suggestion that the biological functions of types I and III collagen are general phenomena whereby specific structural and mechanical requirements are achieved through the unique organization of separate networks.

Figure 6. Nomarski DIC micrograph of unstretched rat intestine (3-month-old) showing wavy fibers crimped in register and biaxially oriented at approximately $+30^{0}$ and -30^{0} to the longitudinal (horizontal) direction. (Oberg, et al., see Ref. 31).

Intervertebral Disc

The intervertebral disc is composed of three anatomic structures (Figure 7). These are the annulus fibrous, a lamellar structure of collagen fibrils, the nucleus pulposis, a gelatinous hydrophilic material, and the vertebral endplates, dense cartilagenous structures that connect the disc with the vertebral bodies (34).

Collagens type I and II together comprised the intervertebral disc. At the periphery of the annulus fibrosis greater than 95 percent of the collagen is type I. This percentage decreases along an approximately linear gradient to a level of less than 5 percent in the nucleus pulposis. An opposing gradient exists for type II collagen which comprises greater than 95 percent of the nucleus and less than 5 percent of the peripheral annulus (35-38). The location of these two collagen networks is not known though it has been proposed that the type I fibrils are restricted to the lamellar framework while type II networks exist in gel-like inter- and intra-lamellar regions (38).

The nucleus pulposis is an oval gelatinous structure composed of chondrocyte-like cells dispersed in a matrix of randomly oriented collagen fibrils associated with chondroitin sulphate (39). The chondroitin sulphate is a hydrophilic molecule and enables the nucleus to imbibe considerable amounts of water, up to 88 percent by weight (35).

The thickness of the lamellae varies with radial location in the annulus fibrous (J.J. Cassidy, A. Hiltner and E. Baer, unpublished results). At the periphery of the human disc the lamellae are approximately 130 μm in thickness. Approximately 2.2 mm from the edge of the disc, at about the 20th lamellae, there is a sharp increase in lamellar thickness to approximately 280 μm. This difference in lamellar thickness permits division of the annulus fibrous into peripheral and transitional regions. In the vicinity of the nucleus, the boundaries between lamallae become less well-defined. There is also a pronounced loss of three dimensional organization of the collagen fibers within lamellae.

In the annulus fibrosis, collagen fibrils are oriented parallel to one another within lamallae. In successive lamellae, the orientation of the fibers alternates with respect to the spinal axis at an angle of about 65 degrees (40). This angle is not constant through the thickness of the annulus but decreases from the periphery of the disc inward (Cassidy, et al.). At a depth of 0.5 mm from the edge, this angle is 62 degrees. At a depth of 1.7 mm, the angle has decreased to 50 degrees.

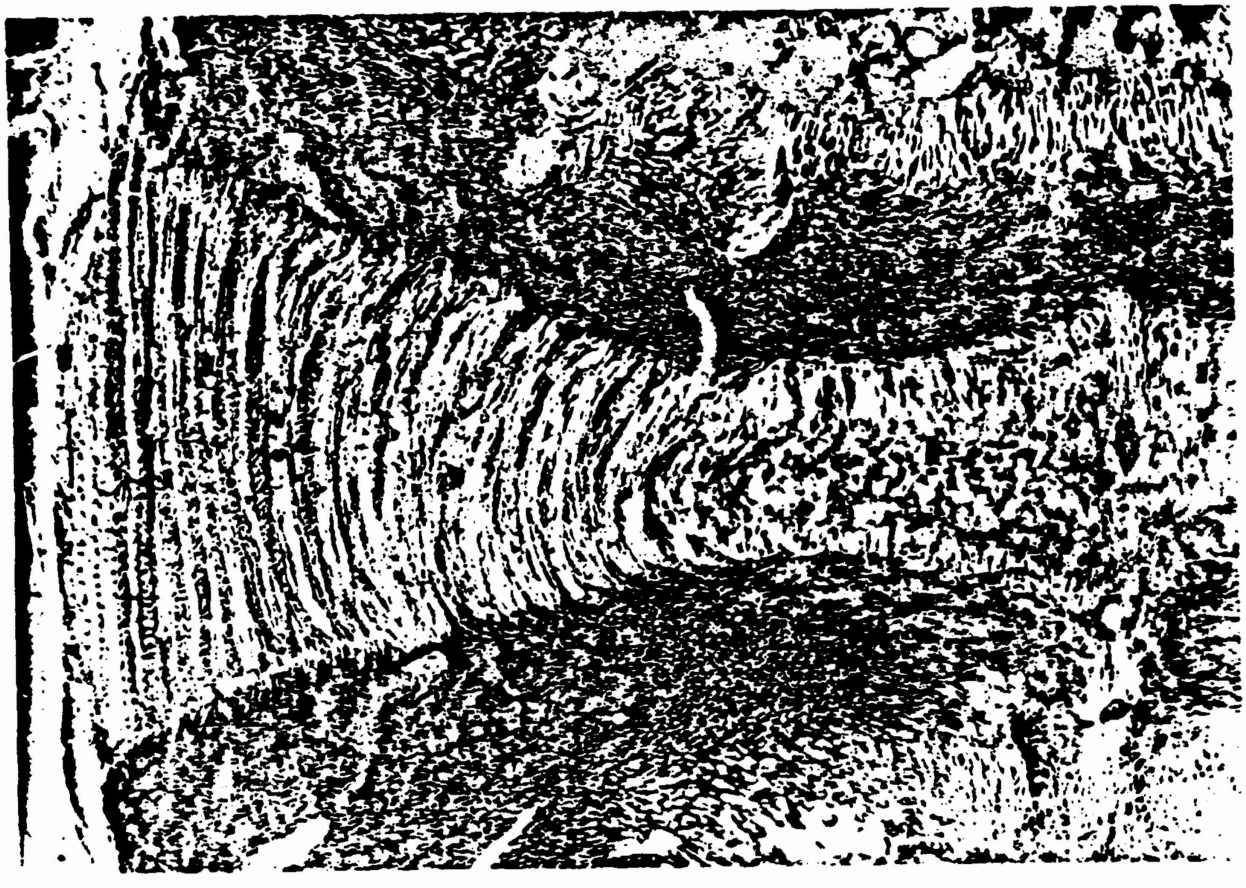

Figure 7. Radial section through the disc showing the annulus fibrosis, nucleus pulposis, and cartilage endplates. Note the change in lamellar thickness between peripheral and transitional regions of the annulus fibrosis. (Cassidy et al., unpublished).

A section through the intervertebral disc cut parallel to the fibers in one set of lamellae shows the concentric lamellae of the annulus fibrosis surrounding the nucleus. Viewed at higher magnification between crossed polarizers, characteristic extinction bands are observed along the fiber direction (Figure 8). This pattern is similar to that observed in tendon, and when analyzed by the technique employed previously (2), it was shown that the characteristic extinction pattern is produced by a planar waveform configuration of the collagen fibers with the plane of the waveform perpendicular to the plane of the lamellae.

The angle and period of the waveform are not constant but vary within the peripheral region of the annulus fibrosis. The angle increases from about 21 degrees at the fourth lamellae to 35 degrees at the fourteenth lamellae. There is a corresponding decrease in the period of the waveform.

A model of the intervertebral disc is proposed based on optical microscope observations of the collagen fiber organization (Figure 9). This model incorporates the structural hierarchy at the micro- and macro-scales. It shows the alternating orientation of collagen fibers in the lamellae that is similar to a layup structure in synthetic composite materials. Undulation of the wavy fibers in and out of the lamellar plane is also shown. From the periphery inward, there is a gradual decrease in the angle the fiber orientation makes with the spinal axis and an increase in the crimp angle.

Mechanical testing of the intact disc in uniaxial compression yields a nonlinear stress-strain curve with an initial low strain region of gradually increasing modulus. By examining specimens fixed under compression, it was shown that increasing strain is accompanied by a gradual increase in the angle of fiber orientation and progressive straightening of the waveform. The response of collagen fibers of the disc to compressive stresses is similar at the micro-scale to the response of collagen fibers in tendon or intestine when deformed in tension. It suggests that the role of the nucleus pulposis is to transmit compressive stresses to the annulus fibrosis as tensile hoop stresses (41). Gradients in the organization at the micro-scale maintain an optimum stress distribution across the disc.

Conclusions

All the tissue examples reviewed in this paper are constructed from a small number of basic macromolecular "building blocks". These macromolecules are organized into hierarchical structures that are anisotropic fiber composites. Their widely varying mechanical functions are derived from the specific composite architecture which makes each tissue unique.

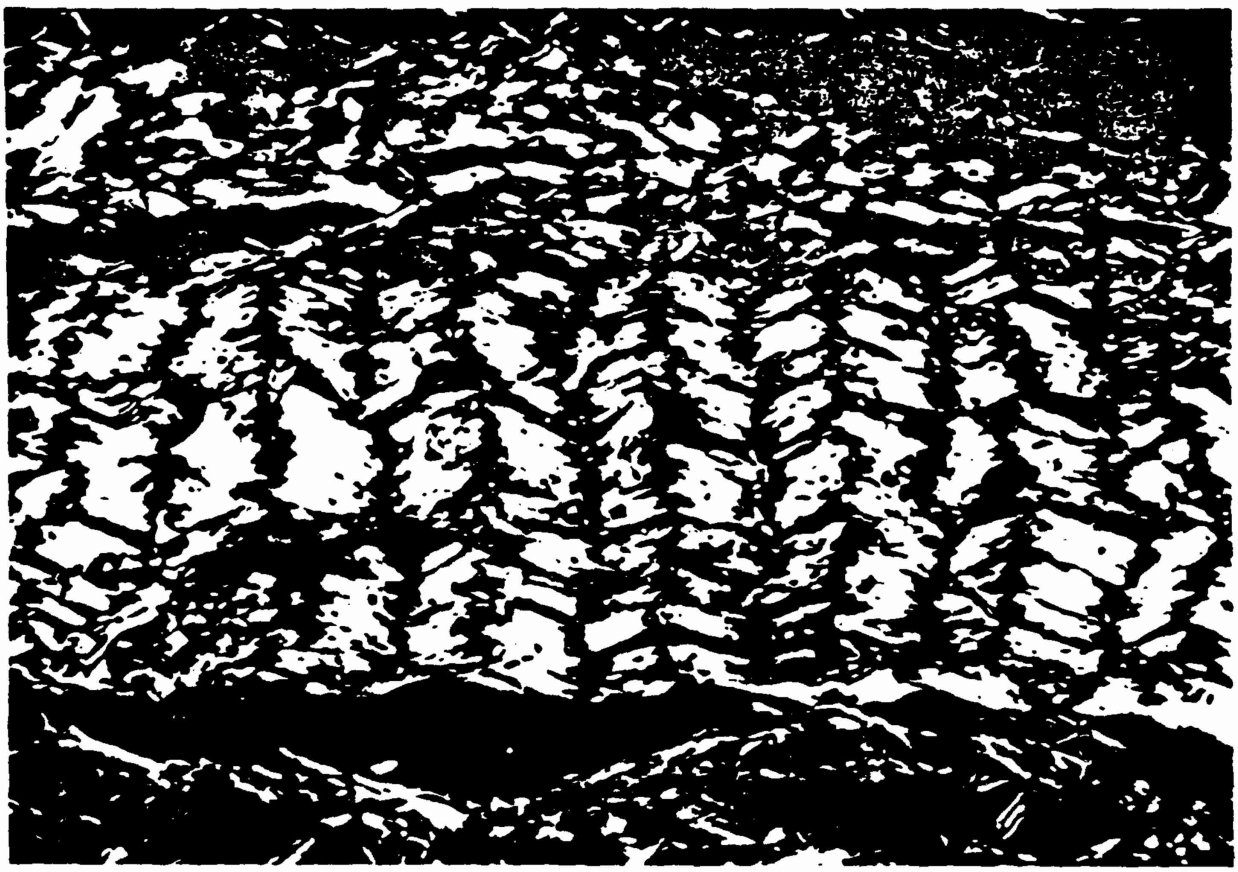

Figure 8. Extinction bands in collagen fibers of a single lamella observed in the optical microscope with crossed polars. (Cassidy et al., unpublished).

Figure 9. Hierarchical model of the intervertebral disc showing lamellar organization, fiber orientation and waveform in the annulus fibrosis. (Cassidy et al., unpublished).

The structural levels at which the properties are resolved occur at a size scale which can be elucidated using the techniques of modern materials science. The relationships between composite structure and mechanical behavior in both reversible and damage regimes of deformation can be understood by using established modeling methodology. Subsequently, from this type of understanding, it seems reasonable to suggest that new concepts and designs in advanced synthetic composites can evolve from the science of these biocomposites.

Acknowledgement

The authors gratefully acknowledge the support of the National Institutes of Health and the Army Research Office in making possible the development of this field of research.

References

1. Baer, E., Gathercole, L.J. Keller, A. 1975. In Structures of Fibrous Proteins, ed. E.D.T. Atkins and A. Keller pp. 189-195. London: Butterworth.

2. Diamant, J., Keller, A., Baer, E., Litt, M., Arridge, R.G.C. 1972. Proc. R. Soc. Lond. B180:293-315.

3. Rigby, B.J., Hirai, N., Spikes, J.D., Eyring, H. 1959. J. Gen. Physiol. 43:265-83.

4. Viidik, A., Ekholm, R. 1968. A. Anat. Entwgesch 127:154.

5. Elliott, D.H. 1965. Biol. Rev. 40:392-421.

6. Gathercole, L.J., Keller, A., Shah, J.S. 1974. J. Microsc. 102:95-106.

7. Dlugosz, J., Gathercole, L.J., Keller, A. 1978. Micron. 9:71-82.

8. Gathercole, L.J., Keller, A. 1978. Biochim. Biophys. Acta. 535:253-71.

9. Viidik, A. 1980. In Biology of Collagen, ed. A. Viidik and J. Vurst pp. 257-80. New York: Academic Press.

10. Dale, W.C., Baer, E. 1974. J. Mater. Sci. 9:369-82.

11. Niven, H., Baer, E., Hiltner, A. 1982. Collagen Rel. Res. 2:131-42.

12. Kastelic, J., Palley, I., Baer, E. 1980. J. Biomech. 13:887-93.

13. Coleman, B.D., Markovitz, H. 1974. J. Polymer, Sci., Polym. Phys. Ed. 12:2195-2207.

14. Viidik, A. 1968. J. Biomech. 1:3-11.

15. Viidik, A. 1973. Int. Rev. Conn. Tiss. Res. 6:127-215.

16. Frisen, N., Magi, M., Sonnerup, L., Viidik, A. 1969. J. Biomech. 2:13-20.

17. Frankel, V.H., Burstein, A.H. 1970. Orthopaedic Biomechanics, Philadelphia; Lea and Fibiger. pp. 188.

18. Kastelic, J., Baer, E. 1980. In The Mechanical Properties of Biological Materials, ed. J.F.V. Vincent and J.D. Currey pp. 397-435 London: Society for Experimental Biology.

19. Torp, S., Baer, E., Friedman, B. 1975. In Structures of Fibrous Proteins, ed. E.D.T. Atkins and A. Keller pp. 223-50. London: Butterworth.

20. Ward, A.G., Courts, A. 1977. In The Science and Technology of Gelation ed. A.G. Ward & A. Courts pp. 396-401. New York: Academic Press.

21. Hass, G.M. 1939. Arch. Path. 27: 334-65.

22. Neuman, R.E., Logan, M.A. 1950. J. Biol. Chem. 186:549-56.

23. Epstein, E.H., Munderloh, N.H. 1975. J. Biol. Chem. 250:9304-12.

24. Klein, L., ChandraRajan, J. 1977. Proc. Natl. Acad. Sci. USA 74:1436-39.

25. Wang, H. 1954. Am Meat. Found. Bull. 17:3.

26. Steven, F.S., Jackson, D.S., Schofield, J.D., Bard, J.B.L. 1969. Gut 10:484-87.

27. Boryski, R. 1977. In Ultrastructure of Protein Fibrils, ed. R. Boryski pp. 396-401. New York: Academic Press.

28. Klein, L., Eichelberger, H., Miriam, M., Hiltner, A. 1983. Conn. Tiss. Res. 12:71-78.

29. Orberg, J.W., Klein, L. Hiltner, A. 1982. Conn. Tiss. Res. 9:187-93.

30. Fackler, K., Klein, L., Hiltner, A. 1981. J. Microsc. 124:305-11.

31. Carrasco, F.H., Montes, G.S., Krisztan, R.M., Shigihara, K.M., Carreiro, J., Junguiera, L.C.U. 1981. Blood Vessels 18:296-302.

33. Junguiera, L.C.U., Montes, G.S., Krisztan, R.M. 1979. Cell Tissue Res. 202:453-60.

34. Koreska, J., Robertson, D., Mills, R.H., Gibson, D.A., Allisser, A.M., 1977. Orthop. Clin. of N.A. 8(1):121-33.

35. Adams, P. Eyre, D.R., Muir, H. 1977. Rheum. Rehab. 16:22-29.

36. Berthet-Colominas, C., Miller, A., Herbage, D., Ronziere, M., Tocchetti, D. 1982 Biochim. Biophys. Acta 706:50-64.

37. Eyre, D.R., Muir, H. 1976. Biochem. J. 157:267-70.

38. Eyre, D.R., Muir, H. 1974. FEBS Letters 42(2):192-96.

39. Akeson, W.H., Woo, S.L., Taylor, T.K.F., Ghosh, P., Bushell, G.R. 1977. Clin. Orthop. 129:133-40.

40. Hickey, D.S., Hukins, D.W.L., 1980 J. Anat. 131(3):81-90.

41. Nachemson, A. 1963. Acda Orthop. Scand. 33:183-207.

NMR AND CONFORMATIONAL ENERGY METHODS IN CARBOHYDRATE CONFORMATION

C. Allen Bush

Department of Chemistry
Illinois Institute of Technology
Chicago, IL 60616 U.S.A

For the purposes of this review, we will define complex carbohydrates as polymers composed of such monosaccharides as mannose, galactose, N-Acetyl glucosamine, N-Acetyl galactosamine, fucose and sialic acid connected in highly varied linkages and anomeric configurations. These macromolecules, which contain glucose only rarely and are not used as energy sources by an organism, are found in glycoproteins, glycolipids and in the capsular polysaccharides of bacteria. The complex carbohydrate structures in these three groups have generally distinct features and each class can be separately defined. On the other hand, they have many similarities and there is considerable biological evidence, such as immunological or lectin receptor activity, which interrelates them. Typical oligosaccharide structures may have from two to 15 sugar residues in a nonrepeating sequence. In a case such as the capsular polysaccharides of bacteria, a structural subunit may be covalently linked into a higher molecular weight polymer with a repeating structure.

Therefore, the problem of structure determination in complex carbohydrates differs substantially from that in either proteins or nucleic acids. Although the structural subunit is generally limited to at most 15 residues and may be composed of usually only five or six different monosaccharides, they may be interconnected by many different linkages (e.g. 1-2, 1-3, 1-4, 1-6 etc.) and anomeric configuration must be determined. Also, since there are multiple substitution points, branching is possible and in fact quite common. It should also be mentioned that the structure of a complex carbohydrate, unlike that of a protein or nucleic acid, is not under the control of a single gene; it is controlled by the interaction of a collection of interacting gene products (glycosyl transferases) whose activities depend not only on the rate of their synthesis but also on other environmental factors.

Concerning the function of complex carbohydrates, a rather large number of functions have been identified. Specific oligosaccharides in heparin have been shown to be active in angiogenesis and other sequences are active in control of blood clotting. Complex carbohydrates have been shown to possess various cell surface receptor functions, which include the activity of ganglioside GM1 as receptor for cholera toxin. The nonreducing terminal galactose residue in serum glycoproteins controls the clearance of glycoproteins from circulation by receptor-mediated endocytosis. Asparagine N-linked glycosylation of newly synthesized glycoproteins in the golgi apparatus is known to control intracellular migration to lysozomes. Antifreeze glycoprotein, a major serum glycoprotein of arctic fish, prevents freezing by noncolligative freezing point lowering. The results from a new technique of blotting onto thin layer chromatograms of glycolipids of the mucosal membranes implies that

they serve as receptors for bacteria. Blood group antigens and a number of closely related tumor and differentiation antigens are known to be complex carbohydrate structures. What is lacking in the catalog of functions for complex carbohydrates given here is some unifying hypothesis. The long list of disparate functions for complex carbohydrates implies that the scientific method has as yet failed to uncover some underlying principle which might contribute substantially to our understanding of such important biological functions as growth, differentiation, immunology, cancer and the organization of multicellular organisms in general.

The problem of structure determination of complex oligosaccharides has been attacked by many techniques over the past 40 years. But the present state of the art continues to be confused by the lack of any single methodology which can be relied upon for any new structural problem. Unlike proteins and nucleic acids, for which well formulated strategies are available for sequencing, a plethora of competing techniques exist for complex oligosaccharides, none of which is truly adequate. Among the classical methods, methylation analysis is extremely difficult and its sensitivity (10 to 100 nanomolar) is unimpressive by modern biochemical standards. Furthermore, methylation analysis determines only linkage position and not the anomeric configuration or sequence of an oligosaccharide. Periodate oxidation of vicinal diols is still widely used in spite of many difficulties. Although enzymatic degradation would appear to be a valuable method, the battery of known exoglycosidases is quite small and the routine use of endoglycosidases, the "restriction enzymes" of complex carbohydrate chemistry, has been possible only in very recent years. Although oligosaccharide mass spectrometry, especially FAB mass spec, seems very attractive on account of its speed and sensitivity, no method now known can give more than partial structural information.

Of all the modern structural determination methods for complex carbohydrates, high field proton Nuclear Magnetic Resonance (NMR) yields the most complete and detailed structural information. It is the only method which can, in principle, give an "ab initio" structure without resort to any other method. In practice, a complete "ab initio" structure determination by NMR is not the easiest way to determine a completely new complex carbohydrate structure and generally other methods are used in conjunction with NMR. The major weakness of NMR spectroscopy as a method for structure determination is its poor sensitivity (100 nanomolar to 10 micromolar). Perhaps the greatest utility of the method will be in providing accurately known structures for callibration then other more sensitive methods, such as enzymatic degradation, mass spectrometry or some as yet undiscovered technique.

The proton NMR spectrum of a typical complex oligosaccharide in D_2O solution shows some isolated resonances which have been called "structural reporter resonances" in the pioneering work of Vliegenthart et al., who have assembled a large body of proton spectra relevant to glycoprotein structure determination (Vliegenthart et al., 1983). As shown in Fig. 1, representing the spectrum of an oligosaccharide from human milk, the

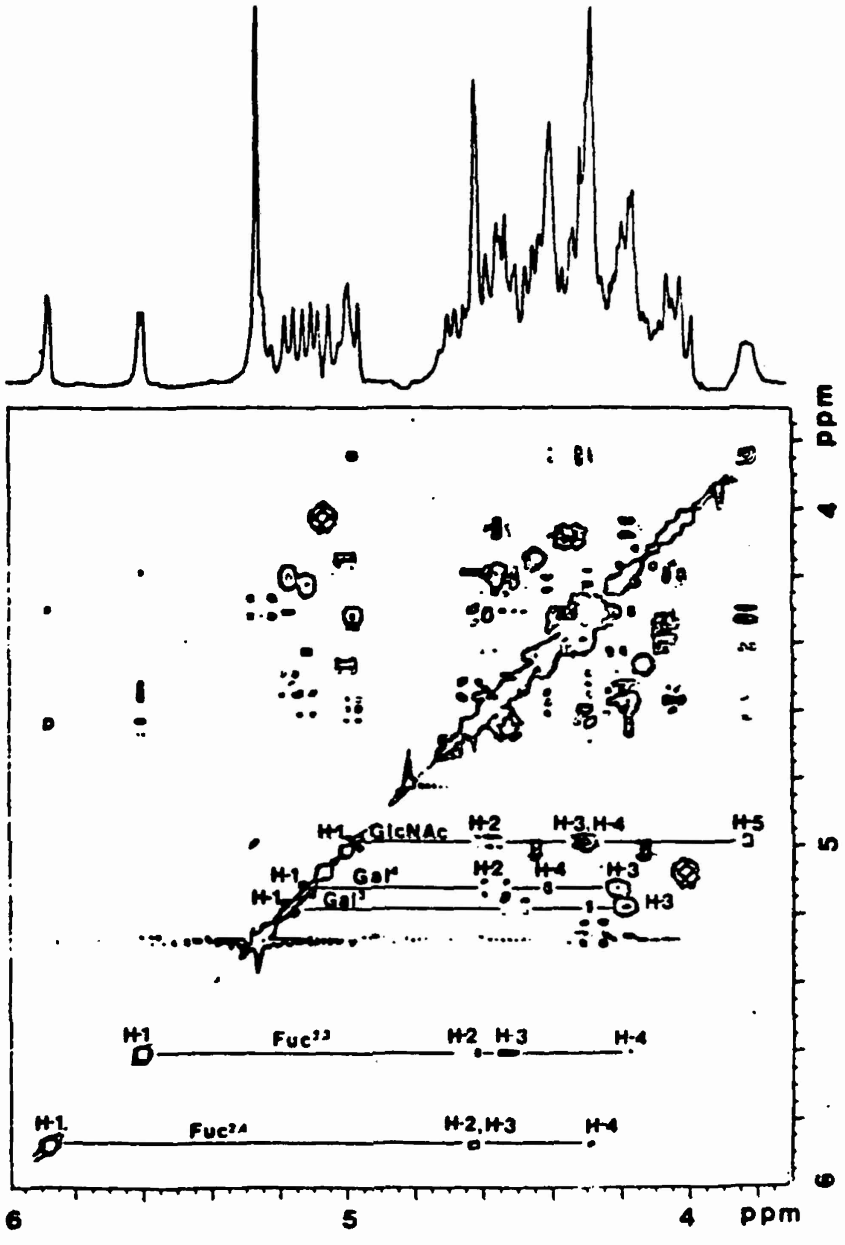

Fig. 1 ^{1}H NMR spectrum in D_2O of the human milk oligosaccharide Lacto-N-difucohexaose 1:

fuc α-1 → 2
↘
gal β-1 → 3glcNAc β-1 → 3gal β-1 → 4glc
fuc α-1 → 4)

chemical shifts of the anomeric protons (4.4 to 5.3 ppm), those of methyl groups (1.2 to 1.4 ppm) and of those protons with equatorial configuration in the pyranoside ring (4.1 to 4.3 ppm) give well isolated resonances. The chemical shifts of these protons have been correlated with known structures to yield a powerful method for use in conjunction with classical structural methods which were outlined above (Vliegenthart et al., 1983).

But proton NMR is capable of giving much more structural information if the methine resonances whose chemical shifts are all similar and contribute to the poorly resolved group of signals in the 3.5 to 4.0 ppm region could be assigned. It has been shown that complete proton assignments in oligosaccharides in a size range up to 10 or 15 residues are in fact generally practical with sufficient observation time on 300-500 MHz NMR instruments. (Dua et al., 1986; Homans et al., 1986). Spin correlation is especially useful in carbohydrates since they are composed of chains of spins which are coupled. Thus, spin correlation by difference decoupling or by 2-d COSY (Fig. 2) can often be used to identify all the protons of a given residue. Since the coupling constants of the axial and equatorial protons of the rigid pyranoside rings are characteristic, their measurement either by 1-d difference spectroscopy or by COSY at high digital resolution indicates the stereochemistry (axial or equatorial) of each proton and thus identifies each sugar residue for correlation with the carbohydrate analysis by chemical methods.

Since there are many resonances crowded into the 3.5 to 4.0 ppm region, one might anticipate that strong coupling could introduce some difficulties in the scheme outlined above even at relatively high magnetic fields. Strong coupling, which arises when two protons which are coupled have similar chemical shifts, leads both to some distortion of the expected multiplet shape and to COSY cross peaks, which lie close to the diagonal. The former effect may interfere with determination of the sugar stereochemistry and the latter interferes with tracing the chain of spins within the sugar residue. If multiplet distortion is not too severe it can be understood by spin simulation, but additional experimental methods are needed to complete tracing the spin connectivity. Two dimensional spin relay experiments and more recently homonuclear Hartmann—Hahn spectroscopy have been shown to be especially valuable in assignments in oligosaccharides (Rao and Bush, 1987). In this technique, cross-peaks can be observed between peaks within a single spin system (e.g. pyranoside ring) among all resonances which share common coupling partners. A complete spin system can thus be identified if there is at least one resonance of the spin system which is well isolated, often the anomeric proton. An example is seen in Fig. 3, which shows several strong and intermediate coupled peaks in the fucosyl and glcNAc rings. Rows containing the anomeric proton resonance show cross-peaks with the H3 and H4 which are far from diagonal even though in the COSY they will be quite difficult to observe. In order to rigorously discriminate acetamide sugars from their neutral counterparts, (e.g. galNAc from galactose) the amide proton resonance can be assigned by its coupling to H2. (Rao et al., 1985; Dua et al., 1986). Although this is not possible in D_2O

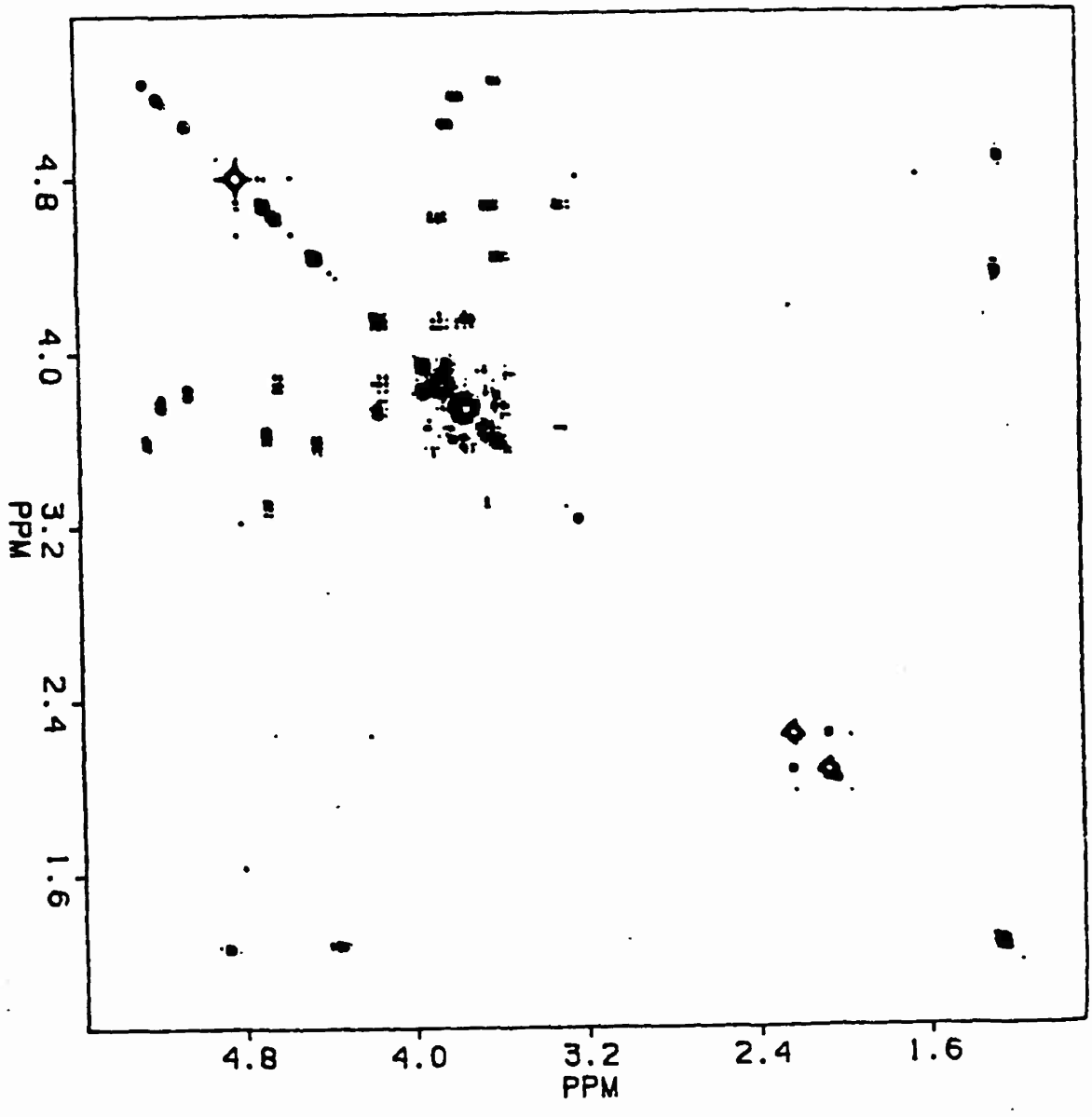

Fig. 2 Proton correlated spectrum (COSY) of the oligosaccharide from Fig. 1 shows that the peaks in the crowded region of 3.5 to 4.0 ppm can be assigned by spin correlation.

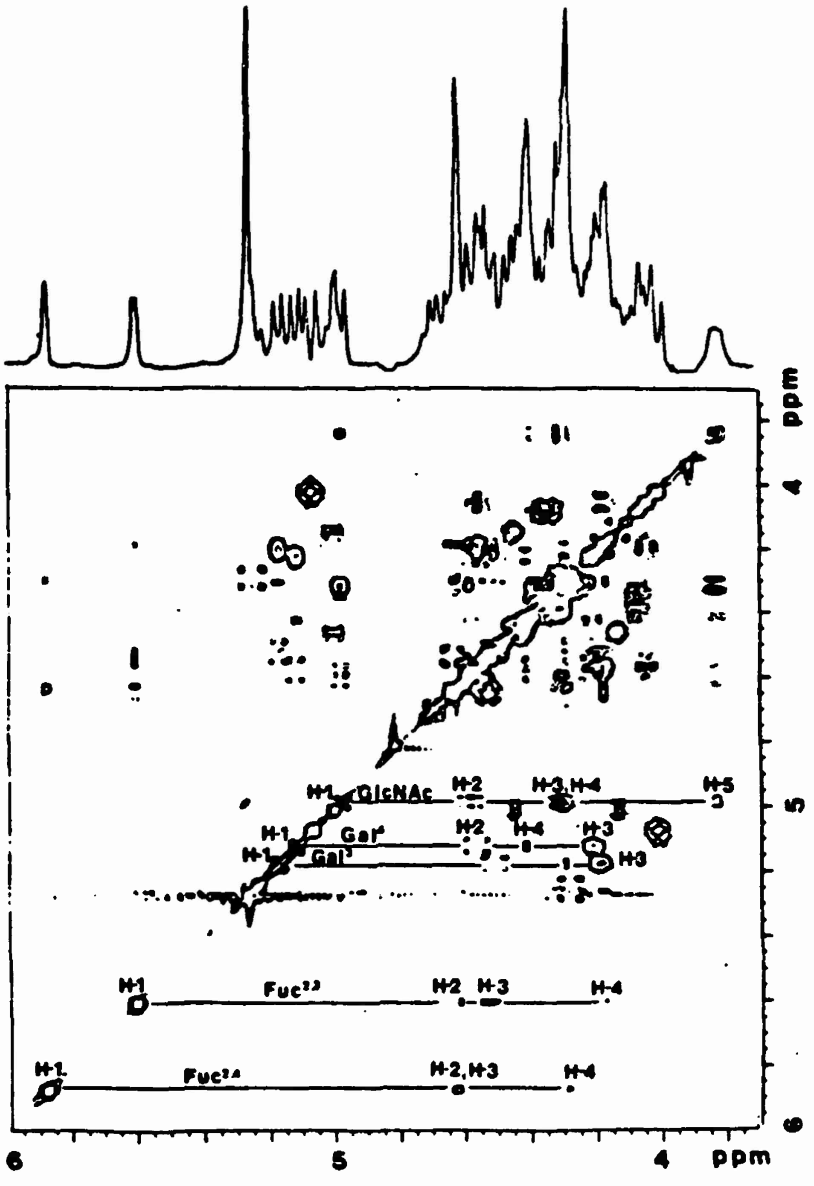

Fig. 3 300 MHz Partial 2D-HOHAHA spectrum of the blood group H-Hexasaccharide alditol:

II.

$$\begin{matrix} & & \text{Fuc}(\alpha 1 \rightarrow 2)\text{Gal}(\beta 1 \rightarrow 3) & \\ & & & \searrow \\ \text{Fuc}(\alpha 1 \rightarrow 2)\text{Gal}(\beta 1 \rightarrow 4)\text{GlcNAc}(\beta 1 \rightarrow 6) & & & \nearrow \text{GalNac-ol} \end{matrix}$$

in pyridine + 2.5% D_2O at 24°C. The total spin propagation time including two 2.5ms spin-lock pulses at the beginning and end of the [MLEV-17] sequence is 55 s. The full data matrix consisted of 512 x 512 real points after zero-filling along t1 (digital resolution 2.9 Hz/point).

Structure of Lacto-N-difucohexaose I[LND 1)

$$\begin{matrix} \text{fuc } \alpha\text{-}1 \rightarrow 2 & & & & \\ & \searrow & & & \\ & & \text{gal } \beta\text{-}1 \rightarrow 3\text{glcNAc} & \beta\text{-}1 \rightarrow 3\text{gal} & \beta\text{-}1 \rightarrow 4\text{glc} \\ \text{fuc } \alpha\text{-}1 \rightarrow 4) & \nearrow & & & \end{matrix}$$

solution due to the exchangeable nature of the amide proton, the amide may be assigned either in H_2O solution or in an H_2O exchanged sample in nonprotic solvents. In aqueous H_2O solution, the assignment can be made either with water suppressed COSY techniques or with 1-d decoupling and selective excitation pulses.

The fully assigned spectrum can be used to identify the anomeric configuration, the stereochemistry and the identity of each of the constituent monosaccharides. The chemical shifts of the anomeric protons and especially of the aglycone protons are often quite characteristic of linkage position and with the extensive data which now exist, chemical shift correlations can often be used to derive the complete oligosaccharide structure. Complete assignments of the type described here have been reported for glycopeptides and oligosaccharides and bacterial polysaccharides in aqueous solution. Considerations of solubility have dictated dimethyl sulfoxide as the solvent of choice for unaggregated glycolipids and a number of studies have been reported for gangliosides and neutral glycolipids. It is clear from comparison of similar oligosaccharides in DMSO and D_2O that the relative proton chemical shifts differ substantially in these two solvent systems. It has been recently shown that even greater differences are observed in pyridine solution, a feature which can be used to advantage in systems for which unfavorable signal overlapping and strong coupling in the D_2O solution occur (Rao and Bush, 1987).

The vicinal proton coupling, which is so useful in the proton assignments of the individual pyranoside rings, cannot be easily used for relating the rings to each other. The four-bond proton coupling across the glycosidic linkage are generally less than 1=Hz. and are difficult to detect in structures larger than a disaccharide. But nuclear Overhauser enhancement (NOE) which depends on proton proximity, can often be measured to indicate the connectivity of the rings. Although NOE is most often observed between the anomeric proton to the aglycone proton, known cases in blood group oligosaccharides and bacterial polysaccharides of major NOE to the adjacent position indicates that some caution must be used in interpretation of NOE for precise linkage position (Dua et al., 1986; Mcintire et al., 1987).

In order to use NOE either for structure determination or for conformational studies, it must be possible to measure it. NOE for small molecules is positive while for larger molecules such as small proteins, the NOE is negative. The rotational correlation times of oligosaccharides having 4 to 6 residues is such that they generally show no NOE when studied at field strengths of 300 to 500 MHz. While substantial negative NOE is generally observed for glycolipids or polysaccharides, NOE measurements on oligosaccharides and small glycopeptides may require special measures. In our work, we have found that the rotational correlation time is a strong function of temperature so that a hexasaccharide showed negative NOE at a temperature 5°C and positive NOE at 70°C, proving that effects can always be measured by the 1-d difference

method, (Rao et al., 1985; Rao and Bush, 1987). In this range of rotational correlation times, 2-dimensional NOE or NOESY spectroscopy generally gives poor results and one must resort to rotating frame NOE measurements (ROESY) for the 2-d method.

Not only have NOE data been valuable for structure determinations but they have been a major source of experimental information for determining the conformation of complex carbohydrates. Since NOE depend on distances between protons, it is in principle possible to determine interproton distances directly from NOE data. In fact this approach suffers from the difficulty that is it generally not possible to measure sufficient NOE data to determine an oligosaccharide conformation. However, when the NOE data are combined with the geometric constraints dictated by the known covalent structure and the conformation of the pyranoside rings, a detailed conformation can often be deduced. The most rigorous solution to the problem of relating NOE data to conformation begins with construction of an oligosaccharide model and the subsequent calculation of the predicted NOE as a function of the glycosidic dihedral angles phi and psi (Brisson and Carver, 1983; Bush et al., 1986). This full matrix method for solving the NOE equations, which can be applied to either the steady state NOE as measured by 1-d difference spectroscopy or the NOESY cross-peak volumes, overcomes difficulties in the interpretation of mutually relaxing spins, which is especially important for carbohydrates that have many closely spaced protons. The discovery of a single geometric model can be found whose calculated NOE agree with the experimental data can be taken as evidence that the complex carbohydrate exists in a single rigid conformation (Brisson and Carver 1983; Bush et al., 1986). Although such single conformations have been found for certain blood group oligosaccharides and for N-linked glycopeptides, it also appears that other structures, especially those involving 1-6 linkages may show some conformational flexibility, which is evidenced by the failure of any single conformation to fully explain the NOE data, (Homans et al., 1986).

The computer model building scheme outlined above for interpretation of the NOE data also lends itself well to calculation of the conformational energy by the method of empirical energy functions. Among the first conformational energy calculations were those of V.S.R. Rao and coworkers who in the mid 1970's adapted to carbohydrates the techniques of the Indian school of calculation, first introduced by Ramachandran for peptides. This rather involves the Kitiagorodsky 6-exp functions in a simple parameterization and ignores electrostatic effects (H-bonding), (Nagarajan and Rao, 1979; Rao and Biswas, 1980). Some poorly justified assumptions about potential are made to simplify the computation. The Rao method was adopted by Lemieux with the minor modification of adding a torsional potential about one of the glycosidic bonds (exo-anomeric effect) and applied to many complex oligosaccharides and polysaccharides, (Lemieux et al., 1980). Although this approach, under the name of HSEA

(Hard-sphere exo-anomeric) method, has been used with success by many other groups, it contains a number of untested assumptions. Bush et al., (1986) have compared the results of the HSEA method with those of several other empirical energy methods for blood group oligosaccharides.

There a number of problems which will determine the direction of the field of conformational calculations in carbohydrates in the next few years. The first serious problem to be addressed is that of how to search a multidimensional conformational energy space. Since this problem must be faced in any complex biopolymer, it has been carefully examined for peptides and nucleic acids. Direct exhaustive searches are prohibitive for more than ten degrees of freedom because computer time increases exponentially with the degrees of freedom. In spite of extensive study, no method of energy minimization has been found which overcomes the problem of trapping in local minima in an acceptable amount of computer time. Recent attempts in our laboratory to use Monte Carlo statistical methods in oligosaccharides have been only moderately successful (Duben and Bush, 1983). Perhaps the new method which shows greatest promise in proteins and nucleic acids is the molecular dynamics or trajectory method.

A second difficult problem is that of how to best calculate the energy. Ab initio quantum mechanical methods are impractical on currently available computers for molecules as large as disaccharides and no semi-empirical quantum mechanical method which gives reliable conformational energy has been found. The most successful calculations employ empirical force fields requiring parameterization which correctly reflects the important interactions. Most workers now agree that it is the nonbonded interactions which predominate in carbohydrates and that electrostatics, hydrogen bonding and solvent effects are less important. But these assumptions must be more carefully tested and better agreement is needed on the correct form of the torsional and nonbonded terms.

Acknowledgement

Research supported by NSF grant DMB 8517421 and by NIH grant GM-31449

References

1. Bothner-By, A.A., Stephens, R.L., Lee, J-M., Warren, C.D. & Jeanloz, R.W. (1984) J. Am. Chem. Soc. 106, 811-813.

2. Brisson, J.R.; Carver, J.P. Biochemistry (1983), 22, 1362-1368.

3. Bush, C.A., Yan, Z.Y. & Rao, B.N.N. (1986) J. Am. Chem. Soc. 108, 6168-6173.

4. Dua, V.K., Rao, B.N.N., Wu, S.S., Dube, V.E. & Bush, C.A. (1986) J. Biol. Chem. 108, 6168-6173.

5. Duben, A.J. & Bush, C.A. (1983) Archives Biochem and Biophys. 225, 1-15.

6. Homans, S.W.; Dwek, R.A.; Boyd, J; Mahmoudian, M.; Richards, W.G. & Rademacher, T.W. Biochemistry (1986), 25, 6342-6350.

7. Lemieux, R.U., Bock, K., Delbaure, T.J., Koto, S. & Rao, V.S. (1980) Can. J. Chem. 53, 631-653.

8. Mcintire, F.C., Bush, C.A. Wu, S.-S., Li, S.-C., Li, Y.-T., McNeil, M, Tjoa, S.S. and Fennessey, P.V. (1987) Carbohydrate Res. (in press).

9. Nagarajan, M. & Rao, V.S.R. Biopolymers (1979), 18, 1407-1420.

10. Rao, B.N.N., Dua, V.K. & Bush, C.A. (1985) Biopolymers 24, 2207-2229.

11. Rao, B.N.N. & Bush, C.A. (1987) Carbohydrates Res. (in press).

12. Rao, V.S.R. & Biswas, M. Biopolymers (1980) 19, 1555-1566.

13. Vliegenthart, J.F.G., Dorland, L. & Van Halbeek, H. (1983) Advan. Carbohydr. Chem. Biochem. 41, 209-374.

LIPID-BASED TUBULE MICROSTRUCTURES*

J. M. Schnur, R. Price, P. Schoen, and P. Yager
Bio/Molecular Engineering Branch, Code 6190
Naval Research Laboratory, Washington, DC 20375-5000

J. M. Calvert, J. Georger, and A. Singh
Geo-Centers, Inc.
Newton Centre, MA 02159

Abstract

Hollow, tubule-shaped microstructures have been fabricated by self-organization of polymerizable diacetylenic phospholipid molecules. These microstructures have potential applications in a number of areas in material science. A wide range of positional isomers of the diacetylenic lipids have been synthesized and all form tubules. A process for deposition of thin metal coatings on the exterior surfaces of the tubules has been developed. Results of spectroscopic and microscopic investigations of the lipids and microstructures are presented. Future issues important to the assessment of the ultimate utility of these materials also are presented.

1. Introduction

Since the early 1960's liposomes have been an area of intensive research.[1] Liposomes are spherical structures composed of a lipid bilayer that encloses an aqueous volume. The need for enhanced stability and greater permeability control in the pursuit of technological applications of these materials has recently led to the development of polymerized liposomes. These materials represent the basic building for biological membranes. Biological membranes, on which both polymerized and unpolymerized membranes are based, are nature's most able self-organizers. In fact, the arrangement of molecules across a membrane are responsible for such important functions as photosynthesis and respiration.

To appear in "Molecular Engineering of Ultra-thin Polymeric Films", a Special Volume of Thin Solid Films and printed by permission of the editor

Portions of this paper have previously appeared in somewhat different form in references; 2. A. Singh and J. M. Schnur, Synth. Comm., 16(7)(1986)847; 3. P. Yager and P. E. Schoen, Mol. Cryst. Liq. Cryst., 106(1984)371; 4. P. Yager, P. E. Schoen, C. Davies, R. Price, and A. Singh, Biophys. J., 48(1985)899; 40. P. E. Schoen and P. Yager, J. Polym. Sci., Polym. Phys. Ed., 23(1985)2203.

In the same way as biological membranes, liposomes can organize many guest molecules in their compartments. The lipid bilayer of liposomes can act as a host to hydrophobic molecules and the liposome-entrapped water pools can allow polar molecules to move about with some freedom.

In our research and development program, we have invested considerable effort in the synthesis and characterization of polymerizable lipids[2]. These materials are important elements in the design of stabilized liposomes and films for biosensor and encapsulation applications, among others. While investigating the phase behavior of the diacetylenic phospholipid 1,2-bis(10,12-tricosadiynoyl)-sn-glycero-3-phophocholine, $DC_{23}PC$, we observed the formation of hollow, cylindrical microstructures[3,4]. These "tubules" are morphologically analogous to soda straws with diameters of approximately 0.5 microns and lengths from 1 to over 200 microns. (Aging under suitable conditions has produced tubules in excess of 1.2 millimeters.)[5] The technological implications of the tubule microstructures, both bare and metal-coated, are large. Application scenarios that have been identified include composites, electro-optics, novel liquid crystalline media, microelectronic elements, reagent delivery vehicles, and microsurgery materials.

To our knowledge, tubules are among the largest self-organized non-living structures yet observed. As such, they may provide insight into the molecular basis of self-organization and bear upon some of the current attempts to model the evolution of life using *self-organizational* materials.

We are currently emphasizing the research areas which are key to the highest number of significant applications. A recent significant result is the successful coating of tubules with nickel and/or copper for the purpose of making them highly conducting[6]. This, coupled with other results, suggests that there is reasonable optimism that this program will lead to several useful technologically important applications.

Currently tubules can be prepared from over 17 different diacetylenic lipids[2]. The tubules are relatively stable before polymerization, but become quite rugged after exposure to UV of Gamma ray radiation and their consequent polymerization. They have, for example, been expelled from a nebulizer without any significant breaking. As a result of an extensive effort in metallization, our group has developed techniques that can uniformly coat the tubule walls with Nickel and/or copper. Tubules so coated are effectively metal cylinders and appear to be quite rugged. A number of interesting properties of the tubules include their very high aspect ratios (up to over 4000), the high reactivity of the surfaces, the existence of two types of surfaces, their uniaxial symmetry, their ability to contain material both in the cylinder or in the wall of the cylinder, and their behavior as anisotropic fluids and phases. Another interesting property is that the uncoated tubules can be oriented in magnetic fields (over 2 KG)[7].

Questions of fundamental interest that are now being pursued by the program are:

What is the molecular basis for the formation of these structures?

What other structures can be fabricated?

What kinds of materials will form these structures?

What is the ultimate utility of these or related structures?

This paper details the synthesis and spectroscopic characterization of tubule-forming lipid molecules. Formation of tubules from aqueous dispersions of lipid, metallization of the tubules, and characterization by spectroscopy and microscopy of the resulting microstructures is described.

2. Lipid Synthesis

Mono- and multilayers from fatty acids and their salts have been studied for some time[8]. Recently there has been a great deal of interest in organically derived films and their properties for a number of potential applications as photoresists, transducers, optical devices, and as matrices for protein based devices. Polymerized forms of these layers have gained considerable attention due to the prospect of increased thermal and mechanical stability. Our beginning studies of polymerized mono- and multilayer films have focused on diacetylene molecules because of their interesting electronic and viscoelastic properties upon polymerization[9]. The initial experiments were designed to study the effect of position of the diacetylenic moiety in the alkyl chain on the polymerization efficiency and its overall effect on the electronic and structural properties of the polymer. In this section we described a simple and convenient method for the synthesis of the diacetylenic acids of the general formula:

$$CH_3(CH_2)_nC{\equiv}C{-}C{\equiv}C(CH_2)_mCOOH$$

where m and n are (5,11); (5,13); (5,16); (6,13); (6,15); (7,9); (7,14); (10,7); (10,9); (10,11); (10,13); and (11,13), respectively[2].

The synthesis of the isomeric diacetylenic acids is achieved in two different steps: first, the synthesis of alkynoic acids; second, coupling of the alkynoic acids with an appropriate 1-haloalkyne, preferable the iodoalkyne. For the synthesis of ω-alkynoic acids we have extended the literature method[10] with some improvements, from alkanes to alkanoic acids which employ lithium acetylide ethylenediamine complex in dry dimethylsulfoxide. In other reports, hexamethylphosphoramide has bee

used as the solvent of choice[11]. We have used both protected and unprotected acids in the reaction and obtained similar yields of acetylenic acids. The 8-bromoctanoic acid was prepared in 80% yield by hydrolyzing 7-bromoheptanenitrile with 70% aqueous sulfuric acid. Table I shows that this method produces acetylenic acids in reasonable yields.

TABLE I

Alkynoic Acid	Yield(%)	MP/BP(^{o}C)
$HOOC(CH_2)_5C{\equiv}CH$	60	84-86/0.6mm
$HOOC(CH_2)_6C{\equiv}CH$	41	23-24 [12,13,14]
$HOOC(CH_2)_7C{\equiv}CH$	71	viscous oil
$HOOC(CH_2)_{10}C{\equiv}CH$	88	39-40
$HOOC(CH_2)_{11}C{\equiv}CH$	71	51-52

This method was also successfully used for making alkynols; 12-tridecyn-1-ol was prepared in 45% yield.

The Cadiot-Chodkiewicz heterocoupling reaction is required to complete the synthesis of the diacetylenic acids. In this reaction the acetylenic acid is coupled to an iodoalkyne. The following iodoalkynes have been used for the coupling reaction:

$$CH_3(CH_2)_nC{\equiv}CI, \text{ where } n = 7, 9, 11, 13, 14, 15, 16$$

The diacetylenic acids produced by the coupling reaction are presented in Table II.

TABLE II

$HOOC(CH_2)_mC{\equiv}C{-}C{\equiv}C(CH_2)_nCH_3$

DIYNOIC ACID m	n	YIELD (%)	MP °C	FOUND% C	H	CALCULATED % C	H
5	11	39	68-69	78.96	11.30	79.46	10.90
5	13	20	70-71	79.30	11.55	9.95	11.70
5	16	37	60-61	82.85	11.79	82.60	11.80
6	13	42	64-66	80.59	11.20	80.15	11.30
6	15	49	75	81.64	11.73	82.60	11.80
7	9	56	49-50	79.42	11.03	79.46	10.91
7	14	51	53-55	80.86	12.28	82.60	11.80
10	7	36	34	79.32	11.66	79.71	11.05
10	9	45	52-54	79.67	11.38	80.15	11.30
10	11	15	38-40	81.89	11.81	82.60	11.80
10	13	36	68-69	81.03	11.88	81.10	11.70
11	13	54	61-62	81.19	11.95	81.01	11.78

A typical NMR spectrum of a diacetylenic acid has the following chemical shifts (recorded on a 90 MHz Varian EM-90 spectrometer in $CDCl_3$ using TMS as internal standard): 0.9 ppm, distorted triplet, CH_2-CH_3; 1.25 ppm, sharp singlet $-(CH_2)-$ (when m=5 or 6 this sharp singlet has a shoulder at 1.45 ppm); 2.1-2.5 ppm, multiplet, $CH_2CH_2C{\equiv}C-$, and $-CH_2COOH$ and 10.8 ppm broad singlet, HOOC-.

2.1. Synthesis of ω-alkynoic acids:

A slurry of lithium acetylide ethylenediamine complex (2.02 g, 22 mmol) in 20 mL of dry dimethylsulfoxide was slowly added over a period of 30 minutes at 4°C to 6-bromohexanoic acid (3.9 g, 20 mmol) in 15 mL of DMSO. After the addition was complete, the contents were brought to room temperature and stirred for 2 hours. The reaction mixture was quenched with 20 mL of water at 8-10°C followed by an addition of 10% HCl to make the contents acidic. The alkynoic acid was extracted with hexane and the extract was dried over anhydrous $MgSO_4$. The acid was distilled (84-87°C/0.6mm) after removal of the solvent to afford 1.7 g of the 7-octynoic acid (60% yield). The compound was characterized by IR and NMR. Iodoalkynes were prepared by a published procedure[15].

2.2 Heterocoupling:

The ω-alkynoic acid 12-tridecynoic acid (1.6 g, 7.6 mmol) was dissolved in aqueous KOH solution (1.1 mol eq.). CuCl (0.25 mol eq.) in ethylamine (70% aq solution) was added, followed by 5 mg of hydroxylamine hydrochloride crystals. To this yellow solution was then added in small portions, the 1-iododecyne (2.01 g, 7.6 mmol) dissolved in 10 mL of methanol-ethyl ether (1:1), causing the reaction mixture to turn blue. Addition of a few drops of 10% aqueous hydroxylamine hydrochloride solution returned the yellow color. These steps, repeated until all the iodoalkyne reacted, were normally complete in 15 minutes. The reaction mixture was then acidified with 30% HCl and extracted with ether. The crude 12,14-tricosadiynoic acid obtained from the ether extract was recrystallized from hexanes and characterized by IR, NMR, MS, elemental analysis and melting point. The coupling for the fatty acid to the head group is described in reference 16.

3. Preparation of Microstructures

Tubular lipid microstructures were formed by a procedure described previously[3]. Briefly, a chloroform solution of the lipid was taken to dryness under nitrogen, then placed in vacuo for 18 hours. Filtered, deionized water was added to the lipid, giving a concentration of approximately 4 mg/mL. The lipid was hydrated by heating the mixture to at least 20 degrees above the melting point of the lipid (T_m for $DC_{23}PC$ = 43°C). Gentle agitation aided hydration. The dispersion was slowly cooled to room temperature at approximately 0.3°C per minute. Tubules formed spontaneously as the temperature passed through the liquid crystal/gel phase transition.

Vesicular dispersions were prepared by hydrating the lipids in distilled water at temperatures above their melting temperatures with vortexing, and were either used immediately or stored frozen under N_2. The appearance of the dispersions was checked by optical microscopy to check for the formation of liposomes or other structures before spectroscopy. Polymerization was performed by brief exposure to 13 mW/cm^2 254 nm light in a Rayonet model RPR-100 reactor at room temperature.

An alternative preparative technique [5,17] was used to produce tubules of somewhat longer dimensions. This technique was used for all the work on metallization of tubules. This alternative procedure involves the addition of lipid to ethanol at concentrations of approximately 0.3 mg/mL. Dialysis or other separation techniques can be used to remove the organic solvents leaving a colloidal suspension of tubules in water.

3.1 Analytical Techniques

Optical microscopy was performed with Leitz Ortholux I with dark-field illumination at room temperature. For transmission electron microscopy tubules in distilled water were pipetted onto carbon-coated grids, air dried, and observed directly. All electron micrographs were taken on a Philips EM200 transmission electron microscope. For freeze fracture, the cryoprotectant glycerol was added to samples to a final concentration of 10% by weight. Specimens were then transferred to Balzers copper specimen plates, equilibrated at room temperature, and quickly frozen by plunging into melting nitrogen. They were then transferred to a Balzers 360 or BAF 400D freeze fracture device, fractured (in some cases briefly etched) and then replicated at -100°C and 10^{-6} Torr. Replicas, which were made with 2 nm Pt-C film and 20 nm C, were floated off onto doubly distilled water, and transferred to sodium hypochlorite for two hours, rinsed in bi-distilled water, and cleaned on 20% ethanol for 1 hour. They were then picked up on coated grids and examined. Unless otherwise indicated, electron micrographs of replicas have been printed with "dark shadows", i.e., with internegative between the final print and the original plate from the microscope. This allows a more natural interpretation of structures that have extreme relief and long shadows, as often is the case for tubules. The samples seen in freeze fracture micrographs in this paper were all originally hydrated in 10 mM EDTA, but no differences between these samples and those prepared in distilled water have been observed.

The samples of lipid dispersion for Raman spectroscopy were pelleted in hematocrit capillaries and maintained in a temperature-controlled block during laser illumination. Above the phase transition temperature over one hundred milliwatts of light could be used, but with the partially polymerized samples, powers were reduced to less than 10 mW in most cases. Slit widths used on the monochromators were such that resolution was between 5 and 7 cm^{-1}, depending on the wavelength of excitation and scattering. Differences between the alignment of the two monochromators limited the accuracy of stated band locations to +/- 3 cm^{-1}.

4. Results

4.1 Microscopy

The first material that we observed to form tubules was di-(10,12tricosadiynoyl) phosphatidylcholine ($DC_{23}PC$)[3]. We therefore concentrated our initial efforts on the characterization on this polymerizable surfactant. When the conditions are optimal quantitative conversion to tubules is possible; as seen in Figure 1, an optical micrograph of nonpolymerized tubules viewed with dark-field optics. At this magnification the walls of the tubules can just be resolved, and at higher powers it can clearly be seen that their ends are open.

Figure 1. Optical micrograph of $DC_{23}PC$ tubules in distilled water taken with darkfield illumination. The walls of the tubules can just be resolved. Scale bar, 25 micrometers[4].

The lipid vesicles from which tubules are to be formed must be larger than a micrometer or so in diameter, otherwise "shards" rather than tubules were formed no matter what the temperature. Conditions that generate excessive numbers of small vesicles include sonication or even more gentle forms of agitation such as vortexing; contamination from decomposition products formed by long-term storage of the lipid in chloroform also seems to promote the formation of small vesicles. Freeze fracture electron microscopy of this nontubular material as seen in Figure 2 reveals that it consists of some small liposomes and shards of curved lipid bilayers that appear to be pieces of incompletely formed tubules. Apparently the formation of complete tubules requires the presence of large liposomes or the aggregation and/or fusion of small liposomes; these processes become impossible if the lipids are supercooled or dispersed too finely. The basic cylindrical structure of the tubules and the approximate radius of curvature is reflected in the shards.

When complete tubules in distilled water are air-dried onto a carbon film and observed under the electron microscope without staining, the lipids scatter enough electrons to produce images such as that shown in Figure 3. Stereo pairs made from this type of sample show that drying flattens the tubules onto the film surface, collapsing the internal hollow space. The electron dosage used to observe the sample and take such micrographs with the EM200 was quite high, and considering the sensitivity of diacetylenes to polymerization by a wide range of radiation, it is likely that the lipid in the beam had been polymerized by the electrons by the time the image was made. This assumes that the hydrocarbon chains were still ordered after drying and then being heated by the electrons. Also, it is possible that the electron beam had decomposed the lipid to amorphous carbon. Nonetheless, it is unlikely that a polymerization or decomposition artifact could generate the startlingly regular wrapping of discrete layers as seen in Figure 3. The apparent spiral wrapping of a strip of lipid about 2 micrometers wide to make up the walls of the structure has been seen consistently in monomeric tubules that are thin enough to allow resolution of their internal structure. A good model is a flattened paper soda straw. It is not apparent from transmission images exactly how thick the piece is that wraps around the tubule axis, although it is certainly as thick as a monolayer and perhaps as thick as two or more bilayers. The actual number of bilayers should provide a clue to the method of formation of the tubules.

Figure 2. Freeze fracture micrograph of lipid fragments too small to appear tubular by optical microscopy. Some of these appear to be partially formed tubules. Scale bar, 0.5 micrometers[4].

Figure 3. Transmission electron micrograph of unstained monomeric tubules. Such samples often show more wrinkling of the tubule walls than is apparent here. The smaller tubule appears to share a sheet of lipid with the larger, as the wrapping lines are continuous from one to the other. Scale bar, 5 micrometers[4].

We have previously observed irregular helical striation on the surface of dry monomeric tubules subjected to electron bombardment[2] that we have attributed to a change in the packing of the lipid hydrocarbon chains during polymerization. This interpretation is supported by the absence of such fibrous structures in micrographs of tubules that have been at least partially polymerized before electron microscopy and then stored in water for at least several days. Such tubules appear to have been "annealed", in that the regular helical banding pattern is often completely absent, leaving a featureless surface, as seen in Figure 4. This sample was formed from a lipid dispersion that was frozen in water, warmed to 45°C, then slowly cooled without any agitation to 38°C. The lack of agitation may have resulted in larger liposomes and hence tubules made from larger pieces of bilayer, or the storage period may have allowed the energetically unstable overlapping edges present in newly formed tubules to fuse.

The flattening of tubules that occurs on drying does not occur when the samples are freeze fractured, allowing visualization of their true cylindrical cross section. To reduce ice crystal artifacts, the samples used in this paper were frozen after addition of 10% glycerol. While we have consistently found that high glycerol concentrations seem to reduce the tightness of lamellar wrapping of the tubule walls, it is still not known how glycerol affects the structure of those bilayers or the mechanism of formation. For aqueous dispersions of dipalmityl phosphatidylcholine, for example, high concentrations of glycerol cause a collapse of the normal bilayer structure into one in which the hydrocarbon chains are interdigitated, so a certain amount of caution is advisable in interpreting samples prepared in glycerol. We have, however, prepared tubules in glycerol concentrations as high as 90% with little change in tubule morphology as observed by optical microscopy.

That tubules are, in fact, filled primarily with water can be seen from the image in Figure 5 of two tubules fractured at a shallow angle near their ends. In one of these tubules there are a few bilayers folded into the tubule interior (lumen), although optical micrographs at high magnification usually give the impression that the tubules are completely hollow. In these samples the glycerol was added shortly before freezing, so that some delamination may have occurred

If the tubules are only formed by rolling up of flattened liposomes, one expects that there would always be numbers of bilayers making up the tubule walls. One can count bilayers from the center of the tubules outward in Figure 5, giving 3 bilayers in one case and 5 in the other. This implies that some un-flattened liposomes may become trapped in the tubule interior as other liposomes wrap around it. This has recently been confirmed using fluorescent microscopy[18],

The wrapping of bilayers is often not completely regular, as can be seen in the tubule in Photograph 6. The apparent taper to the tubule is probably caused by the slight angle between the tubule and the fracture plane. We have so far only utilized the natural chiral

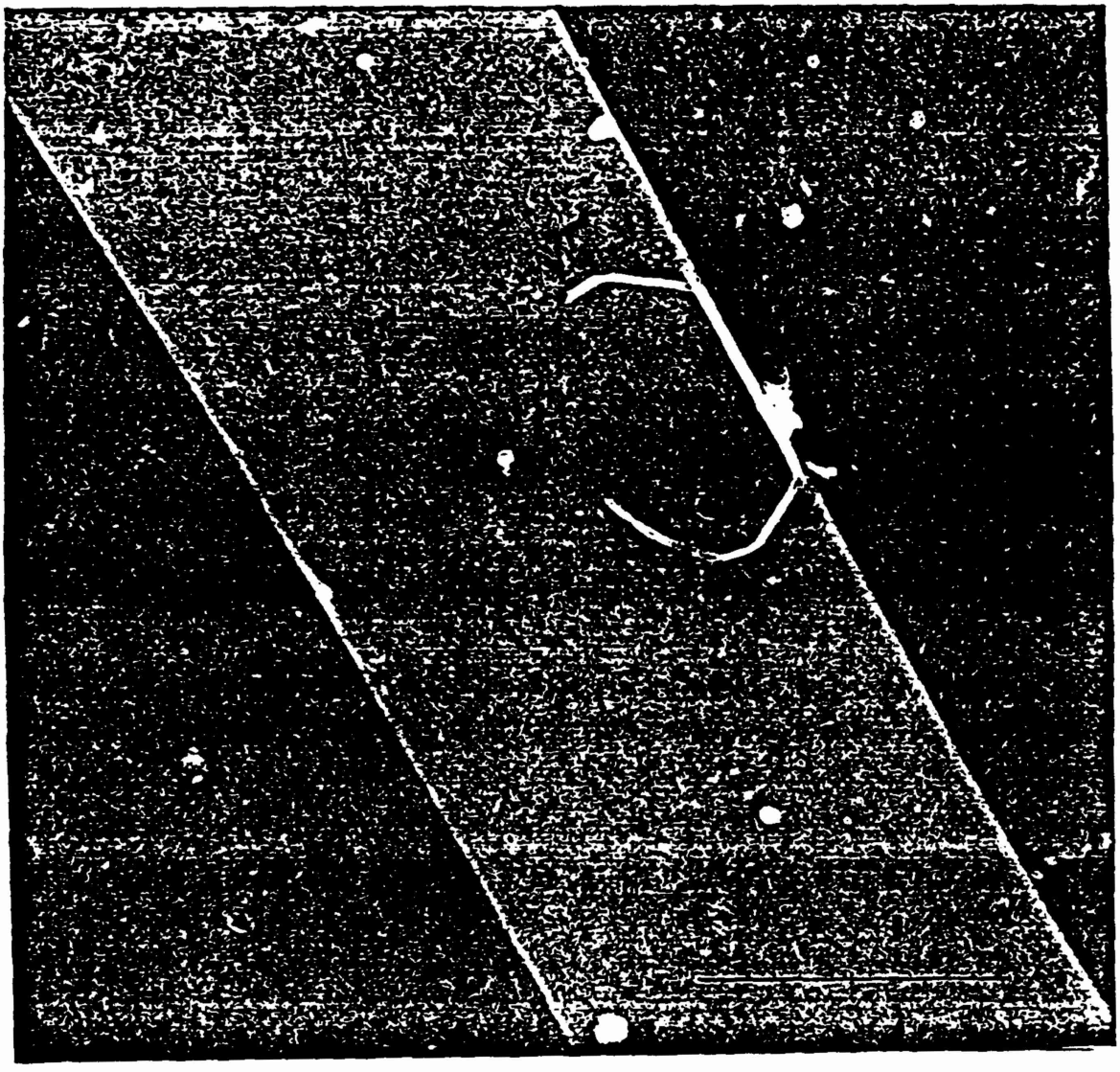

Figure 4. Transmission electron micrograph of tubule which was polymerized and stored for over a month at 4°C prior to observation. It was prepared in the same manner as the sample in Photograph 3. Scale bar, 0.5 micrometers.

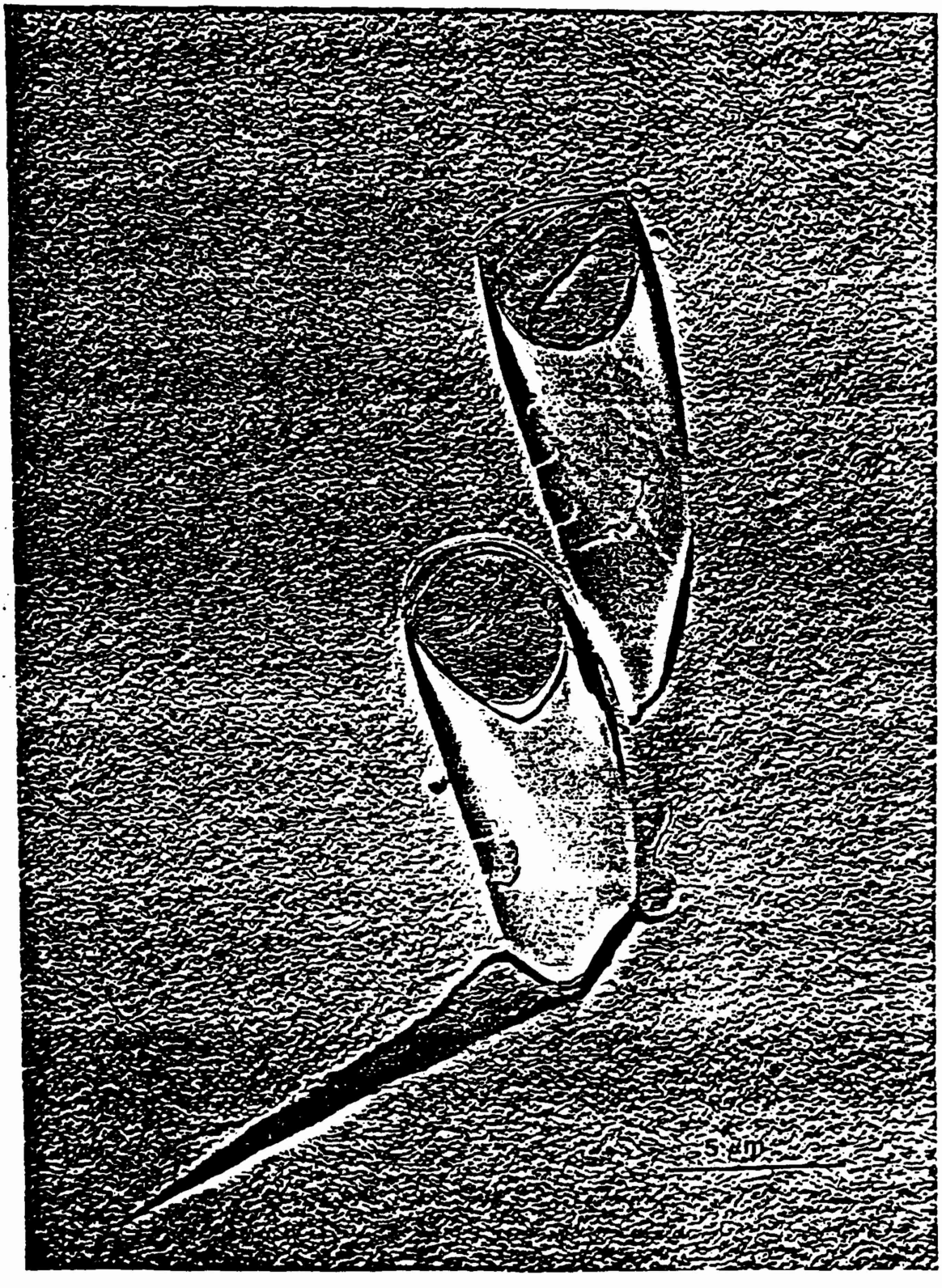

Figure 5. Freeze fracture replica of the concave ends of two tubules. Because of their slightly disordered interiors one can count three bilayers making up the wall of one, and five in the other. The apparent noncylindrical cross section of one of the tubules is not typical and may be the end the tubule. Scale bar, 0.5 micrometers[4].

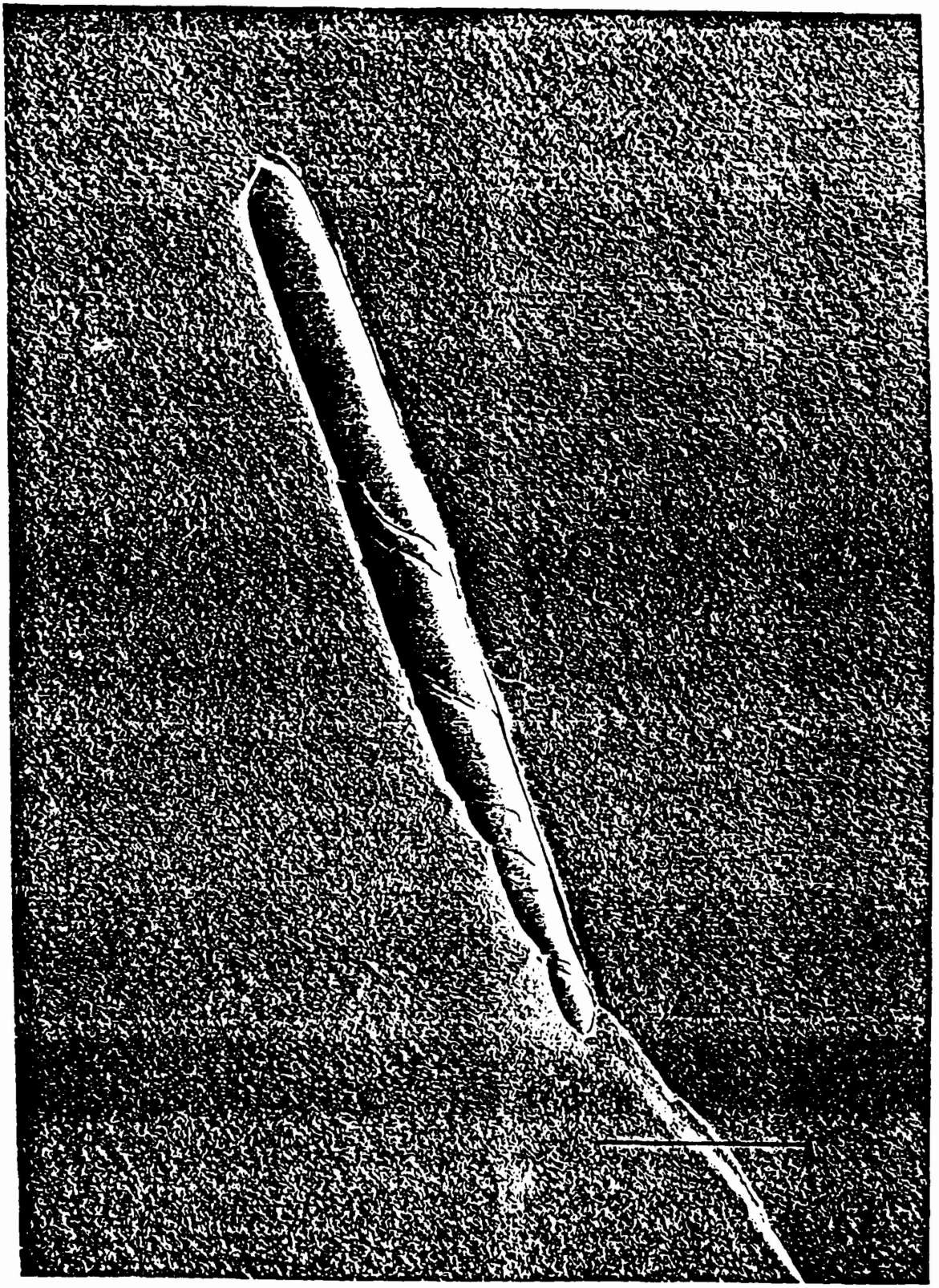

Figure 6. A concave freeze fracture replica of a tubule with stepped helical wrapping. The wrapping forms a right-handed helix, as it does in all tubules formed from this isomer of the lipid. Scale bar, 1 micrometer[4].

phosphatidylcholine head group in our $DC_{23}PC$, which always produces tubules with a right-handed helical wrapping. Note the thinness of the walls of the tubules and the openness of the lumen in Figure 7. The aqueous interior in these tubules is entirely uninterrupted, and the walls are clearly made up of very few bilayers. In other micrographs not shown here, we have seen cross sections of the ends of tubules that clearly were no more than two bilayers in thickness. Close examination of Figure 7 shows what appear to be flattened vesicles making up at least part of the walls. These may even be contiguous with the large liposome floating near the tubule, or to the smaller one apparently attached to the tubule.

A similar situation can be seen in Figure 8, but in this case it is quite clear that there are one or two flattened liposomes of varying width that wind around the tubule to form a helical sheath. That part of the tubule that can be seen in Figure 8 has a completely smooth cylindrical core (that appears to be continuous with one of the cross-fractured liposomes at the tubule's end) around which the liposome is wrapping. As mentioned above, such a structure would be expected to have a wall containing an odd number of bilayers, whereas if tubules were made entirely from flattened vesicles they would always have walls with even numbers of bilayers. The presence of the smooth shaft in the presence of wrapped liposomes again suggests that tubules can be made up of two types of bilayers -- those added by wrapping flattened liposomes, and those made tubular as they were trapped by other liposomes wrapping around them. An alternative possibility is that the tubules are formed by some crystallization and annealing process that takes place within the confines of the wrappings of the bilayers.

Aside from the diameter of the tubules and the linearity of the tubule walls, the most regular feature we have observed associated with them is a shallow rippling of the tubule wall frequently observed in polymerized samples. This ripple, as seen in Figure 9, makes an angle of about 30° to the tubule axis, and has a period of 100 nm along the tubule. The amplitude of the ripple is extremely low, and only fortuitous alignment of the ripple perpendicular to the shadowing direction allows it to be visualized. Along with the possible loss of the overlapping segments as seen in Figure 4, the production of this rippling in the surface is the only polymerization-induced morphological change in the tubules we have observed by freeze fracture. It is interesting that the fibrous striations observed in monomeric tubules in unstained transmission specimens are also arranged at about 30° to the tubule axis. We have previously speculated as to the probable helical alignment of the polymer chains relative to the tubule axis[3]. As it is unlikely that the polymer chain spacing is identical to the spacing of the monomers along the chain propagation direction, formation of the polymer is likely to cause strain and deformation in the tubule structure. While the relation of this pattern to the underlying polymer chains is not proven since the crystal structure of the walls of the tubules is as yet unsolved, this rippling does provide circumstantial evidence for regular helical paths of the polymeric linkages.

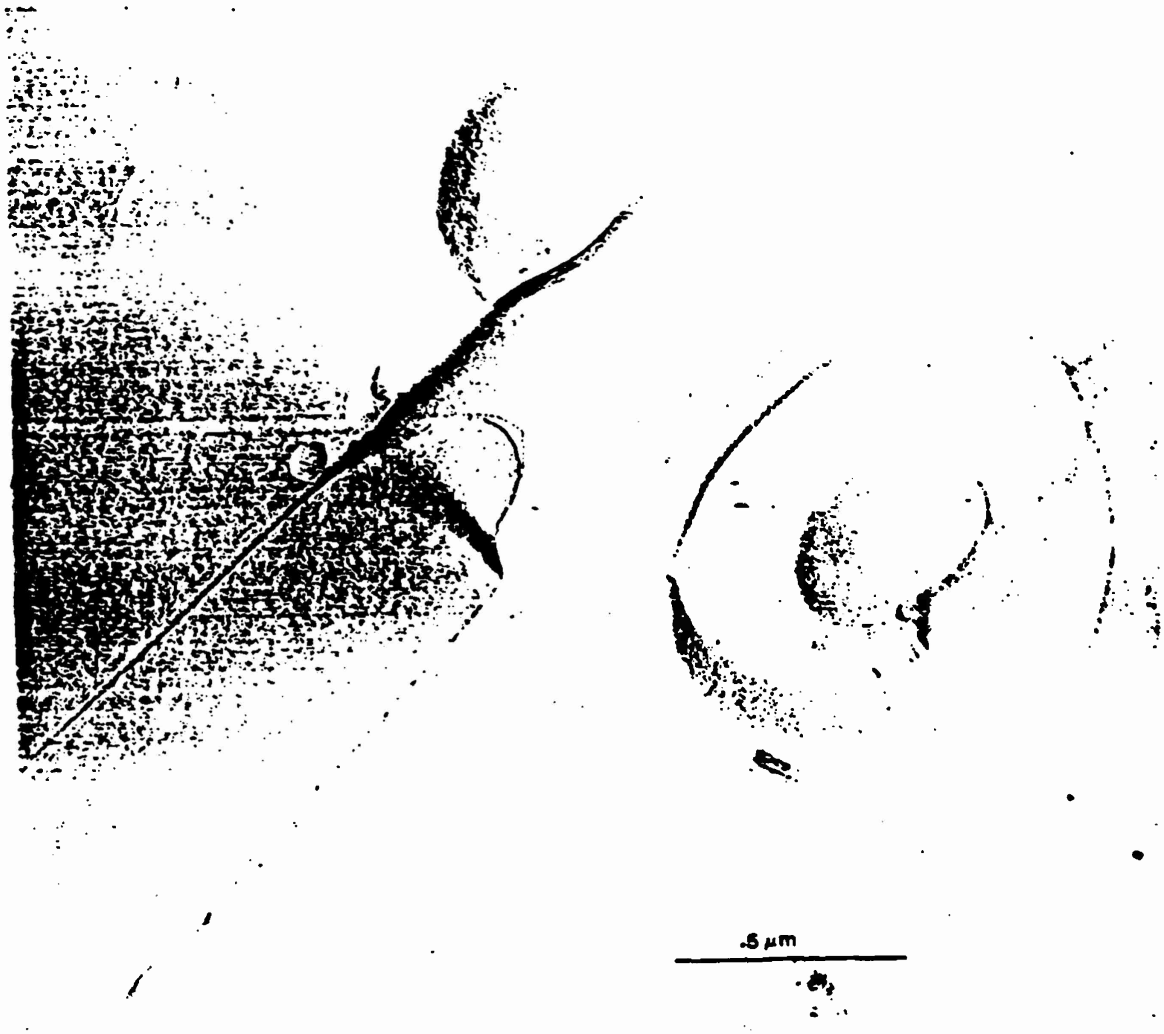

Figure 7. A convex freeze fracture replica of a tubule with thin walls and an adjacent multilamellar liposome. Note the thin walls and adherent liposomes, including an extremely flattened one. Scale bar, Ø.5 micrometers[4].

Figure 8. Freeze fracture micrograph of tubule with flattened liposome wrapping around it and liposome contiguous with the smooth core. Note that the replica is concave[4].

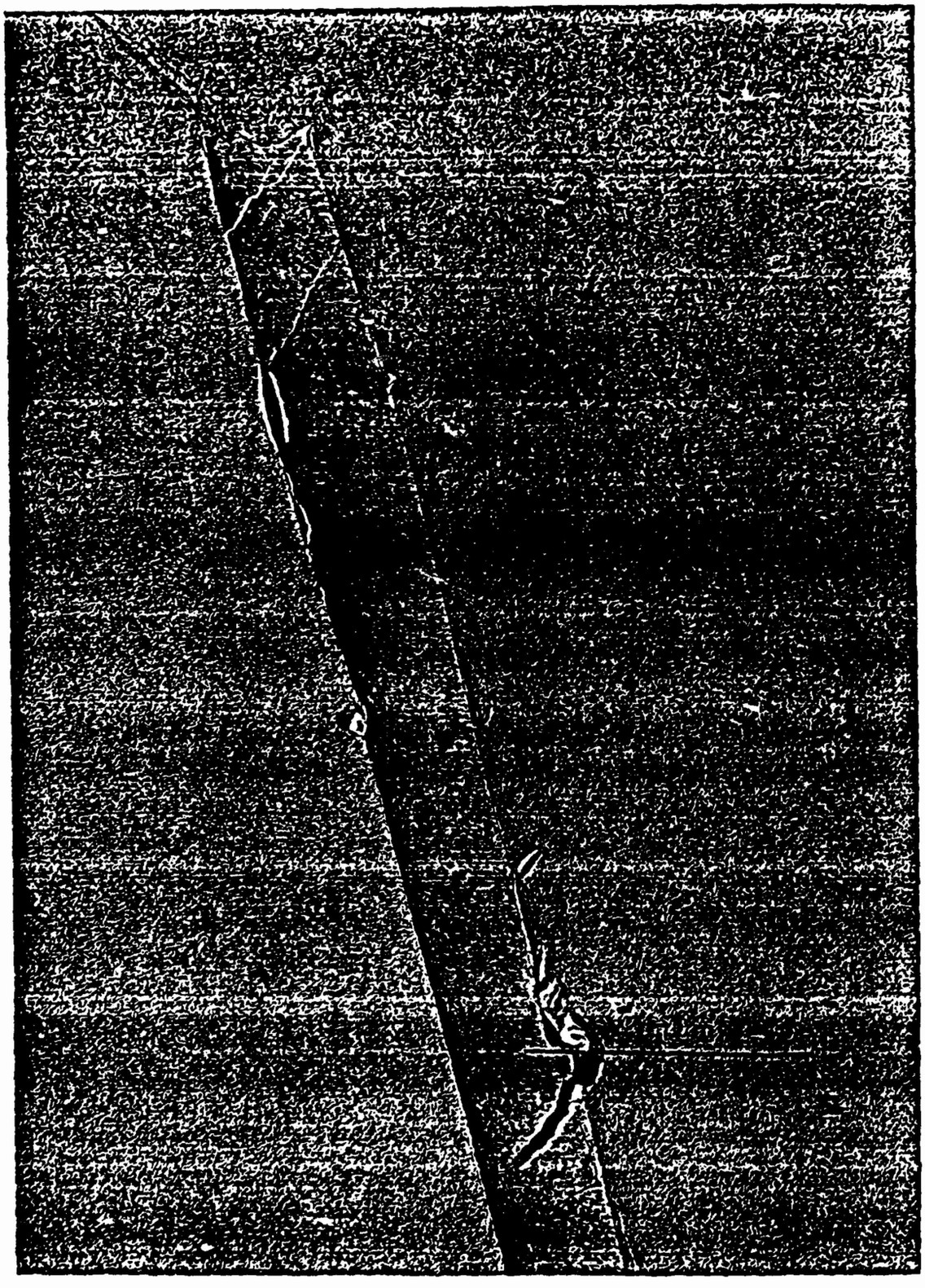

Figure 9. Freeze fracture micrograph of the convex surface of a tubule demonstrating the helical pattern of shallow ridges often seen wrapping around the axis of polymerized samples. Flattened liposomes are also present[4].

4.2 Spectroscopy

Despite their potential importance, there are few spectroscopic studies of polymerizable surfactants. The only well-characterized polymerized surfactants are the polydiacetylenic fatty acids. The polymerization mechanism (1,4 addition) was only recently discovered as a result of studies on crystals of nonsurfactant monomers which become brightly colored on polymerization[19], indicating the formation of polymer concurrent with a solid-solid phase transition. Several groups, particularly that of Ringsdorf, have pioneered the study of polydiacetylenic fatty acids[20,21,22,23]. A significant amount of spectroscopic work has been done on nonsurfactant polydiacetylenes[24,25,26,27]. Lando and coworkers have used electron diffraction from mono- and bilayers of fatty acids to establish the conformation of the diacetylene backbone chains in this ordered surfactant system[28], while others have performed Raman spectroscopy on Langmuir-Blodgett films of similar surfactants[29]. These previous studies provide one with a "basis set" of information from which to study other polydiacetylenic systems.

The surfactants of interest in drug encapsulation and other areas requiring liposomal structures have two alkyl chains, and have more complex behavior than simple fatty acids. Diacetylenic surfactants which have the potential of being far more rugged and perhaps of lower impermeability have been synthesized, most notably by Ringsdorf[30], Chapman[31,32,33], and O'Brien[34,35]. The polymerization can be followed by eye, as the polymers are intensely colored. Although both positively and negatively charged species have been made, the most thoroughly studied of these two-chain amphiphiles is a phosphatidylcholine, which has a naturally occurring head group attached to two diacetylenic hydrocarbon chains. Diacetylenic phospholipids, as these have been called, have a single chain melting phase transition in aqueous dispersion. The transition temperature is dependent on the length of the hydrocarbon chains and the positioning of the diacetylenic groups[33]. The absorption spectra of dispersions of these types of lipids have been monitored during polymerization and before and after heating, and changes in the absorption spectra are observed in both cases[16].

As has been previously reported[3], $DC_{23}PC$ in excess water has a single broad phase transition peaked at about 38°C, above which polymerization does not occur. However, unlike most other phosphatidylcholines, the structures formed by this lipid seem to depend greatly on the history of the sample. Above the phase transition the lipid forms stable liposomes, but as the temperature is dropped, the liposomes may either collapse into an amorphous structure or, if the temperature is lowered slowly and the liposomes are larger than 1 micrometer, the liposomes convert quantitatively to long hollow tubular structures[3]. Such structures also have been observed, but not characterized by Chapman[33] for a shorter chain lipid.

At first glance these appeared to be similar to cochleate cylinders in gross shape; however, upon closer examination, very little was found in common between the two structures other than their both being cylindrical. Tubules differ substantially form cochleate cylinders formed by phosphatidylserines on binding of calcium. The tubules have diameters which range from 0.3 to 1 micrometer and lengths of up to almost one millimeter, depending on conditions of formation. The thickness of the walls varies from as few as two bilayers to tens of bilayers in some longer tubules. Their surfaces have been observed by microscopy to be either smooth, gently rippled, or with spiral steps depending on sample preparation conditions (e.g., whether or not the lipids have been polymerized). The spiral steps may reflect the growth of the tubules by rolling up of flattened liposomes. This approach is not sufficient to predict tubule formation since the ratios for tubule forming lipids are similar to those that also form liposomes. It may be that an inclusion of chirality into these previous models may provide some insights into the mechanism of tubule formation. While chirality may not be essential for tubule formation, it may have an effect on the ultimate structures that are produced.

When dry or in aqueous dispersion below the transition temperature $DC_{23}PC$ has been known to polymerize to a red polymer having an absorption spectrum similar to that seen for many diacetylenes. It has not been reported to form a blue polymer under any conditions, and upon heating the red form turns yellow. In an attempt to elucidate the forces which govern the conversion to tubules from the liposomes, and how the monomeric chain packing affects the polymerization process, we have applied various spectroscopic techniques to the characterization of the $DC_{23}PC$ systems. We report here, the detailed vibrational spectroscopy of one polymerizable lipid, and an analysis of the spectroscopic data for tubules prepared from unpolymerized lipid.

The initially formed polymer of $DC_{23}PC$ is bright red if the lipids are dry or in the form of large hydrated structures. The absorption spectrum shown in Fig. 10 is typical for a sample of polymerized tubules. When $DC_{23}PC$, dried from chloroform solution, is polymerized, "red" polymer peaks near 490 nm and 520 nm are observed, and appreciable portions of the material appear blue under the optical microscope. There appear to be at least two different species of polymer in the dry material. Neither of these absorbs as far to the red as the polymerized 10,12 tricosadiynoic acid (which absorbs at 570 nm and 620 nm), or the polymerized achiral diacetylene two-chain amphiphiles, which can absorb as far to the red as 580 nm and 650 nm[3,33,36]. As can be seen in Fig.10, we find that in tubule preparations there is a small absorption band present near 600 nm, in addition to the main bands near 500 nm, which has not been previously discussed. The monomer structure in the tubules, then,is nearly as ordered as in the dry material, although even dry $DC_{23}PC$ is not so ordered as other polymerizable diacetylenic surfactants.

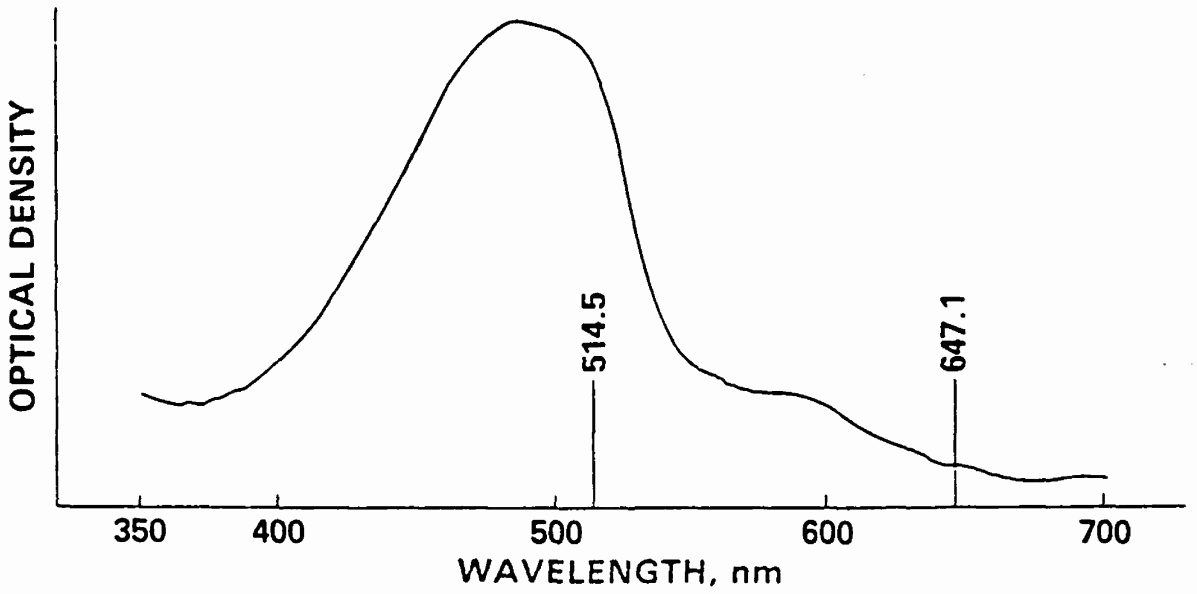

Figure 10. Visible absorption spectrum of partially polymerized tubules of $DC_{23}PC$ in suspension at 22°C. Two identical turbid suspensions were placed in cuvettes and the background was "zeroed", then one cuvette was polymerized to dark red in the reactor, and the spectrum recorded. Note the broad "red" polymer peak near 500 nm and the shoulder near 600 nm. The two laser lines used for Raman studies have been marked on the spectrum for reference[40].

In order to differentiate the structures of the tubules and the "amorphous" cold lipid, we prepared several samples for infrared absorption spectroscopy; both polymerized and unpolymerized tubules and amorphous material. These were then dried in vacuo onto AgBr plates for observation. The IR spectra shown in Fig. 11 include an absolute spectrum (a) of unpolymerized dry tubules, and a difference spectrum (b) between this sample and polymerized tubules. The spectrum of the amorphous material (not shown) was found to differ very little from that of unpolymerized tubules. At the resolution of the instrument used, the difference spectrum of Fig. 11 displays slight but noticeable features. Note that the C≡C stretching is so weak in the infrared as to be invisible in this figure. Particularly large difference bands are observed in the C≡C stretching region at about 1720 cm-1, the CH_2 scissoring region, and the CH_2 rocking mode. These are all similar to the changes seen between the subphase and gel phases of another lecithin, dipalmitoyl phosphatidylcholine[37]. (The subphase of dipalmitoyl PC is known to be nearly anhydrous, and has very highly ordered hydrocarbon chains. In contrast, the gel phase of dipalmitoyl PC is fully hydrated and less ordered.) Small but distinct changes in the $DC_{23}PC$ C-C stretching modes and C-H stretching modes further indicate that the chain packing becomes poorer on polymerization. This is consistent with our observation that the perfectly straight monomeric tubules become twisted and distorted on polymerization, presumably because of changes in unit cell dimensions on formation of the polymer backbone[3].

The Raman spectrum of the unpolymerized $DC_{23}PC$ differs from those of other phospholipids in several respects. The spectra of Fig. 12 was recorded from a (nominally) unpolymerized sample below the transition temperature. The 514.5 nm laser radiation caused a small degree of polymerization as is evidenced by the 2111 cm^{-1} polymer triple bond stretch band. The monomer triple bond stretch occurs at 2261 cm^{-1}. The degree of polymerization was so slight that no color was visible to the eye. Several major differences from what one might expect from a simpler long-chain lecithin are evident, such as the appearance of the CH_2 scissoring (or deformation) modes at approximately 1440 cm^{-1} and the vibrationally coupled C-H stretching region. At first glance, the appearance of the sharp peak at 1420 cm^{-1} in the CH_2 scissoring manifold indicates that the chains are in an orthorhombic packing similar to that seen in dipalmitoyl phosphatidylcholine at very low temperatures[38]. However, the C-H stretching region does not resemble the manifold seen in such cases. The 2825 cm^{-1} peak seen for $DC_{23}PC$ is not observed in any lipid or hydrocarbon of which we are aware, and the presence of a small 2852 cm^{-1} peak and a sharp one at 2912 cm^{-1}, and a shoulder on the high side of the 2890 cm^{-1} compound the discrepancy. It appears that either the coupling between the various modes involved in the complex Fermi resonance-factor group splitting of the hydrocarbons[39] is significantly different in the diacetylenic lipids, or the packing of the hydrocarbon chains is quite different from that observed in other systems.

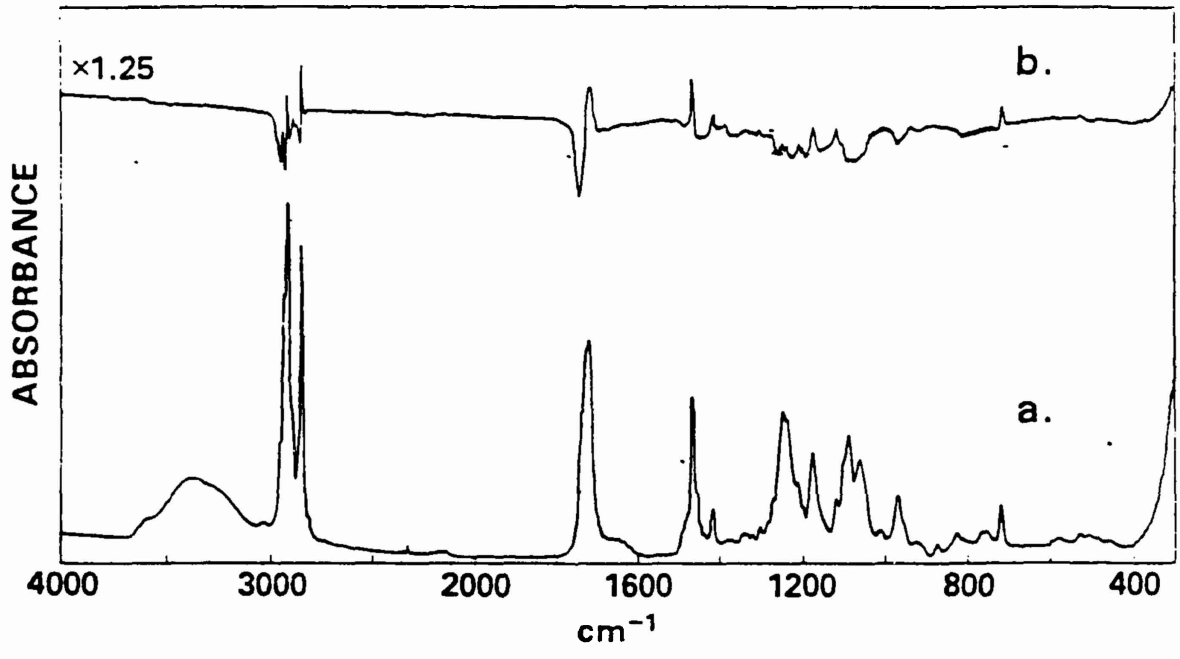

Figure 11. Infrared spectrum of unpolymerized dry $DC_{23}PC$ which was tubular before drying (a) and the difference between this spectrum and the spectrum of polymerized tubules (b). In the difference spectrum the polymer spectrum has been subtracted from the unpolymerized spectrum, following normalization by eye[40].

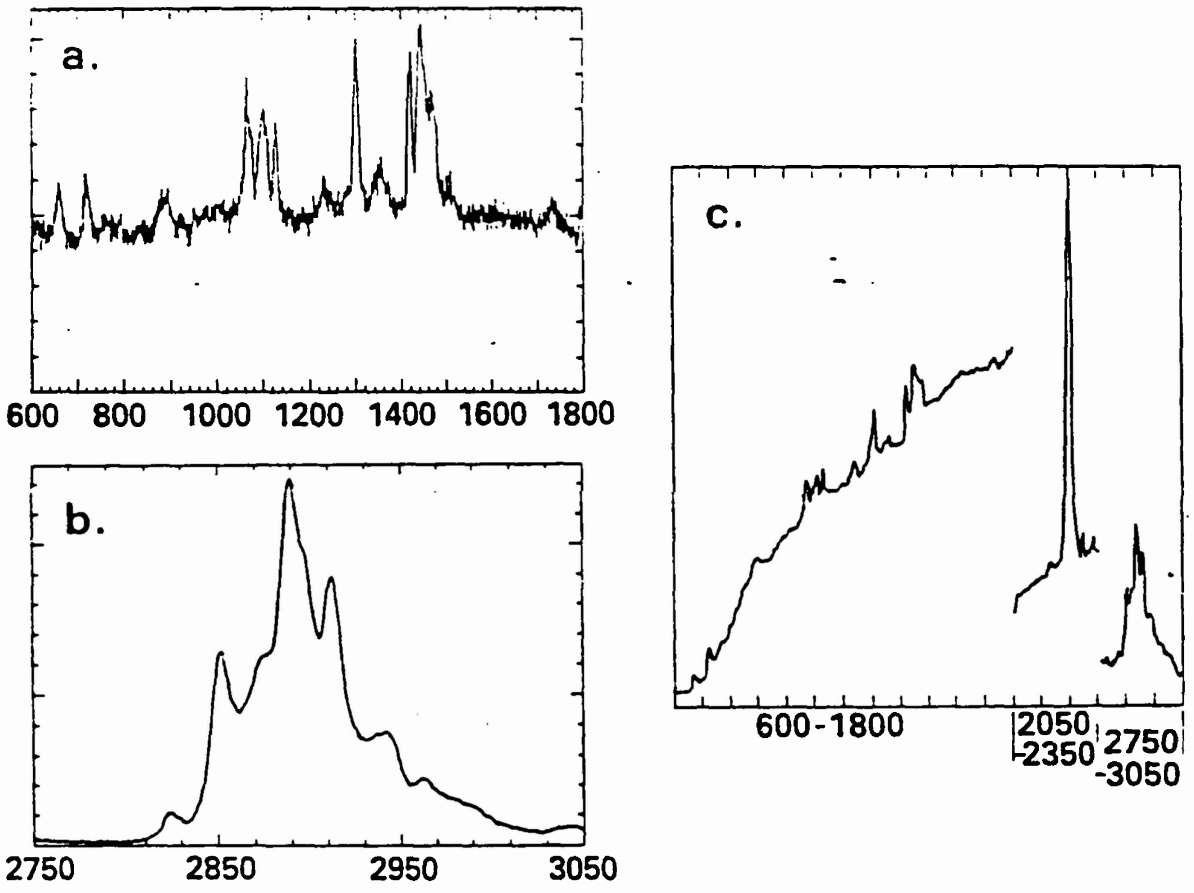

Figure 12. Raman spectrum of monomeric $DC_{23}PC$ dispersed in water at 10°C and recorded with 514.5 nm excitation (a,b) and 647.1 nm excitation (c). The three regions shown in (c) are 600-1800, 2050-2350, and 2750-3050 cm^{-1}. The 514.5 nm spectrum was synthesized as discussed in the text. Note the similarity with (c). The C≡C stretching region is shown only for the 647.1 nm spectrum[40].

To prove that the unusual vibrational structure of this compound is not caused by the great length of the tricosadiynoyl chains, we studied the spectra of two simpler lecithins, dilignoceroyl phosphatidylcholine with two saturated fatty acyl chains of 24 carbon length and dinervonoyl phosphatidylcholine with chains of the same length, but with a single cis double bond at the 15 position. Both lipids form liposomes that are stable above and below their transition temperature. The spectra differ very little from those seen for any other well-packed phospholipids. None of the differences can account for the unusual hydrocarbon chain bands seen in the $DC_{23}PC$ spectrum.

The perturbation of the vibrational structure of hydrocarbon chains by the diacetylenic unit persists even when the motional restrictions of the crystalline state are removed. The spectrum of the monomeric lipid above its phase transition temperature is shown in Fig. 13. In many ways, the changes seen on raising the temperature are typical of those seen in other systems. However, the atypical intensities of the band envelope in the C-H stretch region (4b) emphasize the unusual character of the $DC_{23}PC$ spectrum. The diacetylenic group halfway down the chains must strongly perturb the vibrations of the surrounding hydrocarbon regions, altering the spectrum even when whatever factor group splitting imposed by packing in the crystal is released by melting.

It proved impossible to observe the nonresonance enhanced Raman spectrum of the monomer for long periods of time with 514.5 nm light without obscuration by the polymer spectrum. For this reason, it is preferable to use the 647.1 nm krypton laser line. When the lipid is deliberately polymerized, the resonance Raman effect produces spectra, which depend greatly on the exact conditions of observations, polymerization, and the laser frequency. For further discussion of the resonance spectra of this system see reference[40].

5. Metal-Coated Lipid Tubes

As mentioned earlier, there are a number of potential technological applications for tubular microstructures. A significant fraction of these applications require that the tubules have the additional attribute of being metallic or electrically conductive. We have found electroless plating[41] to be a particularly rapid and effective means of producing thin (20-30 nm), reasonably uniform metal coatings on the exterior and lumen surfaces of tubules. Although most of the experiments employed $DC_{23}PC$ tubules, no difference was observed with any other diacetylenic phospholipid in its receptivity toward metallization.

5.1 Metallization Procedure

Monomeric or polymerized tubules were prepared as described earlier in this paper. The aqueous dispersion was acidified by dialysis against 0.1M HCl The protonated microstructures (at a concentration of ca. 0.5 mg/mL) were slowly added to a four-fold (v/v) excess of commercial Pd/Sn colloidal activator, filtered by gravity through a 0.60 micron filter and

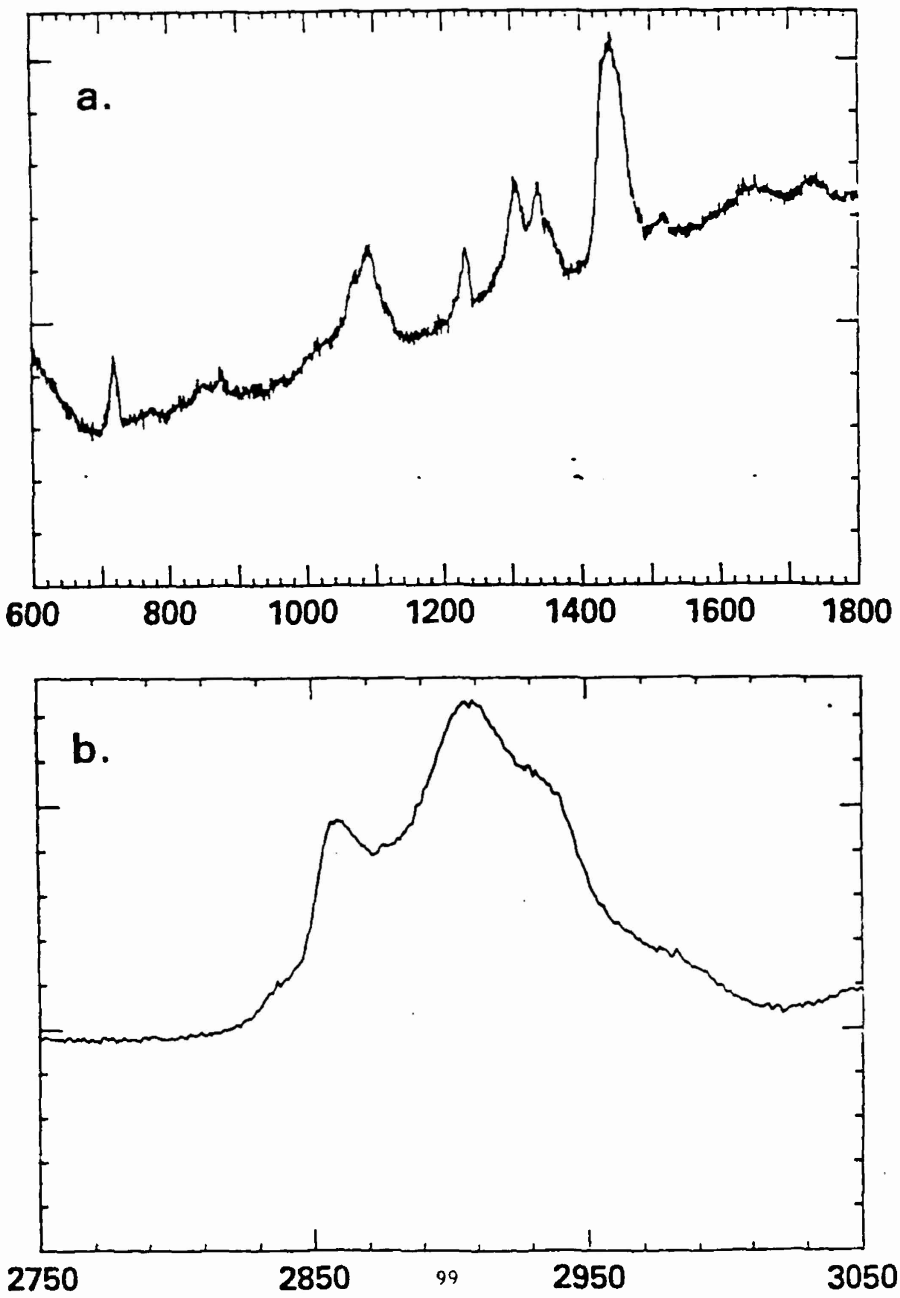

Figure 13. Raman spectrum of monomeric $DC_{23}PC$ dispered in water at 50°C, at which temperature the fatty acyl chains are melted. The skeletal region (a) and the C-H stretching region (b) only are shown[40].

rinsed with excess HCl solution to remove unbound activator. The previously white or red (polymerized) tubules became dark brown due to the color of the activator. The dispersion was rinsed with deionized water until the filtrate reached pH 5, concentrated to the original volume, then added to a four-fold excess of the desired metal plating bath. Among those employed were commercially available electroless Ni-P (low or high phosphorus) and electroless copper. After the desired length of time in the plating bath, typically 1.5 to 6 minutes, the metallized microstructures were added to a twenty-fold excess of water, filtered and rinsed copiously with water. Nickel plated tubule dispersions appeared black; copper-plated samples were red-brown in color.

5.2 Characterization of Metallized Tubules

5.2.1. Optical Microscopy

Examination of the metallized tubules using optical microscopy with bright-field illumination revealed a dense, opaque, relatively uniform black or brown coating on the surface of the microstructures, indicative of the presence of an electroless nickel or copper deposit. By comparison, unmetallized tubules are essentially invisible under bright-field illumination, which appear as distinct parallel lines under dark-field illumination, are unobservable in the metal-coated samples. However, the morphology and aspect ration of the metallized tubules otherwise appears similar to the uncoated material by optical microscopy.

Tubules coated with the magnetic (low phosphorous) electroless nickel deposit were observed under the optical microscope in the presence of a relatively weak ($<10^3$ gauss) magnetic field. The metallized tubules aligned rapidly with the applied field (Fig. 14), and also tracked a rotating magnetic field at over 1000 rpm.

5.2.2. Electron Microscopy/X-ray Fluorescence

The metallized tubules were examined by scanning electron microscopy (SEM), transmission electron microscopy (TEM) and by energy-dispersive x-ray spectroscopy (EDS). For SEM, the tubule dispersion was mounted either on carbon stubs or copper planchettes coated with colloidal carbon paint, air-dried, then examined directly in the microscope equipped with a Kevex EDS detector.

In contrast to the fragile unmetallized samples, microstructures that were plated in electroless copper or nickel baths displayed greatly improved thermal, mechanical and electrical properties. They were intact, undistorted, and could be clearly visualized in the SEM without apparent charging. Fig. 15 is a high resolution image of tubules that were plated in an electroless nickel bath for 1.5 minutes. The relatively homogeneous metal coating allowed visualization of the bilayer wrapping at a resolution of less than 10 nm, and clearly exhibits the hollow nature of

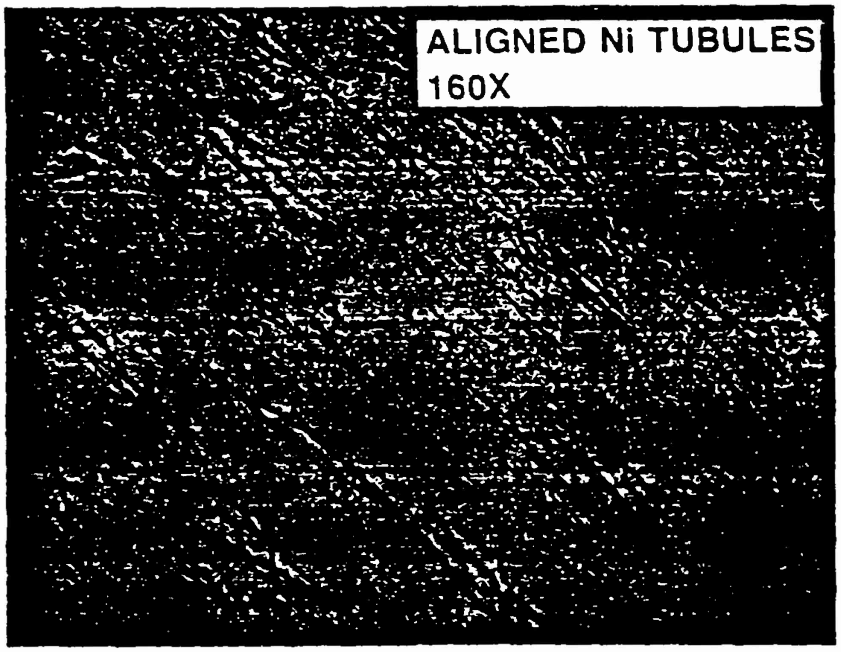

Figure 14. Aqueous dispersion of electroless Ni-plated tubules, aligned with a bar magnet. Bright-field illumination.

Figure 15. SEM of tubules plated with electroless Ni. Note the open-ended tubules and spiral wrapping.

the tubule. Also, SEM provides a direct image of the exterior surface of the microstructure, rather than a replicated image of the inner bilayer surface provided by freeze-fracture. Positive identification of the coating as either Ni-P or Cu was obtained by mapping the x-ray fluorescence from the electron-beam irradiated region in the appropriate elemental energy window.

SEM also demonstrated the improved solvent compatibility of the metallized microstructures -- they were apparently unaffected by exposure to amyl acetate, chloroform, ethanol, 2,2-dimethoxypropane, acetone and propylene oxide. It should be noted that with the exception of acetone, the lipid material is soluble in the solvents listed above. The metal-coated tubules were also essentially unaffected by lyophilization and CO_2 critical point drying, and showed no degradation upon heating to 200°C.

Metallized tubules were prepared for transmission electron microscopy by desiccation with dimethoxypropane or acetone, followed by embedding in epoxy. Tubules were oriented in the matrix by either flow or magnetic alignment during curing of the polymer. The composite was cut with a microtome perpendicular to the axis of alignment to provide a cross-sectional slice of the tubules. TEM clearly demonstrated that the metallized structure remained intact during the embedding procedure. Fig. 16 shows concentric rings of dark, light, and dark regions, which indicate the presence of the metal coating on both the externally accessible surfaces of the tubule. The metal thickness (approx. 20 nm) is nearly identical for the inner and outer layers. The ability to control the morphology and thickness of the metal coating by manipulation of the plating conditions is currently under study in our laboratory. The similarity in gray level of the lumen area to that of the matrix suggests strongly that the polymer had penetrated at least to some extent into the lumen. This points toward the feasibility of using tubules as a sort of "microvial" to entrap, transport and deliver polymeric reagents to a desired site.

6. Discussion

Since the earliest studies on phospholipids in aqueous dispersion[42], pure lecithins have always been found in liposomal form, with an aqueous space contained by single or multiple continuous bilayers. This is true even for synthetic lecithins with complex thermal properties, such as dipalmitoyl phosphatidylcholine, which has at least three phase transitions[43]. The phase transitions may change the bilayer spacing[44] and also the surface areas of the liposomes[45,46], but the topology of the liposomes remains unchanged. Even though sonicated small unilamellarlecithin vesicles below their phase transition temperature are considered "unstable" because they fuse to slightly larger unilamellar vesicles[47,48,49], they still are never seen in nonspheroidal form.

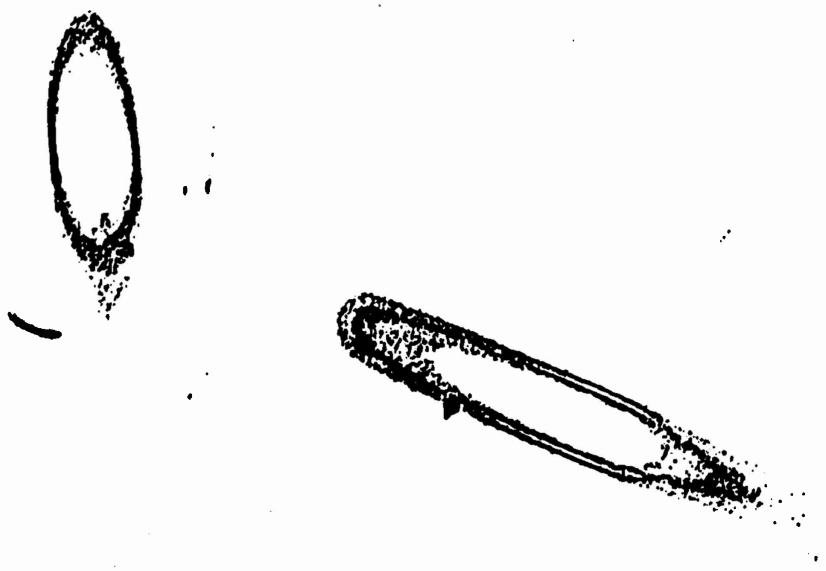

Figure 16. TEM of electroless Cu-plated tubules embedded in epoxy. The apparent ellipticity of the structures is due to the tubules not being oriented at exactly 90° to the plane of the section.

Upon examining the phase transition of a monomeric polymerizable diacetylenic lecithin under the optical microscope, we found that the normal appearing liposomes formed by gentle dispersion of the lipid above its phase transition temperature (T_m) became unstable and seemed to disintegrate on cooling through T_m. If the monomeric lipid was cooled rapidly to below 30°C, the liposomes violently broke into small "shards", but when cooled slowly to 37°C to 38°C, which is within the rather broad melting transition of the compound, the liposomes converted quantitatively to hollow tubules over a period of a minute. These "tubules" were between 0.3 and 1 micrometer in diameter, with fairly thin walls, and ranged in length from a few to hundreds of micrometers. After polymerization, the tubules no longer converted to liposomal form when heated, but did exhibit thermochroism, indicating temperature effects on the conformation of the chromophoric polymer. (See reference 15 for a further discussion of diacetylenic thermochroism in vesicles.)

Other classes of lipids, such as phosphatidylethanolamines, phosphatidylglycerol, cardiolipidin, and other charged lipids, can convert to nonlamellar phases, such as the inverted hexagonal (H_{II}) phase[50] or, in the case of phosphatidylserines in the presence of Ca^{++}, a rolled-up lamellar phase dubbed cochleate cylinders[51]. Structures somewhat similar to the tubules seen here were also observed for a diacetylenic lecithin with 20-carbon long fatty acyl chains and were assumed to be similar to cochleate cylinders[33]. Tubules and cochleate are superficially similar, but our initial electron microscope studies on $DC_{23}PC$ indicated that the tubules were somewhat different from cochleate cylinders in being open ended, and often consisting of only a few bilayers. Cochleate cylinders are similar in diameter, although they are not nearly so long as tubules, and consist of very tightly wrapped multibilayers with little or no internal aqueous space. Recently a tubular lipid structure has been observed to form from an amino acid-based surfactant[52] which is more similar in appearance to the tubules described here than is the cochleate cylinder. In order to differentiate the tubules from cochleate cylinders and further refine our understanding of the tubule structure, we have extended our preliminary studies to include freeze fracture of samples in several states, and transmission electron microscopy of air-dried unstained tubules. We have found that the various images observed suggest not one, but a number of different models for tubule formation.

We have characterized the chemistry and structure of $DC_{23}PC$, including monitoring the conformation of polymerizable hydrocarbon chains, before and after polymerization, using infrared and Raman spectroscopy. While our spectroscopic investigations to date represent more of a survey than an exhaustive study of $DC_{23}PC$, several conclusions may be made about the system. The formation of the highly unusual tubule structure by this phospholipid can only be explained by a fundamental difference between the low temperature phase of $DC_{23}PC$ and that of other better-studied phospholipids. As we have found that neither dilignoceroyl nor dinervonoyl PC forms tubules, the key is likely to be in the

perturbation of hydrocarbon chain packing by the diacetylene group. As quantitative conversion to tubules is possible under our experimental conditions[18], it is clear that other low temperature states are metastable. The tubules differ from liposomes in that they have two quite different radii of curvature -- one narrowly defined near a micrometer and another near infinity. There may be a specific chain crystal packing which exists unaltered throughout the tubules to support such a regular structure. The helical pattern of polymerized fibers within polymerized tubules supports this hypothesis[18].

We see only subtle difference between the nonresonance Raman or infrared spectra of $DC_{23}PC$ samples which appear completely different under the optical microscope; e.g., between the infrared spectra of dry tubules and "amorphous" (presumably microcrystalline) lipid. On the molecular scale, these structures must be similar.

The polymerization itself seems to disturb the hydrocarbon chain packing and the head group conformation, as seen by changes in the infrared spectrum and some indications of changes in the Raman active C-H stretching vibrations.

As yet, we cannot identify the crystallographic packing in which the chains fit because of the difficulty of interpenetrating the $DC_{23}PC$ spectra by analogy with other lecithin spectra. The vibrational perturbation of the diacetylenic group is sufficient to muddy the analysis of the spectra from the rest of the hydrocarbon chains. The spectra do not fit any existing category for alkane chains. However, if the aforementioned similarity between the tubule chain packing and that in fatty acid monolayers is correct, then the packing change on polymerization must be similar to that found by Day and Lando in the fatty acid systems[28]. These include a change from a tilted structure to one in which the hydrocarbon chains are perpendicular to the bilayer, accompanied by a contraction of the packing along the direction of polymerization. The hydrocarbon chain packing of phospholipids is, in general, looser than that in fatty acids, partially because of the unequal penetration of the bilayer by the two hydrocarbon chains imposed on the lipid molecule by the chiral head group, and because of the mismatch in cross sectional area between headgroup and chains. This loose packing may account for the "relaxed" blue polymer forming first in most cases, and for some strained red polymer formed only in the highly crystalline tubule structures and dry lipids. Ongoing work in this laboratory with this and other model compounds should make possible a better analysis of the chain conformations[53].

Much of the interest in the properties of cochleate cylinders derives from the fact that when the Ca^{++} is chelated away from the phosphatidylserine, large unilamellar liposomes are formed that efficiently trap the surrounding aqueous medium[52]. If the $DC_{23}PC$

tubules are not polymerized, they too will convert to liposomes on heating and, for this reason, may also prove useful for entrapping solutes. If present at high concentration, these liposomes would presumably be stable as long as the temperature was kept above about 39°C, but would expel their contents on cooling and reconversion to tubules. Possible uses for selective drug delivery to cool tissues might be envisioned.

To the authors there is, as yet, no obvious physical reason for liposomes, cooled below the melting point of their constituent lipids, to form tubules with a particular narrowly defined diameter, but it is clear that the crystalline lipids making up the tubule walls must favor a finite degree of curvature in one direction, and no curvature in the other to produce the tubule structure. Chirality is necessary but not sufficient to induce helical structure with a consistent handedness. It was first speculated that the kink in the hydrocarbon chains produced by the diacetylene group was responsible for the unusual behavior of $DC_{23}PC$, as most other nondiacetylenic lecithins with long hydrocarbon chains show no inclination to form tubules. At present we have synthesized at least 18 other diacetylenic lipids using the methods described above, which do form tubules, and we are currently in the process of establishing a definitive pattern between chain length, diacetylenic position, and propensity to form tubules.

The simple "kink" theory was severely tested by the aforementioned paper from Kunitake's laboratory,[52] which reports the formation of nearly identical tubule-like structures from a totally dissimilar lipid. Their tubule forming lipid is based on glutamic acid, with two n-dodecyl chains attached to the carboxyl groups and a third long chain with a quaternary ammonium terminal group attached via a peptide linkage. Below the phase transition temperature of this lipid, liposomes convert to long regular helical structures that slowly convert over a period of weeks to straight tubules with dimensions very similar to those produced by $DC_{23}PC$. The glutamate-based lipid is chiral, and the handedness of the helices depends on the chirality of the amino acid, so that racemic mixtures produce no tubules. It appears that the tubule is a thermodynamically stable structure that is common to several lipid systems.

The extremely slow conversion to the final tubules in the glutamic acid lipid system suggests that the formation mechanism in that system may be unrelated to the mechanism that drives the formation of the diacetylenic tubules.

There clearly are differences between the tubules and cochleate cylinders that merit establishing the tubules as a unique class of lipid structure, but there are probably similar processes occurring during the formation of each. The conversions to cochleate cylinders from phosphatidylserine liposomes and to tubules from liposomes of $DC_{23}PC$ appear to be driven by the phase to transition to the gel state of the lipid hydrocarbon chains, induced isothermally by binding of Ca^{++} in one case and by cooling in the other. Also, when the low temperature forms are reheated liposomes are reformed from them. When the warm liposomes

are less than a certain size, tubules will not form at all, and the cochleate cylinders will only form after fusion of small liposomes to much larger ones[54]. Given these superficial similarities one might expect similar molecular mechanisms as well. Dehydration of headgroups is known to play a vital role in allowing the close approach of bilayers that begins the process of cochleate cylinder formation[55] and it may be that similar dehydration occurs when $DC_{23}PC$ liposomes contact as a first step in the formation of tubules. Binding Ca^{++} drives the conversion of the phosphatidylserine bilayer to the gel phase, and the resultant close apposition of bilayers (as reflected by the extremely short bilayer repeat of 5.4 nm) in the cochleate cylinders[51]. We have not yet measured the bilayer repeat in the tubules in distilled water, but we have regularly seen a tendency for some bilayers to be separated by large distances in tubules formed in varying amounts of glycerol. Clearly, close bilayer apposition is not so important a phenomenon for tubules as it is for cochleates.

7. Summation

In this article we have presented a description of the some intriguing self organizing materials and some speculations about the nature of the self organizations. To our knowledge these structures are among the largest self organized nonliving structures yet observed. The potential technological applications of such structures are vast and include possibilities in microsurgery, composites, drug delivery, novel liquid crystals, optical elements, and electronic micro connectors.

In order to determine the ultimate utility of such potential applications a great deal of research and development is required. Process and chemical engineering will be important to evaluate the feasibility of scale up at reasonable cost. Coating techniques must be perfected to ensure the proper mating between the tubules and polymeric host for composite applications. Techniques for encapsulating materials in the tubules must be evaluated and perfected. Manipulation procedures must be developed so that oriented matrices can be fabricated. Mechanical and spectroscopic properties of tubules must be determined for pure and coated tubules. Basic research into the underlying basis for formation is also perhaps the most important of all these issues. It is only by understanding the role of molecular structure in forming microstructures that one of the real promises of bio/molecular engineering may be achieved, if indeed it is possible: bottom up design and engineering of micron-sized structures for specific applications.

Acknowledgments

Our thanks to Barbara Herendeen for synthesis of the lipid used, to Ms. Carol Davies and Ms. Angela Weaver for valued laboratory assistance in the formation of the tubules, to Drs. William Tolles and Mark Nagumo, NRL, and Dr. Ira Skurnick of DARPA for many fruitful discussions. Ms. Sharon Menton is thanked for careful reading of the manuscript.

This work was funded by the Defense Advanced Research Projects Agency, and their support is most gratefully acknowledged.

References

1. D. Chapman, "Biological Membranes", Academic Press, London, 1968.

2. A. Singh and J.M. Schnur, Synth. Comm., 16(7)(1986)847.

3. P. Yager and P.E. Schoen, Mol. Cryst. Liq. Cryst., 106(1984)371.

4. P. Yager, P.E. Schoen, C. Davies, R. Price, and A. Singh, Biophys. J., 48(1985)899.

5. J.M. Schnur, J.H. Georger, R. Price, P. Yager, A. Singh, and P.E. Schoen, "Direct Fabrication of Lipid Microstructures from Solvent/Nonsolvent Solutions", Invention Disclosure, NC #70173, (1986).

6. J.M. Schnur, J.M. Calvert, J.H. Georger, R. Price, P.E. Schoen, and P. Yager, "Fabrication of Metallic Microstructures", Invention Disclosure, NC #70238, (1986).

7. C. Rosenblatt, P. Yager, and P.E. Schoen, Biophys. J., In Press.

8. See for example, D. Mobius, Acc. Chem. Res. 14(1981)63; J.H. Fendler, Monolayers and Organized Multilayer Assemblies, in: "Membrane Mimetic Chemistry", John Wiley & Sons, New York, 1982 and references cited therein.

9. H.J. Canton, ed., "Polydiacetylenes", Springer-Verlag, New York, 1984.

10. W.N Smith and O.F. Beumel, Jr., Synthesis, 441(1974).

11. W.J. DeJarlais and E.A. Emken, Synth. Comm., 10(1980)653.

12. L.D. Bergel'son, Y.G. Molotovskii, and M.M. Shenyakin, Zh.Obsh.Khim., 32(1962)58.

13. A.S. Kovaleva, N.N. Borisov, A.V. Tsyban, L.L. Ivanov, Yu.B. Pyatnova, and R.P. Evstigneeva, Zh.Org.Khim., 8(1972)2472.

14. R.F. Newton, P.L. Pauson, and R.G. Taylor, J. Chem. Res.(M), 3501(1980).

15. T.H. Vaughn, J. Amer. Chem Soc., 55(1933)3456.

16. A. Singh, R.B. Thompson, and J.M. Schnur, J. Am. Chem. Soc., 108(1986)2785-2787.

17. J. Georger, A. Singh, R. Price, J.M. Schnur, P. Schoen, and P. Yager, J. Am. Chem. Soc., In Press.

18. T.G. Burke, A. Singh, and P. Yager, Anal. N.Y. Acad. Sci., In Press.

19. G. Wegner, Z. Naturforsch, 246(1969)824.

20. D. Day and H. Ringsdorf, J. Polym. Sci., Polym. Lett. Ed., 16(1978)205

21. J.P. Fouassier, B. Tieke, and G. Wegner, Israel J. Chem., 8(1979)227.

22. C. Bubeck, B. Tieke, and G. Wegner, Ber. Bunsenges. Phys. Chem., 86(1982)495.

23. C. Bubeck, B. Tieke, and G. Wegner, Ber. Bunsenges. Phys. Chem., 86(1982)499.

24. M.L. Shand, R.R. Chance, M. LePostollec, and M. Schott, Phys. Rev. B., 25(1982)4431.

25. D. Bloor, R.J. Kennedy, and D.N. Batchelder, J. Poly. Sci., Poly. Phys. Ed., 17(1979)1355.

26. D.N. Batchelder and D. Bloor, J. Phys. C. Solid State Phys., 15(1982)3005.

27. D. Bloor, D.N. Batchelder, D.J. Ando, R.T. Read, and R.J. Young, J. Poly. Sci., Poly. Phys. Ed., 19(1981)321.

28. D. Day and J.B. Lando, Macromolecules, 13(1980)1478.

29. B. Tieke and D. Bloor, Makromol. Chem., 180(1979)2275.

30. R. Buschl, B. Hupfer, and H. Ringsdorf, Makromol. Chem. Rapid Commun., 3(1982)589.

31. O. Albrecht, D.S. Johnston, C. Villaverde, and D. Chapman, Biochim. Biophys. Acta., 687(1982)165.

32. M. Pons, D.S. Johnston, and D. Chapman, J. Polym. Sci., Polym. Chem. Ed., 20(1982)513.

33. J. Leaver, A. Alonzo, A. A. Durrani, and D. Chapman, Biochim. Biophys. Acta., 732(1983)210.

34. D.F. O'Brien, T.H. Whitesides, and R.T. Klingbiel, J. Polym. Sci., Polym. Lett. Ed., 19(1981)95.

35. E. Lopez, D.F. O'Brien, and T.H. Whitesides, J. Am. Chem. Soc., 104(1982)305.

36. B. Hupfer and H. Ringsdorf, in, "Polymer Science Overview", G.A. Stahl, ed., A.C.S. Symposium Series (Washington, D.C., American Chemical Society, 1981).

37. D.G. Cameron and H.H. Mantsch, Biophys. J., 38(1982)175.

38. N. Yellin and I.W. Levin, Biochem. Biophys. Acta., 489(1977)177.

39. R.G. Snyder, S.L. Hsu, and S. Krimm, Spectrochim. Acta., 34a(1987)395.

40. P.E. Schoen and P. Yager, J. Polym. Sci., Polym. Phys. Ed., 23(1985)2203

41. C.R. Shipley Jr., Plating and Surface Finishing, 71(1984)92.

42. A.D. Bangham, M.M. Standish, and J.C. Watkins, J. Mol. Biol., 13(1965)238.

43. S.C. Chen, J.M. Sturtevant, and B.J. Gaffney, Proc. Natl. Acad. Sci., 77(1980)5060.

44. Y. Inoko and T. Mitsui, J. Phys. Soc. Japan, 44(1978)1918.

45. P. Yager, J.P. Sheridan, and W.L. Peticolas, Biochim. Biophys. Acta., 693(1982)485.

46. E. Evans and R. Kwok, Biochemistry, 21(1982)4874.

47. J. Suurkuusk, B.R. Lentz, Y. Barenholz, R.L. Biltonen, and T.E. Thompson, Biochem., 15(1976)1393.

48. B.P. Gaber and J.P. Sheridan, Biochim. Biophys. Acta., 685(1982)87.

49. E.L. Chang, B.P. Garber and J.P. Sheridan, Biophys. J., 39(1982)197.

50. P.R. Cullis and B. DeKruiff, Biochim. Biophys. Acta., 559(1979)399.

51. D. Papahadjopoulos, W.J. Vail, K. Jacobson, and G. Poste, Biochim. Biophys. Acta., 394(1975)483.

52. N. Nakashima, S. Asakuma, and T. Kunitake, J. Am. Chem. Soc., 107(1985)509.

53. D.G. Rhodes, S. Blechner, P.E. Schoen, and P. Yager, Biophys. Journal, 51(1987)527a.

54. J. Wilshut, N. Duzgunes, D. Hoekstra, and D. Papahadjopoulos, Biochem., 24(1985)8.

55. A. Portis, C. Newton, W. Pangborn, and D. Papahadjopoulos, Biochem., 18(1979)780.

DEVELOPMENT OF A SYNTHETIC PROTEIN ADHESIVE

Judith P. Kitchell, PhD and Charles C. Stauffer

Dynatech Scientific, Inc.
Cambridge, Massachusetts

Overview

New adhesives that have increased simplicity of application, milder setting conditions, and reduced setting times are required for many structural applications. It is also desirable to develop adhesives that may be applied without the need for special apparatus or technical skills. Repairs to naval aircraft, for example, could be made utilizing such a material on carriers or at remote airfields, reducing downtimes and repair costs. New materials should, of course, compare favorably with available adhesives in strength and resistance to environmental challenges.

To achieve these goals, adhesive setting should be driven not only by local polymerization and cross-linking reactions, but to a large extent by the enthalpy and entropy of formation of an ordered macrostructure. Such organization can occur in short times at low temperatures when self-organizing polymers are incorporated in adhesive formulations. Biological molecules such as proteins are known to assemble spontaneously because of their unique linear structures. Many structural proteins, consisting of simple repetitive sequences, can be recreated synthetically. The intents of this study are: to identify the important structural features of natural proteins that function well in nonaqueous adhesive formulations; to design synthetic polymers offerring the same adhesive properties; and to prepare and evaluate these synthetic polymers.

While it is anticipated that protein-like adhesives could be tailored to many specific adherends, the present work targets aluminum/aluminum bonding. The proposed structure of a phosphoric acid anodized aluminum surface is shown in Figure 1. [Venables et al.; Applications of Surface Science 3, (1979) 88-98] It can be seen that the actual surface area of aluminum oxide is very large because the surface consists of 100 A diameter "whiskers" of perhaps 1,000 Å length. These are regularly spaced with gaps of about 400 Å. The successful adhesive will perform the following functions:

- penetrate and fill the gaps on the surface
- form many hydrogen bonds to the aluminum oxide
- develop a cohesive matrix
- retard moisture penetration

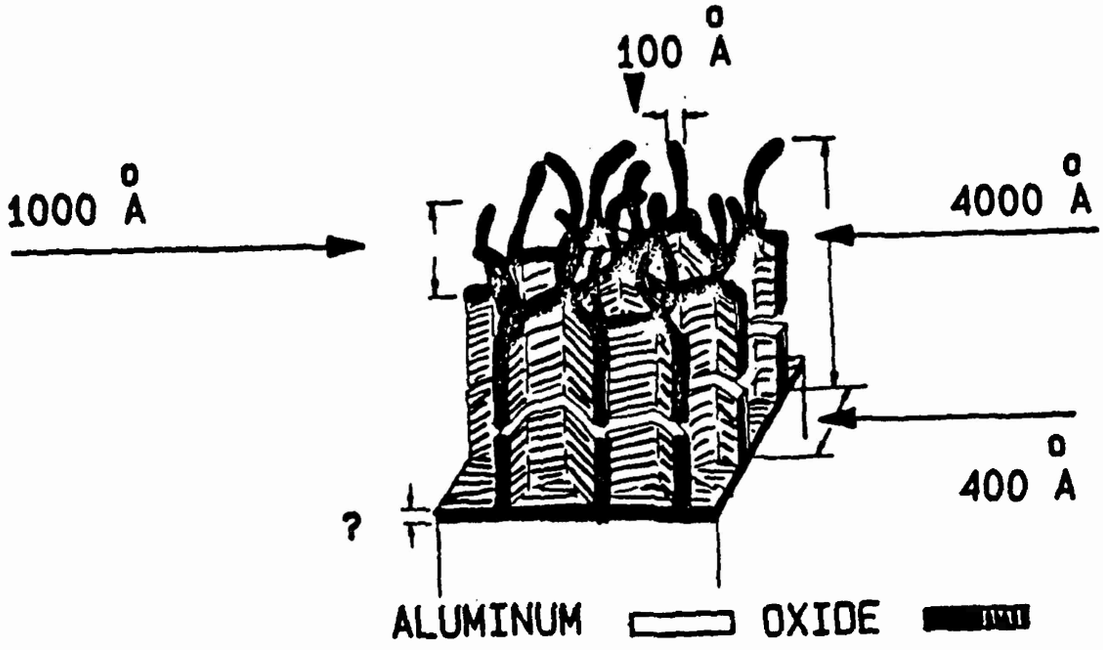

Figure 1. Proposed structure of the surface of phosphoric acid anodized aluminum. From Venables et al.

Approach

Choice of Proteins

Proteins are components of glues used in many commercial applications. These glues are based on the phenomenon of setting of aqueous, denatured proteins (for example, collagen or casein) with precipitants such as salts or cross-linkers. The adhesion attained with these glues to a variety of adherend types is often very good, probably because of the diversity of chemical microenvironments in the protein chains. Such adhesives are not suitable for high performance applications, however, because the adhesive bonds are susceptible to moisture. This is not surprising since they are prepared from soluble proteins and applied in aqueous solution.

A promising route to strong, fast setting, nonaqueous adhesives is the utilization of proteins in nonaqueous formulations. Some proteins which play a structural role in biological environments are not water soluble and are able to maintain rigid conformations in moist environments. Our development program began with screening of several fibrous proteins and reference proteins for ability to form cohesive and adhesive bonds without the incorporation of water. The proteins chosen were as follows:

Collagen - the role of collagen is to resist large physical stresses while offering little resistance to small stresses. Collagen is a component of aqueous glues. Little is known about the properties of dry collagen. Both tendon and hide collagen were chosen.

Elastin - elastin is unique because its function is energy storage. Elastin may be precipitated in fibrous form. It shows a volume decrease with increasing temperature over the range of interest, and might be expected to bind a surface well.

Keratin - keratins are probable model adhesives because of their high strength and insolubility. Wool, feather, and hard tissue keratins were chosen.

Silk - silk fibroin is a compact material with unique properties of strength and pliability. Silk is insoluble in water.

Casein - casein is globular, water soluble protein chosen for comparison with the other proteins.

The above proteins vary in amino acid composition. Some of these are shown in Table 1, where the amino acids have been grouped into descriptive categories for simplified comparison. It can be seen that the horn and feather keratins are distinctive in that they contain high proportions of bulky hydrophobic residues. The hard tissue keratin used in our work, termed "keratin" in the table, is particularly high in aromatic residues as well.

TABLE 1

Amino Acid Compositions of Several Proteins

TYPE	AROMATIC ***	HYDRO-PHOBIC ****	HYDROXY-PROLINE	CYS	POLAR *****
Horn Keratin	7.5%	15.1%		15.4%	62.3%
Keratin **	15.5%	14.3%		*	70.0%
Turkey Barbs	5.1%	11.4%		8.5%	75.4%
Wool Keratin	4.7%	8.2%		16.1%	71.2%
Tendon Collagen	3.3%	6.0%		*	79.0%
Animal Glue	1.4%	4.0%	9.5%	-	85.7%
Silk	5.5%	1.3%		-	93.4%

*CYS not measured **PRO not measured

***PHE, TYR ****MET, LEU, ILE *****ALL OTHERS

Test Methods

The miscibilities and reactivities of the proteins in various organic solvents and liquid organic cross-linkers were examined by placing protein and solution in test tubes, which were held at constant temperatures in a heat block. Samples were examined visually and by mechanical probing at various times.

The tack, cohesive, and adhesive properties of proteins in cross-linking formulations were evaluated first by pressing between two layers of aluminum foil with heat and pressure. Subsequently, various formulations were placed on the ends of aluminum coupons as shown in Figure 2. Aluminum was anodized in a phosphoric acid bath after a standard cleaning procedure. Priming with epoxy or protein solution was done by spraying or direct liquid application. Most of the results given in this report are on unanodized, unprimed coupons. The formulations were placed on the coupon ends by pouring or spatula, usually on both sheets. A die was used to align top and bottom sheets. The joined sheets were pressed under hydraulic pressure between heated plattens. After the bonding procedure, the five-fingered coupons were sawed into single fingers. The ASTM-1002 procedure for single lap shear testing was performed on an Instron mechanical tester.

Formulations

Solutions of protein, or of protein and cross-linker, were either prepared just prior to application, or else the dry ingredients were premixed and refrigerated until used. Solvents and crosslinkers examined included DMF, toluene, halocarbons, alcohols, organic acids and bases, phenol/formaldehyde mixtures, and styrene. Solvents were evaluated for ability to disperse or dissolve all components.

RESULTS AND CONCLUSIONS

The initial screening demonstrated that proteins without solvent did not coalesce when heated, even at temperatures up to a maximum of 180°C; they did char at this temperature, however. Additionally, dry protein did not coalesce when pressure and heat were combined. When solvents were utilized, some mixing was seen with casein, hard tissue keratin, and the collagens; the elastin, wool and silk were notable in immiscibility. None of the solvents facilitated coalescence or adherence when the mixtures were heated.

Screening also included solutions of protein with cross-linkers: phenol/paraformaldehyde mixtures and styrene. Again the elastin, wool, and silk were not miscible with these materials; however, the other proteins did mix and cross-linking did occur upon heating. The results of the qualitative evaluations of the mixtures of protein and cross-linker under heat and pressure for two collagens, casein, and hard tissue keratin are shown in Table 2. The keratin formulations were harder and displayed tighter bonding than the others shown.

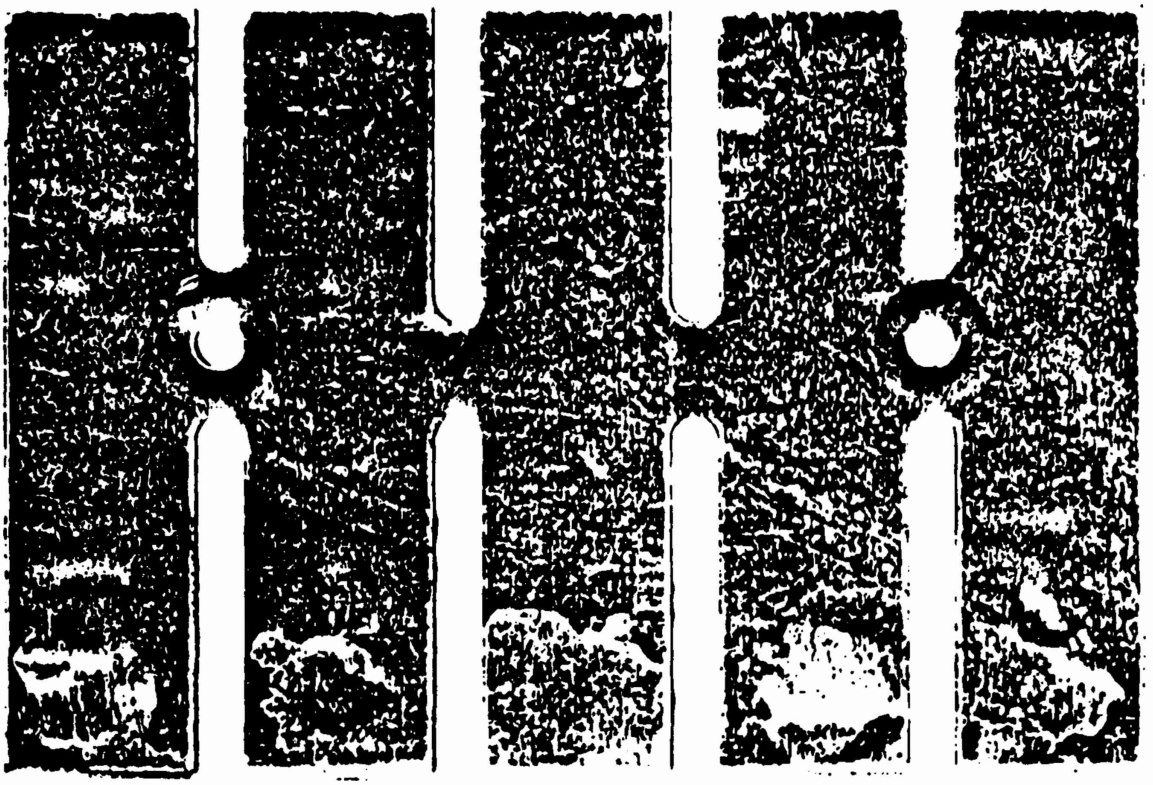

Figure 2. Aluminum coupons.

TABLE 2

TEMPERATURE/PRESSURE SCREENING ON FOIL

	HIDE COLLAGEN	TENDON COLLAGEN	CASEIN	KERATIN
Phenol/paraformaldehyde				
100 °C 15 psi 1 hr	bonds	coarse/tack	bonds	bonds
100 °C 40 psi 1 hr	bonds	coarse/sticky	glassy bond	hard bond
Styrene				
100 °C 15 psi 1 hr	hard bond	crumbles	hard bond	bond
100 °C 40 psi 1 hr	bonds	hard bond	coarse	hard bond

Quantitative measurements with aluminum coupons were made, formulating each protein in the solvent/cross-linker system which seemed to give the best dispersion and reactivity. The results obtained to date reinforce the qualitative observations of the screening tests. Some representative figures for single lap shear tests are shown in Table 3. The collagen and elastin show no adhesion in any of the formulations tested. The values shown for wool and silk (44 and 68 psi) are the only tests in which any adhesion was found; the strength may represent mainly the value of the nonprotein components of the formulations. The problems with these fibers are that as described previously, they are not really wetted by the solvent or reactants and also the fibers are bulky and springy, even when heated under pressure.

The hard tissue keratin performs very well, especially when applied in organic acid or base with paraformaldehyde. For our standard formulation, in tests on unanodized coupons, an average strength of 338.3 psi has been obtained. In these samples, however, the formulation had not fully set in the one hour pressing period, and the failure was adhesive. When surfaces are primed and the formulation is heated long enough for full setting, failure is cohesive. One shortcoming is that, owing to the low viscosity of the application solutions, much of the material is pressed out when pressure is applied during setting. Also, shrinkage of the protein upon solvent removal leaves some of the aluminum surface uncovered. Often the bond failure during testing appears to be due to lack of full surface coverage.

The hard tissue keratin obtained from a commercial source contains a certain amount of peptide material. The high and low molecular weight materials have been separated by dialysis. The low molecular weight fraction appears to contain some fatty material and does not give any adhesion to aluminum. The higher molecular weight keratin fraction, however, is greatly improved in tack and viscosity. While the pull strength obtained with this material on a keratin-primed aluminum surface (166 psi) is less than that obtained with unfractionated material, as shown in Table 3, the cohesion of the set formulation is increased. It is believed that the bonding will be greatly increased with further priming because the bond strength on a keratin-primed aluminum surface is about twice that obtained on unprimed aluminum.

At the initiation of the program, it was envisioned that the ideal formulation would include a helix forming protein which would self-align in a macrostructure stabilized by a number of cross-linking bonds. This is idealized in Figure 3. Presently, the concept of a stretched protein matrix, like a silk sheeted array, but with more bulky groups on one sheet face, seems a better model. This is shown schematically in Figure 4, where the proteins consist of alternating glycines and bulky groups (shown as knobs). It is of interest to consider that a sheet can offer a vast number of potential hydrogen bonds to adherend, and that a strong cohesive strength can be maintained in the hydrophobic planes.

TABLE 3

RESULTS OF SINGLE LAP SHEAR TESTS

FORMULATION 200° F/ 40 psi ~ 1 hr on aluminum coupons	Strength to Break Avg psi
tendon collagen/pf (4: 1) AcOH	0
elastin/pf (4: 1) AcOH	0
wool/pt/pf (1: 5: 10) DBA	44.0
silk/pt/pf (1: 10: 20) DBA	68
hi MWT keratin/pf (3: 1) AcOH	166
keratin/pf (3: 1) AcOH	338.3
EA8	2,050.0
EC2216 B/A 24 hr set time	980.0

pf - paraformaldehydpt - phenylpthalein DBA - dibenzylamine

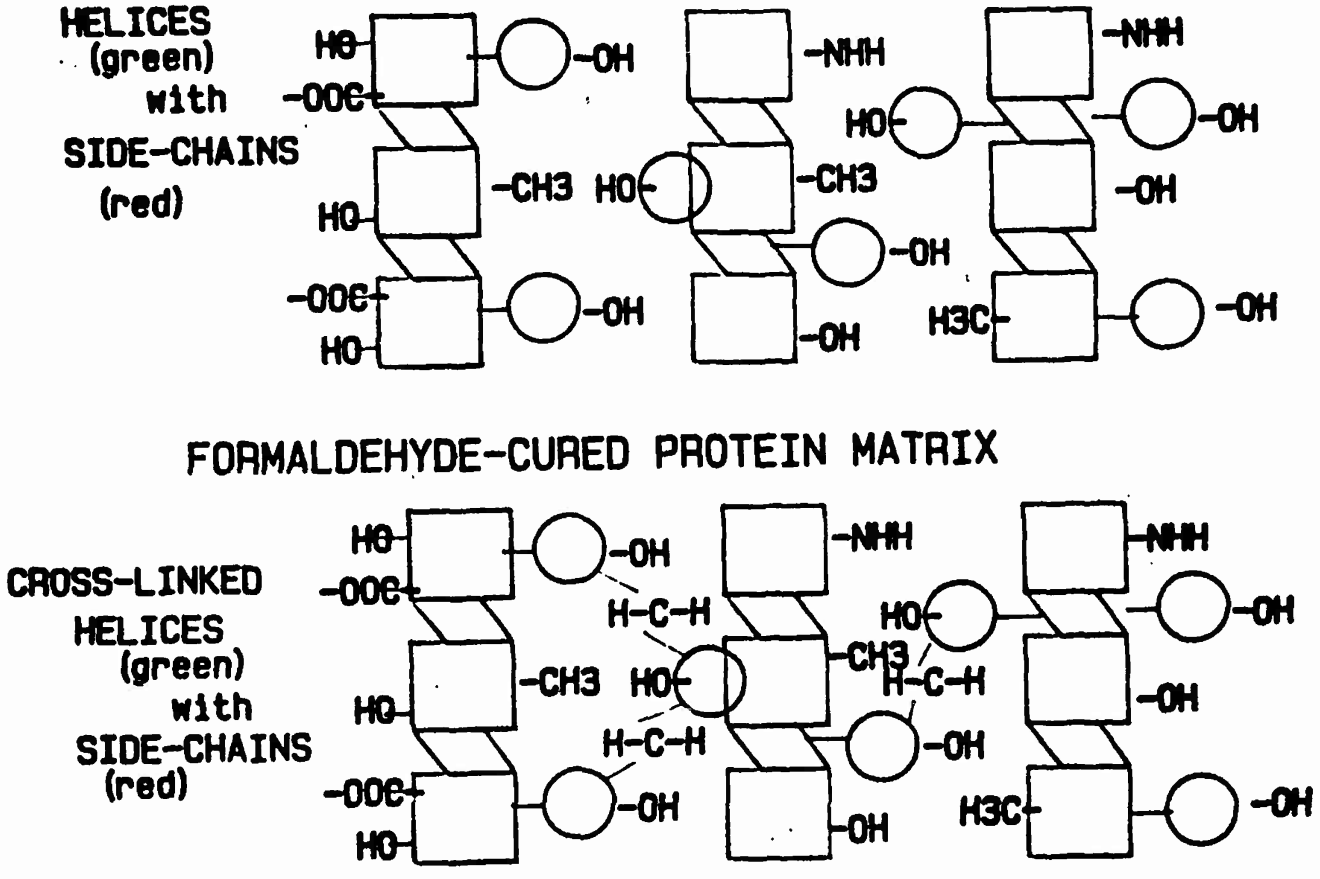

Figure 3. Idealized formulation.

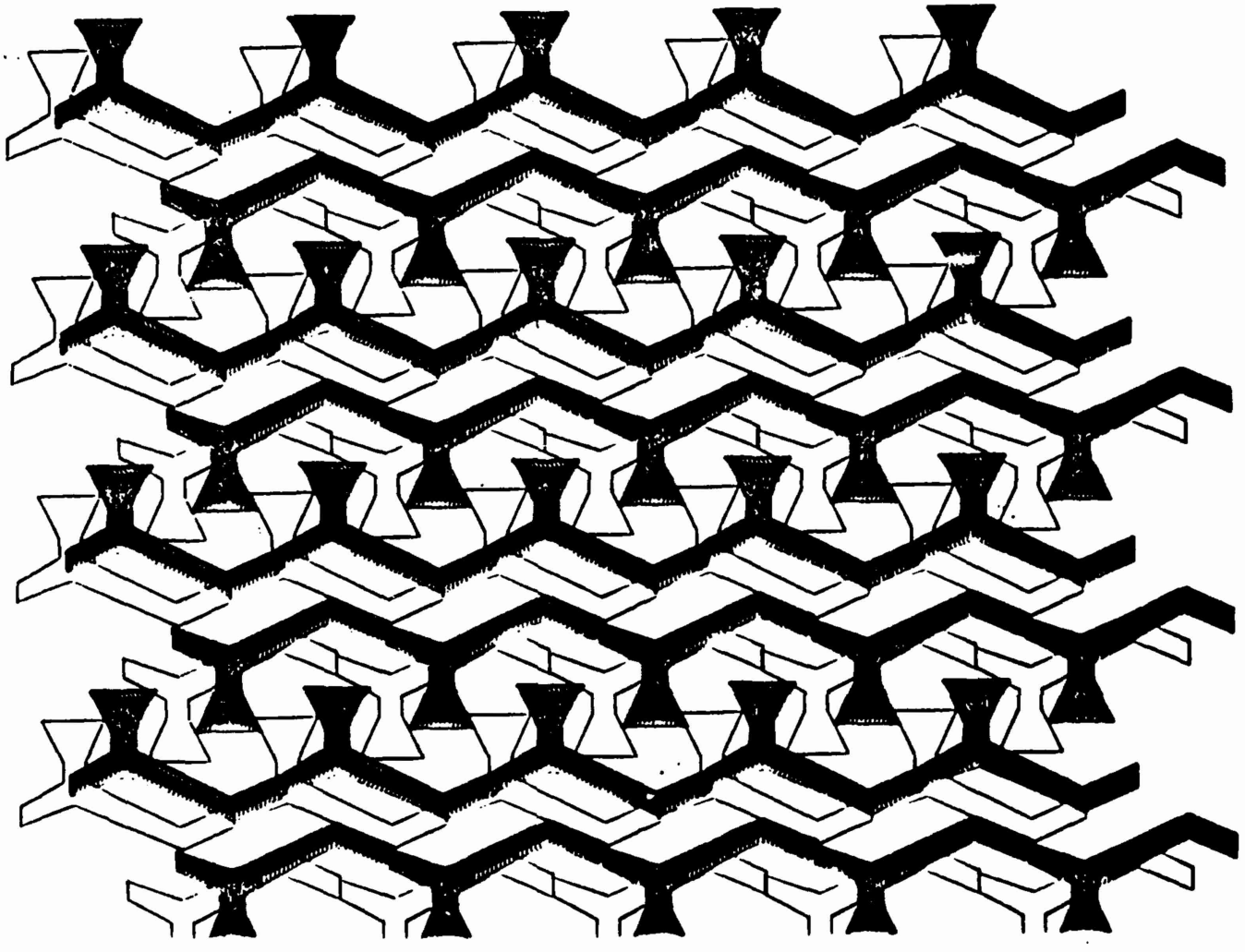

Figure 4. Stylized sheeted array

APPLICATIONS OF RECOMBINANT TECHNIQUES TO BOMBYX MORI FIBROIN

David S. Adams

Department of Biology and Biotechnology
Worcester Polytechnic Institute
Worcester, Massachusetts 01609

Abbreviations: AMT, 4'-aminomethyltrioxsalen; Bm-5, Bombyx ovarian-derived permanent cell line; bp, base pairs; EtBr, ethidium bromide; kb, kilobase pairs; N, nucleotide; pBm-1, recombinant plasmid containing one repeat of Bombyx ribosomal DNA; pBF-36, recombinant plasmid containing 3' repetitive fibroin sequences; pFb-900, recombinant plasmid containing solely fibroin intron DNA; PSG, posterior silk gland; SDS, sodium dodecyl sulfate; Sm, a type of lupus antibody originally isolated from a patient named Smith; SSPE, 0.18 M NaCl, 10mM Sodium Phosphate, 1 mM disodium EDTA, final [Na+]= 0.192 M; TBE, 90 mM Trisma base, 90 mM Borate, 2 mM EDTA, pH 8.3; TMG, trimethylguanosine.

Abstract

Psoralen crosslinking was used to isolate specific small RNA molecules associated with Bombyx mori fibroin messenger RNA (fmRNA) in vivo. The psoralen derivative 4'-aminomethyltrioxsalen (AMT) was perfused into the posterior silk gland (PSG) of fifth-instar larvae, a tissue homogenate was prepared, and covalent crosslinks between RNA molecules were induced by irradiation of the homogenate with longwave ultraviolet light. Total cellular RNA was isolated from the homogenate, and specific fmRNA fractions were purified by hybridization-selection. Total fmRNA was isolated from total cellular RNA by hybridizing to cloned fibroin cDNA representing the 3' region of the gene. This fraction was found to be devoid of pre-fmRNA, thus it represents mature fmRNA. Pre-fmRNA was isolated from total cellular RNA by annealing to DNA containing fibroin intron sequences. The psoralen crosslink was reversed by irradiation of the specific RNA fractions with shortwave ultraviolet light, and the released sRNAs were characterized. Two distinct sRNAs (with sizes of 196 and 163 N) crosslinked to pre-fmRNA. These sRNAs most probably represent U1 and U2b sRNAs, which have been shown to function in mRNA splicing in vertebrates. three distinct sRNAs crosslinked to mature fmRNA. The three sRNAs (named F1, F2, and F3) have sizes approximately 240, 225, and 174 N long, respectively. None of these latter crosslinked sRNAs are capped with trimethylguanosine, or are associated with the lupus type-Sm antigen, thus initially they do not appear to be related to the well-characterized U-RNAs of vertebrates. Interestingly, our data indicate although some Bombyx tissue have two types of U2 (U2a and U2b), and several types of U1, only U2b and one U1-subtype are found in large quantities in the PSG and also crosslink to pre-fmRNA. Our data suggest that molecules U2b and the PSG-U1 may function in the splicing of pre-fmRNA, and that these two molecules only temporarily associate with fmRNA.

Introduction

Our laboratory is interested in the developmental control of gene expression in invertebrate organisms. One system we are currently analyzing is the transcription of the fibroin gene in the lepidopteran Bombyx mori, an organism well suited for an analysis of development. Specifically, we are interested in the role of small RNA molecules (sRNAs) in the splicing of fibroin mRNA (fmRNA) in the posterior silk gland (PSG). Much information is available concerning fibroin gene expression. The PSG of late fifth-instar larvae is a tissue highly specialized for the production of one major gene product, fibroin (for reviews see: Suzuki, 1975; Goldsmith and Kafatos, 1984). On day 6 of the fifth-instar, fmRNA represents 3.5% of total cellular RNA, and 90% of total polysomal mRNA. Although there is only one fibroin gene per haploid genome (Lizardi and Brown, 1975), due to a high degree of polyploidy in the gland, each PSG cell actually contains ~400,000 fibroin genes. The polyploidization represents a repeated uniform replication of the entire genome, rather than a specific amplification of the fibroin gene (Suzuki et al., 1972). The factors responsible for the massive synthesis of fibroin protein include: 1) a selective transcription of fibroin genes, and 2) a stabilization of the fmRNA transcripts (Ibid.). During maximal transcription, fibroin DNA is transcribed at the extremely high rate of ~13 molecules/gene/min. A "Pribnow-type"(TATA/GATG) sequence TATAAAA is located at position -30 to -24 upstream of the cap site (Tsujimoto and Suzuki, 1979a). The sequence of the fibroin gene (including the 5' flanking, mRNA coding, entire intervening, and protein coding regions) has been determined (Tsujimoto and Suzuki, 1979b) from genomic clones (Ohshima and Suzuki, 1977).

The fmRNA transcript is very long (~16 kb, 5.8 x 10^6 daltons) and has a 100N 3' poly(A) tail (Lizardi et al., 1975). Figure 1 shows a diagrammatic representation of the fibroin gene, its transcription product, and protein. About 60% of fmRNA has a fully methylated cap, and the remaining 40% an unmethylated cap (Tsujimoto and Suzuki, 1979a). A 970N intron is located 64-66N from the cap site. The 5' donor splice site occurs at position 64-66, and 3' acceptor site at position 1034-1036 (Tsujimoto and Suzuki, 1979b). Both the 5' and 3' splice junctions share homologous segments of about 10N with the published sequences of -globin (mammal), immunoglobulin (mammal), and ovalbumin (avian) genes (Ibid.). The fmRNA transcript is processed to a mature messenger RNA by removal of the single intron (Lizardi, 1976).

In this paper, we describe the use of the psoralen derivative 4'-aminomethyltrioxsalen (AMT) in the crosslinking of specific sRNAs to fibroin mRNA in vivo. We found three distinct sRNAs crosslinked to mature fmRNA. The three sRNAs (named F1, F2, and F3) have sizes approximately 240, 225, and 174 N long, respectively. None of these crosslinked sRNAs are capped with trimethylguanosine, or are associated with the lupus type-Sm antigen. In contrast, two sRNAs (with sizes of 196 and 163 N) crosslinked to pre-fmRNA. These latter sRNAs may represent U2b and U1 sRNAs, which have been shown to function in mRNA splicing in vertebrates.

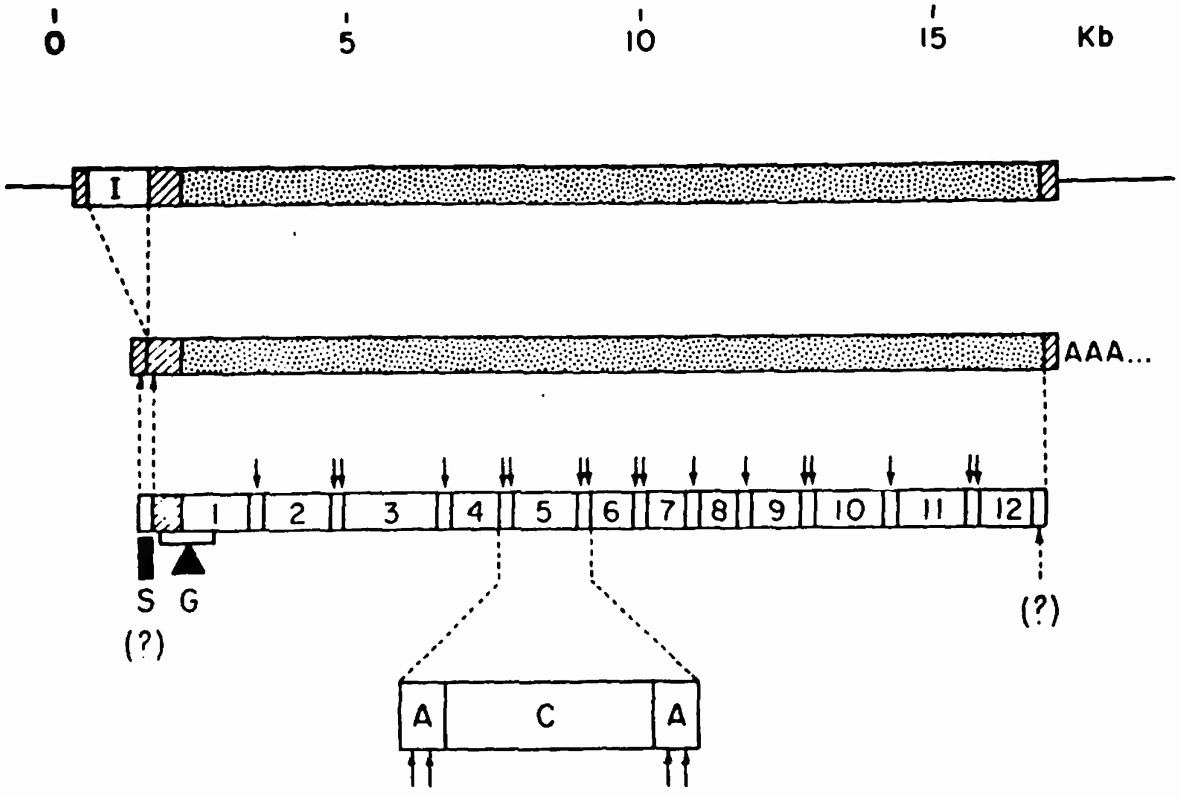

Figure 1. Map of the Bombyx mori Fibroin Gene, Transcript, and Protein. The fibroin gene is represented by the boxed region. The clear boxed region represents the single 970 N intron. Crosshatched and stipled boxed regions represent unique and repetitive fibroin sequences, respectively. the position of the poly(A) addition site is marked with "AAA" on the mature fmRNA. "S" denotes the position of the presumed signal sequence on the protein. Alternating amorphous and crystalline regions withing the repetitive region of the protein are denoted by "A" and "C", respectively. Arrows show the position of several useful restriction sites. This figure was adapted from Gage and Manning (1980).

Materials and Methods

Biological Material: Bombyx mori larvae (strain Gunka x Hoshun) were raised, and Bm-5 cells (a Bombyx ovarian-derived permanent cell line) were cultured as described previously (Adams et al., 1984, 1985, 1986, 1987). Radiolabeling of the larvae or cell line with ^{32}P-orthophosphate (New England Nuclear) or ^{3}H-uridine was for 24 hrs as described (Ibid.).

Isolation of DNA and RNA: Supercoiled plasmid DNA was isolated from chloramphenicol-amplified E. coli cultures by an alkaline/SDS procedure as we described (Adams et al., 1986). It was purified by EtBr/CsCl equilibrium density centrifugation followed by exclusion chromatography (Sepharose CL-4B, Bio-Rad). Total cellular RNA was isolated from posterior silk glands or Bm-5 cells as we described previously (Adams et al., 1984, 1985) using the proteinase K/sodium perchlorate procedure (Lizardi and Engelberg, 1979).

Immunoprecipitations: sRNAs were precipitated from nuclear lysates with lupus type-Sm IgG, or from total cellular RNA with anti-TMG IgG as described (Adams et al., 1984; 1985; 1987).

Crosslinking of RNA in the Posterior Silk Gland: The posterior silk glands of four larvae (day 6 of the fifth-instar) were dissected, rinsed in NET Buffer (50 mM Tris-HCl pH 7.5, 150 mM NaCl, 5mM EDTA), and then resuspended at 0°C in 4.0 mL of AMT Stock [2.0 mg/mL of 4'-aminomethyltrioxsalen hydrochloride (synthesized in our laboratory according to Isaacs et al., 1977) dissolved in NET Buffer]. The glands were incubated for 30 min at 0°C to allow penetration of the AMT. They were then homogenized in a glass ounce homogenizer (type A), and the lysate was transferred to a sterile plastic petri dish floating in ice water in a 4°C cold room. The lysate was irradiated for 90 min using 366 nm UV light (UV-Products Transilluminator, 6500 $\mu W/cm^2$ at the filter surface) with the lamp flush with the top of the petri dish. During this illumination, the lysate was stirred occasionally. Total cellular RNA was then extracted using the sodium perchlorate procedure developed in our laboratory (Lizardi and Engelberg, 1979). Fibroin-mRNA was then isolated from the AMT-treated material by hybridization-selection (see below). The RNA was labeled to high-specific-activity using T4-RNA-ligase (P-L Biochemicals) and [5'-^{32}P]-cytidine bisphosphate (NEN) (England and Uhlenbeck, 1978). The RNAs were repurified by extraction with sodium perchlorate, ethanol-precipitated, and dissolved in 20 µL of sterile water.

Denaturing formamide/sucrose gradients were used to rid noncrosslinked sRNAs from the high-molecular-weight fibroin-mRNA. The 20 µL aqueous sample was mixed with 200 µL of 5% sucrose in formamide, heated at 65°C for 4 min, and layered onto gradients containing 5-20% sucrose in 90% deionized formamide, 10mM Tris-Base, 1 mM EDTA, pH adjusted to 7.5 (Suzuki and Brown, 1972). The 12 mL gradients (14 x 95 mm) were centrifuged at 40,000 RPM for 12 h at 40°C in a SW 40Ti Rotor.

Radiolabeled total PSG RNA was used as a marker since formamide absorbs ultraviolet irradiation preventing spectrophotometric analysis of unlabled markers. Approximately 24 fractions were collected per gradient (0.5 mL/fraction). The fractions containing fibroin-mRNA (6 tubes, 3 mL) were pooled and ethanol-precipitated using 10 µg of carrier tRNA The pellet was dissolved in 10µL of sterile TE Buffer (10 mM Tris-HCl pH 7.5, 1mM EDTA) and was aliquoted into three 0.5 mL plastic eppendorf tubes 3 µL/tube). These tubes (1,2, & 3) were illuminated for 0 min, 2 min, and 60 min, respectively, with 254 nm UV light (UV-Products Transilluminator, 7000 $\mu W/cm^2$) at the filter surface) with the lamp flush with the surface of the eppendorf tube. The preparations were then lyophilized, dissolved in 6 µL of electrophoresis buffer, and electrophoresed as we described previously (Adams et al., 1984, 1985, 1987).

Bombyx Recombinant DNA Clones: Recombinant plasmids containing Bombyx DNA used in this study are listed below:

1. pFb-900: a 902 bp PSG genomic fragment which contains DNA solely within the fibroin intron (from the HaeIII site at position 119 to the HpaI site at position 1021) inserted into the EcoRI site of pBR-322 by AT-tailing. Phenotypic selection: AMP^r, Tet^r. Total length = 5264 bp. This subclone of pFb-29 was prepared by Dr. Seiji Kamijo of our laboratory.

2. pBF-36: a 1.3 kb cDNA complementary to the 3' end of fmRNA to the poly(A) site, inserted into the EcoRI site of pMB9 by AT-tailing (Gage and Manning, 1980). Phenotypic selection: Tet^r. Total vector length = 6685 bp. Supplied by J. Morrow.

3. pBm-1: 6.9×10^6 daltons of EcoRI digested middle silk gland DNA containing one repeat of Bombyx ribosomal DNA (18S, 5.8S, 28S, spacers) inserted into the EcoRI site of RSF2124 (Manning et al., 1978). Phenotype selection: AMP^r, $ColE1^-$. Total length = 21.8 kb, total MW = 14.2×10^6 daltons. Provided by D. Samols.

Isolation of RNA by Hybridization-Selection: Plasmids containing fibroin DNA were linearized by restriction digestion. They were heat-denatured and then hybridized to ^{32}P-labeled (24 hrs, in vivo) total PSG RNA as described (Thireos and Kafatos, 1980) except the incubation temperatures and times were altered (see LEGENDS). The second incubation (to renature the DNA without displacing the hybridization RNA) was conducted as described (Hutton, 1977). The material was then chromatographed on a column (1.5 x 17.0 cm, 25 mL bed volume) containing Biogel A-150m using a high-salt buffer as described (Thireos and Kafatos, 1980). The column flow rate was adjusted to 3.0 mL/h. Each column fraction contained 0.5 mL, and was ethanol-precipitated using transfer RNA as a carrier.

The RNA pellets were either used in sRNA crosslinking experiments or were assayed by electrophoresis. For electrophoresis, the pellets were dissolved in 20 µL of sample buffer (40 mM triethanolamine-phosphate, pH 7.5, 2 mM EDTA, 2.0 M formaldehyde, 50% freshly deionized formamide, 6% sucrose, 0.04% xylene cyanole, and 0.04% bromphenol blue), and were electrophoresed on horizontal gels (3 mm thick, 14 cm wide, 17 cm long) containing 1% agarose, 40 mM triethanolamine-phosphate pH 7.5, 2 mM EDTA, 0.1% SDS, and 1.0 M formaldehyde (Boedtker, 1971). Pre-electrophoresis was for 30 min at 90 volts. Electrophoresis was for 13 h at 70 volts. The gels were then washed for 30 min in fixation solution (20% methanol, 10% acetic acid, 1.5% glycerol) to precipitate the RNA into the matrix of the gel, thereby preventing RNA diffusion and band smearing. After drying, the gel was exposed for autoradiography at -70°C using one intensifying screen.

Computer Analysis of Nucleotide Sequence Information: RNA to be sequenced was end-labeled with pCp (as described above) and sequenced by chemical methods (Peattie, 1979) as we described (Adams et al., 1985; 1987; Skinner and Adams, 1987). the computer program "FASTN" (Lipman and Pearson 1985) was used to search the GenBank DNA sequence database.

Results and Discussion

This project was undertaken to identify, isolate, and characterize specific sRNAs that participate in the splicing of fibroin mRNA. Data accumulated so far using a variety of vertebrate systems (for reviews, see: Lerner and Steitz, 1981; Busch et al., 1982; Maniatis and Reed, 1987) indicate that those sRNAs which participate in mRNA-splicing (U1, U2, U4/U6, U5, and possibly others) associate with the precursor by base-paired hydrogen bonding. For U1, the binding has been localized to the 5' splice junction sequence. U2 has been shown to bind the branch site for lariat formation. U5 binds the 3' splice junction sequence (however this particular binding may be facilitated by a protein). Although the vertebrate sRNAs are relatively abundant (approximately 10^6 copies/cell for U1, 10^4-10^5 copies/cell for other U-RNAs), preliminary evidence indicates that these molecules are 10-100X less abundant in the invertebrates (Wise et al., 1983; Adams et al., 1985). Since these regulatory sRNAs are probably present in low concentrations with Bombyx cells, they may be experimentally identifiable only as they interact with a mRNA. For this reason, we chose to isolate candidate sRNAs on the basis of their ability to bind mRNA in vivo through base-paired interaction.

We chose to analyze the sRNAs associated with one specific mRNA, fibroin mRNA (fmRNA). We chose this system for analysis of sRNA splicing function for several reasons: 1) The splicing of a specific species of messenger RNA (fmRNA) can be analyzed. This is particularly important because specific sRNA regulatory mechanisms may be completely obscured at the level of total cellular mRNA. 2) The tier of sRNA/fmRNA complexes in the posterior silk gland may be increased to accommodate the drastic increases in fmRNA synthesis observed in this gland late in the fifth-instar; this should facilitate the isolation of candidate splicing

sRNAs. 3) Developmental and tissue-specific analyses are easy to perform. Both developmental and tissue-specific variations have been observed in the U-RNAs of a variety of organisms (Forbes et al., 1983; Zeller et al., 1983; Forbes et al., 1984). Knowledge of such variations can provide some insight into potential functions of specific sRNAs. Large amounts of developmentally interesting tissues are easy to dissect. These tissues include the posterior silk gland, the fat body, and the ovarian follicular cells. Each tissue is easy to manipulate experimentally, and can inexpensively be grown in large enough quantities to be analyzed biochemically. 4) An immortalized Bombyx cell line is available. The Bm-5 cell line was originally derived from ovarian tissue (Grace, 1967). This cell line allows the in vivo labeling of RNA to high specific activity (Adams et al., 1985), and also allows developmental comparisons of immortalized versus differentiated tissues to be performed. 5) Several genomic DNA clones are currently available which represent different regions of the fibroin gene. These regions include the 3' flanking, 5' flanking, internal repetitive, and intron portions of the gene. Restriction fragments generated from these clones can be used to isolate specific fibroin RNA populations.

Isolation of Specific RNA Fractions by Hybridization-Selection: The selection procedure we used to isolate fmRNA is analogous to the one used to isolate individual chorion mRNAs from Antheraea polyphemus (Thireos and Kafatos, 1980). During this procedure, denatured plasmid DNA is first hybridized to total cellular RNA under conditions that favor the formation of specific RNA/DNA hybrids (Thomas et al., 1976; Casey and Davidson, 1977). The hybridization conditions are then altered to allow the complete renaturation of the DNA without displacing the hybridized RNA (Hutton, 1977). Chromatography of this solution on Agarose A-150m (developed in solutions containing high concentrations of salt) excludes the plasmid DNA larger that 3kb (including molecules with R-loops), whereas nonhybridized RNA is found in the included volume (Woolford and Roshbash, 1979). The advantage of the technique over other hybridization-selection methods is that it does not entail the time-consuming attachment of plasmid DNAs to a solid support, and both the hybridization and chromatographic conditions can be altered experimentally to provide the purest mRNA preparation.

We used this procedure to isolate three specific RNA fractions from Bombyx posterior silk glands. The three recombinant plasmids used for the selection are listed in MATERIALS AND METHODS. Size verification of each clone is shown in Figure 2. pBm-1 is a control plasmid representing a ribosomal repeat unit, which should fish rRNAs. pBF-36 represents the 3' repetitive end of the fibroin gene, which should fish total cellular fmRNA. pFb-900 represents intron sequence of the fibroin gene, which should fish pre-fmRNA.

Electrophoresis of the RNA fractions excluded from the agarose column (Figures 3 & 4) was used to provide information on the purity and composition of the RNA fractions. The RNA fraction complementary to pBm-1 (Figure 3) contained 99% (by mass) mature ribosomal RNAs and their precursors. The fraction isolated using pBF-36 (Figure 4) contained >95%

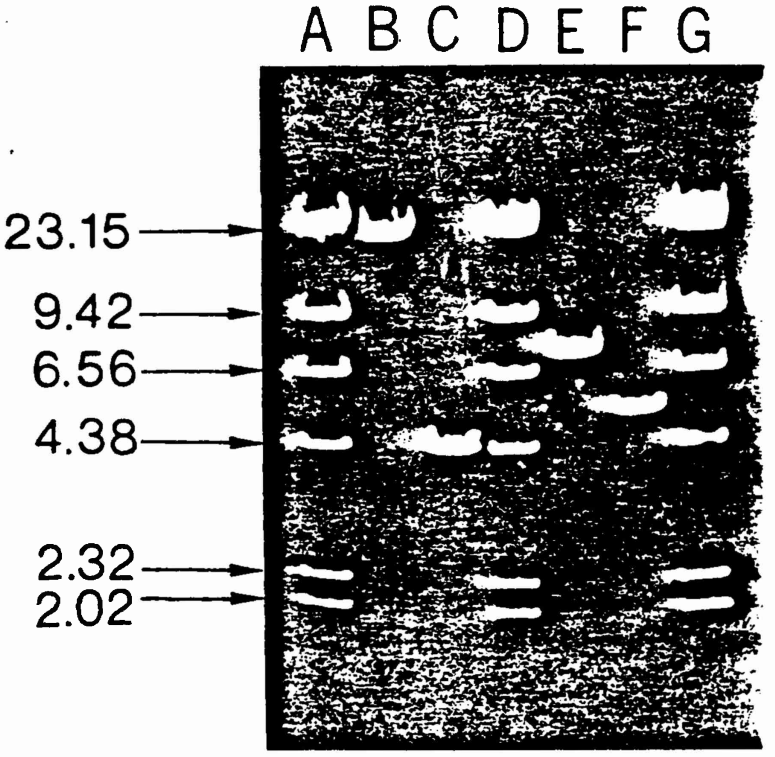

Figure 2. Recombinant Clones Containing Bombyx Fibroin DNA. Plasmid DNAs were purified by cesium chloride density centrifugation as described in MATERIALS AND METHODS and were electorphoresed for 2.5 hrs at 60 volts in a 10 cm gel which contained 0.6% agarose and 90 mM TBE Buffer pH 8.0. The gel was stained with EtBr (0.5 g/ml) for 60 min. The bands were visualized with a 360 nm transilluminator and photographed. Marker DNAs were as follows: Lanes A, D, and G: 0.5 g of lambda DNA digested with HindIII (the sizes of the HindIII fragments are listed (in Kb) in the left-hand margin), and Lane C: 0.2 g of pBR-322 DNA (4.4 Kb) digested with HindIII. Lane B contains 0.2 g of pBm-1 DNA (21.8 Kb) digested with HindIII. Lane E contains 0.2 g of pBF-36 DNA (6.68 Kb) digested with HindIII. Lane F contains 0.2 g of pFb-900 DNA (5.26 Kb) digested with HindIII.

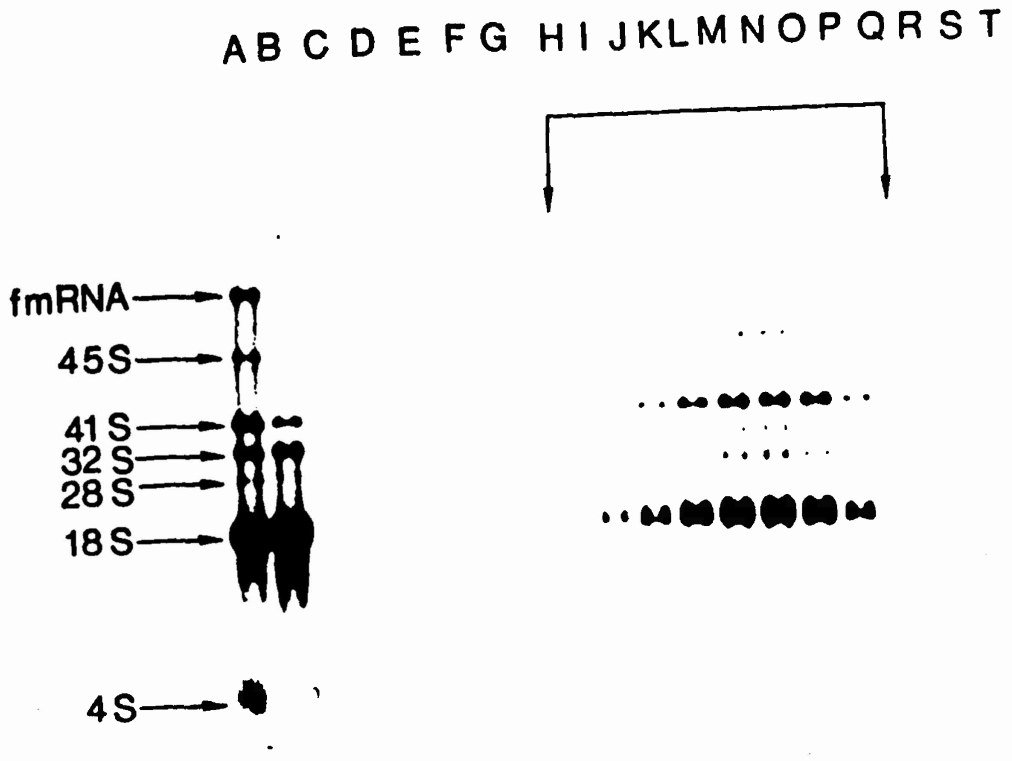

Figure 3. Hybridization-Selection of Bombyx Ribosomal ^{32}RNA. Larvae were labeled from day 5 to day 6 of the fifth-instar with ^{32}P-orthophosphate, and total cellular RNA was isolated from the posterior silk gland. Hybridization of 75 μg of this RNA to 25μg of HindIII digested pBm-1 DNA (1ØX DNA sequence excess) was at 55°C for 6Ø min as described in MATERIALS AND METHODS. RNA/DNA hybrids isolated by exclusion chromatography were collected by ethanol precipitation, denatured, and electorphoresed for 12 hrs at 7Ø volts in 25 cm gels containing 1.0% agarose, 4Ø mM triethanolamine phosphate pH 7.5, 1.Ø M formaldehyde, 2.Ø mM EDTA, and Ø.1% SDS. Lanes A and B are markers. Lane A represents 9,ØØØ CPM of total cellular PSG RNA prior to hybridization. The sizes are (in sedimentation coefficient units) of the major bands are marked in the left-hand side of the figure. 4.ØS represents tRNA, 18S-45S bands represent ribosomal RNAs, and fmRNA represents the 47S (17 Kb) fibroin mRNA. Lane B represents 9,ØØØ CPM of total cellular PSG RNA included in the column. Lanes T-C represent excluded column fractions 11 to 28 (Ø.5 ml per fraction), respectively. Autoradiographic exposure was for 5 days at -7Ø°C intensifying screen.

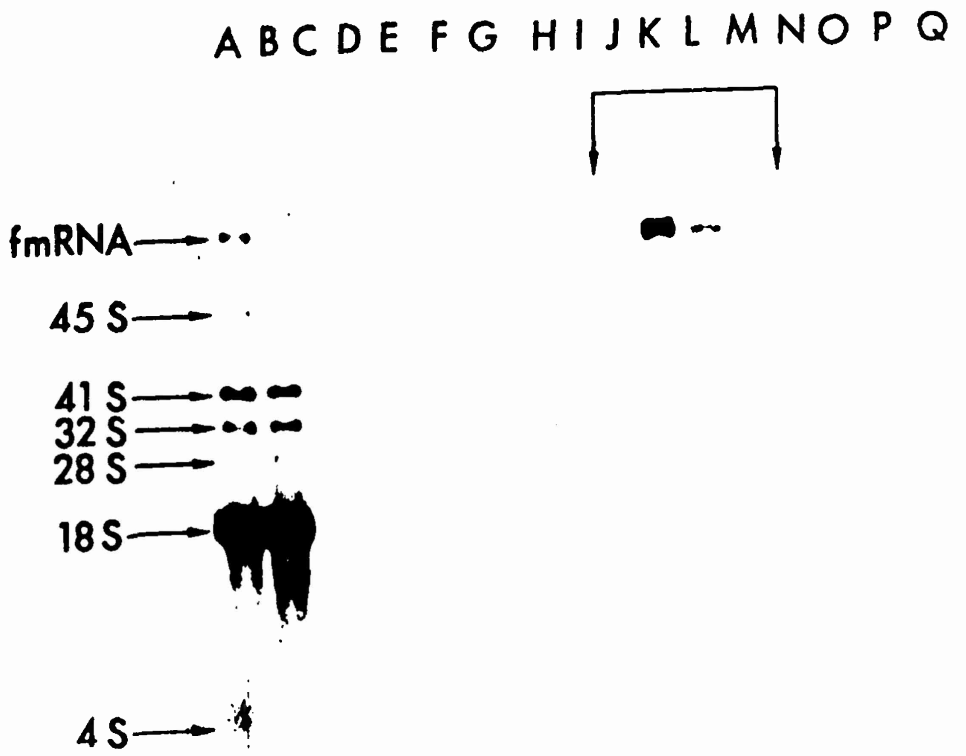

Figure 4. Hybridization-Selection of Bombyx Fibroin mRNA. Details are identical to Figure 3 except that: 20 µg of HindIII digested pBF-36 DNA was hybridized to 36 µg of total cellular RNA, hybridization was at 65°C for 15 min, marker RNA was 45000 CPM, and autoradiographic exposure was for 2 days at -70°C with one intensifying screen. Excluded fractions containing the fmRNA (J-M) are marked.

(by mass) total fmRNA. The purified 47 S fmRNA is found in the excluded column fractions (gel lanes I-M). No contamination with the highly abundant transfer RNAs (4 S) or ribosomal RNAs (45, 41, 32, 28, 18 S) can be discerned in these lanes. No pre-fmRNA (which would be ~17 kb) is detectable in the fraction, which is not surprising since this pre-RNA only represents a small portion of the total fmRNA in the cell (Lizardi, 1976). We estimate that the yield of fmRNA using this technique is approximately 85% [125,772 CPM were applied to the column; since day 6 RNA contains 3.5% fmRNA (Suzuki, 1975), we applied 4,402 CPM fmRNA to the column; 3,939 CPM were excluded from the column, 95% of which (3,742 CPM) is fmRNA (electrophoretic analysis); 3742/4402 = 0.85]. The RNA fraction isolated using pFb-900 (data not shown) contained 70% pre-fmRNA (as assayed by electrophoresis of S1-nuclease-digested radiolabeled intron-DNA which had been previously hybridized to unlabled fished-RNA under R-loop conditions). We conclude that our hybridization-selection protocol is efficient for isolating specific RNA populations.

Crosslinking of sRNAs to Fibroin mRNA: the purification of specific RNA populations by hybrid-selection requires standard R-loop nucleic acid reannealing in the presence of formamide. Under these conditions, sRNAs bound to the sequences will dissociate unless they are covalently crosslinked to the RNA being selected. To alleviate this problem, we used a newly discovered reversible nucleic acid crosslinking compound, 4'-aminomethyltrioxsalen (AMT), to join the sRNA/RNA sequences prior to purification of the latter by hybrid-selection. AMT (Isaacs et al., 1977) is a derivative of psoralen. Psoralens are crosslinking compounds which have proven to be quite useful for studying nucleic acid structures in vivo. They are planar heterocyclic compounds (isomers of the furocoumarin family) which can penetrate intact cells and form interstrand crosslinks between base residues of nucleic acid helices (DNA and RNA) upon irradiation with long-wavelength (365 nm) ultraviolet light. They have some medicinal applications in the UV-treatment of skin diseases, such as psoriasis and vitiligo.

In addition to psoralen-like properties, AMT has several properties that make it specifically well-suited for the analysis of RNA/RNA interactions in vivo. Among these properties are: 1) its ability to cross cell membranes and interact with RNA in all cellular compartments (Calvet and Pederson, 1979a, 1979b), which allows the experiments to be performed in vivo; 2) its reversibility (Rabin and Crothers, 1979), which allows previously crosslinked sRNAs to be analyzed; 3) its nonspecific base-reactive properties (Hochkeppel and Gordon, 1979), which allows short regions of RNA duplexes to be analyzed; and 4) its high solubility in aqueous solutions, which increases the concentration of the crosslinking compound available at a potential reactive site thereby allowing the analysis of rare low-abundance molecules. AMT has been used in other laboratories to demonstrate the in vivo interaction of U1-sRNA with high-molecular-weight nuclear RNA in HeLa cells (Calvet and Pederson, 1981).

We used AMT at its maximum solubility (2.0 mg/mL), and varied the time of exposure to the crosslink-inducing long-wavelength UV to optimize the crosslinking conditions for the maximal recovery of sRNAs while minimizing the UV-induced degradation of the RNA. As a test system, we developed conditions for the specific and efficient crosslinking (and reversal) of Bombyx 5.8 S ribosomal small RNA to 28 S rRNA. This specific system was used as our test system since 5.8 S rRNA is much more abundant than any of the sRNAs proposed to function in splicing (thus it is easier to detect), and the length of the base-paired interaction between these molecules is approximately the same as that demonstrated for the U1/pre-mRNA interaction. Since the posterior silk gland is relatively opaque to long-wavelength UV irradiation, gland homogenates were used as a source of crosslinked material. Conditions were established whereby 80% of total 5.8 S RNA could be crosslinked while leaving 100% of the free 5.0 S ribosomal RNA uncrosslinked (data not shown). About 50% of the crosslinked 5.8 S RNA could be released after irradiation with short-wavelength UV irradiation, with no detectable UV-induced strand-scission of the 5.8 S molecule. A significant finding was that the released 5.8 sRNA could serve as a suitable substrate for direct RNA sequencing (residual AMT monoadducts could have rendered large portions of the sequencing ladders unreadable thereby hindering identification of the crosslinked molecules). This will significantly aid future efforts to identify crosslinked sRNAs.

The crosslinking/reversal conditions established using the ribosomal RNA system were then applied to an analysis of sRNAs associated with fmRNA and its precursor. Total PSG RNA crosslinked as described for ribosomal RNA was used as a source of material for hybridization-selection. Purified RNA fractions were radiolabeled in vitro to high specific-activity using RNA ligase (England and Uhlenbeck, 1978), and the material was then irradiated at 260 nm to reverse the crosslink. Electrophoresis of the samples (Figure 5) was used to reveal sRNAs which were previously associated with the mRNAs. The RNA fraction isolated with pBF-36 containing total cellular fmRNA released three distinct sRNAs (arrows 1, 2, and 3, in Lane D of Figure 5). These three bands were not present in control fmRNA fractions which were prepared: 1) without AMT but were irradiated (data not shown); or 2) with AMT but were not irradiated (Lane B of Figure 5). Based on their migration, these molecules are 240, 225, and 174 N, respectively. Due to their ability to be crosslinked to fmRNA, we named the three molecules F1, F2, and F3, respectively (see Table 1). The RNA fraction enriched for pre-fmRNA released two sRNAs (data not shown). Based solely on their migration in polyacrylamide gels, they have sizes of 196 and 163 N. We conclude that different types of sRNAs associate with pre-fmRNA and fmRNA in vivo, and that the sRNAs associated with pre-fmRNA do not remain associated with the precursor throughout its lifetime.

Figure 5. sRNAs Crosslinked to Bombyx Fibroin mRNA. Crosslinking of sRNAs to PSG fibroin mRNA was performed as described in METHODS. The sRNAs were pCp-labeled, ethanol precipitated, and purified on denaturing formamide/sucrose gradients to rid noncovalently bound sRNAs. The fractions containing fibroin-mRNA were pooled, ethanol-precipitated, and dissolved in TE Buffer. The pooled sample was aliquoted into three 0.5 ml plastic eppendorf tubes (3 1/tube) and illuminated with 254 nm UV light for 0 min (Lane B), 2 min (Lane C), and 60 min (Lane D). Electrophoresis was described in Figure 6. Lane A represents 36,000 CPM of ^{32}P-labeled (24 hr, in vivo) total PSG RNA as a marker. Lanes B, C, and D each contain 2,700 CPM of RNA. The arrows marked 1, 2, and 3 indicate the positions of bands that appeared after reversal of the crosslink, which represent sRNAs F1, F2, F3, respectively, originally associated with the fibroin-messenger RNA. Exposure for autoradiography was 19 days at -70°C with one intensifying screen.

Identification and Characterization of Bombyx sRNAs:

We next set out to identify the sRNAs which crosslinked to fmRNA and pre-fmRNA. In addition to sizing the molecules, five other criteria were used to identify and characterize Bombyx sRNAs: 1) the presence of a trimethylguanosine 5' cap; 2) the presence of a lupus type-SM antigen; 3) developmental specificity; 4) primary sequence; and 5) secondary structure.

With the exception of U6, all vertebrate U-RNAs contain a 5' trimethylguanosine (TMG) cap structure. This cap constrasts with the 7-methylguanosine cap of mRNA, and provides a very strong criterion for the identification of U-RNAs. Antibodies against this structure have been produced (Luhrmann et al., 1982), and have greatly aided the identification, isolation, and characterization of U-RNAs in mouse (Bringmann et al., 1983), human KB cells (Smith and Eliceiri, 1983), pea (Krol et al., 1983), Bombyx (Adams et al., 1984; 1985) and Physarum (Adams et al., 1987). We used this antibody to identify and characterize Bombyx U-RNAs from the PSG (Figure 6). The antibody interacted with at least 12 sRNAs (lanes D & E of Figure 6; Table I). As expected, molecules U1-U7, and U9 interacted with the IgG. Unlike vertebrate U8, Bombyx U8 may not be capped with TMG. Although U1Ø exists in vertebrates, its correlate was not found in Bombyx. Molecules F1-F3 are not capped. Molecules U1 and U2b are the most abundant capped sRNAs in PSG, and they have exactly the same sizes as the two sRNAs that crosslinked to pre-fmRNA.

Antibodies isolated from the sera of human patients with the autoimmune disease systemic lupus erythematosus have been shown to interact with protein antigens associated with vertebrate U-RNAs (Lerner and Steitz, 1979; Lerner et al., 1980). Some evidence exists that lupus IgG also interact with invertebrate U-RNAs: successful precipitations have been performed in fall armyworm (Lerner et al., 1980), Drosophila (Mount and Steitz, 1981; Wooley et al., 1982), dinoflagellates (Reddy et al., 1983), and Physarum (Adams et al., 1987). Different types of the lupus disease produce antibodies with different specificities. We used antibodies of the type Sm (originally isolated from a patient named Smith) to characterize Bombyx U-RNAs since this type interacts with all U-RNAs (except U3) and would thus maximize our chances of characterizing the largest number of U-RNAs. Our data are shown in Figure 7. Our Sm-type IgG interacted with at least 1Ø sRNAs (see lane B of Figure 7, and Table I). Molecules U3a & b did not precipitate as expected. U9 did not precipitate, unlike vertebrate U9. U1Ø has not been found in Bombyx. F1-3 did not precipitate. U1 and U2b were precipitated the strongest, and these sRNAs have the same sizes as those crosslinked to pre-fmRNA.

We also analyzed the developmental expression of Bombyx sRNAs in two tissues: the highly-specialized PSG, and the immortal Bm-5 cell line (Figure 8). Superficially, the patterns of capped sRNAs look similar in the two tissues. Upon closer observation it can be seen that U1 and U2b are the most abundant capped molecules in PSG (Figure 6, lanes D & E; and Figure 8, lane 2), and that the immortal cell line has several U1s and a strong U2a (Figure 8, lane 1). Sequence analysis of each U1 subtype in

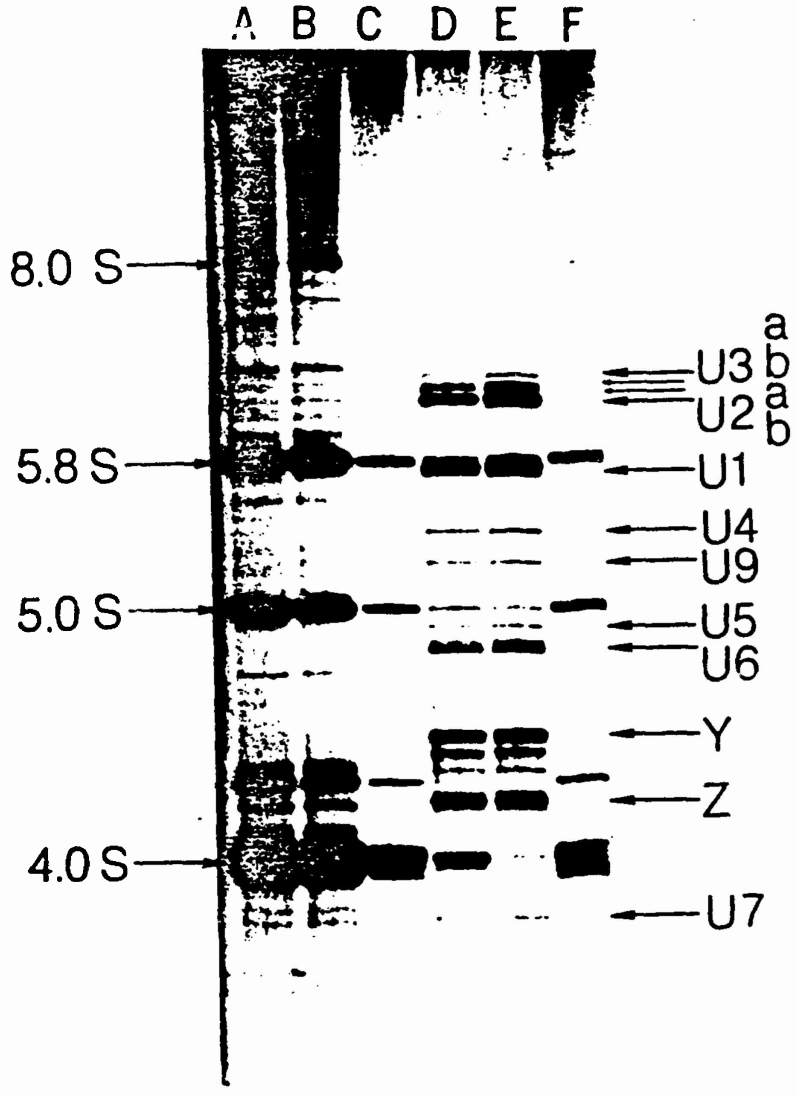

Figure 6. Bombyx Trimethylguanosine-Capped sRNAs. The gland RNA used for precipitation with TMG-IgG was labeled *in vivo* with ^{32}P-orthophosphate for 24 hrs. Lanes A & B, and C & F represent markers containing 80,000 CPM and 8,000 CPM, respectively, of total PSG RNA. Lanes D and E each contain 1,000 CPM of anti-cap-precipitated PSG RNA, where the matrix-bound RNA was washed with a low-stringency wash (Lane D) or high stringency (Lane E) wash. The low-stingency wash was with NET Buffer pH 7.5, 0.05% triton X-100. The high-stringency wash was with 0.4 M NaCl, 0.4 M sodium acetate, pH 5.0, 5mM EDTA, 50mM Tris-HCL, 0.05% triton X-100. Autoradiography was for 3 days at -70° with one screen.

TABLE 1

BOMBYX MORI SMALL RNAs

Tentative sRNA Designation*	Approximate Length (N)§	Presence of 5' TMG Cap	Presence of Lupus Type Sm Antigen	Crosslinked to fmRNA	Crosslinked to pre-fmRNA
8.0S	285	-	-	-	-
F1	240	-	-	+	-
F2	225	-	-	+	-
U3a	210	+	-	-	-
U3b	206	+	-	-	-
U2a	199	+	++	-	-
U2b	196	+++	+++	-	+
F3	174	-	-	+	-
5.8S	167	-	-	-	-
U1	163	+++	+++++	-	+
U8	155	-	+	-	-
U4	144	+	++	-	-
U9	131	+	-	-	-
5.0S	119	-	-	-	-
U5	115	+	++	-	-
U6	109	+	+	-	-
Y	96	++	+	-	-
Z	86	++	+	-	-
U10	--	-	-	-	-
U7	74	+	+	-	-

*Each of the major sRNAs was given a tentative designation based on its approximate length, the presence of a trimethylguanosine cap, the presence of a lupus type-Sm antigen, and (in some cases) nucleotide sequence analysis as described in RESULTS. Molecules F1-F3 are those which crosslinked with total cellular fibroin mRNA and have not been previously characterized. Molecules U2b and U1 crosslinked with pre-fmRNA.

§ The approximate sizes of the sRNAs were estimated from a plot of log of mobility versus square root of molecular weight (Adams et al., 1985) using HeLa cell sRNAs whose sizes are precisely known from complete nucleotide analysis (for a review, see: Reddy, 1985).

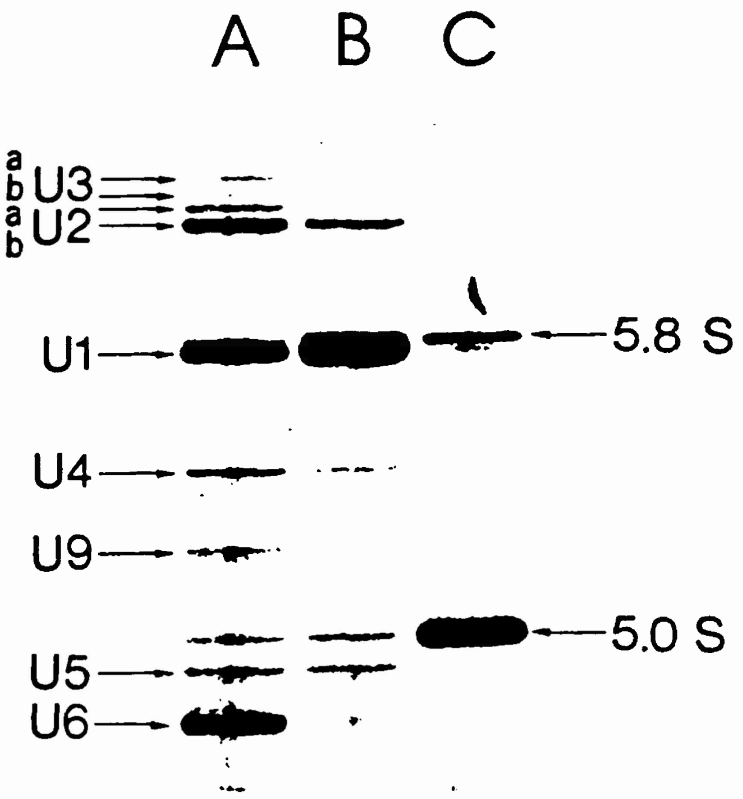

Figure 7. Bombyx Lupus Type-Sm sRNAs. Immunoprecipitation with lupus type-Sm IgG (Lane B) was performed on nuclear sonicates; immunoprecipitation with anti-cap IgG (Lane A) was performed on total PSF RNA (Lane C) isolated from day 6a larvae of the fifth-instar as described in METHODS. RNA was postlabeled with ^{32}P-pCp, and was electrophoresed for 7 hrs at 30 watts (constant power) through 40 cm gels containing 10% polyacrylamide (27:1), 8.0 M urea, and 45 mM TBE pH 8.3. During electrophoresis, the apparatus was placed in a 37°C cabinet; the temperature of the gel during the run was approximately 50°C. The anti-Sm-precipitated sRNAs (2,000 CPM) (Lane B) were chromatographed on Bio-Gel A (1.5 m) to remove tRNA which prevented efficient postlabeling of the U-RNAs. Lane A represents 2,000 CPM of pCp-labeled anti-cap-precipitated total PSG RNA. Lane C represents 5,000 CPM of pCp-labeled total PSG RNA as marker. Autoradiography was for 12 hrs at -70° with one intensifying screen.

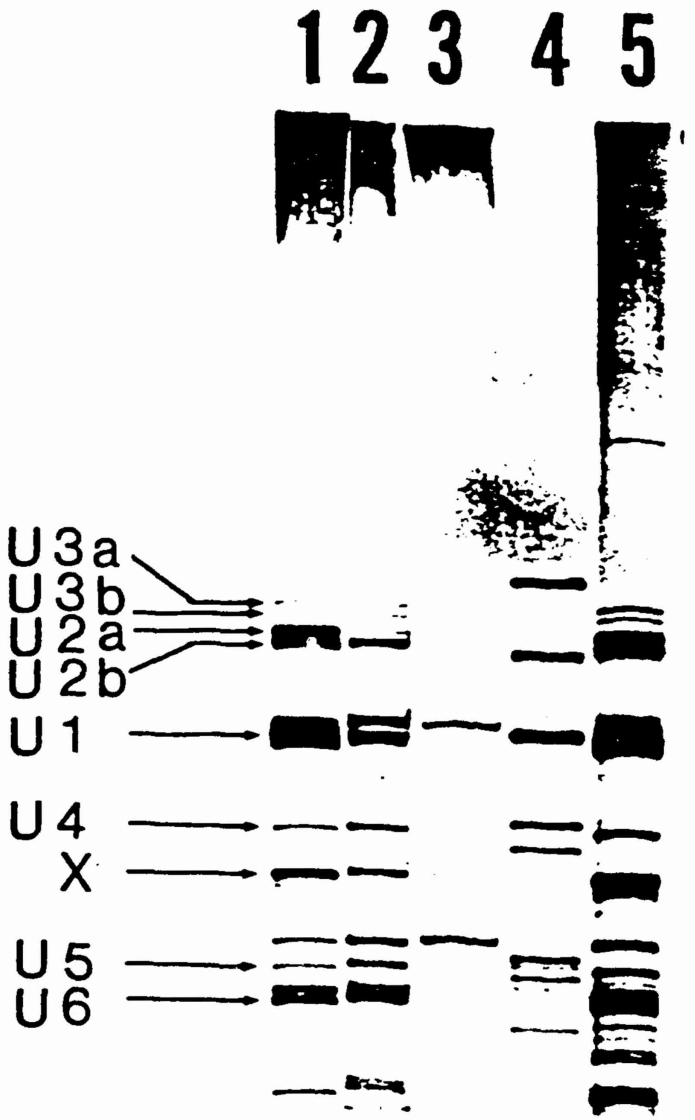

Figure 8. Comparison of the capped sRNAs in PSG Versus Bm-5. Total cellular RNA used for immunoprecipitation with anti-trimethylguanosine antibody was labeled in vivo with ^{3}H-uridine for 24 hr. Lanes 1 and 5 represent 1,000 CPM (but different autoradiographic exposures) of immunoprecipitated Bm-5 RNA. Lane 2 contains 1,000 CPM of immunoprecipitated RNA from larvae labeled from day 5-6 of the fifth-instar. Lane 3 represents 5,000 CPM of total PSG RNA prior to immunoprecipitation, which serves as a marker. Lane 4 represents 1,500 CPM of immunoprecipitated RNA from HeLa cells which also serves as marker. Exposure for fluorography was for 5 days (Lane 1) or 20 days (Lanes 2-5) at -70°C with one intensifying screen.

the Bm-5 cells would be required to verify their U1 homology. If the bands are all U1-like, the data would imply that the immortal cell line expresses several types of U1 genes, and that the PSG expresses only one type, which might serve a specific function in the splicing of fmRNA. These data are in agreement with Xenopus experiments (Forbes et al., 1984) demonstrating seven U1 isoforms expressed in a cultured cell line and in embryonic tissues, but not in specialized tissues. It is also in agreement with studies (Lund et al., 1985) showing that mouse has two U1 isoforms which are expressed in fetal tissues and only one in differentiated adult tissues.

We obtained primary sequence and secondary structure information for some of the Bombyx sRNAs. This type of analysis represents the strongest criterion for the identification of specific sRNAs. To date, we have sequence information for molecules U1-U6 (Adams et al., 1985). Primary sequence comparisons of molecules U3c and d are shown in Figure 9. Potential secondary structures for molecules U3c and d are shown in Figure 10. An important rule appears to be emerging: only relatively short primary sequence domains are conserved, while overall secondary structure is highly conserved. This may imply that only short sequence domains directly interact with mRNAs, and that the overall 2^{o} structure is required for other functions such as binding proteins.

Overall, our data indicate that there are several types of sRNAs in Bombyx, but only two molecules associate with pre-fmRNA through base-paired interaction. There appears to be two types of U2 (U2a and U2b), but only U2b is found in large quantities in the PSG and crosslinks to pre-fmRNA. There appears to be several types of U1 (especially in Bm-5 cells), but only one subtype is found in the PSG and crosslinks to pre-fmRNA. The three sRNAs that crosslink to mature fmRNA (F1-F3) do not appear to be U-RNAs since they are not capped and do not have the lupus type-Sm antigen. Our data indicate that PSG-U1 and U2 transiently associate with fmRNA.

None of the crosslinked sRNAs have been sequenced directly; their identifications are based solely on their migrations with other characterized sRNAs. Northern analysis (hybridization of the released sRNAs to specific radiolabeled cDNA clones) (Calvet and Pederson, 1981) will be required to specifically identify these interesting molecules. It is also possible that other sRNAs base-pair with fmRNA in vivo but were not detectable by our crosslinking method because of their extremely low abundance, or because of their inability to be crosslinked (i.e., the base-paired region may be too short, or the sRNA may bind the mRNA through a protein interaction). For the latter type of molecule, protein/RNA crosslinking studies using UV light may aid in its detection.

PRIMARY SEQUENCE OF TWO BOMBYX U3 sRNAs

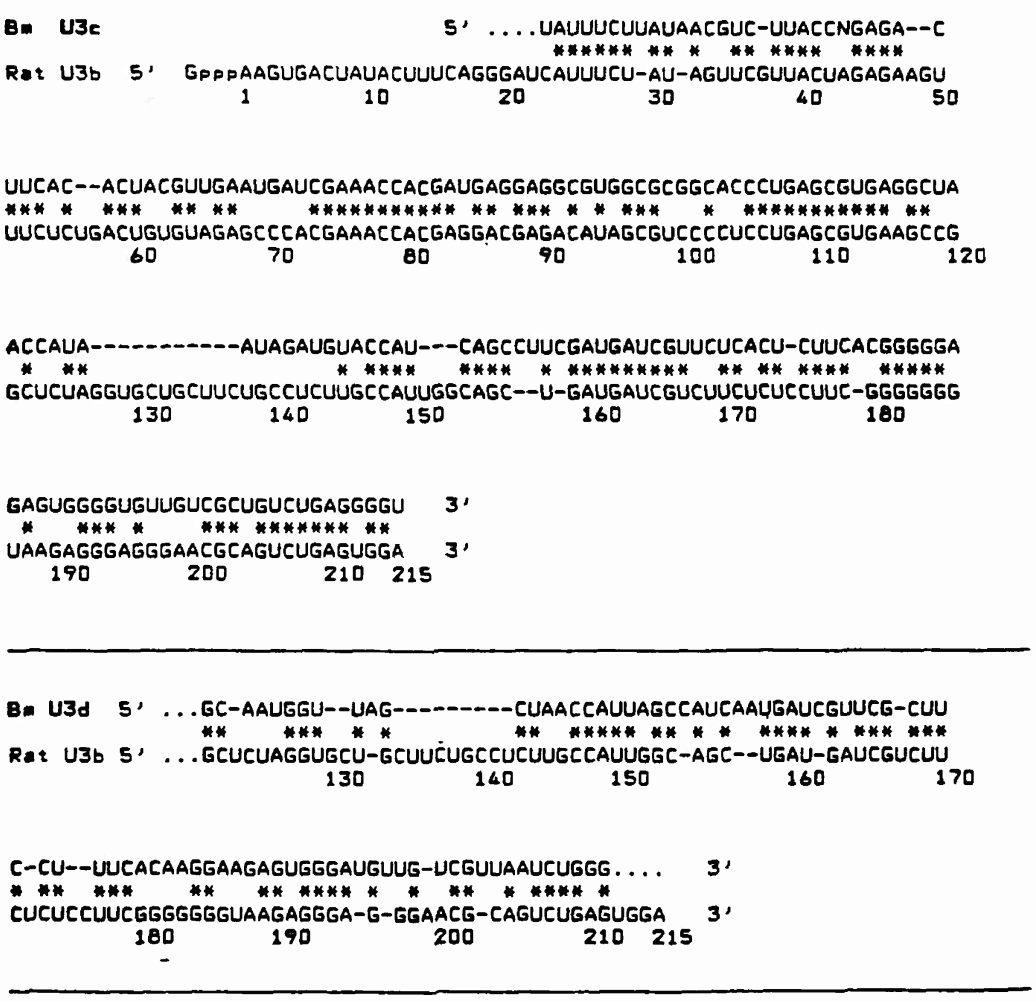

Figure 9. Sequence of Two Bombyx U3 sRNAs. The sequences of Bombyx PSG U3c and d are shown compared to rat U3b. U3c & d were isolated from total cellular RNA by HPLC chromatography (Adams et al., 1985). Sequences were obtained by chemical sequence analysis (Peattie, 1979). Homologous bases are represented by "*", base deletions by "-", and undetermined bases by "N".

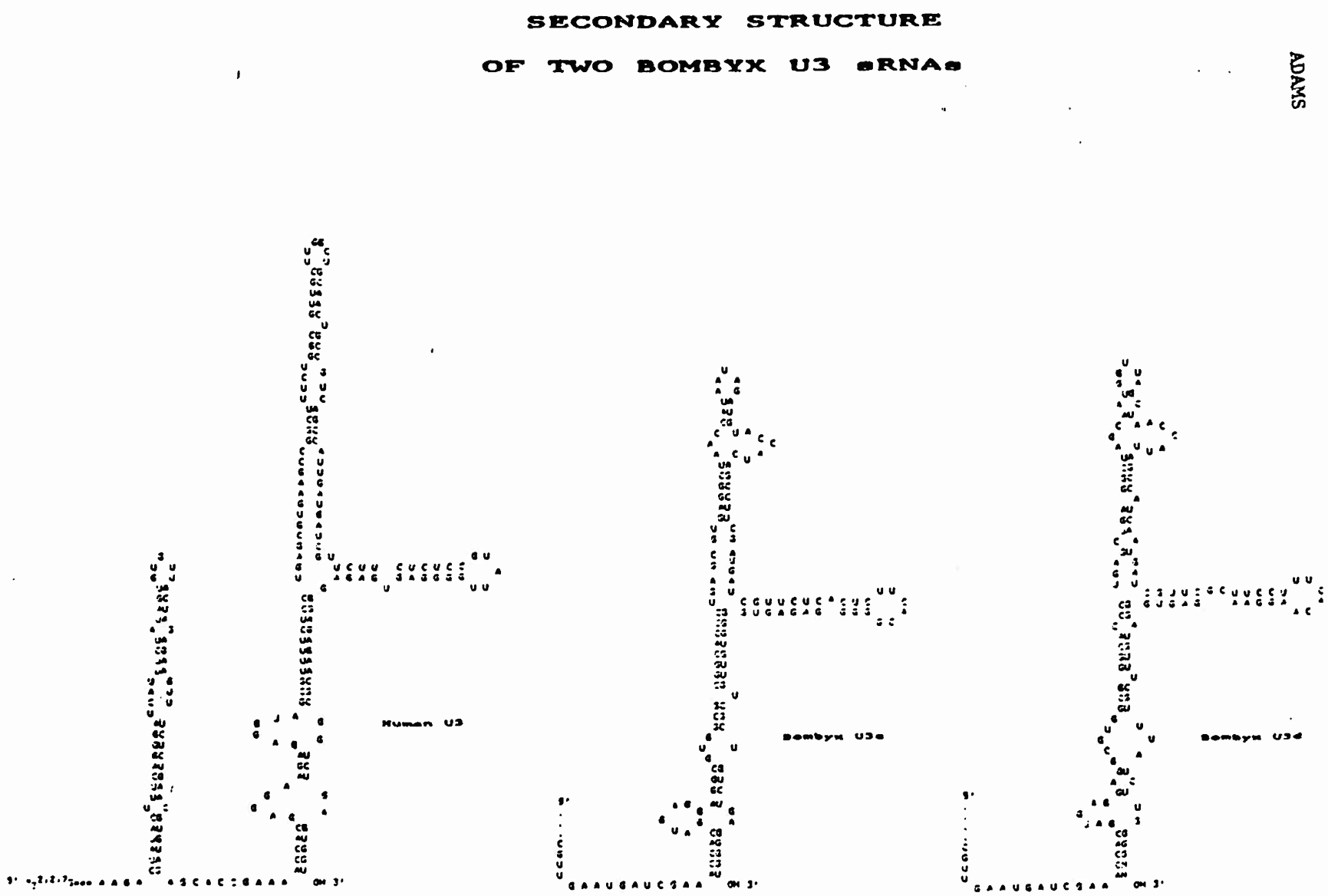

Figure 10. Secondary Structure of Two Bombyx U3 sRNAs. Potential secondary structure for Bombyx U3c & d were derived from the sequence information in Figure 9 using the computer program "RNAFOLD" (Zuker and Stiegler, 1981). The human placental U3 sequence is that of Suh et al., (1986).

Acknowledgements

We would like to thank Dr. Robert Lahita (The Rockefeller University, New York) and Dr. Reinhard Lührmann (Max-Planck-Institut für Molekulare Genetik, Berlin) for providing lupus type-Sm IgG and anti-TMG IgG, respectively; and Dr. Seiji Kamijo (The Rockefeller University), Dr. David Samols (Roche Insititute of Molecular Biology), and Dr. John Morrow (The Johns Hopkins University School of Medicine) for providing clones pFb-900, pBm-1, and pBF-36 respectively. This project was supported in part by grant RDC-1 from the Research Development Council of Worcester Polytechnic Institute awarded to D.S.A.

References

Adams, D.S. and W.R. Jeffery (1978) Biochem. 17: 4519-4524

Adams, D.S., D. Noonan and W.R. Jeffery (1980a) Biochem. 19: 1965-1970.

Adams, D.S., D. Noonan and W.R. Jeffery (1980b) Anal. Biochem. 103: 408-412

Adams, D.S., D. Noonan and W.R. Jeffery (1980c) FEBS Lett. 114: 115-118.

Adams, D.S., D. Noonan and W.R. Jeffery (1981a) Proc. Natl. Acad. Sci. USA 78: 83-87.

Adams, D.S., D. Noonan and W.R. Jeffery (1981b) Differentiation 20: 177-187.

Adams, D.S., R. Luhrmann and P.M. Lizardi (1984) Gene Anal. Tech. 1: 109-115.

Adams, D.S., R.J. Herrera, R. Luhrmann and P.M. Lizardi (1985) Biochem. 24 (1): 117-125.

Adams, D.S., T.H. Eickbush, R.J. Herrera and P.M. Lizardi (1986) J. Mol. Biol. 187: 465-478.

Adams, D.S., D. Noonan, T.C. Burn and H.B. Skinner (1987) Gene 54(1): 91-101.

Adams, D.S. and R.J. Herrera (1987) In Press: Comp. Biochem. Physiol.

Boedtker, H. (1971) Biochem. Biophys. Acta 240, 448-453.

Bringmann, P., R. Reuter, J. Rinke, B. Appel, R. Bald and R. Lührmann (1983) J. Biol Chem. 258 2745-2747

Busch, H., R. Reddy, L. Rothblum and Y.C. Choi (1982) Ann. Rev. Biochem. 51, 617-654.

Calvet, J.P. and T. Pederson (1979a) Proc. Natl. Acad. Sci. USA 76, 755-759.

Calvet, J.P. and T. Pederson (1979b) Nucl. Acids Res. 6, 1993-2001.

Calvet, J.P. and T. Pederson (1981) Cell 26, 363-370.

Casey, J. and N. Davidson (1977) Nucl. Acids Res. 4, 1539-1552.

England, R.E., and O.C. Uhlenbeck (1978) Nature (Lond.) 275, 560-561.

England, R., A. Bruce and O. Uhlenbeck (1980) Meth. Enzymol. 65, 65-74.

Forbes, D.J., T.B. Kornberg and M.W. Kirschner (1983) J. Cell Biol. 97, 62-72.

Forbes, D.J., T.B. Kornberg and M.W. Kirschner (1984) Cell 38, 681-689

Gage, L.P. and R.F. Manning (1980) J. Biol. Chem. 255: 9444-9450

Goldsmith, M.R. and F.C. Kafatos (1984) Ann. Rev. Genet. 18, 443-487.

Grace, T.D.C. (1967) Nature 216, 613.

Hochkeppel, H.-K. and J. Gordon (1979) Biochem. 18 2905-2910

Hutton, J. (1977) Nucl. Acids Res. 4, 3537-3555.

Isaacs, S., C. Shen, J. Hearst and H. Rapoport (1977) Biochem. 16, 1058-1064.

Krol, A., J.-P. Ebel, J. Rinke, and R. Luhrmann (1983) Nucl. Acids Res. 11, 8583-8594.

Lerner, M.R. and J.A. Steitz (1979) Proc. Natl. Acad. Sci. USA 76, 5495-5499.

Lerner, M.R. and J.A. Steitz (1981) Cell 25: 298-300.

Lerner, M.R., J.A. Boyle, S.M. Mount, S.L. Wolin and J.A. Steitz (1980) Nature (Lond.) 283 220-224.

Lizardi, P.M., R. Williamson and D.D. Brown (1975) Cell 4, 199-205.

Lizardi, P.M. and D.D. Brown (1975) Cell 4, 207-215.

Lizardi, P.M. (1976) Prog. Nucl. Acids Res. Mol. Biol. 19, 301-312.

Lizardi, P.M. and A. Engelberg (1979) Anal. Biochem. 98, 116-122.

Luhrmann, R., B. Appel, P. Bringmann, J. Rinke, R. Reuter, and S. Rothe (1982) Nucl. Acids Res. 10, 7103-7113.

Lund, E., B. Kahan and J.E. Dahlberg (1985) Science 229: 1271-1274.
(1978) Cell 15, 687-701.

Maniatis, T. and R. Reed (1987) Nature 325: 673-678.

Manning, R., D. Samols and L.P. Gage (1978) Gene 4, 153-166.

Mount, S.M. and J.A. Steitz (1981) Nucl. Acids Res. 9, 6351-6368.

Ohshima, Y. and Y. Suzuki (1977) Proc. Natl. Acad. Sci. USA 74, 5363-5367.

Peattie, D.A. (1979) Proc. Natl. Acad. Sci. USA 76 1760-1764.

Rabin, D. and D.M. Crothers (1979) Nucl. Acids Res. 7, 689-703.

Reddy, R., D. Spector, D. Henning, M.-H. Liu, and H. Busch (1983) J. Biol. Chem. 258, 13965-13969.

Suh, D., H. Busch and R. Reddy (1986) In Press: Fed. Proc.

Sukuki, Y. and D.D. Brown (1972) J. Mol. Biol. 63, 409-429.

Suzuki, Y., L.P. Gage and D.D. Brown (1972) J. Mol. Biol. 70, 637-649.

Suzuki, Y. (1975) Adv. Biophys. 8, 83-114.

Thireos, G. and F.C. Kafatos (1980) Dev. Biol. 78, 36-46.

Thomas, M., R.L. White and R.W. Davis (1976) Proc. Natl. Acad. Sci. USA 73, 2294-2298.

Tsujimoto, Y. and Y. Suzuki (1979a) Cell 16, 425-436.

Tsujimoto, Y. and Y. Suzuki (1979b) Cell 18, 591-600.

Tsujimoto, Y., S. Hirose, M. Tsuda and Y. Suzuki (1981) Proc. Natl. Acad. Sci. USA 78, 4838-4842.

Wise, J.A., D. Tollervey, D. Maloney, H. Swerdlow, E.J. Dunn and C. Guthrie (1983) Cell 35, 743-751.

Wooley, J.C., R.D. Cone, D. Tartof and S.-Y. Chung (1982) Proc. Natl. Acad. Sci. USA 79, 6762-6766.

Woolford, J.L. and M.R. Roshbash (1979) Nucl. Acids Res. 6, 2483-2497.

Zeller, R., T. Nyffenegger and E.M. DeRobertis (1983) Cell 32, 425-434.

Zuker, M. and P. Stiegler (1981) Nucl. Acids Res. 9: 133-148.

CONTROLLING BIOPOLYMER MOLECULAR WEIGHT DISTRIBUTION - PULLULAN AND CHITOSAN

David L. Kaplan, Bonnie J. Wiley, Steven Arcidiacono, Jean Mayer and Silvino Sousa

U.S. Army Natick Research, Development and Engineering Center
Science and Advanced Technology Directorate
Natick, Massachusetts 01760-5020

Abstract

The influence of culture conditions and processing steps on biopolymer molecular weight distribution and yields is reported for pullulan and chitosan. Batch and continuous cultures, a variety of media and media components, pH controls and processing variables were evaluated. Pullulan, Aureobasidium pullulans, had weight average molecular weights from 100K to 4 million, with a dispersity of around two. Chitosan isolated from the cell wall of Mucor rouxii ranged in weight average molecular weight from 200K to over 1 million with a dispersity of around seven. Gel permeation chromatography was used to evaluate molecular weight distributions. Environmental and processing factors that are critical in controlling the molecular weight distribution of these polymers were identified, and the evaluation of the chemical/physical properties of these defined molecular weight fractions is now under investigation.

Introduction

Pullulan -

Pullulan is a biopolymer, which is released into the extracellular medium as a secondary metabolite by the dimorphic fungus Aureobasidium pullulans (de Bary) Arnaud during the yeast-like phase of the growth cycle, but it is not used during routine metabolism.[15,24] Pullulan is a linear α-D-glucan, predominantly 1,4-linked maltotriose with some maltotetraose units, connected by 1,6-linkages between the terminal glucosidic residues of the trisaccharide.[14,26]

The physiological requirements for pullulan production by A. pullulans have been studied extensively. Ueda et al.[29] studied the production of the polysaccharide by 16 strains of growing cells over time and monitored the pH, dry weight of the cells, and the residual sugar in the medium. They also compared various sugars as carbon sources for the production of the polysaccharide and found the MW of the polysaccharide to be approximately 250,000, when determined by light-scattering. Catley,[6-11] and others also did extensive studies on various physiological requirements for production of the biopolymer, and the influence of these constituents on biosynthesis and elaboration.[19,21,22]

The vegetative cycle of A. pullulans was studied extensively by Ramos and Garcia Acha.[22] They found that an inoculum containing a cell concentration of at least 2 X 10⁷ cells/flask (150 mL) was required to maintain blastospore (yeast cell) production. They also found that nitrate as a nitrogen source could cause the blastospores, after about 46 hours of incubation, to give rise to pseudomycelial forms with low viability that autolyzed as the culture aged. They found that chlamydospores were readily formed in a medium containing ammonium ion as a nitrogen source.

Catley[6,9] and Ono, et al.[21] found that the appearance of extracellular pullulan was not concomitant with an increase in cell mass, but that there was a lag in the rate of elaboration. Catley also studied the role of pH and nitrogen on the production of pullulan and found that the uptake of glucose at more acid pH was diverted to the synthesis of extracellular pullulan, and that high extracellular pH inhibited its production. He found that pullulan elaboration is dictated by depletion in nitrogen availability, and not carbon in the growth medium.[8] Ono et al.[21] found that maintaining a constant, controlled pH gave lower yields of pullulan than an uncontrolled culture. Lacroix et al.[19] described the development of a bistaged pH fermentation process, whereby the first stage of the fermentation was conducted at a very acidic pH (pH 2.0), then the pH was adjusted to a higher value (pH 5.5) to promote the production of pullulan. The amount of pullulan produced was determined by viscosity measurements. Molecular weights were not determined in their study.

Kato and Shiosaka described the effect of phosphate concentration on molecular weight and yield of pullulan.[17] They showed a marked decrease in mean MW of pullulan when comparing various concentrations of phosphate at pH 5.5, pH 6.0, and pH 6.5. Phosphate concentrations of 0.2%-0.4% yielded high MW pullulan at the lower pH level. They reported that using hydrolyzed starch as the carbon source resulted in yields of pullulan as high as 75% or more.[16]

To summarize the nutrient requirements for pullulan elaboration as reported in the literature: hydrolyzed starch yielded the largest amount of pullulan;[16] pH, nitrogen source, and nitrogen limitation affected pullulan elaboration,[8,22] and pH and phosphate concentration affected the MW of pullulan.[17] Culture incubation varied from a few hours to seven days, and most results were reported for batch studies. However, most of this information has not been assembled into a cohesive study. Only a few authors have reported the MW distribution of the pullulan elaborated in their studies.[6,17,29] In most reports, total carbohydrate was determined by a colorimetic procedure, estimation of glucose by glucose oxidase reagent, or by the viscosity of the medium.[19,21,29]

Chitosan -

Chitosan is a cationic polymer consisting of β-1,4 linked 2-amino-2-deoxy β-D-glucan. Chitosan rarely is found in nature. The primary occurrence is in the cell walls of some fungi, particularly the

Zygomycetes which contain chitosan as a cell wall component,[2] in addition to chitin. Chitosan has been identified in the genus Mucor,[25] Aspergillus,[18] and Phycomyces. Commercially, chitosan is derived from chitin which is obtained from shellfish. The strong alkali digestion required to deacetylate chitin to produce chitosan and variability in source material leads to variable physiochemical characteristics. The use of a fungus as a source of chitosan avoids the strong alkali digestion. Therefore, less concern exists about affecting molecular weight distribution of the final product. The use of a fungus also has the potential to provide closer control over the physiochemical properties of chitosan because of the ability to control fermentation and processing parameters. In addition, the potential exists for genetic manipulation using the fungal system.

Chitosan was first identified in 1859 by Rouget[25] from chitin boiled in caustic potassium hydroxide and solubilized in dilute organic acids. Chitosan was first found in nature in 1954 by Kreger[18] in the cell walls and sporangiophores of Phycomyces blakesleeanus, and subsequently in Mucor rouxii by Bartnicki-Garcia and Nickerson[2] in 1962. By 1978, Fenton, et al.[12] found that each family of the Zygomycetes contained chitosan in their cell walls.

The degree of acetylation of the glucosamine polymer determines whether it is chitin or chitosan and influences its solubility properties. Chitosan produced from shellfish chitin ranges from near 0% to 50% acetylation,[13] and cell wall chitosan isolated from M. rouxii has been reported to contain a 5% to 10% acetyl content.[30] The chitosan content of the M. rouxii cell wall is reported to be 33% for the mycelia, and 28% for yeast-like forms.[2] The presence of CO_2 during incubation has been demonstrated to affect the morphology in M. rouxii. Incubation in nitrogen gas or air yields the typical filamentous mycelia, while budding yeast-forms are formed under CO_2.[3]

Previous work concerning chitosan from fungal sources has not dealt with the aspect of molecular weight distributions of the polymer product. White's[30] choice of extraction parameters was based solely on chitosan yield. Molecular weight distributions have been determined for chitosan produced from the commercial conversion of shellfish waste. A commercial chitosan has been reported to have a weight average molecular weight of 2055 K as determined by High Performance Liquid Chromatography (HPLC) using dextran standards for calibration.[31]

Objective -

The objective of this study was to produce and characterize different molecular weight distributions of these two biopolymers.

METHODS AND MATERIALS

Cultures

Nine strains of Aureobasidium pullulans, A. pullulans var. melanigenum, or A. mansonii were evaluated in preliminary studies to compare pullulan elaboration. Strain NRRL-Y 6220 A. pullulans was chosen for further studies, based on product color and yield, when compared with the other cultures. All cultures were maintained on potato dextrose agar slants.

For chitosan production, Mucor rouxii (ATCC 24905) was maintained on yeast extract-peptone-glucose (YPG) agar slants, pH 5.0 and stored at 4°C.

Media

For pullulan production; the following media were used, in grams per liter of distilled H_2O: (A) Ramos and Garcia Acha,[22] K_2HPO_4, 1.0; KCl, 0.5; $MgSO_4 \cdot 7H_2O$, 0.5; $NaNO_3$, 2.0; $FeSO_4 \cdot 7H_2O$, 0.01; $(NH_4)_2SO_4$, 0.6; pH 5.3. (B) Ueda et al.,[29] K_2HPO_4, 5.0; NaCl, 1.0; $MgSO_4 \cdot 7H_2O$, 0.2; yeast extract (Difco, Detroit, MI), 0.4; pH 5.5 and 6.0. (C) Kato and Shiosaka,[7] K_2HPO_4, 2.0; NaCl, 2.0; $MgSO_4 \cdot 7H_2O$, 0.4; $Fe(NH_4)_2SO_4 \cdot 7H_2O$, 0.01; peptone, 2.0 (Difco); pH5.4.

Three different culture media were used for evaluation of biomass production and molecular weight distribution of chitosan. Two complex media were evaluated, BG and YPG. BG consisted of the following ingredients per liter: nutrient broth, 8.0 g; yeast extract, 0.1 g (Difco); KCl, 1.0 g; $MgSO_4 \cdot 7H_2O$, 0.25 g; $FeSO_4$ $7H_2O$, 0.278 mg; $MnCl_2$ $4H_2O$, 0.002 g; glucose, 5.0 g (Fisher Scientific Co., Fairlawn, NJ).[2] YPG components were yeast extract, 3.0 g; peptone, 10.0 g; and glucose, 5 g per liter. A defined medium, TVB, was evaluated which contained the following ingredients per liter: $(NH_4)_2SO_4$, 1.4 g; KH_2PO_4, 2.0 g; $CaCl_2$, 0.3 g; $MgSO_4$ $7H_2O$, 0.3 g; molybdic acid (85%), 0.01 g; glucose, 20.0 g; trace metal solution (see below), 1.0 mL. Citrate buffer, pH 4.4 at 0.05M, consisting of citric acid, anhydrous, 5.38 g/L (J.T. Baker Chemical Co., Philipsburg, NJ) sodium citrate, 6.47 g/L (Fisher) was used if buffering was desired. The trace metal solution contained the following: 495 mL distilled water, 5.0 mL concentrated HCl (12 M) (J.T. Baker) $FeSO_4 \cdot 7H_2O$, 2.5 g; $MnSO_4 \cdot H_2O$, 0.98 g; $ZnCl_2$, 0.83 g; $CoCl_2 \cdot 6H_2O$, 1.0 g (Fisher). For all liquid media, glucose was prepared separately and added aseptically after autoclaving.

Culture Conditions

For pullulan producing batch cultures, an Aquaferm Water Bath Shaker (New Brunswick Scientific Co., Inc., Edison, NJ), temperature 25°C to 28°C, was shaken at 150 and 120 rpm. An Environ-Shaker (Lab-Line Instruments, Inc., Melrose Park, IL), temperature 26°C ± 1°C, was shaken at 125 rpm. A BioFlo Model C30 Fermentor (New Brunswick), temperature 26°C, was set at an agitation rate of 300 rpm, and aeration rate of 0.5 L/min. Media flowrates were controlled with a Rabbit Peristaltic Pump (Rainin Instrument Co., Inc., Woburn, MA) for the continuous fermentation studies. A magnaferm Model MA-114 Fermentor with an Automatic pH Controller and Pump Module (New Brunswick) with a Constant Speed Controller (Cole-Parmer Instrument Co., Chicago, IL) was used for the 10-liter studies, and was set at a temperature of 26°C, an agitation rate of 1,200 rpm, and a variable oxygenation rate.

After initial culture comparisons for pullulan elaboration were studied, all further work with shake flasks used 50 mL/250 mL DeLong flask with 2% inoculum, or 500 mL medium per 2800 mL Fernbach flask and 2% inoculum. Inoculation of batch and continuous fermentations used two- or three-day old cell suspensions grown on the medium being studied.

For the production of chitosan, small-scale batches involved shake cultures of 750 mL in 2800 mL Fernbach vessels, or 100 mL in 250 mL DeLong flasks. Large-scale batch cultures consisted of 10 liters of culture medium in a 14 liter fermentor vessel on a Magnaferm MA-114.

Processing and Purification

For pullulan, the culture medium was neutralized using 1 N NaOH. The medium was diluted with concentrated ROCCAL II (alkyl dimethyl benzyl ammonium chloride, Sterling Drug, Inc., Montvale, NJ) to a final volume of 1% ROCCAL II, then centrifuged at 13,180 X g to 23,430 X g for 20 minutes to remove the cells. The pullulan was then precipitated from the supernatant, using two volumes of acetone for each volume of supernatant, while stirring the suspension to eliminate lumping. After precipitation, the acetone was decanted, the precipitate was washed several times with acetone, and then filtered over vacuum. The pullulan was then dried over $CaSO_4$ in a desiccator.

Extraction of chitosan from the fungal cell wall was based on the procedure developed by White *et al.*[30] with some modifications. These changes included the elimination of lyophilization of NaOH treated (cell wall) material, homogenization of the cell wall material with a Waring blender in 2% acetic acid prior to refluxing, and an increase in cell wall-acid ratio to 1:≥100. These modifications of White's method were examined in relation to their effect on molecular weight distribution (MW) of chitosan and yield of product. Other changes were evaluated visually by using Lugol's stain. Modifications included pretreatment of mycelium

by soaking or boiling in water; placement of mycelium in -70°C acetone to disrupt the cell wall; sonification of mycelium homogenate prior to NaOH treatment, also for cell wall disruption; and homogenization of cell wall material prior to acetic acid extraction by refluxing.

Chitosan samples were clarified by one of two methods, centrifugation at 3000 x or filtration using one of the following systems: a Swinnex filter (0.45 µm); a Millex-HV filter (0.45 µm) (Millipore); or a 0.5 µm sintered stainless steel GPC filter (Waters Chromatography Div., Millipore Corp., Milford, MA). Three methods were evaluated for determining the degree of acetylation of chitosan. They were infrared spectrophotometry,[27] first derivative of UV absorbance spectrum,[20] and titration.

Analytical Methods

Determination of pullulan and chitosan MW distribution and dispersity was performed on a Waters 150-C ALC/GPC Gel Permeation Chomatograph (Waters). Standards and samples were run through three Bio-Gel (Bio-Rad Laboratories, Richmond, CA) columns; a TSK-60, separating in the 40,000 to 8,000,000 molecular weight range, and two TSK-50 columns, effective from 4,000 to 800,000 molecular weight. The TSK-60 column preceded the two TSK-50 columns in line. A third order calibration curve was generated correlating MW distribution with retention time on the columns. Standards and samples were solubilized at a concentration of 0.1% in the carrier solvent, which consisted of an aqueous solution of sodium acetate, 0.1 M; acetic acid, 2% (v/v), and sodium azide, 0.05% (w/v). The instrument was adjusted to 1.0 mL/min flow-rate. The injection volume was 200 to 300 µL and the run time was 40 minutes.

Results

A sampling of results from our studies on pullulan and chitosan are presented here. The full publications on each of these biopolymers are currently under review.

Pullulan -

Figures 1 and 2 illustrate the effect of incubation time on pullulan yield and MW distribution using NRRL-Y 6220. The highest MW distribution product was attained on the first day of incubation, but the greatest yield was afforded after seven days of incubation.

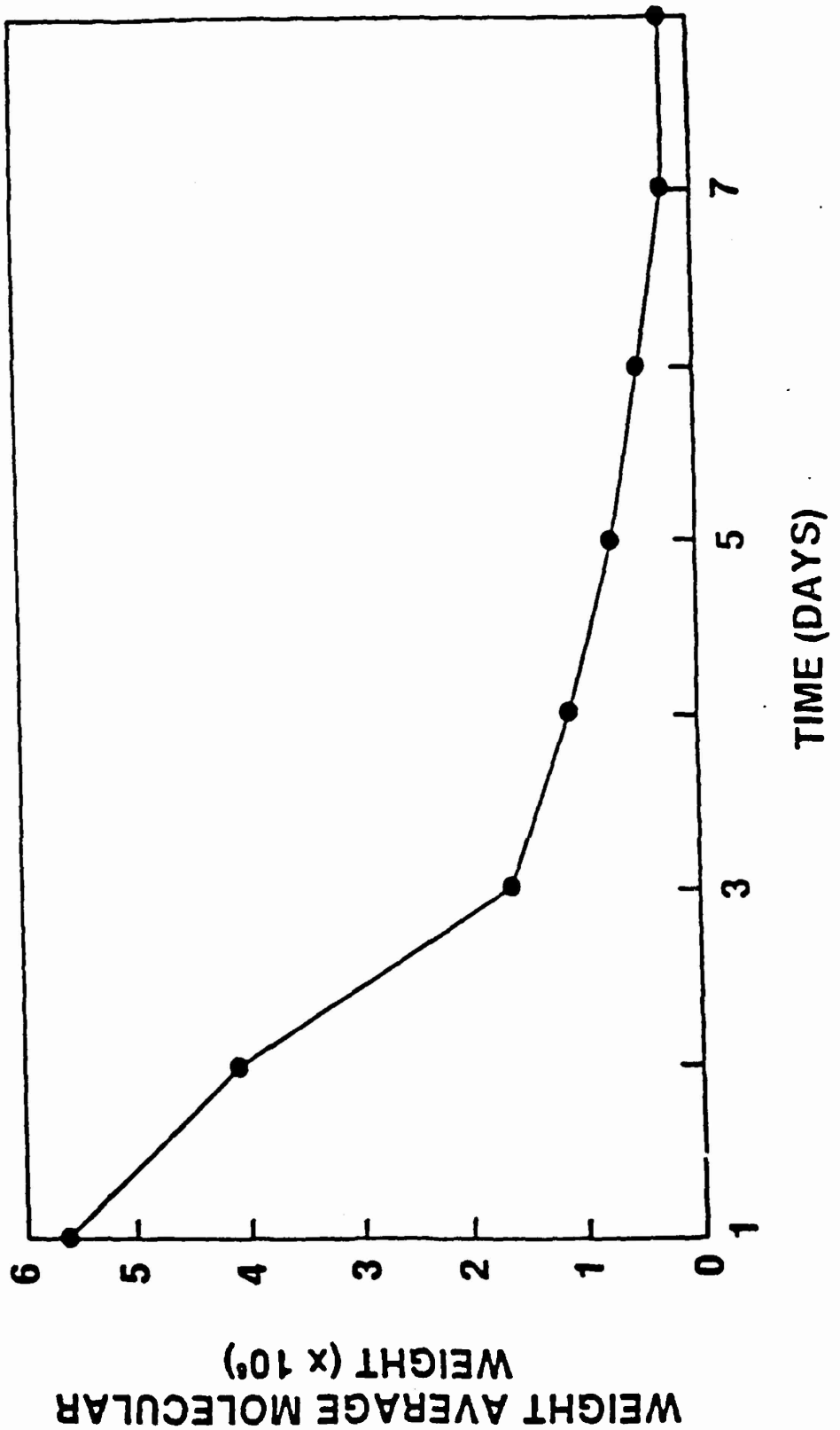

Figure 1. Weight average molecular weight pullulan vs. time (NRRL-Y 6220).

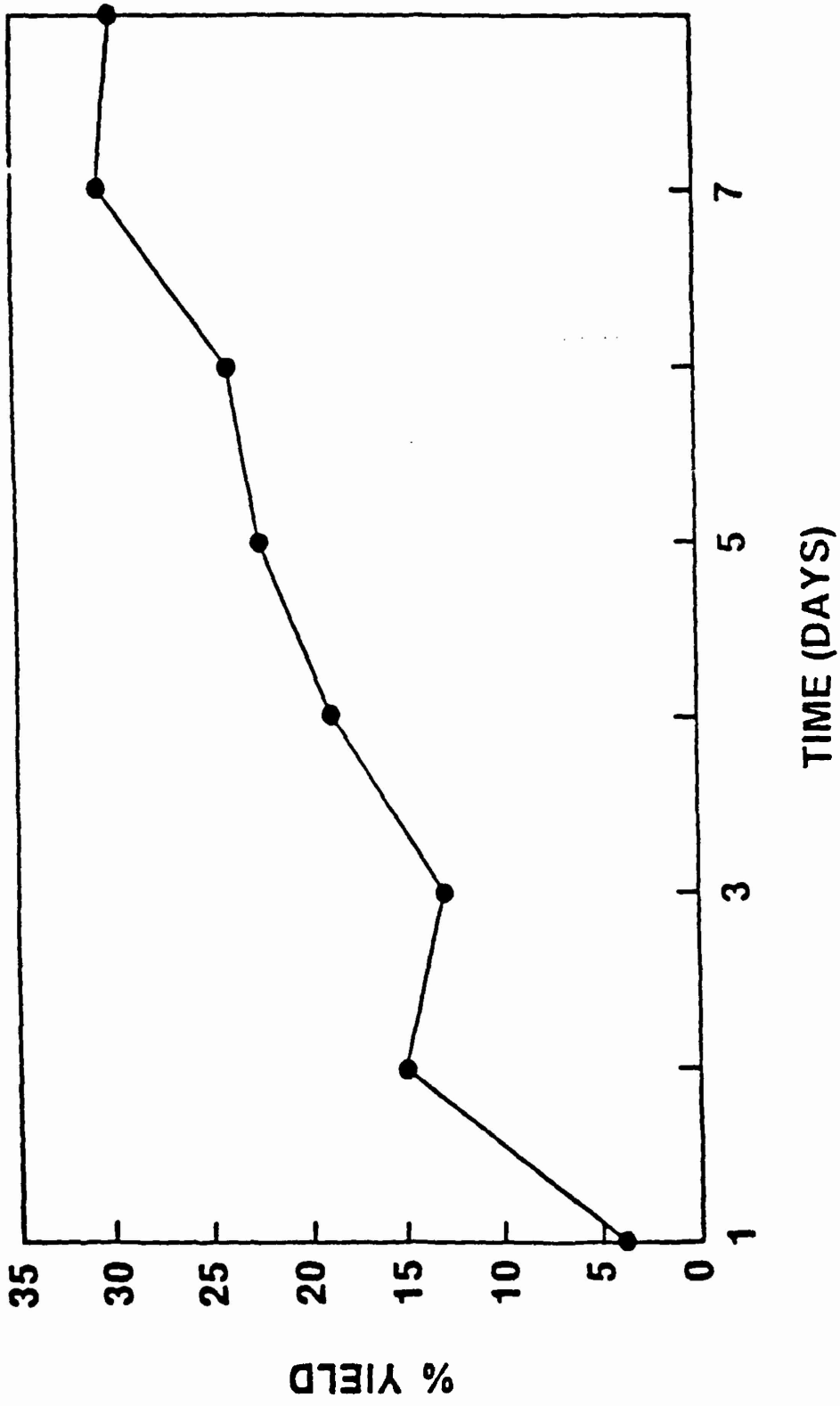

Figure 2. Percent yield of pullulan vs. time (NRRL-Y 6220).

The effects of carbon and nitrogen sources, and phosphate concentration on pullulan yield and molecular weight are shown in Tables 1, 2, and 3, using NRRLY-6220 and the medium of Kato and Shiosaka. Fructose used as a carbon source resulted in the highest MW distribution of pullulan, but the use of sucrose yielded a greater amount of product (Table 1). The use of soluble starch resulted in the highest yield of pullulan; however, the MW distribution of the product was relatively low. Various nitrogen sources were evaluated for use in pullulan production. A combination of peptone and ammonium sulfate gave the highest MW distribution of product, and yields varied from 5% to 9%. The use of urea, and urea with ammonium sulfate resulted in a high MW distribution of product, and yields were between 10% and 11% (Table 2).

As can be seen in Table 3, the phosphate concentration, within the range evaluated, seemed to have little effect on the MW distribution or the product yield, at least during the time period studied. Kato and Shiosaka reported, however, that using a medium containing glucose, phosphate concentration and initial pH value affected the yield and MW distribution of pullulan. Their culture period was from four to seven days, whereas a time period of from two to three days was used in this study. We found that length of incubation and initial pH had more of an effect than phosphate concentration.

The method of Ueda et al.[29] was first used to process the pullulan. This involved diluting the culture medium with an equal amount of distilled water, neutralizing with 4% NaOH, and centrifuging at 7,000 X g for 15 min. The supernatant was diluted with an equal amount of 95% ethanol, then refrigerated overnight at 5°C. The mixture was centrifuged at 2,500 X g for 15 min. The precipitate was washed twice with 55% ethanol, then washed with absolute ethanol and twice with ether. The product was then dried. A simpler and easier method was devised (Fig. 3), using acetone, eliminating the second centrifugation step, and the petroleum ether drying. The use of ROCCAL II aided the processing of the culture medium and helped remove the discoloration in the older cultures. Acetone-precipitated polymer yielded a fine white powder when all excess moisture was removed.

Chitosan -

Initially, the two complex media BG and YPG were compared in 750 mL shake cultures (Fig. 4). The weight average MW for BG was a maximum of 643 K at 72 hours, while YPG reached 539 K at 72 hours. The biomass achieved in BG was relatively low, a maximum 3.9 g/L at 72 hours compared to 10.3 g/L for YPG (Fig. 5). Each study used a plug inoculum and initial sampling times of 16 hours and 7 and 10 days.

TABLE 1. Effect of Carbon Source on Pullulan Yield and Molecular Weight Using NRRL-Y 6220 *Aureobasidium pullulans**

Carbon Source (10%)	Initial pH	Final pH	Yield (%)	Mol. Wt. (k)	Dispersity
Fructose	5.44	3.76	27.0	1122	2.5
Sucrose	5.44	3.69	34.4	895	2.4
Maltose	5.44	4.08	25.4	881	2.1
Corn Syrup	5.44	3.85	29.3	840	3.3
Dextrose	5.44	3.91	23.3	563	1.8
Lactose	5.44	3.79	5.8	518	1.6
Sol. Starch	5.44	4.24	70.3	137	1.4
Dextrin	5.44	2.99	21.6	9	1.1

*Culture Conditions: K & S Medium, 0.2% K_2HPO_4, 26.5°C, 120 rpm Environ-Shaker, 4 Days Incubation, 50 mL/250 mL DeLong Flask, 2% Inoculum.

TABLE 2. Effect of Nitrogen Source on Pullulan Yield and Molecular Weight Using NRRL-Y 6220 *Aureobasidium pullulans**

Nitrogen Source (%)	Initial pH	Final pH	Yield (%)	Mol. Wt. (k)	Dispersity
$NaNO_3$ (0.2)	5.31	6.67	2.00	78	1.1
$NaNO_3$ (0.2): Y. Ext. (0.25)	5.30	6.49	5.30	85	1.4
Peptone (0.2)	5.30	3.64	6.30	1935	2.3
Peptone (0.2); $(NH_4)_2SO_4$ (0.01)	5.50	3.50	9.00	1384	2.8
Peptone (0.1); $(NH_4)_2SO_4$ (0.01)	5.31	3.27	4.95	2940	4.9
$(NH_4)_2SO_4$ (0.14)	5.30	2.26	1.17	-	-
Urea (0.3)	5.30	4.93	10.20	2061	2.6
Urea (0.3); $(NH_4)_2SO_4$ (0.14)	5.32	5.08	11.02	1898	2.7
Y. Ext. (0.25)	5.31	4.16	18.80	859	6.7

*Culture Conditions: K & S Medium w/o Nitrogen, 10 % Sucrose, 26.5°C, Environ-Shaker 120 rpm, 3 Days incubation, 50 mL/250 mL DeLong Flask, 2% Inoculum.

TABLE 3. Effect of Phosphate Concentration on Pullulan Yield and Molecular Weight Using NRRL-Y 6220 *Aureobasidium pullulans**

Culture Period	Phosphate Conc. (%)	Initial pH	Final pH	Yield (%)	Mol. Wt. (k)	Dispersity
2 Days	K_2HPO_4					
	0.1	5.42	3.43	8.50	2704	2.0
	0.2	5.42	3.65	11.10	2659	2.1
	0.3	5.42	3.58	11.20	2646	1.8
	0.4	5.42	3.88	13.70	2165	2.3
	0.5	5.42	3.93	14.00	2477	2.2
2 Days	KH_2PO_4					
	0.2	5.42	3.50	9.20	2608	2.1
3 Days	K_2HPO_4					
	0.1	5.42	3.65	11.60	1968	2.2
	0.2	5.42	3.79	14.40	1551	2.3
	0.3	5.42	3.82	13.10	1629	2.2
	0.4	5.42	3.97	16.20	1369	2.3
	0.5	5.42	4.10	18.40	1169	2.4
3 Days	KH_2PO_4					
	0.2	5.42	3.77	11.00	1933	3.7

*Culture Conditions: Kato & Shiosaka Medium, 10% Sucrose, 26°C - 26.5°C, 125 rpm New Brunswick Shaker, 50mL/250 mL DeLong Flask, 2% Inoculum.

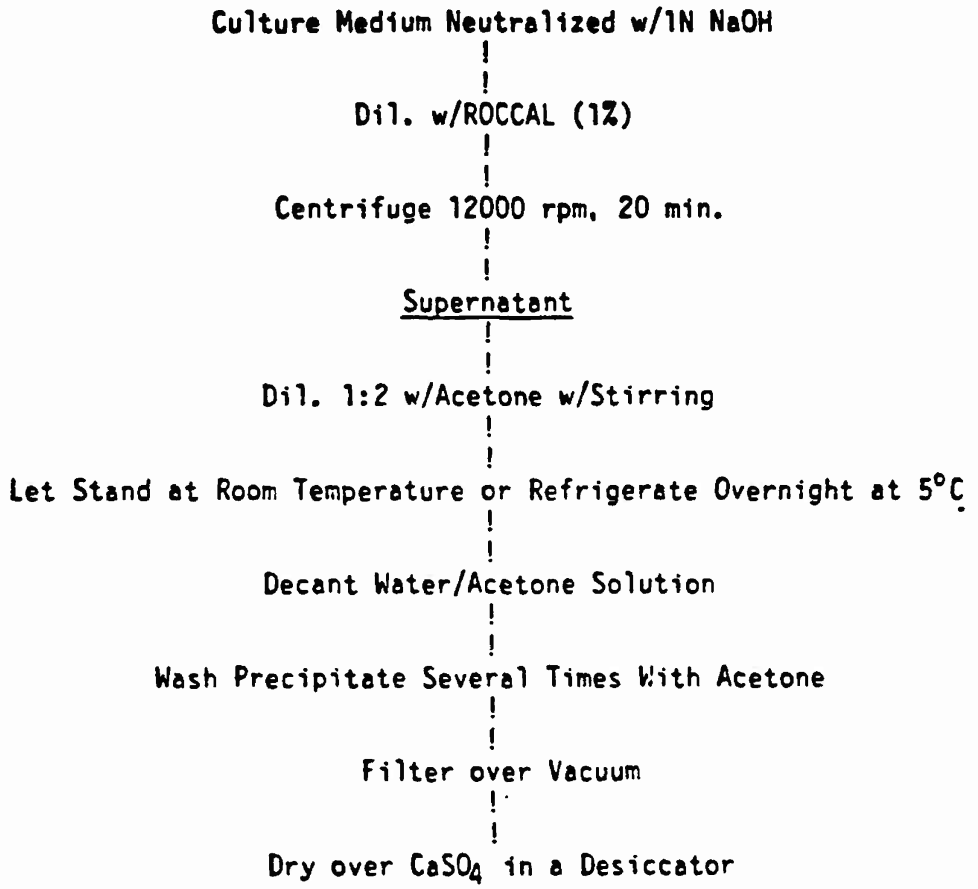

Figure 3. Pullulan processing conditions.

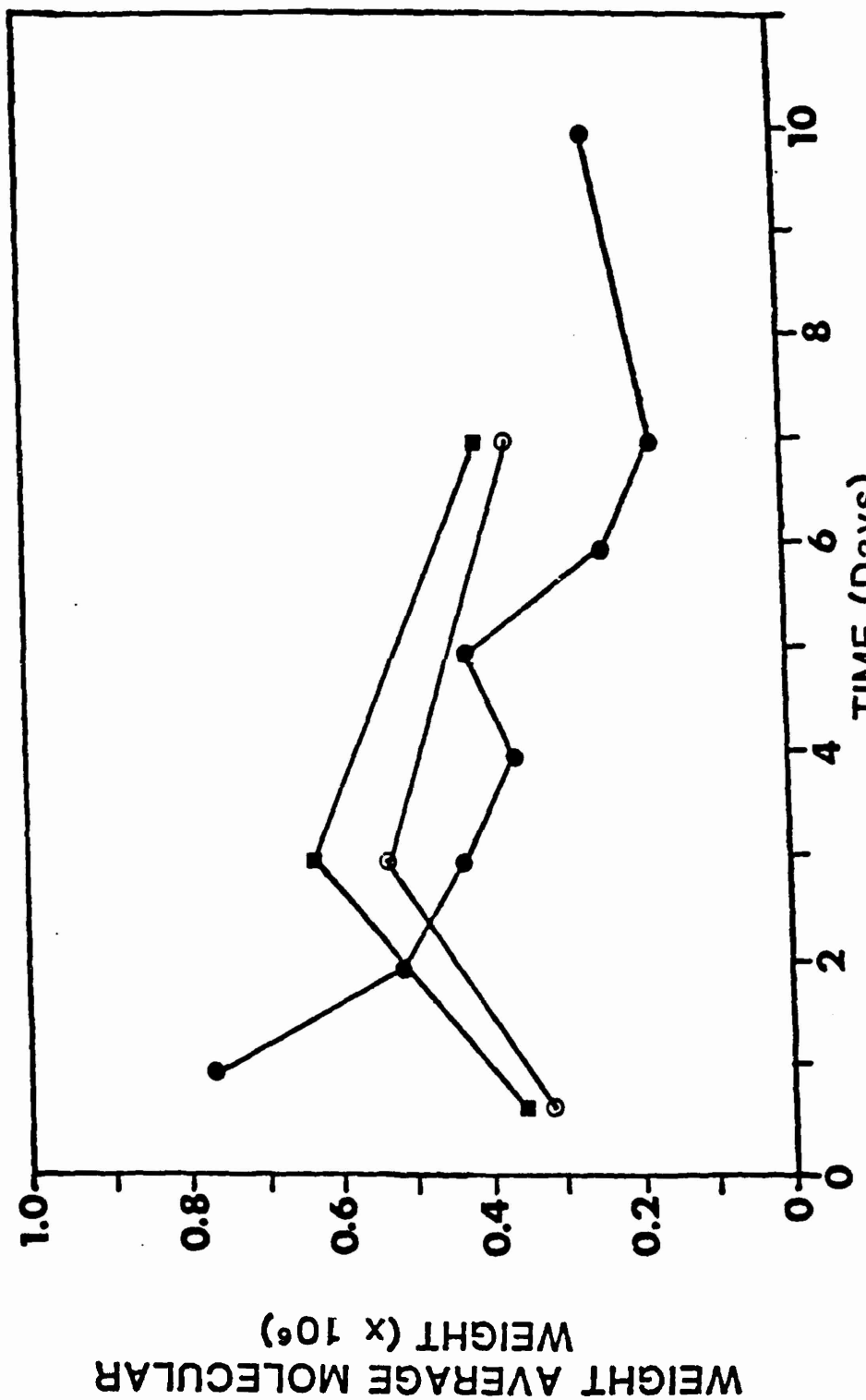

Figure 4. Weight average molecular weight of chitosan vs. time in complex media. 750 ml. YPG (1) (●), YPG (2) (○), BG (■)

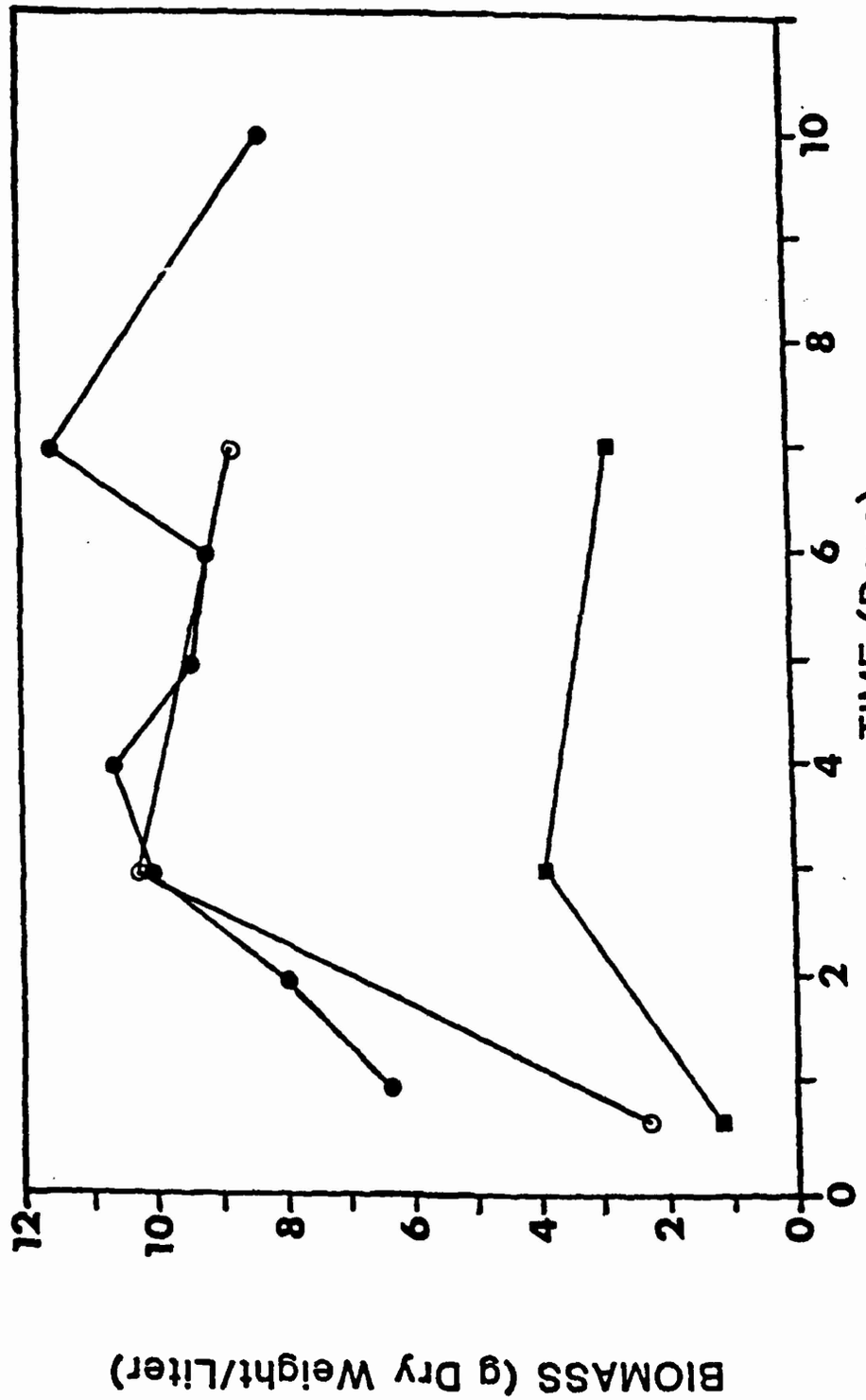

Figure 5. Effect of time on biomass production in complex media. 750 ml. YPG (1) (●), YPG (2) (○), BG (■)

Further study involving 750 mL YPG shake cultures was carried out to determine the effect of length of incubation on weight average MW distribution and yield. Flasks were processed every 24 hours for a period of seven days and at ten days (Fig. 4). The maximum weight average MW was 769 K at 24 hours. Weight average MWs continued to decline reaching 200 K to 300 K after 6 days. Biomass increased up to 72 hours before stabilizing in the range of 9 to 11 g/L (Fig. 5).

In 10 liter batch cultures MW increased rapidly, reaching maximum weight average MW values of approximately 1 million to 1.1 million by two days for plug and spore inoculated cultures (Fig. 6). There was a decline in weight average MW during the three to seven day period. While biomass in the plug inoculated cultures leveled off after two days, biomass levels in cultures inoculated with spores decline steadily from 10.3 g/L at three days to 5.0 g/L at seven days (Fig. 7). Although maximum biomass levels are similar, the 10 liter YPG batches showed a more rapid rate of biomass production than the 750 mL cultures (10.4 g/L at 30 hours vs. 10.1 g/L by 72 hours).

A second set of experiments was conducted by growing M. rouxii in small scale defined buffered (TVB-citrate) and complex (YPG) media in which pH was adjusted to a constant value twice daily. The pH values of 3.0, 4.0, 5.0, and 6.0 were evaluated (Fig. 8). The same media, without pH adjustment served as controls. Optimal pH for the production of highest weight average MW chitosan was 6.0 for the YPG (521 K) medium and 4.0 for the defined medium (594 K), although differences were small over the pH range studied. The unadjusted YPG control weight average MW was 16% less at 437 K (final pH of 4.2), while in TVB, the weight average MW was 490 K (final pH 5.0). Optimal pH for biomass production was 5.0 in both media. At this pH, 9.7 g/L biomass was produced for YPG and 6.28 g/L in TVB-citrate. The unadjusted pH YPG control yielded 8.1 g/L and had a final pH of 4.6, while the defined medium control resulted in 2.58 g/L at a final pH of 2.3. YPG yielded more biomass over the pH range evaluated. Adjustment of both media to pH 3.0 inhibited fungal growth (Fig. 9).

DISCUSSION

In order to evaluate different cultures for pullulan production, nine strains of Aureobasidium pullulans were examined. Of these strains, only QM 3090 had been reported previously as being used for the study of pullulan production (cited erroneously as QM 3092),[7-9] except for the QM strains used by Dr. E. T. Reese of this Center (unpublished data, 1965). Three of the cultures produced an acid-soluble glycan, probably that first fractionated by Bouveng et al.[4,5] as discussed by Catley.[8,9,10] The fraction was not investigated further in this study. The criteria used in evaluating the cultures were: product color, yield, and MW distribution. Both cultures of QM 5752 and NRRL-Y 6220 produced a white product, but the MW distribution of QM 5752 was low when compared over time. The culture of NRRL-Y 6220 also produced a low MW product initially, but when the culture medium was changed, greater yields and higher MW distributions were obtained.

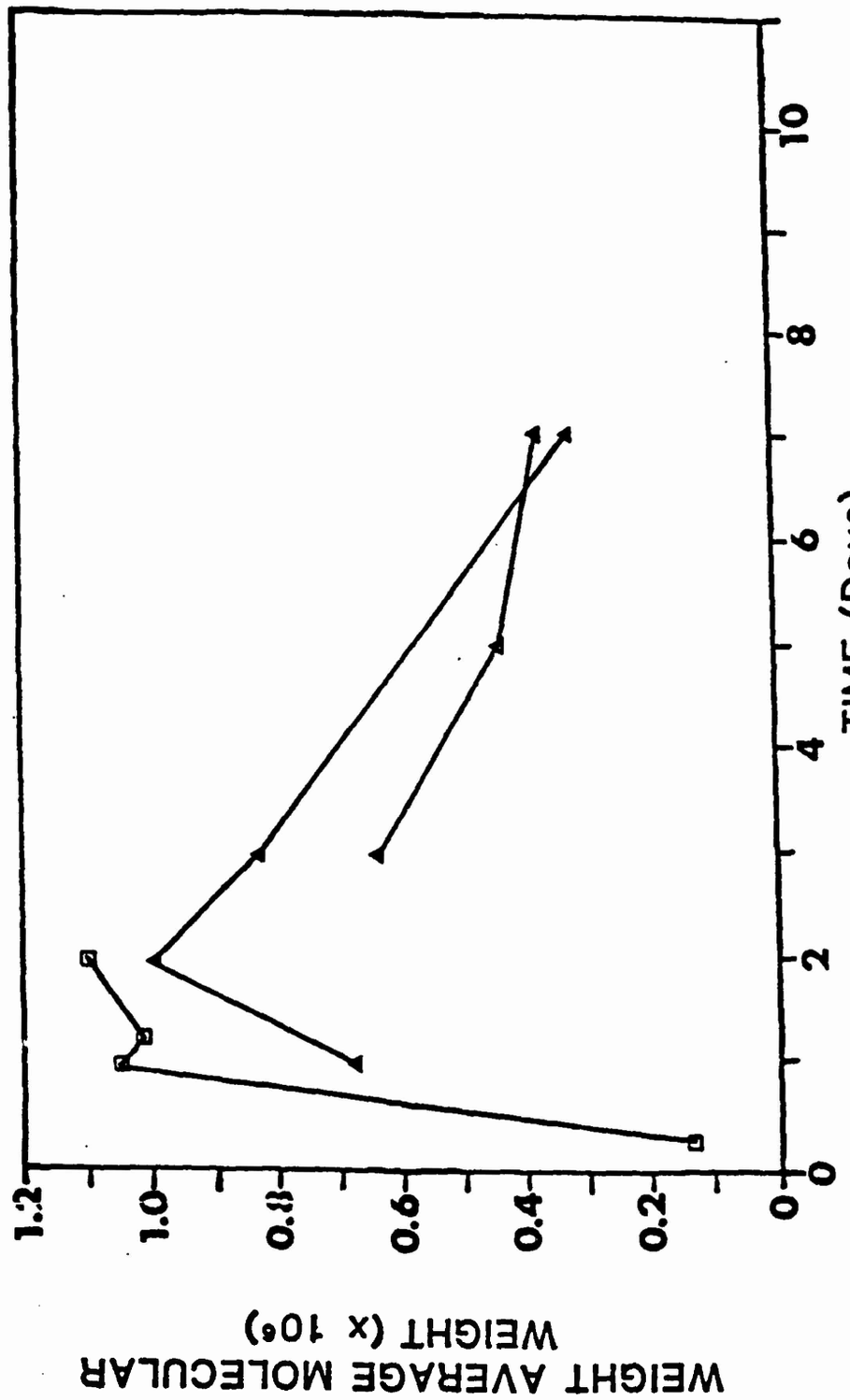

Figure 6. Weight average molecular weight of chitosan vs. time in complex medium, 10 L. YPG (1) (□), YPG (2) (▲), plug inoculum, YPG spore inoculum (△)

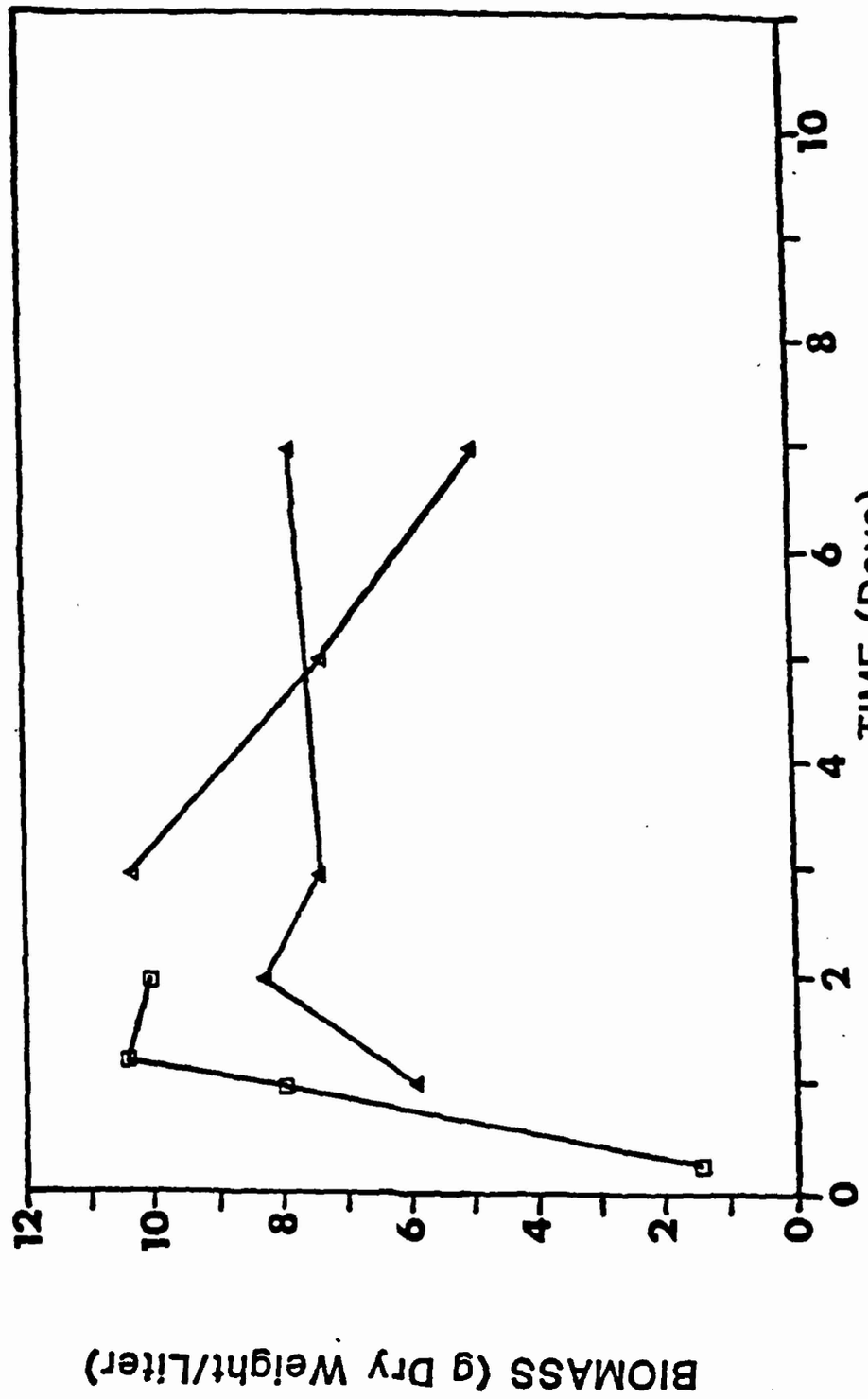

Figure 7. Biomass production vs time in complex medium, 10 L. YPG (1) (□), YPG (2) (▲), plug inoculum, YPG (Δ) spore inoculum

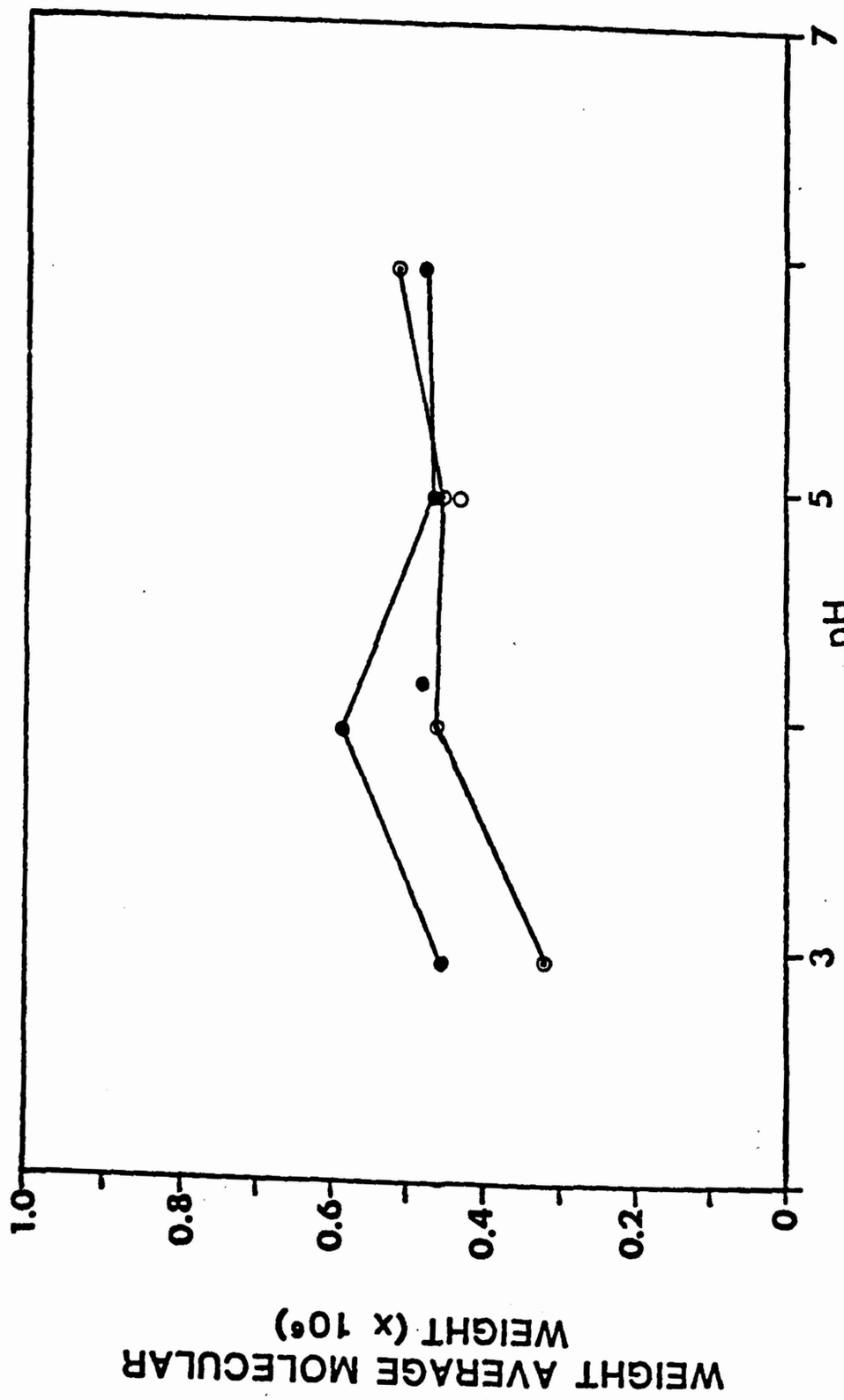

Figure 8. Effect of pH on weight average molecular weight in defined (●) and complex (○) media. Isolated points represent weight average molecular weight when pH is not controlled (initial pH = 4.2 and 5.0 for defined and complex media, respectively)

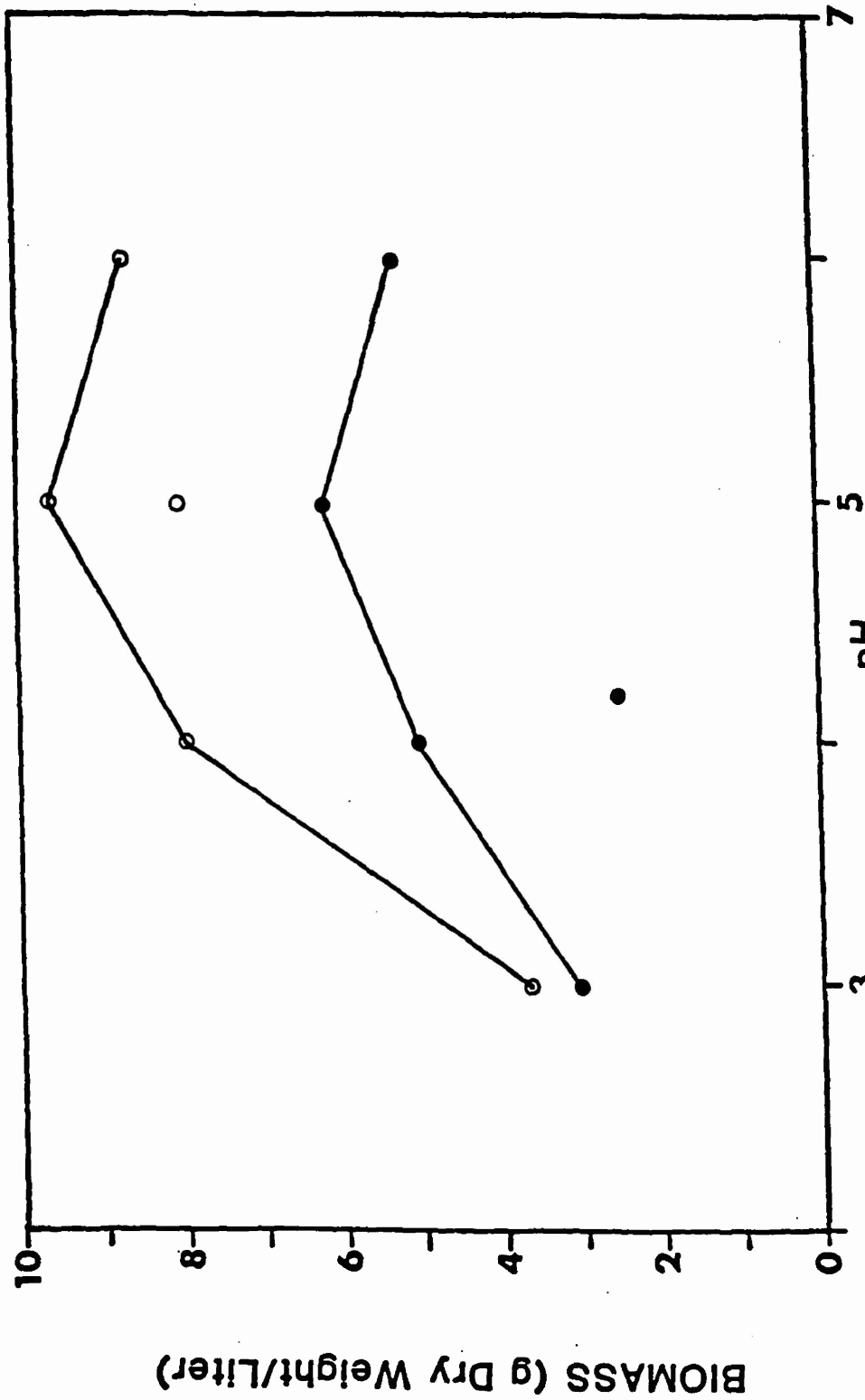

Figure 9. Effect of pH on biomass in defined (●) and complex (○) media. Isolated points represent biomass when pH is not controlled (initial pH = 4.2 and 5.0 for defined and complex media, respectively)

Studies of carbon and nitrogen sources, and phosphate concentration, determined that 10% sucrose was the best carbon source of those evaluated in terms of availability and economy, although the use of fructose produced the highest MW product, and soluble starch gave the best yield of low MW product. Combinations of peptone, ammonium sulfate, and urea were the best nitrogen sources evaluated, in terms of yield and MW distribution. Phosphate concentrations at pH 5.4 seemed to have little effect on MW distribution, at least during the incubation periods studied.

The processing procedure used in this study is shown in Fig. 3. The use of ROCCAL II (suggested by Dr. E. T. Reese, unpublished data[28]) in processing the polymer was with reference to the work of Scott[28] and that of Bouveng et al.[4,5] who used long-chain quaternary ammonium compounds to precipitate acid-soluble glycans and β-linked glucans from α-linked glucans. The neutral α-linked glucans remain in solution, and after the precipitated products are removed by centrifugation, can then be precipitated by solvents such as ethanol or acetone. Fuller's earth or activated carbon can also be used to adsorb the quaternary ammonium compound from the solubilized polymer; also, these substances aid in removing the discoloration products excreted into the medium by older cultures.[16,17,28]

In summary, defined MW fractions of pullulan were produced by varying fermentation conditions such as constituents of the culture medium, pH, length of incubation, etc. Pullulan biopolymer products with weight average MWs from 100 thousand to 4 million have been produced. The appropriate conditions were then established to produce sufficient quantities of low (below 500 thousand weight average MW), medium (1 to 2 million weight average MW), and high (above 2 million weight average MW) molecular weight pullulan products. Films and fibers, and chemical derivatives made from these different preparations are now under evaluation in terms of physical/chemical characterization.

A number of growth and processing variables influenced the yield of biomass production and the weight average molecular weight of the chitosan. Growth conditions included length of incubation, culture vessel volume, the form of inorganic nitrogen salt in defined medium, and medium component concentration. The processing variables affecting the yield of chitosan extracted were the type and strength of acid, and homogenization of cell wall material in acid before refluxing.

In complex media, weight average MW distribution increased rapidly over 72 hours of incubation, then declined as length of incubation increased. This was especially evident in YPG medium. It may be that the chitosan is degraded or turned over in the cell wall, or modified in the cell wall making extraction more difficult. There is documentation of the production of chitosanases in a strain of M. rouxii[23] which undergoes autolysis. In the strain of Mucor used in the study, autolysis did not begin until seven days.[23] We have found that the decline in weight

average MW begins prior to seven days. It is not believed that chitosanases are responsible. The chitosan must become accessible for the enzyme to be functional. Chitosan does not appear to become increasingly accessible, as the amount of chitosan extracted from the cell wall does not increase with time of incubation.

The difficulty in extracting high weight average MW chitosan may be due to the formation of an increased number of arthrospores with time as environmental stress occurs.[2] As was observed by Lugol's stain, the arthrospores proved to be more difficult to break apart during the extraction procedure, resulting in the chitosan being more difficult to extract. In addition, in the early stages of arthrospore production, the mycelium cell wall continues to surround the arthrospore cell wall.[1] In mature arthrospores, the mycelium cell wall becomes degraded. There appears to be no data on the chitosan of arthrospores, but it may be of a different nature than the chitosan in the mycelium, or less accessible to disruption and extraction from the cell wall.

Processing steps for the isolation and purification of chitosan are important in terms of the yields and MW distribution of the polymer. The type of acid used for extraction is important. White[30] determined that 1N (8.3%) hydrochloric acid was the acid of choice; however, this decision was based on yield and the of degree of acetylation. There were no MW determinations made. We tested hydrochloric acid but discontinued its use when the cell wall material turned brown and appeared to be degraded during the extraction. Acetic acid at different concentrations was evaluated. There were differences in the extraction efficiency, with 2% acetic acid producing the highest yield when compared to 1N and 4% acetic acid. It may be possible that the 1N (5.75%) and 4% acetic acid treatments were too strong and hydrolysis of the chitosan occurred. Homogenization of the cell wall prior to refluxing in acetic acid increased the efficiency of chitosan extraction, probably due to increased surface area of the cell wall material.

We evaluated a number of growth conditions that did not have an effect on the yield of biomass or MW distributions of the chitosan including; adjustment of culture media to a constant pH, addition of inorganic nitrogen salts to YPG, and supplementation of YPG with iron, manganese, or biotin in trace quantities. Adjusting the pH (pH 3.0, 4.0, 5.0, and 6.0) in defined and complex media to a constant value did not appear to affect the weight average molecular weight of chitosan. Biomass was not affected over the range pH 4.0 to 6.0; however, at pH 3.0 reduced biomass was observed.

In summary, while average molecular weight of chitosan extracted from the cell wall of M. rouxii can be controlled to some extent, low yields of chitosan (5% to 10% of total dry weight of biomass, 30% to 35% of cell wall) make M. rouxii unattractive at this time as a fungal source of chitosan until more efficient processing procedures or controls over biosynthesis can be developed.

Acknowledgement: We thank Drs. Elwyn Reese and Mary Mandels for their expertise and support.

REFERENCES

1. Barrera, C.R., Formation and Ultrastructure of Mucor rouxii Arthrospores. J. Bacteriol. 155:886-895 (1983).

2. Bartnicki-Garcia, S., and W.J. Nickerson, Isolation, Composition, and Structure of Cell Walls of Filamentous and Yeast-Like Forms of Mucor rouxii. Biochim. Biophys. Acta 58:102-119 (1962).

3. Bartnicki-Garcia, S., and W.J.Nickerson, Nutrition, Growth, and Morphogenesis of Mucor rouxii. J. Bacteriol. 84:841-858 (1962).

4. Bouveng, H. O., H. Kiessling, B. Lindberg, and J. McKay, Polysaccharides Elaborated by Pullularia pullulans. Part I. The Neutral Glucan Synthesized from Sucrose Solutions. Acta Chem. Scand. 16: 615-622 (1962).

5. Bouveng, H. O., H. Kiessling, B. Lindberg, and J. McKay, Polysaccharides Elaborated by Pullularia pullulans. Part III. Polysaccharides Synthesized from Xylose Solutions. Acta Chem. Scand. 17:1351-1356 (1963).

6. Catley, B. J., Pullulan, a Relationship Between Molecular Weight and Fine Structure. FEBS Letters 10:190-193 (1970).

7. Catley, B. J., Utilization of Carbon Sources by Pullularia pullulans for the Elaboration of Extracellular Polysaccharides, Appl. Microbiol. 22:641-649 (1971).

8. Catley, B. J., Role of pH and Nitrogen Limitation in the Elaboration of the Extracellular Polysaccharide Pullulan by Pullularia pullulans, Appl. Microbiol. 22:650-654 (1971).

9. Catley, B. J., The Rate of Elaboration of the Extracellular Polysaccharide, Pullulan, during Growth of Pullularia pullulans, Jour. Gen. Microbiol. 78:33-38 (1973).

10. Catley, B. J., Chapter 4, Pullulan Synthesis by Aureobasidium pullulans, p. 69-84, in Microbial Polysaccharides and Polysaccharases, Edited by R. C. W. Berkeley, G. W. Gooday and D. C. Ellwood, Special Publications of the Society for General Microbiology 3, Academic Press, New York, 1979.

11. Catley, B. J., The Extracellular Polysaccharide, Pullulan, Produced by Aureobasidium pullulans: A Relationship between Elaboration Rate and Morphology, Jour. Gen. Microbiol. 120:265-268 (1980).

REFERENCES (cont'd)

12. Fenton, D., B. Davis, C. Rotgers, and D. E. Eveleigh, Enzymatic Hydrolysis of Chitosan. pp 169-181 In Proceedings of the First International Conference on Chitin/Chitosan. Edited by R. A. A. Muzzarelli and E.R. Pariser. MIT Sea Grant MITSG 78-7, Index No. 78-307-Dmb. Massachusetts Institute of Technology, Cambridge, MA, (1978).

13. Foster, A.B. and Webber, J.M. Chitin. pp 371-393 In Advances in Carbohydrate Chemistry. Volume 15 Edited by M.L. Wolfrom and R.S. Tipson. Academic Press, New York, (1960).

14. Gorin, P. A. J., and E. Barreto-Bergter, Chapter 6, The Chemistry of Polysaccharides of Fungi and Lichens, p. 365-409, in The Polysaccharides, Volume 2, Edited by G. O. Aspinall, Academic Press, New York, (1983).

15. Hoog, G. S. de, and E. J. Hermanides-Nijhof, The Black Yeasts and Allied Hyphomycetes, Studies in Mycology 15, 222 pp., Centraalbureau voor Schimmelcultures, Baarn, Netherlands, (1977).

16. Kato, K., and M. Shiosaka, United States Patent 3,827,937, Method of Producing Pullulan (1974).

17. Kato, K., and M. Shiosaka, United States Patent 3,912,591, Process for the Production of Pullulan (1975).

18. Kreger, D. R. Observations on Cell Walls of Yeasts and Some Other Fungi by X-ray Diffraction and Solubility Tests. Biochim. Biophys. Acta 13:1-9 (1954).

19. Lacroix, C., A. LeDuy, G. Noel, and L. Choplin, Effect of pH on the Batch Fermentation of Pullulan from Sucrose Medium, Biotechnol. Bioengineer. 27:202-207 (1985).

20. Muzzarelli, R. A. A. and R. Rocchetti, Determination of the Degree of Acetylation of Chitosans by the First Derivative Ultraviolet Spectrophotometry. Carbohydrate Polymers 6:461-472. (1985).

21. Ono, K., N. Yasuda, and S. Ueda, Effect of pH on Pullulan Elaboration by Aureobasidium pullulans S-1, Agric. Biol. Chem. 41:2113-3118 (1977).

22. Ramos, S., and I. Garcia Acha, A Vegetative Cycle of Pullularia pullulans, Trans. Br. Mycol. Soc. 64:129-135 (1975).

23. Reyes, F., R. Lahoz, M. J. Martinez, and C. Alfonso, Chitosanases in the Autolysis of Mucor rouxii. Mycopathologia 89:181-187. (1985).

REFERENCES (cont'd)

24. Romano, A. H., Chapter 7, Dimorphism, p. 181-209, in The Fungi, Volume II, The Fungal Organism, Edited by G. C. Ainsworth and A. S. Sussman, Academic Press, New York, 1966.

25. Rouget, C., Des Substances Amylacees Dans les Tissues des Animaux, Specialement des Articules (Chitine). Compt. Rend. Acad. Sci. Paris. 48:792-795. (1859).

26. Sandford, P. A., and J. Baird, Chapter 7, Industrial Utilization of Polysaccharides, p. 412-490, in The Polysaccharides, Volume 2, Edited by G. O. Aspinall, Academic Press, New York, (1983).

27. Sannan, T., K. Kurita, K. Ogura, and Y. Iwakura, Studies on Chitin: 7. I.R. Spectroscopic Determination of Degree of Acetylation. Polymer 19:458-459. (1978).

28. Scott, J. E., Aliphatic Ammonium Salts in the Assay of Acidic Polysaccharides from Tissues, p. 145-196, in Methods of Biochemical Analysis, Vol. VIII, Edited by D. Glick, Interscience, New York, (1960).

29. Ueda, S., K. Fujita, K. Komatsu, and Z. Nakashima, Polysaccharide Produced by the Genus Pullularia, I. Production of Polysaccharide by Growing Cells, Appl. Microbiol. 11:211-215 (1963).

30. White, S.A., P. R. Farina, and I. Fulton, Production and Isolation of Chitosan from Mucor rouxii. Appl. Environ. Microbiol. 38:323-328 (1979).

31. Wu, A. C. M., B. A. Bough, E. C. Conrad, and K. E. Alden, Jr, Determination of Molecular-Weight Distribution of Chitosan by High-Performance Liquid Chromotography. Journal of Chromotography, 128:87-99 (1976).

HOST AMYLASES AND PULLULAN PRODUCTION

Timothy D. Leathers

Northern Regional Research Center
Agricultural Research Service
U.S. Department of Agriculture†
1815 N. University Street
Peoria, Illinois 61604

Introduction

Pullulan is a unique polysaccharide with biomaterial applications that include compression moldings, films, and fibers.(9) Starch, an agricultural commodity currently in vast surplus, is the most commonly employed feedstock for pullulan fermentations.(9)

Exceedingly little is understood about the enzymology of pullulan biosynthesis. But, clearly, fermentations from starch require amylase as a prerequisite step. Amylase may also play a less obvious role in the post-synthetic alteration of pullulan. The internal α-1,4 linkages of the maltotriose subunits of pullulan have been found resistant to attack from amylases of all types, since these subunits are themselves linked α-1,6. However, studies by Catley and coworkers have demonstrated that maltotetrose subunits occur in pullulan, randomly distributed and representing up to 7% of total subunits.(1) These maltotetrose subunits can be specifically hydrolyzed by α-amylase from human saliva and porcine pancreas. Catley has proposed that host amylase activities may also attack pullulan, and account for the distinct drop in pullulan molecular weight often observed in late stationary-phase cultures. Molecular weight control is an important concern, especially for pullulan film and fiber applications.

Although host amylases may thus function as the first and last enzymatic steps in pullulan fermentation, and they should be by far the most accessible enzymes of pullulan biosynthesis, no quantitative information has been available concerning amylases from Aureobasidium pullulans, particularly as they might affect the quantity and quality of pullulan produced.

† The mention of firm names or trade products does not imply that they are endorsed or recommended by the U.S. Department of Agriculture over other firms or similar products not mentioned.

LEATHERS

Culture Sources

In a soon-to-appear survey, we identified 8 strains of A. pullulans as capable of authentic pullulan production with at least 20% conversion efficiency of substrate to polysaccharide under our culture conditions (Table 1). Included were strain NRRL Y-2567 (QM-3090), studied by Catley and a number of other workers, and four other strains previously described as outstanding sources of pullulan (Y-6220, Y-12,996, Y-12,997, and Y-12,999). For subsequent graphic illustrations, these strains are sequentially numbered from 1 to 8.

Results and Discussion

Figure 1 presents pullulan yields from parallel 9-day starch- and sucrose-grown cultures. Starch fermentation consistently resulted in higher pullulan yields, with conversion efficiencies of up to 50%. Substrate preference varied considerably, however, on a strain-specific basis; strain 5 performed nearly as well on sucrose as on starch.

As a relative measure of pullulan molecular weight, culture supernatant viscosities were assayed (Figure 2). Relative viscosity divided by polysaccharide yield should be a function of molecular weight. Viscosity/yield is not a true intrinsic viscosity, but should serve as a valid relative measure. Results indicated that pullulan molecular weights were always higher from sucrose cultures (from which yields were lowest). Starch cultures were consistently of low viscosity, whereas sucrose cultures varied considerably, on a strain-specific basis.

We next determined the cellular location of amylase from A. pullulans (Figure 3). Starch-grown cultures of strains 1 and 5 were employed. Amylase assays were by dinitrosalicylic acid detection of reducing sugar equivalents of maltose released from starch. This method should equally represent potential endo- and exoglucanases. Activities were expressed in international units (IU). Cells suspended in their original culture medium were compared with cognate cell-free medium. Within error, cells added no activity to cleared culture medium. We concluded that amylases from A. pullulans were not cell-bound.

Amylase yields from all 8 strains, grown on either starch or sucrose, are shown in Figure 4. Starch-grown cultures uniformly produced from 10 to 20 IU amylase per liter. With one obvious exception, sucrose cultures exhibited low to negligible amylase activity, which suggests that amylase production is regulated, possibly by induction or catabolite repression. Strain 3 (YB-4587) was exceptional in the production of relatively high amylase levels from cultures grown on sucrose. For reasons described below, we suspect that this activity includes little or no α-amylase.

LEATHERS

TABLE 1. STRAINS OF *Aureobasidium pullulans* IN THIS STUDY

1.	NRRL	Y-2567	QM-3090, QM-3092, ATCC 9348, F-44
2.	NRRL	YB-4026	
3.	NRRL	YB-4587	
4.	NRRL	Y-6220	ATCC 34647, M-42
5.	NRRL	Y-12,974	
6.	NRRL	Y-12,996	ATCC 42023
7.	NRRL	Y-23,997	IFO 4464
8.	NRRL	Y-12,999	PBR-P_P-Km-3

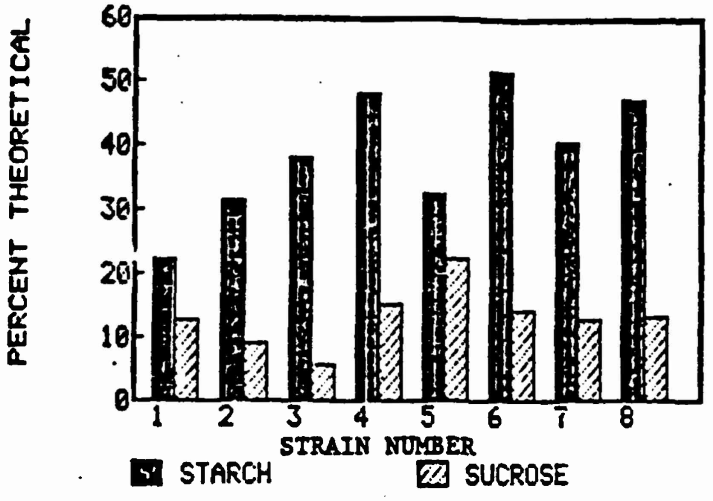

Figure 1. Extracellular polysaccharide yields from 8 test strains grown on starch or sucrose. Tetrahydrofuran precipitates of culture supernatants were baked under vacuum to constant weight; yields are expressed as percentages of initial carbon.

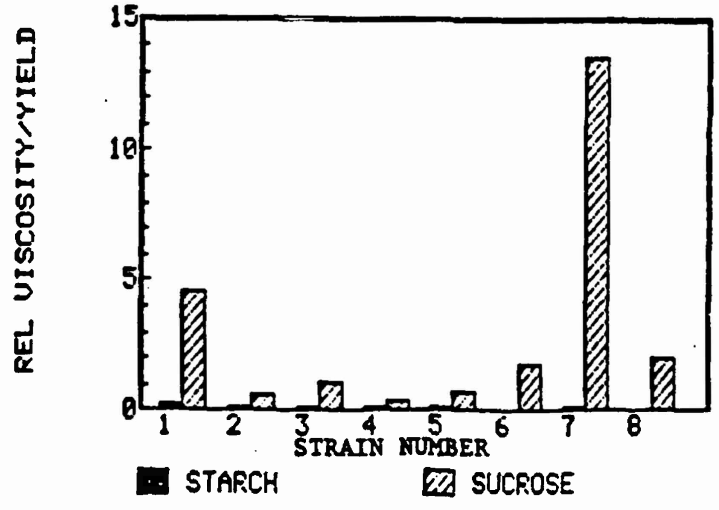

Figure 2. Relative viscosities of 8 test strains grown on starch or sucrose. Viscosities were normalized for total polysaccharide yield, to provide a value that is a function of product molecular weight.

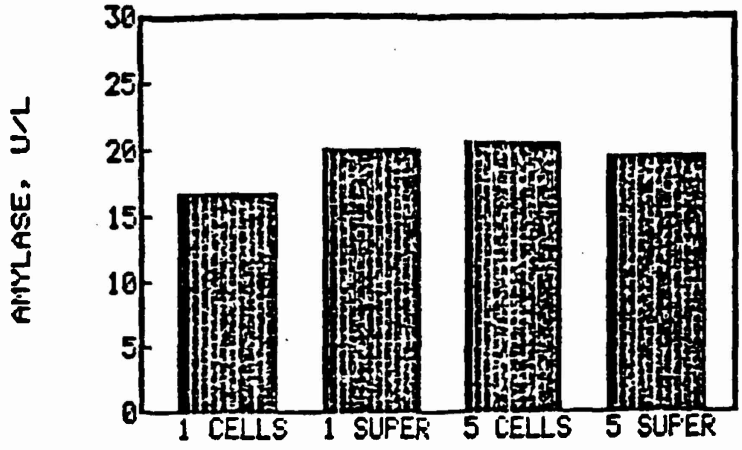

Figure 3. Cellular localization of amylase from representative strains 1 (Y-2567) and 5 (Y-12,974). Activities from cells suspended in original culture medium,"CELLS", were compared with those from medium cleared of cells,"SUPER".

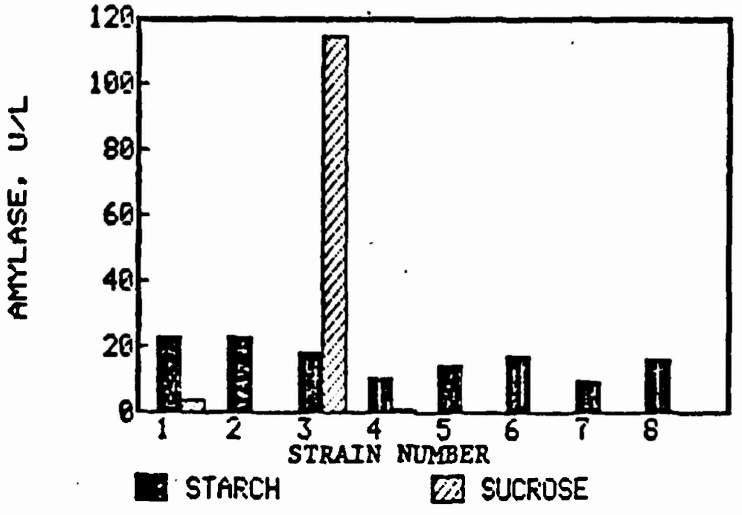

Figure 4. Amylase yields from 8 test strains grown on starch or sucrose. Culture supernatants from 9-day cultures were assayed by dinitrosalicylic acid-detection of reducing sugar equivalents (of maltose) released from starch.

Perhaps not immediately apparent are the comparatively low levels of all of these amylase measurements. Amylase yields from a number of fungi (published work of various authors) are summarized in Table 2. Although most hyphal fungi (molds) produce amylases, the trait has been found to be rare among yeastlike fungi. Table 2 includes most of known amylase-producing yeasts. Well-characterized hyphal sources of amylase were approximately 1000 times more active than those we measured from A. pullulans. Unfortunately, amylase yields for many of the yeastlike species shown in Table 2 were expressed in nonstandard units so that a meaningful comparison is impossible. Data from Table 2 are biased, in that they were derived from surveys for high amylase sources. But our results are also selective, as these 8 strains of A. pullulans were chosen for high pullulan production. If free sugar in culture medium were responsible for reduced pullulan yields (perhaps through catabolite control), it is conceivable that superior pullulan-producing strains might express minimal amylase activities. The work of Federici, while largely qualitative (involving + plate assays), indicated that at least certain strains of A. pullulans may be active amylase producers.(2) We have not yet surveyed amylases from poor pullulan sources. It is possible, however, that amylase assays could serve as a new rapid screen for potential high pullulan producers.

Crude specific activities of amylase from A. pullulans cultures were also quite low compared to those from other fungal sources (data not shown). These results suggest that pullulan strains either secreted low levels of amylase with respect to other extracellular proteins or produced amylase with distinctively low activity.

Total extracellular proteins from A. pullulans cultures were subsequently resolved on denaturing polyacrylamide gels (data not shown). Previously characterized fungal amylases ranged from 30 kd to 50 kd in molecular weight.(3-8,10) Although most cultures contained proteins of about 45 kd, these were abundant only in cultures (both sucrose- and starch-grown) from strain 3. No abundant protein species were clearly common to all high amylase samples examined and absent from low amylase samples. Low amylase yields and crude specific activities may, therefore, reflect low amylase protein levels rather than low specific activities. Sucrose-grown strain 3 cultures contained an abundant, unique protein of about 18 kd that may be correlated with its unusual amylase activity, as discussed below.

To directly test the possibility that host amylases recognize pullulan, culture activities against commercial pullulan (300 kd, Fluka Chemical) were measured. In preliminary experiments, we confirmed that commercial pullulan was susceptible to human salivary amylase (HSA). As Figure 5 shows, only culture supernatants that contained significant activity against starch also showed activity against pullulan (i.e., all starch cultures, plus sucrose cultures of strain 3).

TABLE 2. FUNGAL AMYLASES

SPECIES	MORPHOLOGY	CRUDE AMYLASE LOCATION	CRUDE AMYLASE YIELD U/ml	CRUDE AMYLASE SPECIFIC ACTIVITY U/mg	REFERENCE
Aspergillus niger	Mycelial	Extracellular	250	100	Ramachandran et al., 1978
Aureobasidium pullulans	Yeastlike	?	?	?	Federici, 1982
Candida tropicalis	Yeastlike	Extracellular	?	?	Sawai, 1958
Endomycopsis figuliger	Yeastlike	?	?	?	Wickerham et al., 1944
Endomyces sp.	Yeastlike	Extracellular	1.2	?	Hattori, 1961
Lipomyces starkeyi	Yeastlike	Cell-bound	NA	600	Moulin & Galzy, 1979
Mucor pusillus	Mycelial	Extracellular	702	704	Somkuti & Steinburg, 1980
Torulopsis ingeniosa	Yeastlike	Cell-bound	NA	206	Moulin & Galzy, 1978

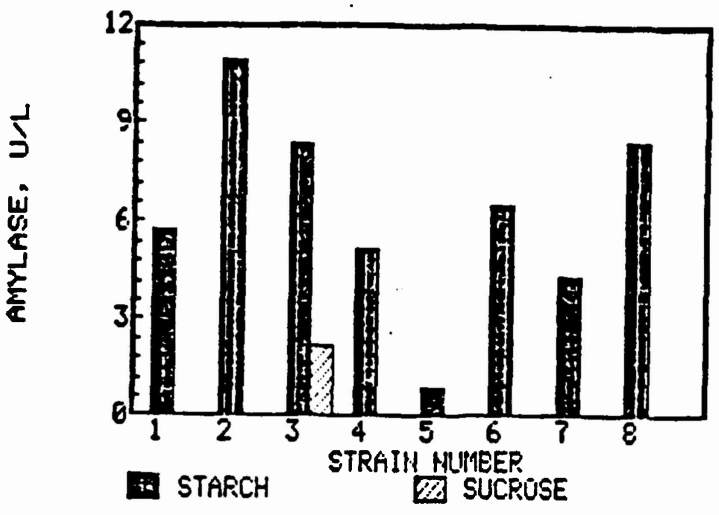

Figure 5. Amylase activities against pullulan were measured from 8 test strains grown on starch or sucrose. Commercial pullulan (300 kd, Fluka Chemical Co.) was used as substrate in reducing sugar assays.

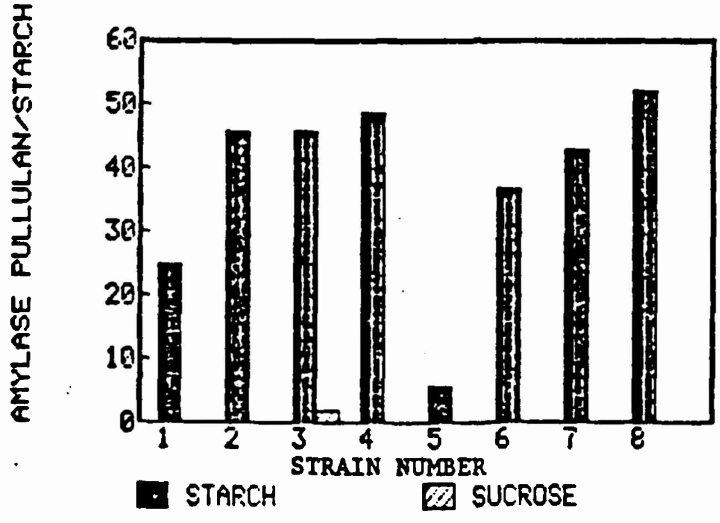

Figure 6. Amylase activities against pullulan from 8 test strains grown on starch or sucrose, expressed as percentages of culture activities against starch.

Figure 6 presents (as percentages) the ratios of culture activities against pullulan to activities against starch. Among starch cultures of 6 strains, these percentages were fairly constant, falling between 20 and 50%. These results suggest that pullulan-specific activity (presumably α-amylase) is typically a constant proportion of total amylase. Quite possibly, most strains produce only α-amylase when grown on starch. These amylases may also have an exceptionally high affinity for pullulan. By comparison, the ratio of pullulan-to-starch activity of HSA was less than 1%. The inclusion of maltotetrose residues may, therefore, be a purposeful mechanism, designed to permit cells to reduce environmental viscosity under certain conditions.

Starch-grown cultures of strain 5, and sucrose-grown strain 3, had much lower ratios of pullulan-to-starch activity. These strains may have produced exoglucanase activities (e.g., glucoamylase) or another hydrolase with partial activity on starch. Interestingly, sucrose-grown cultures of strain 3 were found to have exceptionally high invertase levels (data not shown).

Figure 7 summarizes culture amylase levels and relative viscosities. While not all cultures with low amylase were of high viscosity, no viscous culture contained over 5 IU amylase per liter, and no culture with over 10 IU/L was highly viscous. We conclude that relatively low amylase (less than 5 to 10 IU/L) may be a necessary but insufficient condition for high molecular weight pullulan production.

Conclusions

To summarize our conclusions: 1. Amylases from A. pullulans were not cell-bound. 2. Amylases were regulated by growth on starch. 3. Pullulan-productive strains had overall low amylase yields, specific activities, and protein abundances. 4. Host amylases had a relatively high specificity for pullulan. 5. Amylase levels in excess of 5-10 IU/l may have been detrimental to pullulan molecular weight. 6. Significant strain variability was found in both amylase and pullulan production.

Host amylases may, therefore, be critical to both pullulan yields and molecular weight. In order to optimize both, a strain might be desirable that expresses only a regulated, low-level α-amylase, or perhaps only exoglucanase activity. A combination of rational mutant selections and genetic engineering may have real potential to address these possibilities.

I thank Stanley L. Janson for his dedicated efforts and technical skill in the performance of these studies.

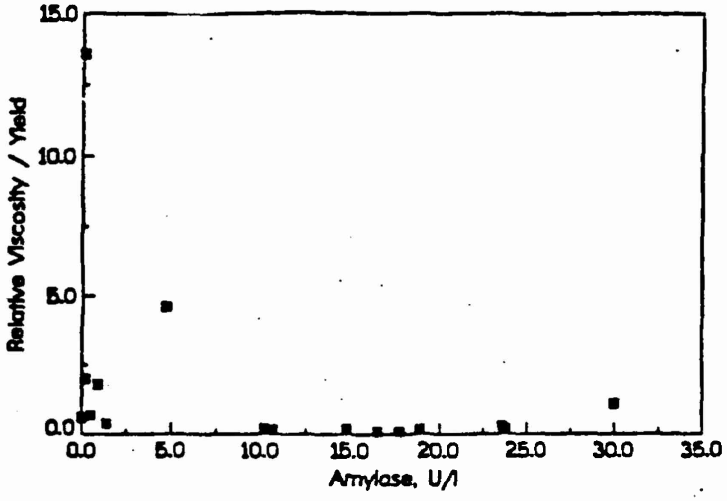

Figure 7. Correlation of amylase yields from 8 test strains grown on starch or sucrose, and normalized culture viscosities. Extreme amylase value from sucrose-grown strain 5 (Y-12,974) omitted for figure clarity.

References

1. Carolan, G., Catley, B. J., and McDougal, F. J. 1983. Carbohydr. Res. 114:237.

2. Federici, F. 1982. Mycologia. 74:738.

3. Hattori, Y. 1961. Agric. Biol. Chem. 25:737.

4. Moulin, G., and Galzy, P. 1978. Folia Microbiol. 23:423.

5. Moulin, G., and Galzy, P. 1979. Agric. Biol. Chem. 43:1165.

6. Sawai, T. 1958. J. Biochem. 45:49.

7. Somkuti, G. A., and Steinburg, D. H. 1980. Dev. Indus. Microbiol. 21:327.

8. Ramachandran, N., Sreekantiah, K. R., and Murphy, V. S. 1978. Starch/Starke 30:272.

9. Yuen, S. 1974. Process. Biochem. 9:7.

10. Wickerham, L. J., Lockwood, L. B., Pettijohn, O. G., and Ward, G. E. 1944. J. Bacteriol. 48:413.

CHITOSAN, NATURE'S MOST PLENTIFUL CATIONIC BIOPOLYMER: COMMERCIAL USES OF ITS POWDER, FIBER, FILM BEAD AND SOLUTION FORMS

Paul A. Sandford, PhD

Protan Laboratories, Inc.
Redmond, WA 98052

ABSTRACT

Chitosan, a natural, nontoxic, biodegradable, high molecular weight polymer, is produced commercially on a large scale. For some time, it has been sold commercially as a solution, flaked and fine powder, and more recently in bead and fiber forms. Chitosan's availability in a variety of useful forms and its unique chemical and biological properties make it a very attractive biomaterial. Chitosan's key properties are its ability to act as a cationic flocculant, humectant, viscosifier, and chelator of selective metal ions. Chitosan's ability to be made into films, fibers and beads as well as powders and solutions, lead to many commercial applications. The main objective of this work will be to give an overview of the wide variety of useful forms of chitosan that are now commercially available or are soon to be commercialized.

CHITIN/CHITOSAN STRUCTURE

Even though chitosan was first described in 1811 and named by Odier in 1823, chitin and chitosan are not as well known as the related biopolymer cellulose (refs. 1-2), which has been used commercially for some time. Like cellulose, chitin is a $\beta(1\rightarrow4)$-linked glycan composed of 2-acetamido-2-deoxy-D-glucose (N-acetylglucosamine) (see Fig. 1). Chitosan is the name used for low acetyl forms of chitin and is composed of glucosamine, 2-amino-2-deoxy glucose. Glucosamine and its N-acetylated form are the most abundant amino sugars occurring in polysaccharides, glycoproteins, cell walls, etc.

FIGURE 1

STRUCTURAL SIMILARITIES
OF CHITIN, CHITOSAN AND CELLULOSE

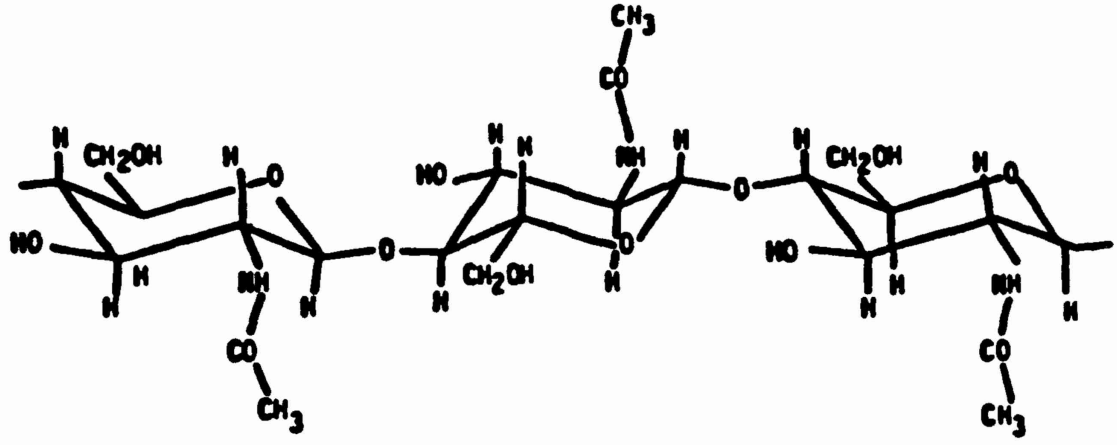

(a) CHITIN

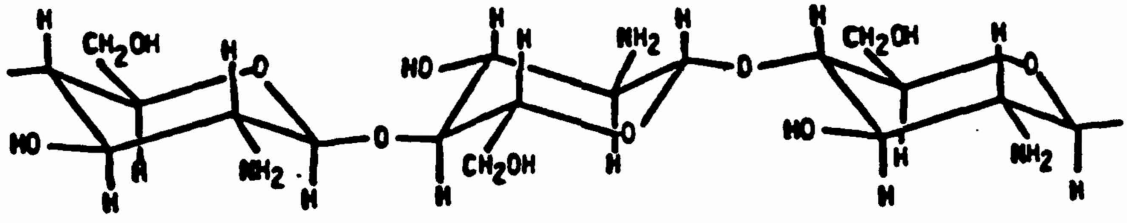

(b) CHITOSAN

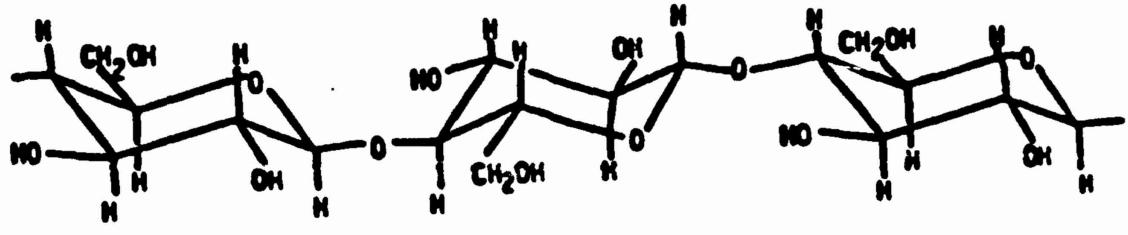

(c) CELLULOSE

COMMERCIAL SOURCES

Chitin is the second most abundant natural biopolymer, cellulose being the most abundant. Chitin is widely distributed throughout nature. The most easily exploited sources are the protective shells of crustaceans such as crabs and shrimp. Allan (refs. 3-5) has estimated that worldwide annually there is over 39,000 tons of chitin available from shellfish. This estimate does not include krill, which has a potential of 56,000 tons annually.

Table 1 lists the main sources of shellfish that are used in the U.S. to make chitosan.

TABLE 1

MAIN U.S. SOURCES OF CHITIN

* CRAB SHELLS
  - *Cancer magister* (Dungeness crab)
  - *Paralithodes camschatica* (King crab)
* SHRIMP SHELLS
  - *Pandalus borealis* (Pacific shrimp)

Since crab and shrimp are harvested in different seasons, raw materials for chitin production are always readily available.

CHITIN MANUFACTURING PROCESS

Figure 2 outlines the key steps in the extraction of chitin from shellfish by-products. First, proteins are removed from ground shell by treating with sodium hydroxide. Minerals such as calcium carbonate and calcium phosphate are extracted with hydrochloric acid. After rinsing, the chitin is dried as a flaked material. Maintaining inventories of chitin allows processing of vast amounts of shellfish waste without processing to any one particular grade of chitosan.

FIGURE 2

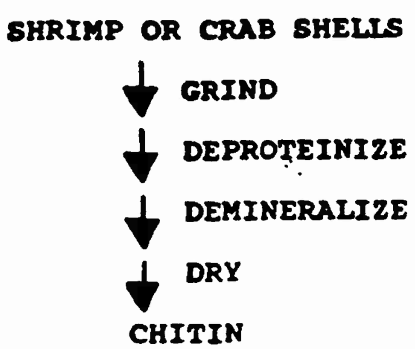

CHITOSAN MANUFACTURING PROCESS

Figure 3 illustrates the scheme to make chitosan. Chitin is first treated with very strong NaOH to hydrolyze the N-acetyl linkage, then rinsed, pH adjusted and dewatered. At this state, the chitosan can be dried to give what we call flaked chitosan. This is a course mesh product whose particle size can be reduced by milling to give a finer mesh powder. Chitosan powder in turn can be dry blended with an organic acid, such as adipic acid, to give a chitosan acid blend that is self-dissolving. It should be remembered that chitosan in its free amine form is not usually soluble in water at pH above 6.5 and requires acid to prepare aqueous solutions.

FIGURE 3

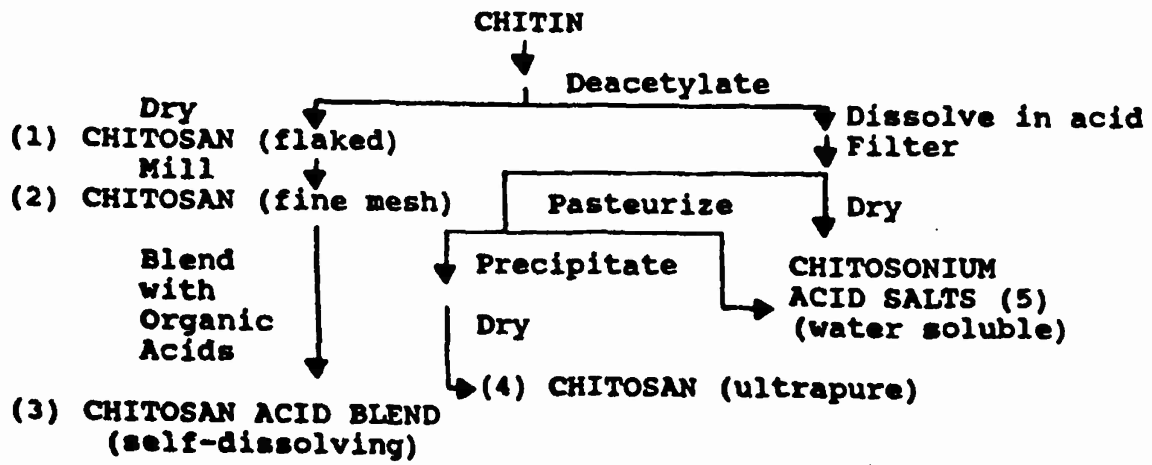

CHITOSAN MANUFACTURING PROCESS

One scheme to prepare chitosan of improved purity is to dissolve it in an acid (e.g. acetic acid) and to filter it to remove extraneous materials. Depending on the application, the clarified solution can then be pasteurized and reisolated to give an ultrapure product, or the solution can be dried to give water soluble chitosonium acid salts. It should be pointed out that covalent chitosan derivatives can also be made, but derivatives will not be covered here.

QUALITY ASSURANCE

Key to any successful manufacturing process is quality control. We at Protan take pride in the quality of our products. We have made great strides in producing more uniform products, even within the last year.

The type of routine analyses we perform are listed in Figure 4. For example, we measure % deacetylation and intrinsic viscosity and calculate viscosity average molecular weights on each chitosan lot. For ultrapure chitosan, new Q.A. procedures are being devised and will include the analysis of most commonly encountered metals. Currently, we are measuring metals by atomic absorption and inductively coupled plasma emission analyses.

KEY PROPERTIES RELATING TO COMMERCIAL USES

Cationic Properties

Many of chitosan's uses depend upon its cationic nature. (See Table 2)

TABLE 2

CHITOSAN: CATIONIC PROPERTIES

* Linear Polyelectrolyte

* High charge density

* Excellent flocculant

* Adheres to negatively charged surfaces

* Substantive to hair, skin

* Chelates metal ions

  - Iron (Fe), Copper (Cu)
  - Toxic metals (Cd, Hg, Pb, Cr, Ni)
  - Radionucleides (Pu, U)

SANDFORD

FIGURE 4

CHITOSAN QUALITY ASSURANCE
DATA SUMMARY

CHITOSAN LOT #: _____ GRADE: _____

Q.A. CODE 3	PROCEDURE	MEAN VALUE $\bar{X}$	STANDARD DEVIATION σ
100	% Moisture		
200	% Ash		
400	Solids Qualitative Observation		
	a. Form		
	b. Glossiness		
	c. Color		
500	% Protein		
600	Solution Qualitative Observation		
	a. Color		
	b. Insolubles		
	c. Odor		
700	Viscosity (cps)		
725	% Deacetylation		
750	Intrinsic [dl/g] viscosity		
775	Viscosity average molecular weight x 10^6		
800	Turbidity [NTU]		
900	% Insolubles		

COMMENTS:

Prepared By: _____ Date: _____

Approved By: _____ Date: _____

Chitosan is a linear polyelectrolyte at acidic pH. It has a high charge density, one charge per glucosamine unit. Since many materials carry negative charges (e.g., proteins, anionic polysaccharides, nucleic acids, etc.), the positive charge of chitosan interacts strongly with negative surfaces to give an electric neutrality.

Chitosan is an excellent flocculant due to its vast number of $-NH_3^+$ groups that can interact with negatively charged colloids. Chitosan adheres readily to natural polymers such as hair and skin, which are composed of negatively charged mucopolysaccharides and proteins.

Chitosan forms complexes with many metal ions. Thus, it is useful in chelating iron, copper and magnesium and can also be used to remove toxic heavy metal ions such as silver, cadmium, mercury, lead, nickel and chromium (ref. 6).

Biological Properties

Many of chitosan's biomedical applications rely on its nontoxic and biodegradable properties (Table 3). Chitosan has been shown to accelerate wound healing (see Tables 9 & 10 later) (ref. 7), reduce serum cholesterol levels (ref. 8) and stimulate the immune system (ref. 9). Chitosan, when coated on seeds, results in increased crop yields, apparently due to chitosan inducing a protective response by the germinating plant (ref. 10).

TABLE 3

CHITOSAN: BIOLOGICAL PROPERTIES

* Biocompatible
  - nontoxic
  - biodegradable
  - natural polymer
* Bioactivity
  - wound healing accelerator
  - reduce blood cholesterol levels
  - immune system stimulant

Chemical Properties

Chitosan, being a high molecular weight polymer, is a linear polyamine whose amino groups are readily available for chemical reactions and salt formation with acids (Table 4).

Since chitosan can be viewed as a cellulose derivative, the primary (C-6) and secondary (C-3) hydroxyl groups can be used to make derivatives. The scientific literature contains many interesting chemical derivatives of chitosan with commercial potential (ref. 6).

TABLE 4

CHITOSAN: CHEMICAL PROPERTIES

* Linear polyamine (poly D-glucosamine)

* Reactive amino groups

* Reactive hydroxyl groups

COMMERCIAL PRODUCTS

The type of chitosan used commercially is determined by its physical form (flake, powder, solutions), its purity (ultrapure, standard, industrial) and its molecular form [high to low viscosity, percent deacetylation (>75%), free amine or acid salt], and ultimately the cost (Table 5).

TABLE 5

CHITOSAN: COMMERCIAL PRODUCTS

PROTASAN™

- Ultrapure quality
- In vivo biomedical uses
- Powder/solution

SEA CURE™

- High Quality
- Flake/powder/beads/fibers
- Low, medium, high viscosity grades
- Cosmetics/personal care
- Enzyme/cell immobilization
- Pharmaceutical/medical
- Membranes
- Food related

PRO FLOC™

- Flake/powder
- Self-dissolving blends
- Low, medium, high viscosity grades
- Waste treatment
- Agriculture uses
- Industrial uses
- Metal recovery
- Detoxification

Protasan(TM), having the highest purity, has the quality needed for internal body uses where the product must be nontoxic, nonpyrogenic and completely absorbable. Sea Cure(TM) is a standard but high quality material useful for cosmetics, personal care, topical medical applications, enzyme immobilization, etc. Pro Floc(TM), designated for industrial applications where quality requirements are not as stringent, is used in agriculture, waste management, metal recovery and many general applications.

Another product, Sea Klear(TM), is a solution of chitosan being marketed successfully as a swimming pool and spa natural clarifier (ref. 11).

CHITOSAN: VERSATILE BIOMATERIAL

The interest in chitosan as a biomaterial is partly due to the large variety of useful forms that either are commercially available or can be readily obtained. Table 6 lists many of the forms of chitosan that are being actively pursued commercially.

TABLE 6

CHITOSAN: NATURE'S MOST VERSATILE BIOMATERIAL

POWDER	- course to fine - coating - spray - fast dissolving - high purity
FILM	- tough, clear, flexible - O_2 permeable - adheres to negative surfaces
FIBER	- strong - flexible - biodegradable
SHAPED OBJECTS	- suitable for orthopedics - bioerodable - readily molded
GEL	- high gel strength - formed easily with poly anions
BEADS	- easy to make - encapsulate - size selectable - porosity can be varied - easy to crosslink/attach enzymes

TABLE 6 CONT.

PASTE/SALVE/LOTIONS	- excellent feel - moisture retention - easy to formulate
SOLUTIONS	- high to low viscosity - many salt forms - high clarity - water clear

---

CHITOSAN APPLICATIONS

1. Clarification and Purification of Water and Beverages

Flocculant -- The largest single use of chitosan is in the clarification of wastewater in Japan. Since chitosan is a natural polymer, it is preferred over synthetic polymer flocculants which may contain hazardous monomers. (See Table 7.)

In conjunction with the Division of Animal Feed, Department of Health and Human Service, and the U.S. Food and Drug Administration (FDA), the Association of Animal Feed Control Officials, Inc. (AAFCO) has issued the following description of chitosan as a flocculant for recovering proteinaceous material (ref. 12). (See Table 8.)

"Chitosan is a cationic carbohydrate polymer intended for use as a precipitating agent of proteinaceous material for food processing plants. It is chemically derived by deacetylation of the naturally occurring chitin in crab and shrimp shells. It may be used in an amount not to exceed that necessary to accomplish its intended effect. Chitosan, when fed as a component of feed to livestock, shall be present at no more than Ø.1% of the feed. Proteinaceous material coagulated with chitosan must have safety and efficacy data approved before it can be registered or offered for sale." (Proposed, 1984, Adopted 1985)

According to the U.S. Environmental Protection Agency, chitosan is acceptable for potable water applications when used within the stated rates and under the restrictions listed (ref. 13):

1. A bed of flaked chitosan may also be used as filter medium in potable water treatment.

2. Whereas deacetylated chitin is newly proposed as a potable water treatment chemical, and whereas such new chemicals do not fulfill the requirement of "virtual identity" in FR 44, No. 141, below, chitosan is acceptable for use only on an experimental or pilot basis, under conditions which are carefully controlled by the appropriate state.

TABLE 7

CHITOSAN APPLICATIONS: CLARIFICATION AND PURIFICATION
Not-Food Related

KEY USES	KEY FUNCTIONS
* Sewage effluents	* Nontoxic
* Sand & gravel wash	* Biodegradable
* Metal finishing electroplating wastes	* Chelate metal ions
* Paper mills	* Flocculant
* Radioactive wastes	* Used extensively in Japan

TABLE 8

CHITOSAN APPLICATIONS: CLARIFICATION AND PURIFICATION
Food Related

KEY USES	KEY FUNCTIONS
* Drinking water	* Nontoxic
* Recover protein for animal feed - rendering plants - vegetable processing - poultry/egg processing	* Biodegradable * Remove tannin/acids * EPA approved (pilot) * FDA/AAFCO approved ($\leq$0.1%)
* Fruit juices	
* Microalgae recovery	
* Muddy fishing lakes	

2. Chelation

Since chitosan is an excellent chelator of many harmful metals (e.g., copper, nickel, chromium, cadmium, manganese, cobalt, lead, mercury, zinc, uranium and silver), a sharp increase in interest in using chitosan to detoxify hazardous wastes has developed (refs. 3,6,14-16). Chitosan's ability to chelate iron, as well as its flocculating activity, makes it a very useful pool and spa clarifier.

3. Pharmaceutical (Tables 9 & 10)

There are several reasons why chitosan is being actively pursued by pharmaceutical companies. First, it has many useful as well as biological characteristics that allow it to be used in wound healing (see Table 10). In drug delivery, it is chitosan's biocompatibility and its ability to be totally absorbed in vivo (e.g., lysozyme) that allow its use in bioerodable and orthopedic devices.

TABLE 9

CHITOSAN APPLICATIONS: PHARMACEUTICAL

* Wound Healing

* Drug Delivery

* Bioengineering Material

  - orthopedic
  - contact lens

* Cholesterol Reducing Agent

  - Investigative New Drug (IND) application
  - human feeding trials

Since chitosan has been shown to be effective in lowering serum cholesterol when added to the diet, human feeding trials are scheduled requiring the filing of an Investigative New Drug (IND) with FDA (ref. 17).

TABLE 10

CHITOSAN APPLICATIONS: WOUND HEALING

Key Properties

- Biocompatible
- Accelerate wound healing
- Absorb liquids
- Reduce fibroplasia (scar tissue)
- Hemostatic
- Form protective film/coating

Variety of Useful Forms

- Powder
- Paste/salve
- Solution/gel
- Film
- Fiber
- Spray

Potential Uses

- Bandages
- Sutures
- Synthetic skin
- Eye bandage

4. Cosmetics/Personal Care

Since chitosan is an excellent humectant and is cationic, it is being used in both skin and hair applications.

TABLE 11

CHITOSAN APPLICATIONS: COSMETICS/PERSONAL CARE

* Natural, Nontoxic, Cationic Polymer

* Hair Treatment

  - clear solutions for clear films
  - substantive to hair
  - obtain gels in water:alcohol mixtures
  - viscosity can be varied; low to high to suit application

* Skin Care

  - moisturizer
  - substantive to skin
  - excellent tactile properties

5. Agriculture

Chitosan has been used several seasons as wheat seed coating. This application grew out of research at Washington State University, where it was shown that chitosan-coated wheat resulted in increased crop yields (ref. 18). EPA permits the use of chitosan for coating wheat seed and it is being used in 11 states so far. Apparently, chitosan triggers a response in the seed, signaling the plant to protect itself from natural predators, such as pathogenic fungi, most of which have chitin in their cell walls.

TABLE 12

CHITOSAN APPLICATIONS: AGRICULTURAL

* Coat Seeds (wheat, rice, peas)
  - fungistatic, protect plants
  - nontoxic, biodegradable, biocompatible
  - increase crop yields
  - EPA approved

* Animal Feed
  - approved flocculant for recovering proteinaceous wastes (FDA/AAFCO, $\leq$ 0.1% feed)
  - natural binder for fish feed

* Fertilizer (8.7% N)/Soil Stabilizer/Metal Chelator

5. Biotechnology

Chitosan has been used to immobilize cells containing useful enzymes and to immobilize enzymes directly (refs. 19-22).

TABLE 13

CHITOSAN APPLICATIONS: BIOTECHNOLOGY

* Immobilization of Enzymes and Cells
  - entrapment and absorption
  - crosslinked with dialdehydes (e.g. glutaraldehyde)
  - charge complexes with anionic polymers

* Chitosan Gels
  - stable to phosphate buffers, Na^+ and K^+ ions
  - easily prepared at room temperature
  - nontoxic
  - high cell loads/activities

* Purify/Recover Biologicals

Cells and enzymes can merely be entrapped or adsorbed into ionotropic chitosan gels formed by mixing chitosan solutions with solutions of anionic polymers (e.g., polyphosphate, alginates, pectin, carrageenan).

Alternately, chitosan beads can be crosslinked to render them insoluble before attaching the enzymes. By attaching protein antigens or antibodies to chitosan, affinity type columns can be fabricated.

REFERENCES

1. H. Braconnot, Sur la nature des champignons, Am. Chi. Phys. 79 (1811), pp. 265-304.

2. A. Odier, Memoire sur la composition Chimique des parties cornees des insects, Mem. Soc. Hist. Nat. Paris (1823), pp. 29-42.

3. R.A.A. Muzzarelli and E.R. Pariser (Eds.), Proc. 1st Inter. Conf. on Chitin/Chitosan, MIT Sea Grant Report MITSG 78-7, 1978.

4. R.C.W. Berkeley, Chitin, Chitosan and their Degradative Enzymes in Microbial Polysaccharides and Polysaccharidases, C. W. Gooday & D.C. Elwood (Eds.), 1979, Soc. Gen. Microbiol. Academic Press.

5. F. Nicolaysen, Naturen (1980) 273.

6. R.A.A. Muzzareli, Chitin, Pergamon Press, NY, 1977.

7a. G.G. Allan, L.C. Altman, R.E. Bensinger, D.K. Ghosh, Y. Hirabayashi, A.N. Neogi and S. Neogi, Biomedical Applications of Chitin and Chitosan, Ref. 15, pp. 119-133.

7b. L.L. Balassa and J.F. Prudden, Applications of chitin and chitosan in wound healing acceleration, Ref. 15, pp. 296-305.

7c. W.G. Malette, H.J. Quigley, R.D. Gaines, N.D. Johnson and W.G. Rainer, Chitosan: a new hemostatic, Am. Thoracic Surgery, 36 (1983), pp. 55-58.

7d. W.G. Malette and H.J. Quigley, Method for the therapeutic occlusion of blood vessels, U.S. Pat. 4,452,785, June 5, 1984.

7e. W.G. Malette and H.J. Quigley, Method of achieving hemostasis inhibiting fibroplasis and promoting tissue regeneration in a tissue wound, U.S. Pat 4,532,134, July 30, 1985.

7f. W.G. Malette and H.J. Quigley, Method of achieving hemostasis, U.S. Pat. 4,394,373, July 19, 1983.

8a. I. Furda, Non-absorbable lipid binder, U.S. Pat. 4,223,023, Sept. 16, 1980.

8b. J.J. Nagyvary, J.D. Falk, M.L. Hill, M.L. Schmidt, A.K. Wilkins and E.L. Bradbury, The hypolipidemic activity of chitosan and other polysaccharides in rats, Nutrition Reports Int'l. 20 (1979), pp. 677-684.

8c. J.E. Maltz, Semi-synthetic chitin derivative, the process for its preparation and the therapeutic compositions which contain it as active principal, U.S. Pat. 4,436,731, March 13, 1984.

9. S. Suzuki, Y. Okawa, Y. Okura, K. Hashimoto and M. Suzuki, Immunoadjuvant effect of chitin and chitosan, Ref. 14, pp. 210-212.

10a. L.A. Hadwiger, Chitosan, a natural regulator in plant-fungal pathogen interactions increases crop yields, Ref. 15, pp. 291-302.

10b. R.L. Rawls, Prospects brighten for converting chitin wastes to valuable products, C & E News, May 14, 1984, pp. 42-45.

10c. L.A. Hadwiger, D.F. Dendra, B.W. Fristensky and W. Wagoner, Chitosan both activates genes in plants and inhibits RNA synthesis in fungi, Ref. 16, pp. 209-222.

11. Polychite Corp., Sea Klear--A Natural Pool Cleaner & Clarifier from the Sea, Redmond, WA.

12. Protan Laboratories, Inc., Pro Floc™ -- Natural Cationic Polymer for Recovering Valuable By-Products from Food Process Wastes, PLI-006, Redmond, WA, 1987.

13. Protan Laboratories, Inc., Chitin and Chitosan--General Properties and Applications, PLI-002, Redmond, WA, 1987.

14. S. Hirano and S. Tokura (Eds.), Chitin and Chitosan, Proc. 2nd Intern. Conf. on Chitin and Chitosan, Jap. Soc. of Chitin and Chitosan, Tottori, Japan, 1982.

15. J.P. Zikakis, (Ed.), Chitin, Chitosan and Related Enzymes, Academic Press, San Diego, 1984.

16. R. Muzzarelli, C. Jeuniaux and G.W. Gooday (Eds.), Chitin and Nature in Technology, Proc. 3rd Intern. Conf. on Chitin and Chitosan, Plenum Press, New York, 1986.

17. I. Furda, Aminopolysaccharides -- their potential as dietary fiber, ACS Symp. Ser. 214 (1983), pp. 105-122.

18. Agricultural Applications of Chitosan, Sea Grant Res. Adv. Res. Note 2, 1986.

19. Protan Laboratories, Inc., Chitosan for Cell Immobilization, PLI-004, Redmond, WA, 1987.

20. Protan Laboratories, Inc., Sea Cure™ Chitosan for Immobilization of Enzymes, PLI-003, Redmond, WA, 1987.

21. O.J. Lantaro, New immobilized whole cell glucose isomerase for fructose syrup production, Eng. Foundations Conf., White Haven, PA, Sept. 25-30, 1983.

22. Miles Laboratories, Inc., Taka-Sweet®- Immobilized glucose isomerase for high fructose syrup production, Elkhart, IN.

POLYSACCHARIDE CHARACTERIZATION BY AQUEOUS SIZE EXCLUSION CHROMATOGRAPHY AND LOW ANGLE LASER-LIGHT SCATTERING: A REVIEW

A. Corona and James E. Rollings

Department of Chemical Engineering
Worcester Polytechnic Institute
Worcester, MA 01609

Synopsis

Aqueous size exclusion chromatography (SEC) coupled with on-line low-angle laser light scattering (LALLS) is a valuable analytical tool for characterization of polysaccharides and other important biopolymers. This work reviews the fundamental size separation mechanism of polymers chromatographed via SEC, the development SEC/LALLS methods for characterization of eluted polymers, and applications of this technique to determine polysaccharide physical and chemical properties. Important nonsize exclusion effects encountered in aqueous SEC of polysaccharides are discussed, and attributed to intramolecular and polymer-support interactions, as well as flow related anomalies. The necessity of absolute molecular weight detection as a direct means of calibration is presented. Low-angle laser light scattering coupled to SEC provides a simple method of direct calibration and allows determination of polymer molecular weight and molecular weight distribution. Recent applications of SEC/LALLS to determine polysaccharide branching characteristics are detailed. The combined knowledge of molecular weight distributions and branching distributions provides insight into the molecular kinetic events of polysaccharide processing operations.

Introduction

Size Exclusion Chromatography (SEC) is now regarded as one of the most important analytical techniques in polymer characterization. The application of this technique to water-soluble polymers, especially naturally occurring biopolymers, is of special interest. These interests now exist as many new uses for naturally occurring polymers are envisioned. In particular, the utilization of polysaccharides as a renewable source for fuel, food, and specialty chemical production has stimulated investigators to develop specific analytical tools to characterize these important polymers. Aqueous size exclusion chromatography coupled to on-line low-angle laser light scattering (SEC/LALLS) appears to be the most promising method for measuring physical and chemical properties (e.g. average molecular weights (MW), molecular weight distribution (MWD) and branching). Reliable determination of these properties is essential in understanding many fundamental chemical processes, most notably the kinetics of polysaccharide synthetic and degradative reactions, which convert abundant low-value raw materials to high-value products.

The advances of aqueous SEC have recently been reviewed by Barth [1], Rollings et al. [2] and Dubin [3]. Rollings et al. [2] have pointed out that development of SEC methods for water-soluble polymers has lagged behind SEC techniques for polymers soluble in organic solvents. This exists for numerous reasons, which include the lack of readily available monodispersed calibration standards and suitable chromatographic supports of sufficient separation ranges for characterizing aqueous soluble polymers. In addition, SEC of water-soluble polysaccharides can be complicated by non-size-exclusion effects that result from intramolecular and polymer-support ionic interactions and flow related anomalies (see below).

With the development of on-line low-angle laser light scattering detection in the late 70's, molecular weights, molecular weight distributions, and polymer branching can now be rapidly determined as a function of polymer molecular size. On-line light scattering detection provides a simple and direct calibration method. The combination of SEC molecular size separation, on-line concentration and molecular weight detection, and microcomputer data acquisition provides an efficient method of determining polymer physical properties. A review of SEC/LALLS and its applications in determining molecular weight and long-chain branching has recently been published by Hamielec and Meyer [4].

The purpose of this work is to review the fundamental size separation mechanism of polymers in aqueous solvents chromatographed via SEC, discuss SEC/LALLS methods for characterizing eluted polymers, and briefly discuss applications of this valuable technique. Important non-size-exclusion effects encountered in SEC resulting from interactions between the polymer, solvent, and support, as well as other effects (e.g. shear degradation) will be discussed briefly. Commonly used calibration techniques will be presented, including the use of secondary standards, universal calibration methods, and direct calibration from light scattering. The development of low-angle laser light scattering detection, as it applies to SEC, will be detailed. Finally, a survey of aqueous SEC/LALLS applications for determining polysaccharide physical/chemical properties will be presented. Specifically, SEC/LALLS will be demonstrated to be a key analytical tool useful in gaining a fundamental understanding of polysaccharide synthesis and degradation processes.

SIZE-EXCLUSION CHROMATOGRAPHY DEVELOPMENT

SEC Separation Mechanism

The fundamental separation mechanism in SEC is due to the partitioning of macromolecules between the flowing solvent in the interstices of the column and the nonflowing solvent within the porous matrix of the column packing [5,6]. Smaller macromolecules spend a longer time in the stationary solvent inside the porous matrix compared to larger macromolecules. Larger macromolecules, therefore, elute from the SEC column before smaller macromolecules. They "see" a smaller effective column pore

volume. Since the column separation is based on the solution size of the macromolecule, the polymer conformation in dilute solution is of great importance. In applying SEC to polysaccharides, polyelectrolytic interactions between the polymer, the solvent, and the support may lead to other non-size-separation effects. Macromolecular solution size and polyelectrolytic effects will be addressed in the next sections.

The retention mechanism in SEC can be best described by the following equation, which relates the elution volume of a polymer, Ve, to the bed interstitial volume, V_o, and the bed pore volume, V_i.

$$V_e = V_o + K_d V_i \qquad (1)$$

K_d represents an effective partition coefficient and is defined as the ratio of the polymeric solute concentration within the pores of the packing and its concentration in the bulk fluid [1]. For a chromatographic separation solely controlled by macromolecular size, K_d ranges from Ø to 1. Figure 1 displays a typical SEC chromatogram constructed by plotting the eluting polymer's concentration (usually measured from differential refractometry) versus retention volume. For a macromolecule that is too large to diffuse into the porous matrix, K_d = Ø and elution occurs at the interstitial bed volume; $V_e = V_o$. A value of K_d = 1 represents a polymer that can penetrate the entire available bed pore volume, and hence, the polymer elutes at an elution volume equal to the total volume of the bed; $V_e = V_t = V_o + V_i$. Pore size, pore shape, and pore size distribution will also influence the values of the partition coefficient [7]. More complete reviews of theoretical SEC mechanisms are presented by Yau et al. [5] and Barth [8].

Relating the partition coefficient to elution volume can be carried out through a direct calibration procedure. Direct calibration is made by plotting known molecular weight samples versus column performance. Direct calibration can be done only with well characterized standards of the polymer of interest. Unfortunately, primary standards are available for few water-soluble polymers. A listing of commercially available standards can be found in Barth's review [1]. The use of secondary standards, such as sodium polystyrene sulfonate (NaPSS) and dextran, has been employed for aqueous SEC calibration [9]. Secondary standards that differ significantly in chemical nature (e.g. structure and ionic behavior) from the sample must be used cautiously. If polymer molecular weight information is desired and suitable calibration standards are not available, a correlation between molecular weight and solution size is needed.

Molecular Size - Molecular Weight Relationship

Fundamental separation in SEC occurs via a mechanism that is dependent upon the polymer's molecular size. As a consequence, the relationship between the macromolecule's size in solution and the molecular weight must be available to interpret SEC data correctly. Pioneering work by P. J. Flory (using statistical mechanical arguments)

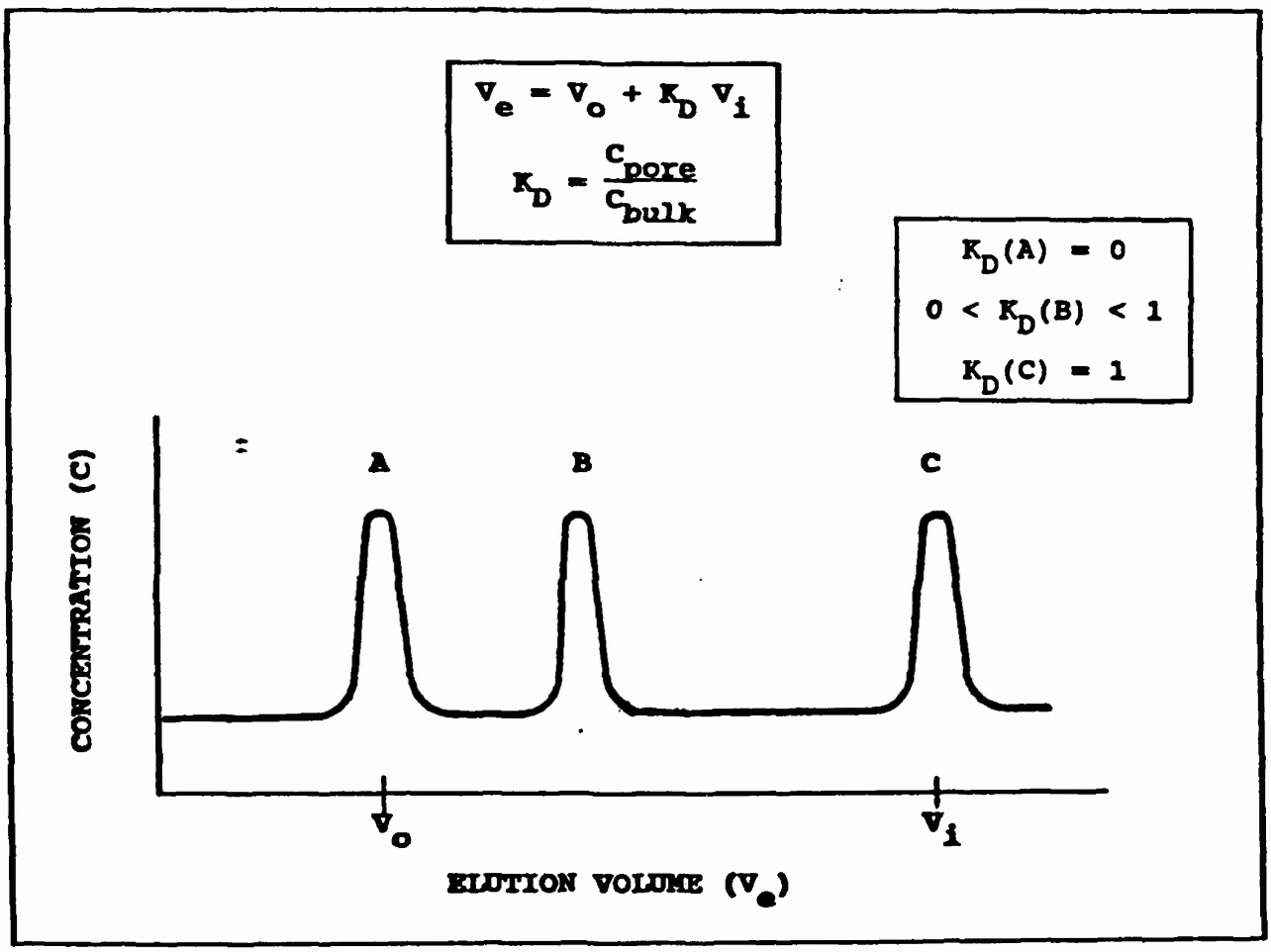

Figure 1. Typical SEC chromatograph depicting variation of K_D with elution volume for a polymer mixture; A - High MW (totally excluded), B - Intermediate MW, C - Low MW (totally retained).

laid the foundation for determining the desired molecular size - molecular weight relationship. Flory's initial interests were in describing dilute solution rheological behavior of polymeric solutions. He determined that the intrinsic viscosity [η] of a polymer solution is described by Equation 2 [10],

$$[\eta] = \Phi_o \langle r^2 \rangle^{3/2}/M = \Phi_o \alpha^3 \langle r_o^2 \rangle^{3/2}/M \qquad (2)$$

where M is the polymer molecular weight, $\langle r^2 \rangle$ is the mean-square end-to-end distance, $\langle r_o^2 \rangle$ is the unperturbed mean-square end-to-end distance, α^3 is the expansion factor, and Φ_o is Flory's constant (3.6×10^{21} dl/cm^3). Intrinsic viscosity is a molecular parameter obtained from linear extrapolation to zero concentration of other rheological properties. More complete discussions of these subjects can be found elsewhere [11]. Concentrations approaching infinite dilution prevail in SEC experiments. Therefore, the applicability of Flory's equation may be useful in SEC analysis.

Grubisic, Rempp, and Benoit [12] employed Flory's relationship and demonstrated that molecular size separation can be correlated for various polymers differing in their specific chemical nature and configuration. They showed that plotting the product of log [η] and MW vs. volumetric throughput is applicable for many neutral polymers in nonpolar solvents. Figure 2 demonstrates that linear, comb branched, and star branched polymers of differing chemical make-up scale to this common separation index. This secondary calibration technique (called universal calibration) has found wide applicability in similar polymer-solvent systems. Universal calibration has not been demonstrated to be generally applicable for polymers soluble in polar solvents. Reasons for this failure have been presented [13,14] and suggested to result from the polymer's polyelectrolytic nature in polar solvents (e.g. water). The possibility of intramolecular polymer-polymer, polymer-solvent, and polymer-support interactions also exists. These complications must be considered in SEC analysis in order to assure that their contributions have either been accounted for or eliminated.

Polymers in dilute solution are subject to two major forms of interactions, which affect their molecular size and, hence, their physical properties: polymer-solvent interactions and intramolecular polymer-polymer interactions [15]. In a poor solvent, intramolecular associations dominate, the polymer conforms to a tightly coiled structure, and the molecular size is small. In a good solvent, polymer-solvent interactions are greater than polymer-polymer interactions and, consequently, the polymer exists as a large, loosely coiled structure [16,17]. For polyelectrolytes in solution, conformation is strongly dependent on bulk solution ionic strength [17,18]. In solvents of low ionic strength, the ionizable moieties of the polyelectrolyte dissociate. The electrostatic interactions among charged groups along the polymer backbone cause the molecule to expand [15]. These repulsive effects are suppressed in high ionic strength solvents by a process that shields the polymer's ionic groups [19]. This leads to a contracted molecular conformation in solution. Therefore, polyelectrolyte expansion and contraction (i.e. molecular size) is strongly dependent on the solvent's ionic strength.

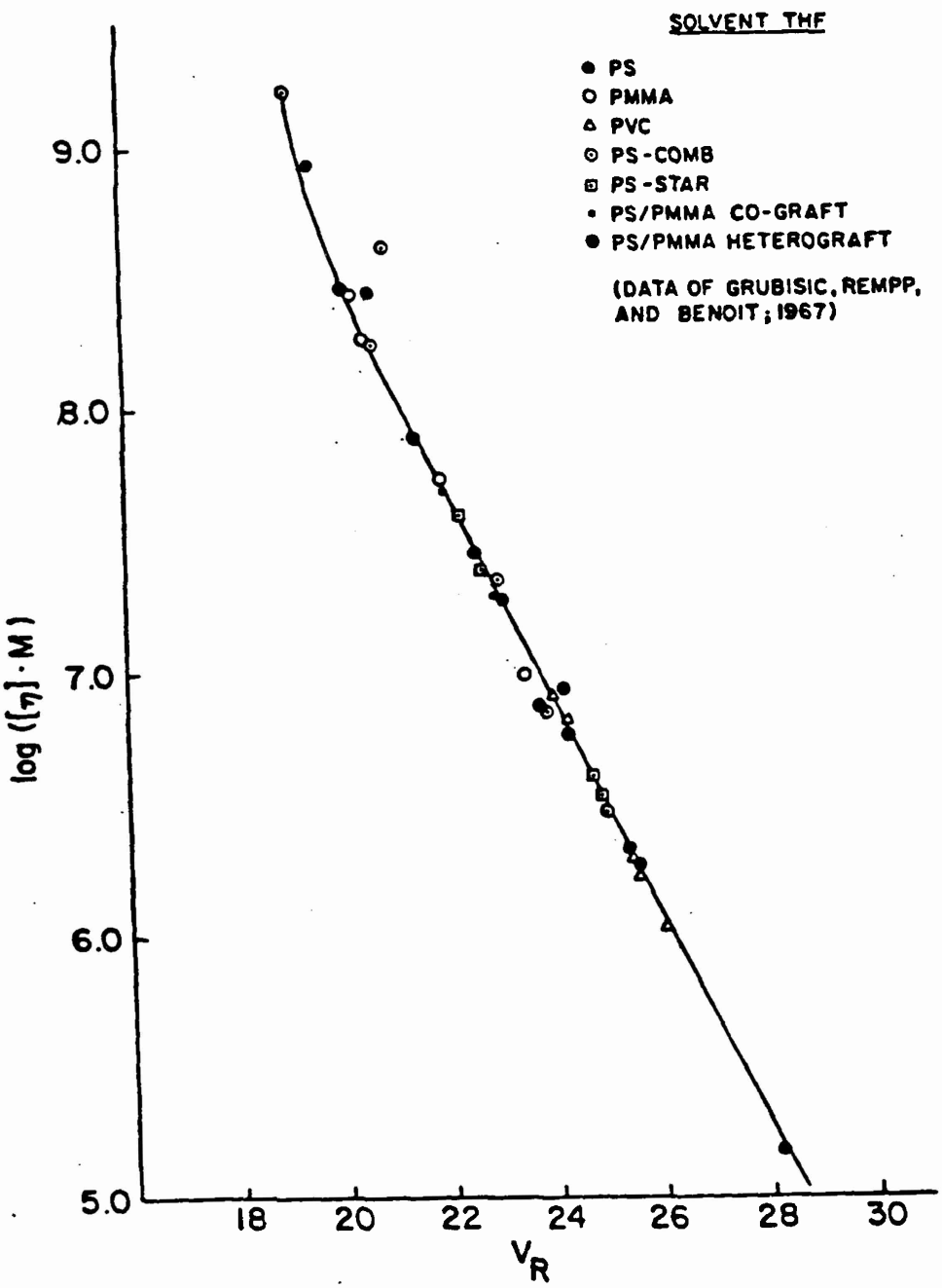

Figure 2. Universal calibration plot of Grubisic et al. [12].

Coll and Prusinowski [20] proposed an alternative calibration scheme more suitable for highly expanded polymers. They argued that significant variation in the Flory constant exists for such systems due to solvent drainage through the coil. Coll and Prusinowski suggested a modification of the universal calibration procedure to account for this behavior. Their calibration procedure plots [η] MW/f(E) vs. elution volume. The function f(E) is an excluded volume function, which accounts for nonconstancy in the Flory parameter. Although in some systems use of the Coll-Prusinowski procedure has been shown to be applicable [14], these reported systems have not been exhaustively studied, and the possibility exists of other, unaccounted for separation phenomena. [13,21]. Detailed work on these and other systems must be performed before concrete conclusions regarding separation phenomena are established.

Secondary Separation Phenomena in SEC

Secondary aqueous SEC separation mechanisms (nonsize) of polyelectrolytes can occur due to ionic interactions between the polymer in solution and the porous support matrix. These interactions have been reviewed by Stenlund [22]. Ionic interactions for these systems can lead to adsorption, ion exclusion, and ion inclusion effects. This section discusses these phenomena and their potential effects on aqueous chromatography of large molecules.

Adsorption of a macromolecule to the chromatographic support has been well documented for polymers in nonpolar solvents (e.g. polystyrene) [23,24,26-28]. Polymer adsorption depends on numerous parameters, which include contributions due to the particular solvent used and the presence of co-solutes [23,25,27-30]. Van der Waals forces are the primary driving forces for polymer adsorption of neutral polymers in nonpolar solvents. The mechanism is more complex for charged polymers in polar solvents undergoing separation on a support surface that also may be charged. When the chromatographic support and solute are oppositely charged, electrostatic attractions retard the movement of the polyion through the porous matrix, resulting in delayed elution. Multiple elution peaks have been reported for mono-dispersed polymers and attributed to adsorption [30,31]. Irreversible adsorption of the polymer to the support matrix is also possible and some authors have discussed this situation [30].

When the surface of the chromatographic support and the polyelectrolyte are of like charge, electrostatic repulsion or ion-exclusion occurs, which prevents the polyion from freely diffusing into the pores of the matrix [22,32-35]. This repulsion essentially reduces the effective pore volume available to the polymer and results in polymer elution from the column prior to that expected from a neutral polymer of the same size. This leads to an overestimation of the polymer's molecular weight. The addition of co-solutes, most often alkaline halides, has been shown to retard this exclusion effect [22,35].

In solutions containing two or more ionic solutes where one ionic species is excluded from a region of porous packing and the other species can penetrate the region, in a Donnon equilibrium is established [22,36-41]. This phenomenon can occur SEC of polyelectrolytes because the size of the pore opening can exclude large polyions while allowing smaller electrolytes to completely permeate. The ionic solutes of lower permeability will force smaller ions of like charge to migrate into the pore. This ion-inclusion effect leads to further retention of low molecular weight ionic solutes. This effect can be observed with the use of on-line conductometric detection [39,41]. If ion-inclusion exists, a baseline perturbation in solution conductivity is evident in the vicinity of the solvent peak. Suppression of this effect is often possible by the addition of a simple electrolyte to the eluent [36-39,41].

Other nonsize exclusion effects can be generated in SEC due to shear degradation and viscosity differences between the injected sample and the solvent. Shear degradation in SEC has recently been reviewed by Barth and Carlin [42] and others [43,44]. High molecular weight polymers are fairly sensitive to shear forces prevalent in SEC, which could cause mechanical chain scission. Barth and Carlin outline the most probable sources of shear degradation in a SEC system. These sources include the injection valve, capillary tubing, column frits, and the packed column [42]. Shear degradation is a function of polymer configuration in solution [45,46] and flow rate [44,47], as well as polymer molecular weight.

Concentration effects on the eluting chromatogram in SEC have been attributed to differences in viscosity between the eluent and the injected sample [48-51]. As the sample concentration is increased, the elution volume of the peak increases. At even higher concentrations, the eluting peak becomes quite distorted. This effect is usually explained by two mechanisms: viscous fingering and molecular crowding [8]. In viscous fingering, the rear boundary of the polymer sample in the column is unstable; especially if the polymer viscosity is significantly higher than the solvent. As the solvent finds the easiest pathway through the column, fingers of solute are formed. This channeling effect leads to a distortion of the elution chromatograph, most notably at the high molecular weight end of the chromatograph (larger size and viscosity) [6]. Molecular crowding results from the compression of individual macromolecules to hydrodynamic volumes smaller than those found at infinite dilution. This reduction in size causes the elution peaks to be shifted toward higher elution volumes [6]. Reduction in sample concentration will help to reduce both viscous fingering and molecular crowding effects. The viscosity of polyelectrolytes (and hydrodynamic volume) can be reduced by adding small amounts of electrolyte to the solvent or by increasing column temperatures.

In general, aqueous SEC is more complex than SEC of neutral polymers in nonpolar solvents due to the additional phenomena enumerated above. The origins of these complexities, for the most part, arise from the polyionic nature of aqueous soluble macromolecules. Often times, these additional separation phenomena can be suppressed by an appropriate choice of system conditions. It is necessary to explore these effects in greater detail if aqueous SEC is to be routinely used. Specifically, if secondary calibration is utilized in biopolymer analysis, detailed investigation of other nonsize separation mechanisms must be studied. Alternatively, more sophisticated instrumentation can be employed, which avoids these complexities and leads to direct calibration of the aqueous SEC chromatograph. The next sections detail state-of-the-art developments in this area.

DIRECT SEC CALIBRATION VIA LIGHT SCATTERING DETECTION

The scattering of light through dilute solutions of macromolecules is a well known phenomenon [16]. Zimm developed the initial theoretical framework for this technique, and many reviews of this subject are available elsewhere [52,53]. Experimentally, the intensity of scattered light is dependent upon polymer concentration and the angle from the incident beam at which the scattered light intensity is measured. From these two independent parameters, light intensity can be mapped in a Zimm plot (see Figure 3). These relationships were formulated mathematically by Rayleigh and are given in Equation 3 [52].

$$Kc/R(\theta,c) = 1/M_w P(\theta) + 2A_2C + 3A_3C^2 + \ldots\ldots, \quad (3)$$

$$\text{where } K = (2\pi^2 n^2/\lambda^4 N)\ (dn/dc)^2 (1 + \cos^2\theta)$$

In this equation, the weight-average molecular weight of the polymer (M_w) can be determined from the solution concentration (c), the excess Rayleigh factor for unpolarized incident radiation at the scattering angle ($R(\theta,c)$), the solution refractive index (n), the wavelength in vacuo (λ), Avogadro's number (N), the second and third virial coefficients (A_2, A_3). The term $P(\theta)$ is the form factor, which is a function of the size and shape of the macromolecule in solution, and represents the modulation of light intensity due to the finite molecular size and to the polymer's deviation from sphericity. At the limit of zero scattering angle, $P(\theta) = 1$. The term dn/dc is the specific refractive index increment and represents the change in solution refractive index as a function of polymer concentration. In extremely dilute solutions, terms containing c^2 can be neglected. In constructing a Zimm plot (Figure 3), experimentally determined values of $Kc/R(\theta,c)$ are plotted vs. $\sin^2\theta/2 + kc$, where k is an arbitrary constant. The resulting rectilinear grid allows extrapolation to both $c = \emptyset$ and $\theta = \emptyset$. The weight-average molecular weight is the inverse of the dual intercepts.

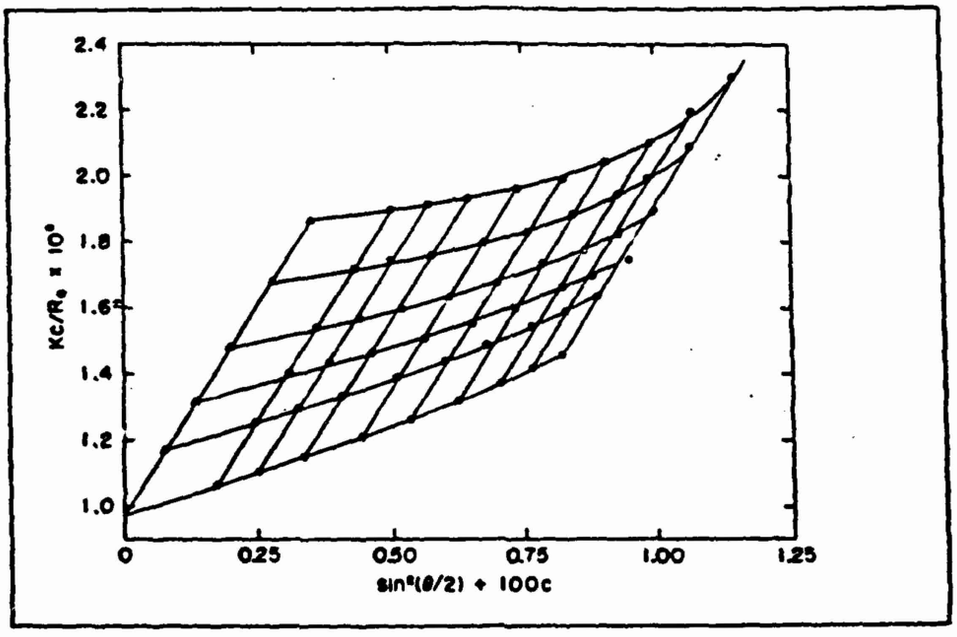

Figure 3. Zimm plot for the light scattering of polystyrene in methyl ethyl ketone (from P. Doty and R. F. Steiner, J. Chem. Phys., 18, 1211 (1950)). Filled triangles: extrapolation to $c = 0$. Filled circles: extrapolation to $\theta = 0$. Courtesy of the American Institute of Physics.

Equation 3 can be simplified if light scattering intensity measurements are collected at low angles (approximating the zero angle extrapolation), and at dilute solution conditions (approximating the zero concentration extrapolation) to yield the LALLS working equation

$$Kc_v/R(\theta,c_v) = 1/M_v + 2A_2c_v \qquad (4)$$

where the subscript v is used to denote the constant elution volume comparison. M_v represents the weight-average molecular weight of a sample within the LALLS detector cell. Thus, the molecular weight of a polymer in solution can be determined using Equation 4 and the material's second virial coefficient.

APPLICATIONS OF SEC/LALLS IN POLYSACCHARIDE CHARACTERIZATION

Recent advances in commercial light scattering instrumentation now provide for direct coupling to SEC. Reviews of the overall SEC/LALLS technique have been presented by Kaye [54], Ouano [55], Jordan [56], and Hamielic and Meyer [4]. The enormous volume of data collected from such devices has necessitated the use of data acquistion and processing machines. Information obtained from these state-of-the-art systems provides molecular weight and molecular weight distributions of eluting polymers. Determination of polysaccharide molecular weight information via SEC/LALLS has been carried out for cellulosic materials [57,58], lignins [59], dextran [60], and others [61,62]. The reader is referred to these publications for a more complete discussion. Although these two fundamental molecular parameters are of primary importance, additional molecular information is desired in many systems. More recently, Yu and Rollings [62,63] (for polysaccharides) and others [64-67] (for polymers in organic solvents) have extended basic light scattering theory to obtain some of this much needed information. Specifically, they have demonstrated that polymer branching as a function of column separation is obtainable with the same commercial instrumentation.

Yu and Rollings [62] employed SEC/LALLS to obtain data about the branching parameters, g_v and g_m, for samples of homopolymeric polysaccharides of increasing degrees of branching (amylose, amylopectin and glycogen), and for starch (a mixture of amylose and amylopectin). The branching parameter, g_v is obtained from molecular weight (M) comparisons of linear and branched molecules at a constant molecular size (or elution volume, v), and is defined as

$$g_v = (M_l/M_b)_v \qquad (5)$$

where the subscripts l and b denote linear and branched polymers. The branching parameter, g_m, was defined by Zimm and Stockmeyer [68] as the ratio of the mean-square radius of gyration $\langle R^2 \rangle$ of branched and linear polymers of the same molecular weight. Yu and Rollings [62] show that g_m can be obtained from the SEC/LALLS branching parameter g_v as follows:

$$g_m = (M_1/M_b)_v \ (a + 1)/e = g_v \ (a + 1)/e \qquad (6)$$

where a is the Mark-Houwink coefficient and e is a polymer draining parameter which can vary between 0.5 and 1.0 depending upon the particular theoretical assumptions used in developing the model. Their branching results are shown in Figure 4. For the three homopolymers, branching frequency (as measured by chemical means) and branching parameters are inversely related, as theoretically predicted. For starch (Amylomaize VII), a nonhomogeneous branching distribution is observed as a function of molecular weight. This observation has led to a greater understanding of basic starch physical and chemical properties and opened new areas of study in biopolymer kinetics.

Theoretical advancements of SEC/LALLS-determined branching parameters continues. Yu and Rollings [63] theoretically related two measurable branching parameters $g_{v(m)} = (M_1/(M_N)_m)_v$ and $g'_{v(m)} = (M_1/(M_M)_m)_v$ of a sample mixture to the mixture's composition. Here, the subscripts M and N denote weight-average and number-average molecular weights respectively and m denotes that measurements are performed on mixed polymer samples. They have determined that there exist linear relationships between $g_{v(m)}$ and $W_{b,v}$ (the mass fraction of branched component in the mixture) as well as between $g'^{-1}_{v(m)}$ and $W_{b,v}$. The latter correlation was demonstrated experi- mentally using SEC/LALLS and displayed excellent agreement with theoretical predictions. A representative linear plot of $g'^{-1}_{v(m)}$ vs. $W_{b,v}$ for amylose/ glycogen mixtures at different elution volumes is shown in Figure 5.

Armed with the ability to efficiently determine molecular weight distribution and branching characteristics for polymer mixtures, Yu and Rollings [63] employed SEC/LALLS in the examination of an industrially important biopolymer, and in particular, to study enzymatic starch hydrolysates products. Starch samples were extracted from the reaction mixture and analyzed via SEC/LALLS. For example, the observed molecular weight distribution and branching distribution are shown in Figure 6; a) before hydrolysis, and b) after a 2 min hydrolysis time. Here, the area under the main solid-line chromatographic trace represents the total mass of material eluted from the SEC column as a function of either elution volume or molecular weight (based on amylose hydrodynamic volume). The total branched polysaccharide material (expressed as amylopectin; narrow dashed line chromatographic region) and the mass fraction of branched material at each elution volume ($W_{b,v}$, right hand side axis) is displayed, also. From this type of analysis, Yu and Rollings determined that starch branched components are preferentially hydrolysed by the particular enzyme chosen (endo-acting linear depolymerase α- amylase). Combined SEC/LALLS analysis of mixed polymer systems (e.g. starch) now provides many parametric values never before obtainable. The resulting "snapshot" of this or any similar processing operation provides insight into the molecular kinetic events that occur.

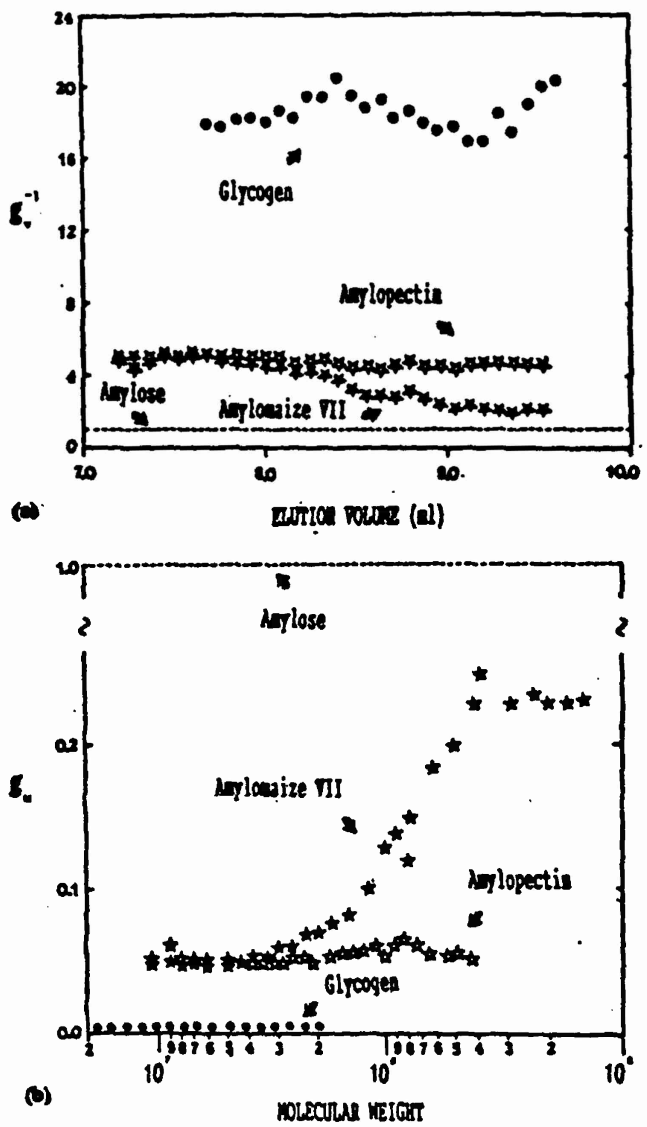

Figure 4. Branching distribution of polysaccharides: a) the plot of g_v^{-1} vs. elution volume and b) the plot of g_M vs. molecular weight for three branched polysaccharides as compared to amylose (linear) [62]. Courtesy of John Wiley & Sons.

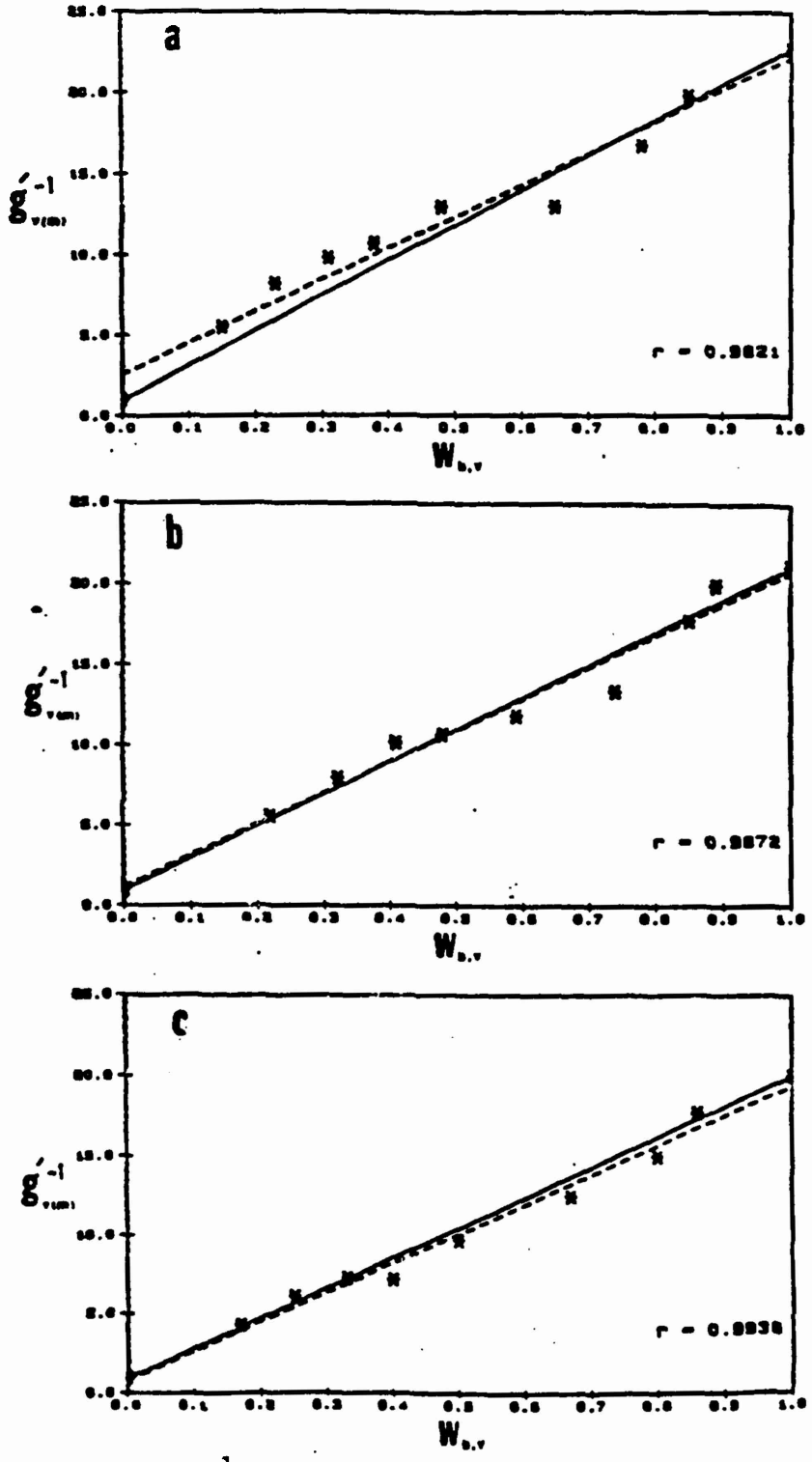

Figure 5. The plot of g'^{-1}_{v} vs. weight fraction of branched material ($W_{b,v}$) for amylose/glycogen mixtures at three elution volumes (EV); a) EV = 8.5 ml; b) EV = 9.0 ml; c) EV = 9.5 ml [63]. Courtesy of John Wiley & Sons.

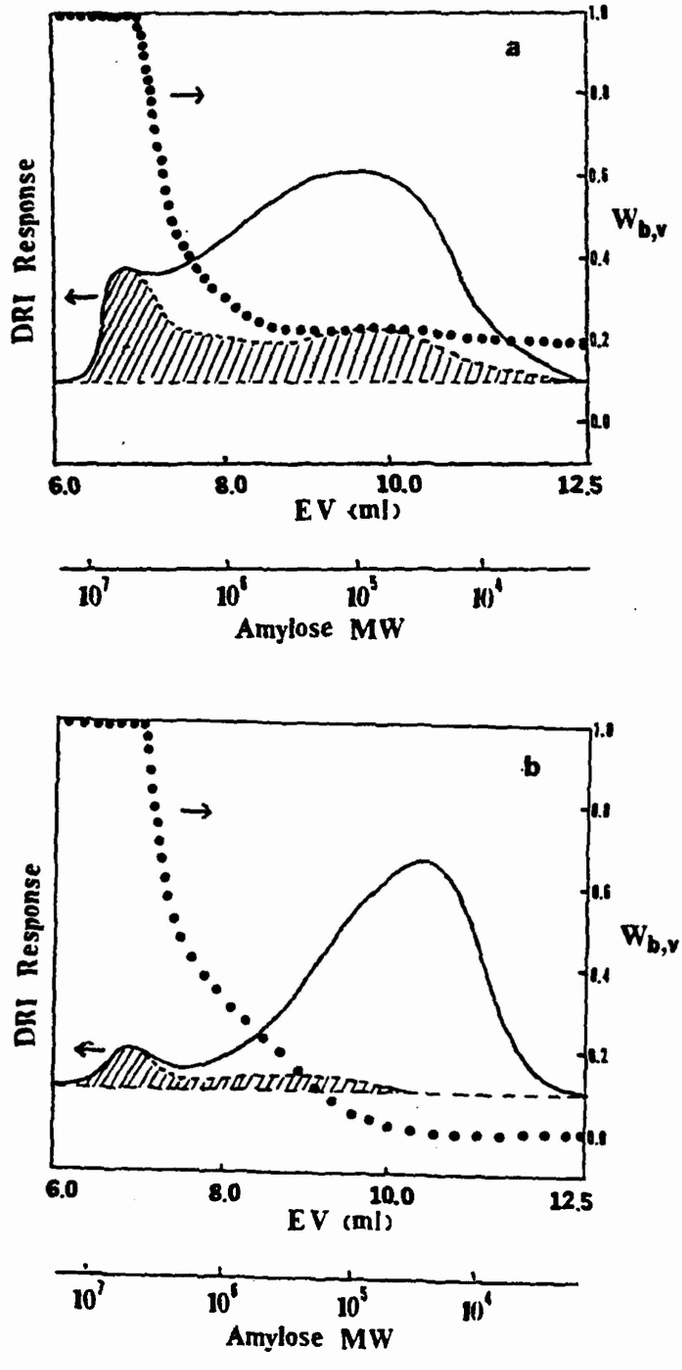

Figure 6. Molecular weight distribution and branching distribution (dashed region) of Amylomaize VII starch; a) before enzymatic hydrolysis and b) after 2 min. hydrolysis time [63]. Courtesy of John Wiley & Sons.

CONCLUSIONS

Aqueous size exclusion chromatography coupled with on-line low-angle laser light scattering detection is a valuable tool for characterization of polysaccharides and other polyelectrolytes. The principal separation mechanism in SEC is based on the solution size of the macromolecule. The ionic strength of the solvent influences the molecular conformation of the polyion in solution and therefore the elution behavior in SEC. The use of polar solvents or ionic solutions in aqueous SEC requires consideration of possible polymer-support interactions such as adsorption, ion-exclusion, and ion-inclusion. These secondary separation phenomena usually can be suppressed by controlling solvent ionic strength. Flow-related anomalies such as shear degradation and viscosity differences between solvent and polymer sample may lead to other nonsize separation effects. Since primary calibration standards for most polysaccharides of interest are not available, secondary calibration techniques have been employed. These methods have met with limited success due to the inability to account for complex ionic effects present in aqueous SEC. The use of on-line light scattering as an absolute molecular weight detector has revolutionized calibration in SEC.

SEC/LALLS has been applied in determining molecular weight information about polysaccharides. Quantitative branching measurements of both polysaccharide homopolymers and mixtures can be obtained via SEC/LALLS. The combined knowledge of molecular weight and branching distributions allows insight into the molecular kinetic events of polysaccharide processing operations. Further developments of the SEC/LALLS technique, including the use of additional on- and off-line detectors, may provide the key to greater understanding of polysaccharide physical and chemical properties.

REFERENCES

1. H. G. Barth, Am. Chem. Soc. Adv. Chem., 213, 31 (1986).

2. J. E. Rollings, A. Bose, J. M. Caruthers, M. R. Okos, and G. T. Tsao, Adv. in Chem., 203, 345 (1981).

3. P. L. Dubin, Amer. Lab. Fairfield CT, 15, 62 (1983).

4. A. E. Hamielec and H. Meyer, in "Developments in Polymer Characterization - 5", J. V. Dawkins, Ed., Elsevier, 1986, p. 93.

5. W. W. Yau, J. J. Kirkland, and D. D. Bly, "Modern Size Exclusion Liquid Chromatography", John Wiley, New York, 1979.

6. L. H. Tung and J. C. Moore, in "Fractionation of Synthetic Polymers - Principle and Practice", L. H. Tung, Ed., New York, 1977, 545 (1978).

7. W. W. Yau, C. R. Ginnard, and J. J. Kirkland, J. of Chromatogr., 149, 465 (1978).

8. H. G. Barth, J. Chromatogr. Sci., 18, 409 (1980).

9. Y. Bao, A. Bose, M. R. Ladisch, and G. T. Tsao, J. Appl. Polym. Sci., 25, 263 (1980).

10. T. G. Fox and P. J. Flory, J. Am. Chem. Soc., 73, 1904 (1951).

11. P. Rodriquez, "Principles of Polymer Systems", McGraw-Hill, New York, 1982.

12. Z. Grubisic, R. Rempp, and H. Benoit, J. Polym. Sci., Polym. Letters, 5, 753 (1967).

13. P. L. Dubin and C. M. Speck, Proc. Am. Chem. Soc. Div. PSME, 54, 194, (1986).

14. A. Bose, J. E. Rollings, J. M. Caruthers, M. R. Okos, and G. T. Tsao, J. Appl. Polym. Sci., 27, 795 (1982).

15. J. E. Rollings, Ph.D. thesis, Purdue University, 1981.

16. P. J. Flory, "Principles of Polymer Chemistry", Cornell University Press, Ithaca, NY, 1953.

17. B. Vollmert, "Polymer Chemistry", Spring-Verlag, New York, 1973.

18. A. Eisenburg and M. King, "Ion Containing Polymers - Physical Properties and Structure", Academic, New York, 1977, Chap. V.

19. C. Tanford, "Physical Chemistry of Macromolecules", John Wiley, New York, 1977.

20. H. Coll and P. Prusinowski, J. Polym. Sci., Polym. Letters, 5, 1153 (1967).

21. J. E. Rollings, Private communication.

22. B. Stenlund, Adv. Chromatogr., 14, 37 (1976).

23. D. Bakos, T. Bleha, A. Ozima, and D. Berek, J. Appl. Polym. Sci., 23, 2233 (1979).

24. O. Chiantore, J. Liq. Chromatogr., 7(1), 1 (1984).

25. T. Ogawa and M. Sakai, J. Liq. Chromatogr., 6(8), 1385 (1983).

26. J. V. Dawkins, Polymer Preprints Am. Chem. Soc. Div. Polym. Chem., 18(2), 198 (1977).

27. C. Booth, J. L. Forget, I. Georgii, W. S. Li, and C. Price, Eur. Polym. J., 16, 255 (1980).

28. A. Campos, V. Soria, and J. E. Figueruelo, Makromol. Chem., 180, 1961 (1979).

29. G. Coppola, P. Fabbri, B. Pallesi and U. Bianchi, J. Appl. Polym. Sci., 16, 2829 (1972).

30. W. Siebourg, R. D. Lundberg, and R. W. Lenz, Macromolecules, 13, 1013 (1980).

31. C. Y. Cha, J. Polym. Sci., Polym. Letters., 7, 343 (1969).

32. P. A. Neddermeyer and L. B. Rodgers, Anal. Chem., 40, 755 (1968).

33. M. Rinaudo and J. Desbrieres, Eur. Polym. J., 16, 849 (1980).

34. R. M. Wheaton and W. C. Bauman, Ind. Eng. Chem., 45, 228 (1953).

35. A. R. Cooper and D. P. Matzinger, J. Appl. Polym. Sci., 23, 419 (1979).

36. T. Miyajima, Y. Yoshikawa, N. Yoza, and S. Ohashi, J. Liq. Chromatogr., 5(1), 73 (1982).

37. I. J. Levy and P. L. Dubin, Ind. Eng. Chem. Prod. Res. Dev., 21, 59 (1982).

38. P. L. Dubin and I. J. Levy, J. Chromatogr., 235, 377 (1982).

39. C. Rochas, A. Domard, and M. Rinaudo, Eur. Polym. J., 16, 135 (1980).

40. E. A. Buytenhaus and F. P. B. Van der Maeden, J. Chromatogr., 149, 489 (1978).

41. A. Domard, M. Rinaudo and C. Rochas, J. Polym. Sci. Polym. Phys. Ed., 17, 673 (1979).

42. H. G. Barth and F. J. Carlin, J. Liq. Chromatogr., 7(9), 1717 (1984).

43. J. H. Aubert and M. Tirrell, J. Liq. Chromatogr., 6(S-2), 219, (1983).

44. J. C. Giddings, Adv. Chromatogr., 20, 217 (1982).

45. A. Nakaro and Y. Minovra, Macromolecules, 8, 677 (1975).

46. A. Nakaro and Y. Minovra, J. Appl. Polym. Sci., 22, 2207 (1978).

47. C. Huber and K. H. Lederer, J. Polym. Sci., Polym. Letters, 18, 535 (1980).

48. J. E. Figueruelo, A. Campos, V. Soria, and R. Tejero, J. Liq. Chromatogr., 7(6), 1061 (1984).

49. J. Janca, S. Pokorny, J. Zabransky, and M. Bleha, J. Liq. Chromatogr., 7(9), 1887 (1984).

50. O. Chiantore and M. Guaita, J. Liq. Chromatogr., 7(9), 1867 (1984).

51. R. Tejero, V. Soria, A. Campos, J. E. Figueruelo, and C. Abad, J. Liq. Chromatogr., 9(4), 711 (1986).

52. C. Strazielle, in "Light Scattering from Polymeric Solutions", M. B. Huglin, Ed., Academic, New York, 1972, p. 663.

53. H. Yamakawa, "Modern Theory of Polymer Solutions", Harper & Row, New York, 1971.

54. W. Kaye, Anal. Chem., 45(2), 221A (1973).

55. A. C. Ouano, J. Chromatogr., 118, 303 (1976).

56. R. C. Jordan, J. Liq. Chromatogr., 3(3), 439 (1980).

57. J. J. Cael, D. J. Cietek, and F. J. Kolpack, J. Appl. Polym. Sci., Appl. Polym. Sym. No. 37, 509 (1983).

58. J. J. Cael, R. E. Cannon, and A. O. Diggs, in "Solution Properties of Polysaccharides", D. A. Brant, Ed., ACS Symposium Series No. 150, ACS, Washington, D.C., 1981, p. 43.

59. F. J. Kolpak, D. J. Cietek, W. Fookes, and J. J. Cael, J. Appl. Polym. Sci. Appl. Polym. Sym. No. 37, 491 (1983).

60. C. J. Kim, A. E. Hamielec, and A. Benedek, J. Liq. Chromatogr., 5(3), 425 (1982).

61. S. Hizukuri and T. Takagi, Carbohydrate Res., 134, 1 (1984).

62. L. P. Yu and J. E. Rollings, J. Appl. Polym. Sci., 33, 1909 (1987).

63. L. P. Yu and J. E. Rollings, J. Appl. Polym. Sci., submitted.

64. R. C. Jordan and M. L. McConnell, in "Size Exclusion Chromatography (GPC)", T. Provder, Ed., ACS Symposium Series No. 138, ACS, Washington, D.C., 1980. p. 107.

65. R. C. Jordan, S. F. Silver, R. D. Sehon, and R. J. Rivard, in "Size Exclusion Chromatography" Methodology and Characterization of Polymers and Related Materials", T. Provder, Ed., ACS Symposium Series No. 245, ACS, Washington, D.C., 1984, p. 295.

66. D. E. Axelson and W. C. Knapp. J. Apl. Polym. Sci., 25, 119, (1980).

67. V. Grinshpun, A. Rudin, K. E. Russell, and M. V. Scammell, J. Polym. Sci. Polym. Phys. Ed., 24, 1171 (1986).

68. B. H. Zimm and W. H. Stockmeyer, J. Chem. Phys., 17, 1301 (1949).

PRODUCTION OF PHENOLIC POLYMERS CATALYZED BY HORSERADISH PEROXIDASE IN ORGANIC SOLVENTS

Jonathan S. Dordick

Department of Chemical and Materials Engineering
University of Iowa
Iowa City, Iowa 52242

Abstract

Horseradish peroxidase has been shown to vigorously polymerize phenols on a gram scale in dioxane, acetone, methyl formate, and dimethylformamide, containing 15% aqueous buffer, pH 5. Polymers and copolymers with m.w.'s up to 26,000 daltons were produced. Similar catalysis in aqueous media resulted in low molecular weight coupling products. In the case of p-phenylphenol polymerization in dioxane, the polymer was found to exhibit significant electrical conductivity (10^{-5} $ohm^{-1}cm^{-1}$) following chemical doping. Peroxidase-produced phenolic polymers may represent a viable alternative to traditional phenol-formaldehydes.

1. Introduction

Phenol-formaldehyde resins are the mainstay of the phenolic polymer industry. These highly cross-linked three dimensional polymers have widespread uses as molding, casting, binding, adhesive, impregnation, and surface coating agents (1). The future for their general use, however, is threatened by the severe health and environmental concerns associated with the toxicity of formaldehyde (2). Furthermore, the method of preparation of phenol-formaldehyde resins via simple acid- or base-catalyzed condensation of phenols with formaldehyde does not afford rigid control over the desired physico-chemical characteristics of the final polymer (e.g., molecular weight, degrees of cross-linking and crystallinity, etc.). Hence, the use of phenol-formaldehydes as specialty resins is also limited.

For these reasons, various alternatives to phenol-formaldehyde resins are needed. The chemical literature contains a wide variety of methods for polymerizing phenols in the absence of cross-linking agents such as formaldehyde instead relying on free radical polymerization (3-5). These procedures fail, however, to offer much control over polymerization and are therefore severely limited.

Enzyme-catalyzed polymerization of phenols is an attractive alternative to synthetic approaches. While a number of enzymes are mechanistically capable of carrying out phenolic polymerizations in the absence of condensation cosubstrates (such as formaldehyde) (6), and offer the possibility of mild conditions and high selective control over the reactions, horseradish peroxidase appears the most logically suited for such reactions. In nature, peroxidases catalyze the polymerization of phenols in plants under highly controlled conditions to give lignin (7).

Under far less rigorous conditions in vitro, however peroxidase-catalyzed polymerization of phenols has resulted only in low molecular weight coupling products (8). The most likely explanation given for this phenomenon has been that the poor solubility of these coupling products (predominantly dimers and trimers) in aqueous solutions results in their precipitation out of solution and termination of polymerization.

While phenols and their coupling products are poorly water-soluble, they are readily soluble in a large number of organic solvents. It occured to us that by carrying out peroxidase-catalyzed polymerization of phenols in nonaqueous media, higher molecular weight polymers would be produced. Our previous studies have shown horseradish peroxidase to be a highly active catalyst in organic solvents (9-12). In the present study we have extended peroxidase catalysis in organic media to preparative scale phenolic polymerizations.

2. Materials and Methods

Horseradish peroxidase (EC 1.11.1.7) was obtained from Sigma Chemical Co., (St. Louis, MO) as a salt-free powder with a specific activity of 150 Purpurogallin units/mg solid. Hydrogen peroxide (30% solution in water) was purchased from Mallinckrodt (Paris, KY); the actual H_2O_2 content was determined by volumetric titration with $KMnO_4$ (13). All other chemicals used in this work were obtained from various commercial suppliers and were of the highest purity available.

Polymerization studies were performed in volumes of 20 to 100 mL with a variety of phenols and organic solvents (see "Results and Discussion"). In a standard reaction mixture 5-100mM of phenol and an equimolar concentration of H_2O_2 (no more than 20mM added at any one time) were dissolved in dioxane containing 15% v/v acetate buffer, 0.01M, pH 5.0 and 0.5mg/mL horseradish peroxidase. Horseradish peroxidase was completely insoluble in concentrations of dioxane in water above 60%. The decrease in phenolic concentrations was followed by HPLC (Waters Assoc. Milford, MA) equipped with a uBondapak C_{18} reverse-phase column (30cm x 3mm) with a solvent system consisting of 30% acetonitrile in water at a flow rate of 2 mL/min. Detection was carried out at 254nm with a model 440 absorbance detector (Waters Assoc.). Preparative polymerization of p-cresol and p-phenylphenol were carried out in 50mL of the above reaction mixture but 1M of the phenol and 1M H_2O_2 (added slowly throughout the reaction) were employed.

To characterize the polymeric products from aqueous reactions, the enzyme reaction was filtered to remove the water-insoluble polymers and the solids dissolved in dimethylformamide (DMF). For organic reactions, the solvent was evaporated and the solids washed with water to remove the peroxidase. The solids were then dissolved in DMF (in some cases complete dissolution was not obtained). In both aqueous and organic reactions, the DMF-soluble polymers were then analyzed by gel-filtration chromatography using Sephadex LH-60 (Pharmacia, Sweden) packed in a glass column (22 x 1.5cm) equilibrated with anhydrous dioxane at a flow rate of 0.6 mL/min.

Standardization was made with polystyrenes (M.W.'s 500-50,000) obtained from Polysciences (Warrington, PA). The molecular weight cut-off under these conditions was determined to be 10,000 daltons. Molecular weight determinations of polymers in excess of 10,000 daltons were performed by capillary viscometry with 3mL DMF:methanol (4:1) as solvent (viscometer size no. 25, Industrial Research Glassware, Ltd., Union NJ). Standardization was performed with polystyrenes (M.W.'s 10,000-110,000). Melting/softening temperatures (uncorrected) were carried out using a bench-top melting point apparatus (Electrothermal Engineering Laboratory, England).

Electrical conductivity measurements on poly(p-phenylphenol) were carried out as follows: poly(p-phenylphenol) was packed into 0.5cm pellets, placed in a dry box to remove residual moisture, and added to 5mL nitromethane containing 75mg nitrosylhexafluorophosphate. The doping solution was left for 24h, after which the polymer pellets were extensively washed with nitromethane and dried. Surface resistivities were measured using a two-point conductivity probe.

3. Results and Discussion

Aqueous Reactions: We initially studied the polymerization of phenols in aqueous solutions. In this manner, a direct comparison between organic and aqueous based phenolic polymerizations could be made. p-Phenylphenol was chosen as a model substrate of peroxidase because it is a commercially important phenolic monomer for oil-soluble resins (14), has poor solubility in water and extremely high solubilities in a wide variety of organic solvents. A saturating concentration of p-phenlyphenol (1.5mM) in 20 mL aqueous buffer (0.01M acetate, pH 5.0) containing 10% dioxane was prepared and 10mg horseradish peroxidase was added. The reaction was initiated by adding 2mM H_2O_2 and the mixture magnetically stirred at 25°C. The solution immediately turned black and a solid formed. Complete conversion of the p-phenylphenol occurred after 0.5h and the solids were filtered and dissolved in DMF. Chromatography on Sephadex LH-60 yielded a broad peak with an average molecular weight of 500 daltons (dimers and trimers) (Figure 1). Thus by using p-phenylphenol in aqueous solutions we confirmed previous workers failed attempts to carry out effective polymerizations using horseradish peroxidase (8). Presumably, polymerization ceased at such low molecular weights due to the poor solubility of the products in the aqueous solution. To overcome this, we endeavored to carry out the polymerization of p-phenylphenol in organic media.

Organic Reactions: In previous papers (9-12) we described peroxidase catalysis in a number of organic solvents, both water-immiscible and water-miscible. Dioxane, containing 15% v/v aqueous buffer (horseradish peroxidase was shown to be inactive in anhydrous dioxane) was chosen as a suitable solvent for phenolic polymerizations based on high solubility of nearly all phenols in the solvent. The polymerization of 25mM p-phenlyphenol in 85% dioxane was carried out as described under "Materials and Methods". Once again, the reaction mixture blackened and

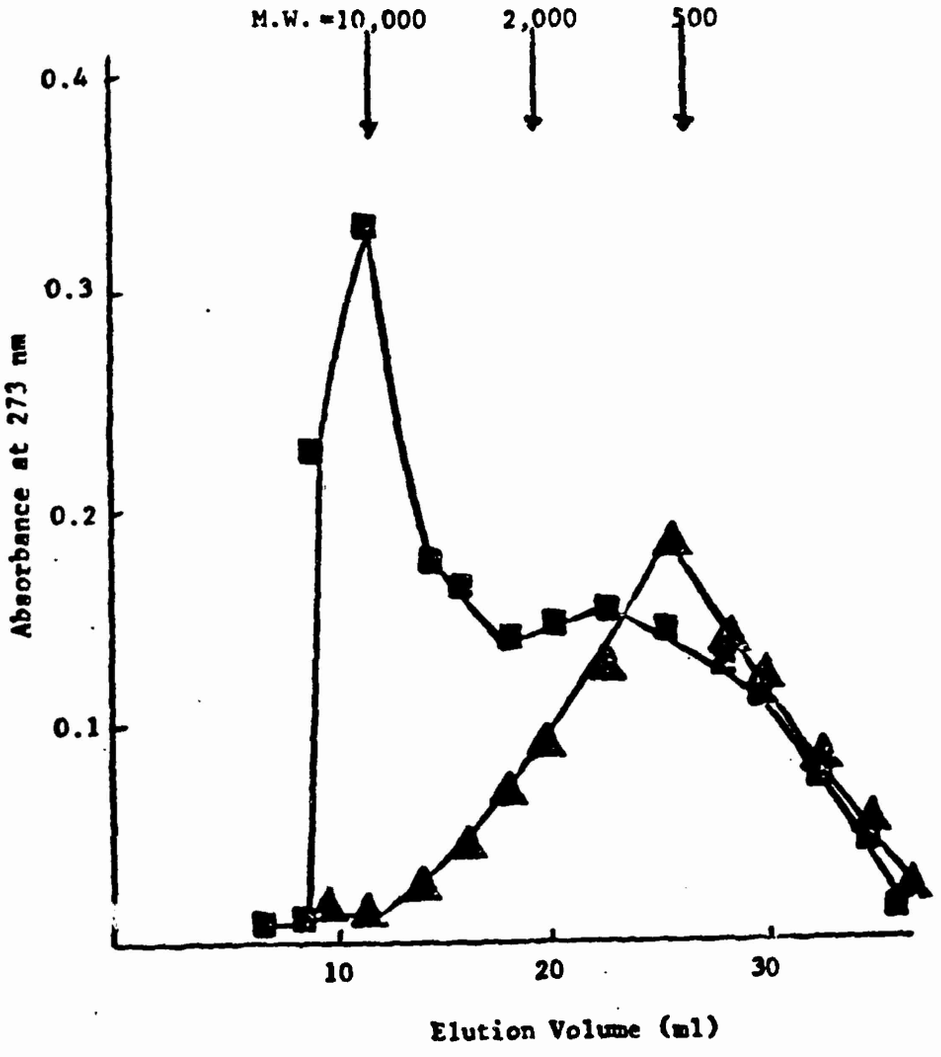

(▲), Aqueous reaction - (HRP) = 0.5 mg/ml, (p-phenylphenol) = 1.5 mM, (H_2O_2) = 2 mM. (■), Reaction in 85% dioxane/15% aqueous buffer - (HRP) = 0.5 mg/ml, (p-phenylphenol) = 25 mM, $(H_2O_2)_{total}$ = 25 mM. Reaction volumes = 20 ml. T = 25°C.

FIGURE 1. Polymerization of p-Phenylphenol in aqueous vs organic media

solids formed. After 2.5h the p-phenylphenol was completely consumed, the reaction worked up as described above, and the polymer placed in DMF where only 70% dissolved. The dissolved polymer was subsequently chromatographed on Sephadex LH-60. As shown in Figure 1, polymerization of p-phenylphenol in 85% dioxane gave a significant amount of high molecular weight polymer. Further analysis by viscosity indicated that the average molecular weight was 26,000 daltons (DP=153) - an increase in polymer size of 52 fold over the aqueous case. Hence, before the poly(p-phenylphenol) precipitated out of solution in 85% dioxane, a high polymer formed supporting our hypothesis that the increased solubility of polymeric species in organic media as opposed to water would lead to high polymer formation. The DMF-insoluble fraction is intriguing. Apparently, this fraction must have had a molecular weight in excess of 26,000 daltons or it would have easily dissolved in DMF. No further characterization on this material, however, was performed.

It occurred to us that because such a large difference in molecular weight of poly(p-phenylphenol) was obtained in organic media with respect to water, it is possible to selectively control polymer size by simply varying the concentration of dioxane in water. To that end, p-phenylphenol was polymerized in different dioxane-aqueous buffer mixtures ranging from pure aqueous buffer to anhydrous dioxane. As expected, no reaction occurred in anhydrous dioxane. In all other reactions, however, conversions exceeding 90% were obtained. The polymeric solids were isolated, dissolved in DMF (at dioxane concentrations from 80-90%, roughly 30% w/w of the polymeric solids failed to dissolve), and their molecular weights determined by Sephadex LH-60 chromatography and viscosity. The results are shown in Figure 2. Dioxane at 85% concentration supported the highest polymer formation (26,000 daltons) with a sharp drop in polymer size on either side of this maximum. The drop-off in molecular weights at lower dioxane concentrations undoubtedly was due to the reduced capacity of the solvent to keep the growing polymer chains in solution. While the cause of lower molecular weights obtained at concentrations above 85% dioxane was not further investigated, the dramatic effect of dioxane concentration on polymer size indicates that the progress of peroxidase-catalyzed phenolic polymerizations can easily be controlled by varying solvent concentrations. This is a major advantage in polymer production as it is often more important to obtain selectivity in molecular weights than to achieve very high molecular weight, highly dispersed polymers.

Dioxane was by no means a unique medium for peroxidase-catalyzed polymerization of p-phenylphenol: acetone, methyl formate, and DMF, all containing 15% v/v aqueous buffer, supported the polymerization reaction giving molecular weights from 2,000 to above 10,000 daltons (data not shown). In addition, horseradish peroxidase was capable of polymerizing a wide variety of phenols (and an aromatic amine, aniline) in 85% dioxane (Table 1). Once again, polymerizations in aqueous buffer resulted in low molecular weight coupling products (approximately 500 daltons). Of the 13 substrates polymerized in 85% dioxane, 8 gave molecular weights of 1350-1950 daltons, the optimal size for novolak and small resole-type phenolic resins prior to curing. The relatively low molecular weights

TABLE 1

HORSERADISH PEROXIDASE-CATALYZED POLYMERIZATIONS

Compound	Polymer m.w.
phenol	1350
p-methoxyphenol	1950
p-cresol	1900
aniline	1650
coniferyl alcohol	1800
ethyl ferulate	1850
β-naphthol	1950
p-tert-butylphenol	1850
p-chlorophenol	550
2,6-dimethylphenol	480
4,4'-biphenol	375
p-phenylphenol	26,000
α-naphthol	Insoluble

Conditions

Concentration = 25 mM, $(H_2O_2)_{total}$ = 25mM,
reaction volumes = 20 ml, T = 30 C, [HRP] = 0.5 mg/mL.
Solvent = 85% dioxane/15% aqueous buffer, pH 5.

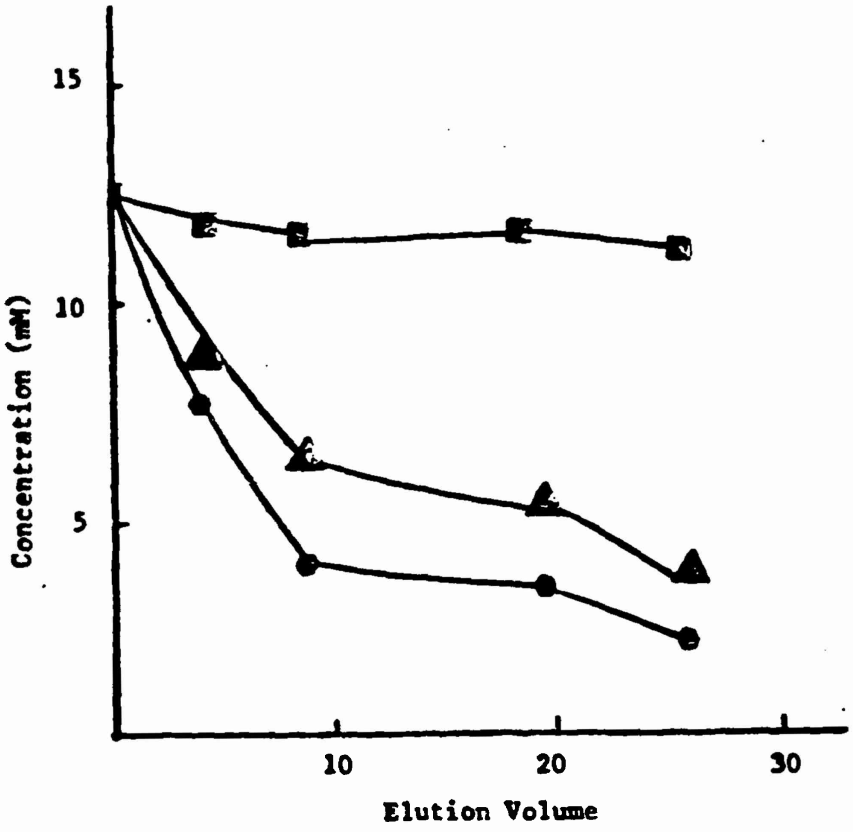

(■), 2,6-dimethylphenol (12.5 mM). (▲), 2.6-dimethylphenol (12.5 mM) in the presence of p-phenylphenol (12.5 mM) (●). (HRP) = 0.5 mg/ml, $(H_2O_2)_{total}$ = 15 mM for (■) and 25 mM for (▲),(●)
Reaction volume = 25 ml.

FIGURE 2. Effect of Dioxane Concentration on the molecular weight of Poly(p-Phenylphenol)

obtained for polymerization of p-chlorophenol, 2,6-dimethylphenol, and 4,4'-biphenol may stem from the fact that the two former phenols are poor substrates for the peroxidase while the latter biphenol reacts rapidly to the 4,4'-diphenoquinone and thus is unable to be polymerized further . The disparity in polymer size of p-phenylphenol and perhaps α-naphthol (which gave a polymeric solid that could not be dissolved, even in boiling DMF and, therefore, must be a high molecular weight polymer) with respect to the other phenols may be explained by free radical chemistry. Both p-phenylphenol and α-naphthol are high-resonance stabilized phenols. Hence, the lifetimes of their respective phenoxy radicals are long and radical transfer is enhanced resulting in larger polymers.

Copolymerization: It is often worthwhile to simultaneously polymerize two or more phenols in order to incorporate the chemical and physical properties of each phenol into a copolymer. We examined the potential of horseradish peroxidase to carry out copolymerization in 85% dioxane. In order to show the generality of such an approach, a poorly reacting phenol, 2,6-dimethylphenol, was copolymerized with p-phenylphenol. After 2.5h, less than 10% of the 2,6-dimethylphenol had reacted whereas in the presence of an equimolar concentration of p-phenylphenol over 75% of the 2,6-dimethylphenol had reacted (Figure 3). The resulting polymer had a molecular weight of approximately 1000 daltons, significantly different than either mono-polymer (see Table 1). This phenomenon can be explained, mechanistically, based on the nature of horseradish peroxidase catalysis. Horseradish peroxidase initiates the one-electron oxidation of a phenol to the corresponding phenoxy radical. The radical then can undergo recombination with another radical species or initiate radical transfer. A series of radical transfer and chain termination reactions leads to the growth of the polymer chain. This is clearly depicted in Figure 4. In the aforementioned copolymerization reaction, the p-phenylphenoxy radicals produced by peroxidase catalysis can engage in radical transfer with the poorly reactive 2,6-dimethylphenol thereby initiating copolymerization. In this case, the nonenzymatic radical transfer reaction is less susceptible to steric hindrance by the ortho methyl groups than is the peroxidase-catalyzed one-electron oxidation of 2,6-dimethylphenol. Therefore, poorly reactive phenols that would otherwise not be expected to undergo facile polymerization can be copolymerized with a fast reacting peroxidase substrate. This significantly expands the scope of peroxidase-catalyzed phenolic polymerizations as it is not always possible to use fast reacting phenols as monomers.

Preparative Scale Polymerizations: The ability of 85% dioxane to solubilize phenols and their respective polymeric products to a much greater degree than water has enabled preparative-scale polymerizations to be carried out. This was clearly shown using p-phenylphenol and p-cresol. To 1M p-phenylphenol in 50mL 85% dioxane, 25mg horseradish peroxidase and 20 mM H_2O_2 were added (a total of 1M H_2O_2 was added during the reaction). The mixture was magnetically stirred at 25°C, aliquots periodically removed and p-phenylphenol concentration measured by HPLC. After 6.5h, nearly 0.5M p-phenylphenol was converted into a black

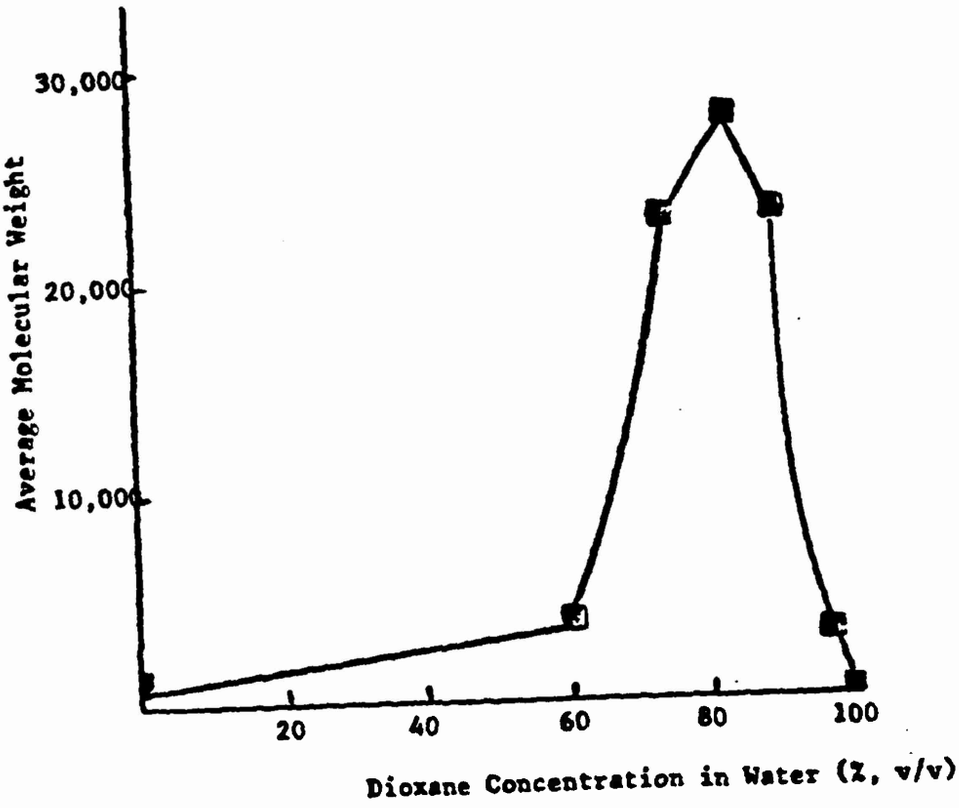

(HRP) = 0.5 mg/ml, (p-phenylphenol) = 0.1 M (except 1.5 mM at 0% dioxane), (H_2O_2) = 100 mM (except 2 mM at 0% dioxane). Reaction volumes = 100 ml, T = 25°C.

FIGURE 3. Copolymerization of 2,6-Dimethylphenol with p-Phenylphenol in 85% dioxane

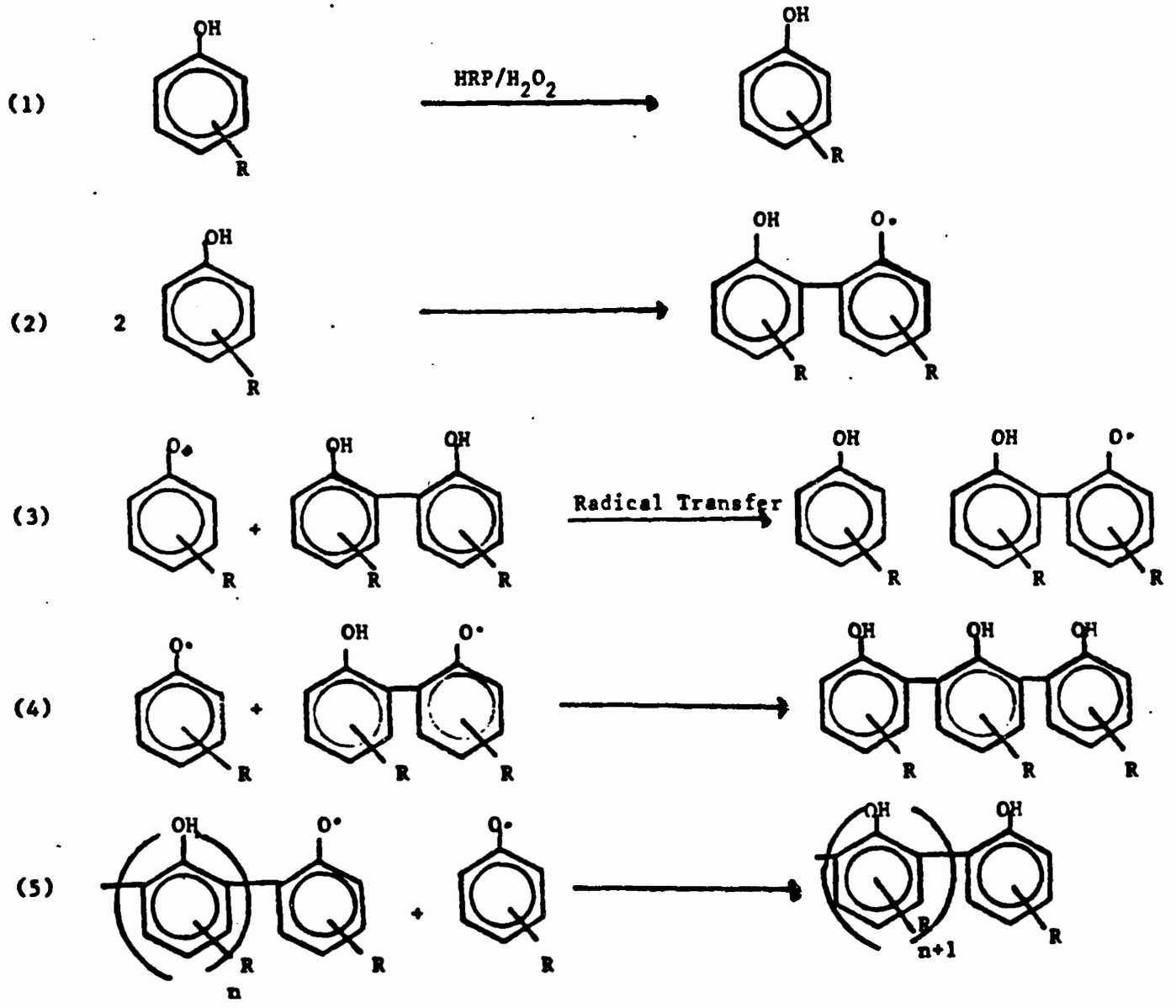

FIGURE 4. Mechanism of horseradish peroxidase-catalyzed polymerization of phenols via radical transfer

polymeric solid and the reaction continued for a total of 75h to give a conversion of 90% (Figure 5). Following solvent removal a black oil remained which was washed with water to remove the enzyme and then with 50% aqueous acetone to remove the unreacted p-phenylphenol. Nearly 7.5g (86% recovered yield) of poly(p-phenylphenol) were obtained (300g polymer per g horseradish peroxidase in 75h). Viscosity measurements indicated an average molecular weight of 13,500 daltons, approximately one-half of what was routinely obtained in smaller scale experiments. The cause of the lower polymer size may have been due to the slow decay of the high molecular weight polymer over such long (relative to small scale experiments) reaction times. A similar procedure was carried out using 1M p-cresol giving 4.5g (83% recovered yield) of the yellow-orange poly(p-cresol) (M.W. of 2000) after 100h (Figure 5).

The large amounts of polymer enabled us to carry out several characterizations other than molecular weight determinations and compare the polymers to typical phenol-formaldehydes. For example, the melting/softening temperatures of poly(p-phenylphenol) and poly(p-cresol) were 208-212°C and 165-170°C, respectively. These temperatures are far higher than typical novolaks or resols which have typical melting/softening temperatures of 90-110°C (15). The higher melting temperatures of peroxidase-produced phenolic polymers may be advantageous for producing thermoresistant resins which do not require curing or for producing resins with a much larger operating temperature regime for chemical modifications prior to curing.

Another property further investigated was the ability of peroxidase-produced phenolic polymers to conduct electricity. Unlike phenol-formaldehyde resins, peroxidase-produced phenolic polymers are highly conjugated by virtue of carbon-carbon coupling, which also gives them a highly colored nature. The surface resistivity of a hardened pellet of poly(p-phenylphenol) after doping with the strongly oxidizing nitrosylhexafluorophosphate, was approximately 10^5 ohm-cm. A comparison to other polymers is given in Table 2. Peroxidase-produced phenolic polymers were considerably more conductive than the nonconjugated phenol-formaldehydes or polystyrene (16).

4. Conclusions and Future Prospects

In summary, the data obtained in this work clearly show that horseradish peroxidase is an effective catalyst for preparative scale phenolic polymerizations in nonaqueous media. It appears that most, if not all, substrates of peroxidase - including phenols and aromatic amines - can be polymerized in organic media by the approach developed herein, either individually or by copolymerization. From an applied standpoint, selective control over polymer size can be obtained by simply varying the organic solvent concentration in water. This may be important for specialty uses of these polymers, including adsorbants for chromatography,

TABLE 2

PEROXIDASE-PRODUCED POLY(p-PHENYLPHENOL): ELECTRICAL CONDUCTIVITY IN RELATION TO OTHER COMMERCIALLY IMPORTANT POLYMERS

Polymer	Electrical Conductivity $(ohm\text{-}cm)^{-1}$
polyacetylene (doped)	10^{1}
Poly(p-phenylene)	10^{1}
Peroxidase-produced (doped)	10^{-5}
Polyacetylene (undoped)	10^{-8}
Phenol-formaldehyde (typical)	10^{-14}
Polystyrene	10^{-18}
PTFE (Teflon)	10^{-20}
Diamond	10^{-20}

Literature values from ref. 16.
Peroxidase-produced polymer doped with nitrosylhexafluorophosphate as described in the text.

surface coating materials, and as fire-resistant foams of variable physical properties. Furthermore, the polymers appear to have significant electrical conductivities and, therefore may have potential use in semiconducter plastics.

Peroxidase-catalyzed phenol oxidations in aqueous solutions have long been studied (17). The use of peroxidase as a polymerization catalyst in organic media is only beginning to be examined. Such reactions, in concert with other enzyme-catalyzed polymerizations in nonaqueous media (18) will usher in a new era in enzymatic catalysis.

Acknowledgements: Part of this work was carried out in the laboratories of Professor Alexander M. Klibanov and Professor Michael A. Marletta in the Department of Applied Biological Sciences at the Massachusetts Institute of Technology. The author wishes to express his gratitude to both of them for their guidance and cooperation.

References

1. Brode, G.L. 1981. in Kirk-Othmer Encyclopedia of Chemical Technology. 3rd Edition, Vol. 18 John Wiley and Sons: New York. pp. 384-416.

2. Clary, J.T., Gibson, J.F., and Waritz, R.S. (eds.). 1982. Formaldehyde: Toxicology-Epidemiology-Mechanisms. Marcel Dekker: New York.

3. Endres, G.F., Hay, A.S., and Eustance, J.W. 1967. J. Org. Chem. 28: 1300-1305

4. Hay, A.S. 1979. in Proc. of China-US Bilateral Symposium on Polymer Chemistry and Physics, Oct. 5-10, Beijing. Science Press: New York. pp. 351-357.

5. Schwartz, M.A., Rose, B.F., Holton, R.A., Schott, S.W., and Vishnuvajjala, B. 1977. J. Am. Chem. Soc. 99: 2571-2578.

6. Walsh, C. 1977. Enzymatic Reaction Mechanisms. W.H. Freeman and Co.: San Francisco.

7. Sarkanen, K.V. and Ludwig, C.H. (eds.). 1971. Lignins-Occurrence, Formation, Structure, and Reactions. Wiley-Interscience: New York, Pts 1 and 2.

8. Schwartz, R.D. and Hutchinson, D.B. 1981. Enzyme Microb. Technol. 3: 361-363.

9. Dordick, J.S., Marletta, M.A., and Klibanov, A.M. 1986. Proc. Natl. Acad. Sci. USA 83: 6255-6257.

10. Kazandjian, R.Z., Dordick, J.S., and Klibanov, A.M. 1986. Biotechnol. Bioeng. 28: 417-421.

11. Boeriu, C.G., Dordick, J.S., and Klibanov, A.M. 1986. Bio/Technology 4: 997-999.

12. Dordick, J.S., Marletta, M.A., and Klibanov, A.M. 1987. Biotechnol. Bioeng. 29: (In Press).

13. Schumb, W.C., Satterfield, C.N., and Wentworth, R.L. 1955. Hydrogen Peroxide. Reinhold Publishing Co.: New York. pp. 553-557.

14. Whitehouse, A.A.K., Pritchett, E.G.K., and Barnett, G. 1967. Phenolic Resins. American Elsevier: New York.

15. Zaks, Y., Lo, J., Raycher, D., and Pearce, I.M. 1982. J. Appl. Polym. Sci. 27: 913-930.

16. Potember, R.S., Hoffman, R.C., Hu, H.S., Cocchiaro, J.E., Viands, C.A., Murphy, R.A., and Poehler, T.O. 1987. Polymer 28: 574-580.

17. Saunders, B.C., Holmes-Seidle, A.G., and Stark, B.P. 1964. Peroxidase. Butterworths: Washington.

18. Margolin, A.L., Crenne, J.Y., and Klibanov, A.M. 1987. Tetrahedron Lett. 28: 1607-1610.

POTENTIAL BIOTECHNOLOGY APPLICATIONS TO AIR FORCE MATERIALS NEEDS

Frederick L. Hedberg

Structural Materials Branch
Nonmetallic Materials Division
Materials Laboratory
Air Force Wright Aeronautical Laboratories
Wright Patterson Air Force Base, Ohio 45433

The general objectives for Air Force Materials Laboratory programs involving biotechnology are: (1) to significantly lower materials preparation costs through biosynthesis; (2) to significantly lower the cost of processes such as paintstripping by utilizing biotechnology; (3) to obtain materials with structural complexity not conventionally obtainable; and (4) to learn improved materials design concepts through understanding biomaterials.

To attain these objectives, a small cadre of senior Materials Laboratory technical personnel with diverse backgrounds, led by the Chief Scientist, have engaged in a continuing and growing dialogue with the biotechnology community. The dialogue has been enlarged to include other members of the aerospace materials community through the organization and support of workshops, and through active participation with the Air Force Biotechnology Advisory Group (BIOTAG). A community of people has thus been created with knowledge of biotechnology and its potential contributions to the Air Force. For example, a distinguished university professor is spending a sabbatical with us, with AFOSR support, investigating natural materials with electrooptical properties. With the knowledge gained, small probing programs have been planned and initiated, utilizing funding from a variety of sources, including Materials Laboratory, Laboratory Director's Funds, Focal Area 6.2 Development Funds, Small Business Innovation Research Funds, and Biotechnology Initiative Funds from the Air Force Office of Scientific Research. It is anticipated that successful programs will be transitioned either to Materials Laboratory 6.2 development programs or to industry through Phase II and Phase III SBIR programs. Current investment strategy extends to FY 91. Fiscal planning beyond that time will be coordinated with the BIOTAG.

The investment criteria for these programs take into consideration the payoff for the Air Force, the risk factor, and the time factor.

Within the Materials Laboratory there are a variety of technical problem areas which are being considered for biotechnology related programs. These areas include: Organic matrix resin based structural composites; Carbon matrix based composites; Transparent materials; Elastomers and seals; Fluids; Lubricants; Paints and coatings; Ceramic materials; Structural metals; Electrooptical materials; Laser hardened materials; and Electronic materials. We are seeking suggestions for novel, biotechnological related approaches to attaining our specified objectives in these areas. This will necessitate the development of a dialogue between biotechnology people and aerospace people with back-

grounds in these areas. Workshops, such as the ones we have supported, are one method of dialog development. It is hoped that publicizing our interest and needs will stimulate technical people in the private sector to take the initiative of bridging the gap between these diverse disciplines of biotechnology and aerospace materials.

One approach to determining the types of chemistry or design required for materials exposed to harsh environments is to ascertain what types of structural modifications nature uses to respond to such environments.

Current on-going and planned programs include the following:

Biologically assisted mining or purification of metals through bioleaching processes or bioaccumulation is an area with a number of possibilities. Bioleaching methods have been quite successful for copper mining and are currently being used for more than 25% of U.S. copper production. The greatest potential for bioleaching methods is considered to be for metals occurring in low natural abundance. A number of relatively rare metals have been identified with potential applications to aerospace systems, including scandium, erbium, yttrium, iridium, and gallium. A current program is concerned with lowering the cost of preparation of gallium, a metal of strategic importance for Air Force electronic and electrooptic applications. Bioaccumulation processes may be applicable to the purification of some metals which are particularly difficult to purify, such as removing zirconium from hafnium, or, alternatively, as a supplement to bioleaching operations to recover a desired metal from a leach mixture. Bioaccumulation of metals of Air Force interest may interrelate with government and commercial interests in removal of toxic metals or recovery of rare metals.

The program on biomining of gallium will explore the use of bioleaching methods (conversion of water insoluble metal species in ores to water soluble species by microorganisms instead of by expensive chemicals) to obtain gallium from ores in which it is commonly present at a level of 0.1% or less. Gallium has not been mined in the U. S. since 1982 due to economic considerations. Our on-going Phase I Small Business program has been notably successful in that a new high temperature microorganism has been discovered which leached 91% of the gallium from the ore. Encouragement and technical support for a Phase II program has been offered by the U. S. Bureau of Mines. The technical developments arising from this program may be applicable to other strategic metals found in low natural abundance.

A current program area is concerned with lowering the cost of preparation of acetylenic molecules which are candidate materials for structural composites, circuit boards, conductive polymers, and nonlinear optical devices. A major limitation to their development in aerospace is their cost. The only acetylenic material commercially available today for aerospace applications costs $200 per pound.

Molecules with a high acetylenic content have correspondingly high theoretical char yields, which are desirable for carbon matrix composites. Naturally occurring acetylenes of this type are currently being explored. One compound, 1-phenylhepta-1,3,5-triyne, showed very good processing conditions with a melting temperature of 52 degrees C, a cure in the range of 150 to 200 degrees C, and a nonoptimized char yield of 76%.

This program will address the use of biosynthesis routes for the general preparation of the acetylene group itself as well as for the preparation of useful acetylenic chemical intermediates such as meta-hydroxyphenylacetylene. This molecule has been demonstrated to be a useful intermediate for acetylene terminated resins. Acetylenic materials are found in great abundance in nature. Dialogue with the biotechnology community indicates that this area of preparation of aerospace chemicals may be most amenable to biotechnological assistance, but may require a significant investment.

An example of the potential payoff from this area of research is the commercial biologically aided preparation by ICI Ltd. of the structural composite candidate material, polyphenylene. The projected cost of this material is $6.00 per pound, as contrasted with $25-$50 per pound for conventional "inexpensive" aerospace composite materials, and hundreds of dollars per pound for materials with the thermal performance characteristics possible for polyphenylene.

We are interested in suggestions for low cost biotechnological aided routes to other high cost chemical intermediates for aerospace applications.

The program area designated as modeling mechanical properties of natural systems is concerned with learning improved materials design concepts through analysis of the chemical and morphological design of natural structural composite systems, which have optimized strength, stiffness, and damage tolerance for survival considerations without a severe weight penalty. Candidate systems include cartilage, bone, wood, and insect and marine exoskeletons. Although the chemistry of natural systems is not suitable for the harsh thermal environments encountered by Air Force structural composites, natural design appears to be much more complex. The overall goal of this program is to combine natural design features with aerospace high temperature chemistry.

The program on deuterated materials is concerned with lowering the cost of preparation of candidate materials for lubricant and structural composite applications. The program will explore the growth of certain species of algae in deuterated (heavy) water for the production of deuterated chemical intermediates, which can be converted by conventional chemistry to deuterated lubricant, composite resign and composite fiber materials. These deuterated materials have been found by Naval researchers to provide five- to fifteenfold increases in lifetimes under thermal/oxidative conditions. The biological method of preparing

deuterated intermediates may provide a significant savings over the conventional chemical method. An earlier program in this area was co-funded with the Naval Air Systems Command.

An on-going Small Business program will provide deuterated chemical intermediates, which Materials Lab inhouse personnel will chemically convert to silahydrocarbon lubricant molecules. The compounds will then be compared with their hydrogen-containing analogs for relative thermo-oxidative stability. A major purpose of this evaluation is to identify if deuterated materials have sufficient potential for further pursuit.

A planned program on biological paintstripping is concerned with lowering the cost, decreasing the toxicity, and reducing the substrate damage associated with state-of-the-art methods of paint removal from aircraft. The program will investigate the use of natural enzymatic methods for removal of Air Force polyurethane paint formulations. Current methylene chloride solvent based or polymer bead blasting based paint-stripping methods create environmental problems due to toxic chemicals or dust and also have a propensity to damage underlying composite aircraft structures.

The following pages summarize the goals, strategy, and possible technical payoffs of the Air Force efforts in potential biotechnology applications for materials needs.

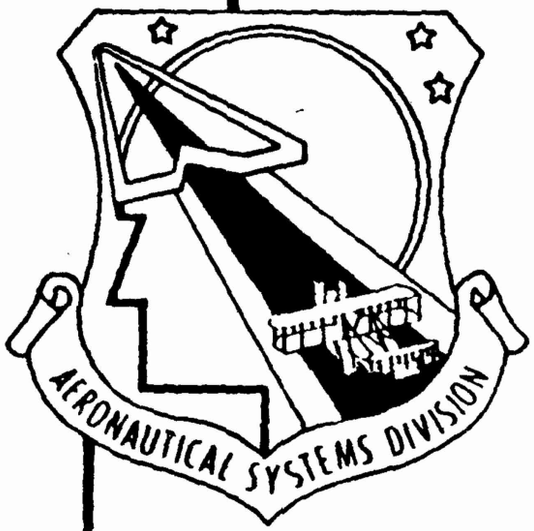

AIR FORCE WRIGHT AERONAUTICAL LABORATORIES MATERIALS LABORATORY

POTENTIAL BIOTECHNOLOGY APPLICATIONS TO AIR FORCE MATERIAL NEEDS

DR. FREDERICK L. HEDBERG
AFWAL/MLBC

POTENTIAL AIR FORCE PAYOFFS FROM BIOTECHNOLOGY

- LOWER COST MATERIALS PREPARATION THROUGH BIOSYNTHESIS
- LOWER COST PROCESSING METHODS
- MATERIALS WITH STRUCTURAL COMPLEXITY NOT OTHERWISE OBTAINABLE
- IMPROVED MATERIALS DESIGN CONCEPTS THROUGH UNDERSTANDING BIOMATERIALS

INVESTMENT STRATEGY PLAN

HEDBERG

- MATERIALS LABORATORY BIOTECHNOLOGY PLANNING GROUP LED BY CHIEF SCIENTIST
- CONTINUING AND GROWING DIALOGUE WITH THE BIOTECHNOLOGY COMMUNITY
- WORKSHOP ORGANIZATION BRINGING TOGETHER MEMBERS OF THE BIOTECHNOLOGY AND AEROSPACE COMMUNITIES
- SMALL PROBING PROGRAMS TO ESTABLISH CONCEPT FEASIBILITY
- POTENTIAL TRANSITIONING OF SUCCESSFUL PROGRAMS THROUGH NORMAL 6.2 DEVELOPMENT PROGRAMS OR THROUGH SMALL BUSINESS PROGRAM
- WORK WITH BIOTAG TO DETERMINE INVESTMENT STRATEGY BEYOND FY 91

CRITERIA FOR INVESTMENT STRATEGY PROGRAMS

- PAYOFF FOR AIR FORCE
- RISK FACTOR
- TIME FACTOR

HEDBERG

PROBLEMS AREAS POTENTIALLY ADDRESSABLE BY BIOTECHNOLOGY

HEDBERG

- ORGANIC MATRIX RESIN BASED STRUCTURAL COMPOSITES
- CARBON MATRIX BASED COMPOSITES
- TRANSPARENT MATERIALS
- ELASTOMERS AND SEALS
- FLUIDS
- LUBRICANTS
- PAINTS / COATINGS
- CERAMIC MATERIALS
- STRATEGIC METALS
- ELECTRO OPTICAL MATERIALS
- LASER HARDENED MATERIALS
- ELECTRONIC MATERIALS

NEW CHEMISTRY OR DESIGN FROM STRESS ENVIRONMENTS

- HEAT
- MECHANICAL - DAMAGE TOLERANCE
- RAPID CHANGES IN LIGHT INTENSITY
- MAGNETIC FIELD
- OXIDATION
- ABRASION

HEDBERG

Biologically Assisted Mining or Purification of Metals

- Biomining Established for Copper
- Biomining Most Effective for Rare, High Cost Metals
- Metals of Interest for Metal Matrix Composites or Oxidation Protective Coatings for Carbon Matrix Composites: Scandium, Erbium, Yttrium and Iridium
- Current USAF Program Addressing Biomining for Gallium
- Biopurification May Have High Metal Specificity
- Interrelates with Government and Commercial Interests in Bioremoval of Toxic Metals

HEDBERG

BIOMINING GALLIUM

HEDBERG

OBJECTIVE:	EXPLORE THE USE OF MICROORGANISMS FOR BIOLEACHING AND BIOACCUMULATION OF GALLIUM FROM LOW-GRADE ORES
PAYOFF:	• LOWER COST DOMESTIC SUPPLY OF GALLIUM FOR FUTURE ELECTRONIC REQUIREMENTS • TECHNOLOGY TO OBTAIN OTHER STRATEGIC METALS WITH LOW NATURAL ABUNDANCE AT LOW COST
STATUS:	ON-GOING PHASE I SBIR PROGRAM TO ESTABLISH TECHNICAL FEASIBILITY AND COST POTENTIAL OF BIOLEACHING
ACCOMPLISHMENTS:	NEW HIGH TEMPERATURE MICROORGANISM DISCOVERED WHICH LEACHED 91% OF GALLIUM FROM ORE
FUTURE PLANS:	PHASE II PROGRAM TO DEVELOP COMMERCIAL PROCESS

BIOSYNTHESIS OF ACETYLENIC MOLECULES

HEDBERG

OBJECTIVE: DEVELOP LOW COST BIOSYNTHETIC ROUTES TO ACETYLENIC MOLECULES

PAYOFF: LOWER COST MATERIALS WITH APPLICATIONS TO ORGANIC MATRIX RESIN COMPOSITES, CARBON MATRIX RESIN COMPOSITES, CIRCUIT BOARDS, CONDUCTIVE POLYMERS, AND NONLINEAR OPTICAL DEVICES

STATUS:

- PLANNED IN-HOUSE PROGRAM TO STUDY CARBON MATRIX COMPOSITE POTENTIAL OF MATERIALS PRODUCED UNDER AFOSR PROGRAM
- PLANNED PHASE I SBIR PROGRAM TO HYDROXYLATE PHENYLACETYLENE
- PLANNED PROGRAM ON BIOSYNTHESIS OF TERMINAL ACETYLENES

ACCOMPLISHMENTS: ACETYLENIC MOLECULE PREPARED FOR STUDY WITH THEORETICAL 95% CHAR YIELD AND PROCESSABILITY FOR CARBON MATRIX COMPOSITES

ACETYLENE TERINATED MATRIX RESIN THROUGH BIOSYNTHESIS

HEDBERG

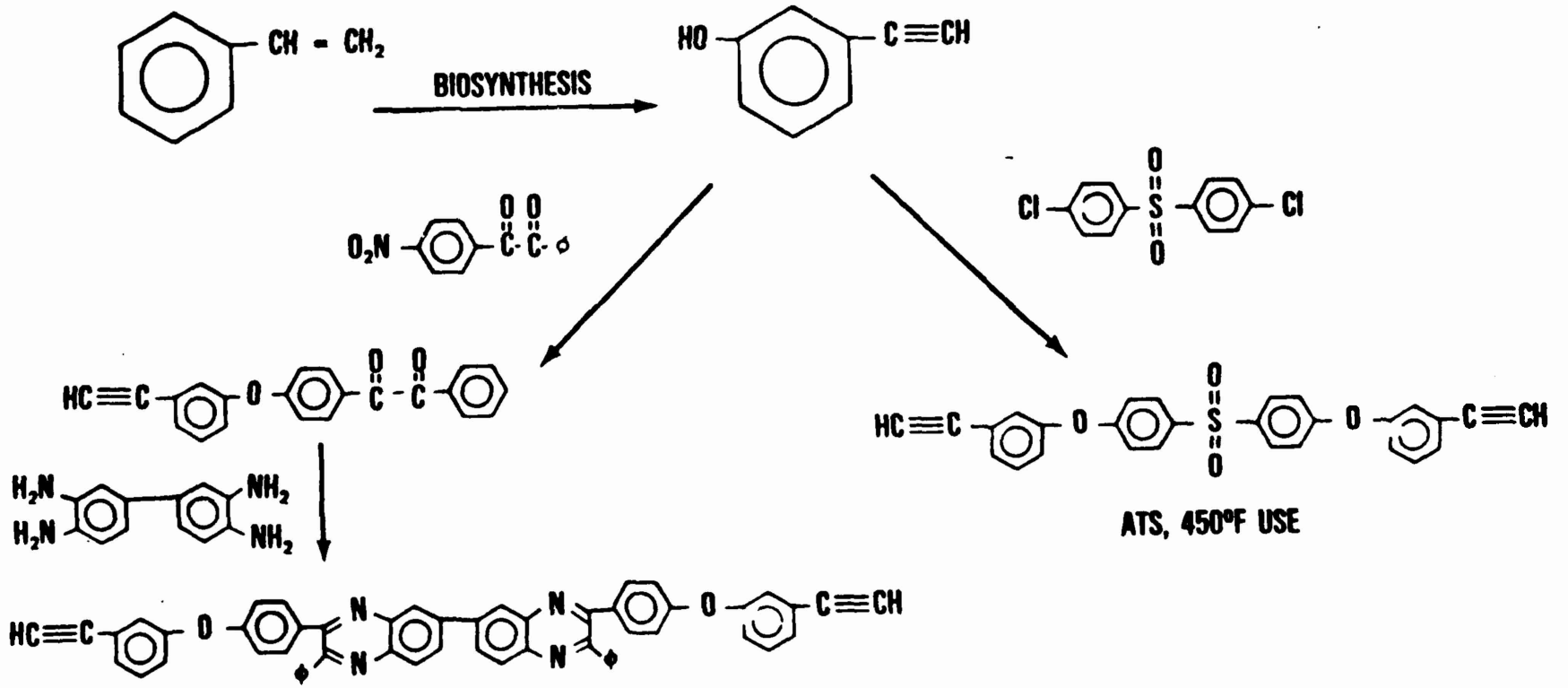

Biomaterials For Carbon-Carbon Composites

HEDBERG

$CH_3-(C\equiv C)_5-CH=CH_2$ 96% Th. Char Yield

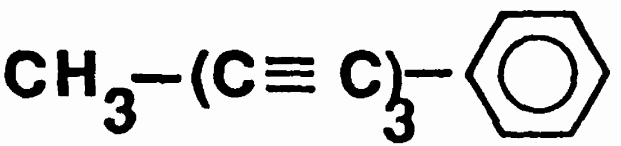

95% Th. Char Yield
76% Obtained Char Yield
M.P. 52°C
Cures 150°-200°C
Natural Insecticide

POLYPHENYLENE THROUGH BIOSYNTHESIS (ICI)

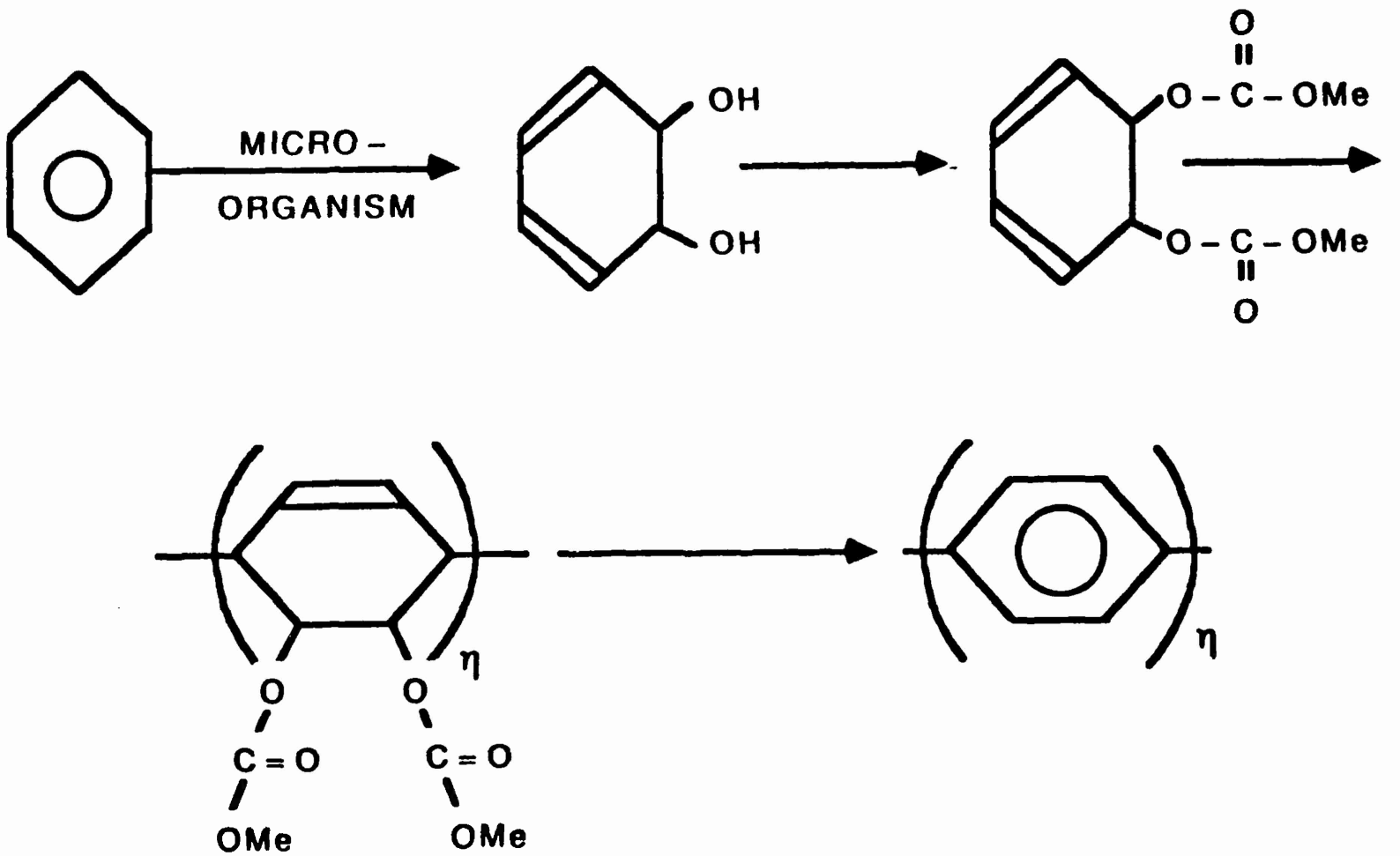

HEDBERG

HIGH COST CHEMICAL INTERMEDIATE FOR AEROSPACE APPLICATIONS

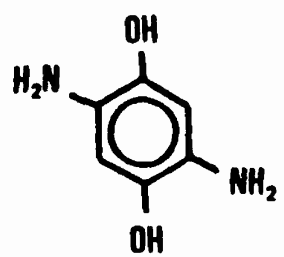

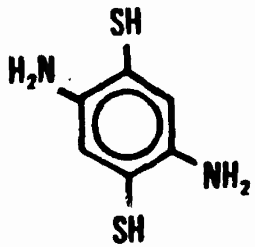

HOOC-R-COOH

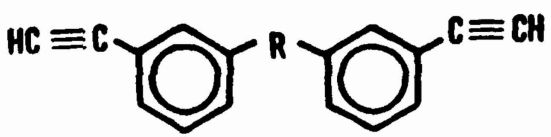

R = COOH OR NH_2

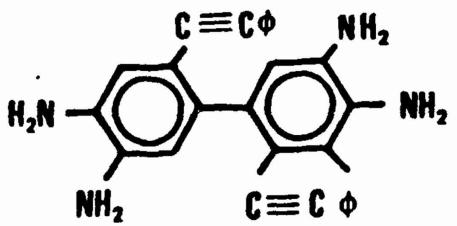

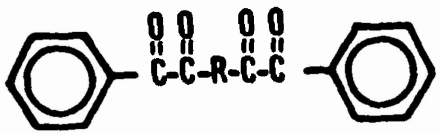

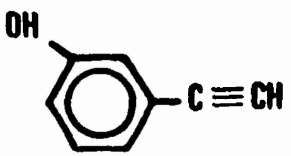

HEDBERG

MODELING MECHANICAL PROPERTIES OF NATURAL SYSTEMS

HEDBERG

OBJECTIVE:	UNDERSTAND NATURAL STRUCTURES FOR MECHANICAL PROPERTIES SUCH AS STRENGTH, STIFFNESS AND DAMAGE TOLERANCE
PAYOFF:	LIGHTER WEIGHT STRUCTURAL COMPOSITES
STATUS:	ON-GOING ON-SITE CONTRACTUAL PROGRAM
ACCOMPLISHMENTS:	ORGANIZED AND SUPPORTED WORKSHOP BRINGING SCIENTISTS FROM STANFORD, CASE-WESTERN, AND DUKE UNIVERSITIES TOGETHER WITH AIR FORCE PERSONNEL
FUTURE PLANS:	IDENTIFY AND EXAMINE APPROPRIATE NATURAL MATERIALS

DEUTERATED MATERIALS

HEDBERG

OBJECTIVE: DEUTERATED CHEMICAL INTERMEDIATES FROM ALGAL GROWTH IN DEUTERIUM OXIDE (HEAVY WATER)

PAYOFF: LOW COST LUBRICANTS AND POLYMERS WITH LONGER LIFETIMES IN THERMAL AND RADIATION ENVIRONMENTS

STATUS: ON-GOING PHASE I SBIR PROGRAM TO PREPARE DEUTERATED FATTY ACIDS

FUTURE PLANS:

- IN-HOUSE SYNTHESIS AND THERMAL TESTING OF DEUTERATED SILAHYDROCARBON LUBRICANTS AND RIGID ROD POLYMERS
- IF PROPERTIES SHOW ADEQUATE POTENTIAL POSSIBLE PHASE II SBIR PROGRAM TO ESTABLISH TECHNICAL AND ECONOMIC FEASIBILITY OF SCALED UP PRODUCTION

DEUTERATED LUBRICANTS

HEDBERG

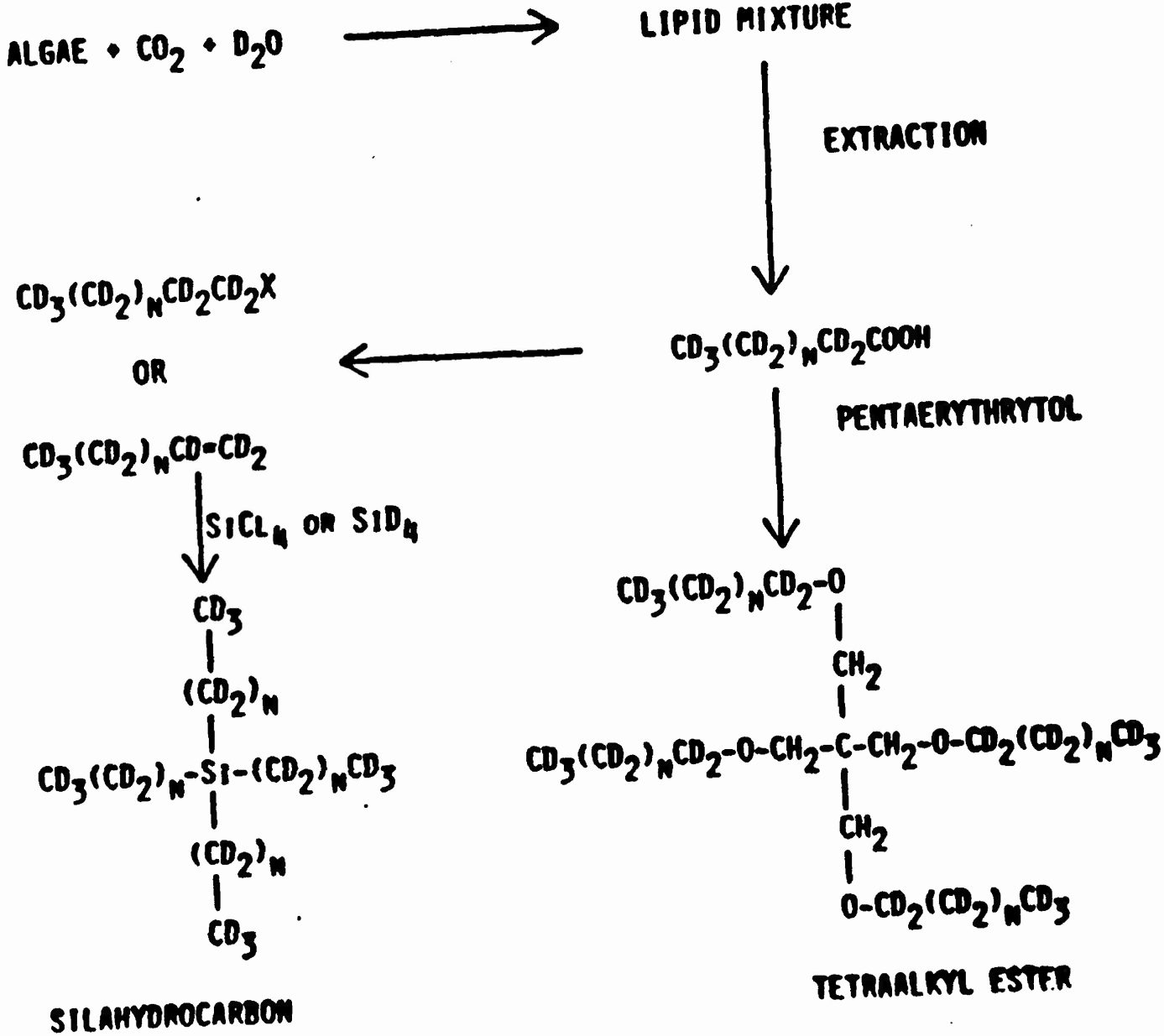

BIOLOGICAL PAINTSTRIPPING

OBJECTIVE: DEVELOP AN ENZYMATIC PAINT REMOVAL METHOD FOR AIRCRAFT

PAYOFF: A PAINT REMOVAL METHOD WHICH IS LOW COST, ENVIRONMENTALLY ACCEPTABLE, AND NON-DAMAGING TO COMPOSITE AIRFRAME STRUCTURES

STATUS: PLANNED PHASE I SBIR PROGRAM TO SCREEN POLYURETHANE-DEGRADING MICROORGANISMS FOR THEIR EFFECT ON AIR FORCE PAINTS

BIOLOGICAL MATERIALS IN OPTICAL MEMORIES AND SIGNAL PROCESSING

Albert F. Lawrence and Robert R. Birge

Center for Molecular Electronics
Carnegie-Mellon University
4400 Fifth Avenue
Pittsburgh, PA 15213

Abstract

Application of molecular physics to electronics offers the possibility of substantial increases in speed, as well as decreases in size and power consumption. We show how optically coupled molecules can serve in the role of memory devices and gates for digital and analog computers.

Role of molecular physics.

In essence, the physical limitations on the size and speed of electronic and optical devices, as we presently conceive them, are determined by the quantum nature of matter and the speed of light. As the size of electronic circuitry continues to decrease, our conceptual view of the processes inside electronic devices is beginning to shift away from the classical picture of solid-state physics in which electrons and thermal vibrations are treated as statistical ensembles of free particles. To a great extent, the discovery of new types of extended quantum systems (the quantum Hall effect), the observation of the Aharanov-Bohm effect in small wire loops, and the recent advances in superconductivity have made the quantum field view much more fashionable in device physics than it was a few years ago. If we are to continue along this path, we will be faced with the problem of information transfer in structured matter at the nanometer level. At this scale, any device must resemble a large molecule in its physics.

There are also practical as well as theoretical reasons for looking toward molecular physics. Figure 1 gives comparisons between speed and power dissipation for various types of electronic devices and for molecular processes. The developments in superconductivity will, of course push Josephson speeds up by one or two orders of magnitude, but taken altogether molecular structures offer the ultimate attainable speed, power dissipation and size. (See Figure 2.) Molecular physics is where we need to look both to obtain examples of useful phenomena and to solve the problems of scaling conventional microelectronics.

Molecular electronics.

Molecular electronics is basically the study of transduction (production of excited states) and transport (movement of charge and energy) in molecular systems. As such the study of molecular electronics adds a dynamical component to the molecular orbital theory, which has long been the major tool of chemical physics. Rather than discussing the details of what is required to add time dependence to our well-developed picture of molecular states, we will turn to two examples where dynamical processes in molecules might be of interest in electronics. The first example is the application of a bio-molecule to computer memories, the second, the application of a synthetic molecule (based on substances found in biological organisms) to signal processing.

Optically coupled molecular devices.

Quantum statistics plays a determining role in the interaction of a molecule with external fields. For example, the absorption of a photon of light by a chromophore has a certain quantum amplitude. That amplitude corresponds to a probability of observation which is never unity. Thus, a highly reliable device based on optical coupling will invariably require more than one molecule to participate in the transformation of interest. Equally important is that the observation of the transfer of an electron from one part of a molecule to another is also governed by quantum statistics. Thus it is unlikely that a practical molecular electronic device can rely on the motion or translocation of a single electron. Ensemble averaging is one solution and provides a means of averaging out quantum fluctuations so that the expectation value governs the final result.

Optical memory.

Memory storage is an essential for any type of digital computer. What is required for a molecular optical memory is a molecule which exhibits two or more stable states and switches predictably between these states in response to absorption of light. Bacteriorhodopsin, the light-harvesting protein found in the purple membrane of Halobacterium halobium, is one such molecule. Figure 3a shows how the protein aggregates in the bacterial membrane. This drawing, derived from x-ray diffraction data, shows three molecules arranged symmetrically around a central point. The part of the protein which spans the membrane is either composed of seven alpha-helices (Figure 3b) or a beta sheet and three alpha helices. This structure can be seen from the diffraction data. The light-adapted form of the protein undergoes a photochemical cycle that is responsible for transporting protons from the inside (cytoplasm) to the outside (extracellular) of the membrane. The proton almost certainly moves along a channel enclosed by the protein alpha helices. The primary event ($bR_{568} \rightarrow K_{601}$ in chemical notation) is the only process of the cycle that requries energy input in the form of light. This event involves an extremely rapid conformational change, less than 10 pico-seconds, in a portion of the molecule known as the chromophore. A

schematic representation of the position of a bacteriorhodopsin molecule in the lipid bilayer, and location of the chromophore on the molecule is given by Figure 4. The structure of the chromophore before and immediately after the conformational change is shown in Figure 5. As can be seen from the figure the major change is a trans- cis shift around carbon number 14. This rapid change is driven by a shift in molecular orbitals (not shown) which, before photon absorption are stabilized by interaction with a charged group on the protein substrate. The geometric relations between the chromophore and the protein are shown in Figure 5. The complete photocycle for bacteriorhodopsin is shown in Figure 6. At liquid nitrogen temperature (77K) both of the species bR and K are stable, and the photocycle is halted after the primary event. In addition the two species have distinctly different absorption maxima--568nm for bR and 610 nm for K. Figure 6 also gives the absorption curves for the two species. Bacteriorhodopsin satisfies the criteria for an optical molecular memory. Furthermore, the data on interconversion rates, the distinctness of the absorption curves and the high photochemical stability of the protein make it an attractive candidate for further investigation.

Application of bacteriorhodopsin.

Bacteriorhodopsin may be dispersed in a lipid solvent and deposited on a substrate in multiple composite monolayers. This is shown in Figure 7. Such a film, deposited on a sapphire or quartz substrate, would be the basis for an optical read/write memory. Information may be stored by assigning bR to bit = 0 and K to bit = 1. Irradiation at 500nm converts bR to K with quantum efficiency of 0.33. Resetting the bit is accomplished with 633nm laser radiation, which converts K to bR with a quantum efficiency of 0.67. Thus, an optical disc configuration would require two lasers. In such a device, the read operation would be performed using both lasers in a coupled mode such that the 633nm beam reads the track and the "1" bits are immediately resent as the site of the bit is carried under the focus of the 500nm laser. This technique is an optical analog of microelectronic refresh techniques. (Figure 8).

Gating optical signals.

The second optically-coupled molecular device is the equivalent of a logic gate. Numerous examples of molecular gates have been proposed in recent literature. Although all such devices have, to this point remained hypothetical, molecular orbital calculations lend some support to the ideas behind this particular implementation. The basic idea is to use molecular groups which will give up charge and change their absorption spectra when exposed to light. These input groups are present in the same molecule with groups which pick up charge and also change their absorption spectra. Given that the absorption wavelengths are sufficiently separated, so that input and output do not interfere, communication with a film of these molecules consists of exposing the film to laser light and noting how much light gets through.

Optical NAND gates.

One example of an optical gate is the molecular structure shown in Figure 9. Two zwitterionic n-σ-n systems are attached to a porphyrin unit, the latter acting as a charge integrator. In the resting state the cyanine donors have both transferred an electron across the tunneling barrier (sigma bridge) to the quinone acceptors ($D^+ -A^-$ state). Both acceptors are connected to the porphyrin ring by conjugated double bonds to produce a delocalized two-electron excess charge, which stabilizes the output chromophore. The output chromophore is actually a protonated Schiff base, a situation reminiscent of the example of bacteriorhodopsin. The output chromophore absorbs light at approximately 520nm under the electrostatic perturbation provided by the nearby charge integrator system. When one or the other of the acceptor moieties absorbs a photon of light from an external laser pulse, an electron is transferred in the excited state back to the donor section to produce a neutral input species (D-A state). The other input, however is not activated so that an additional electron remains delocalized in the porphyrin unit. This firing of a single input module maintains electrostatic stabilization of the output chromophore and shifts its absorption maximum only slightly to approximately 535nm. Hence the excitation of a single input does not "fire" the gate. We see a very different situation when both acceptors absorb a photon and transfer electrons back to the donor portions. In this case, the porphyrin returns to a closed shell ground state and a delocalized electron is no longer available to stabilize the output chromophore. The protonated Schiff base chromophore is now situated as an electrostatically unstable environment and the absorption maximum shifts to approximately 590nm. Input selectivity can be provided by having slightly different absorption maxima for the input quinones. Figure 10 shows the results of molecular orbital calculations for the molecular system of Figure 9. Accordingly, the model system in Figure 9 can serve as an optically coupled molecular electronic NAND gate. Figure 11 shows the optics required for switching the molecule.

Applications.

Many of the algorithms required in image processing, signal processing and numerical methods can be realized as 2-D transforms of optical waves. The repertoire of transforms available from reflection, refraction and phase conjugation could be augmented by nonlinear point-to-point operations, such as afforded by a molecular NAND gate, the inputs of which respond only to specific wavelengths of light. A thin film of such molecules would give a point by point transform on a 2-D pattern. Serial processing by a sequence of thin films separated by optical couples gives a very fast analog signal processing machine.

References

Birge, R. R., "Photophysics of Light Transduction in Rhodopsin and Bacteriorhodopsin," Annual Review of Biophysics and Bioengineering 10:315 (1981).

Birge, R.R., A.F. Lawrence, T.M. Cooper, C.T. Martin, D.F. Blair, and S. I. Chan, "The Energetics and Molecular Dynamics of the Proton Pumping Photocycle in Bacteriorhodopsin," in Nonlinear Electrodynamics in Biological Systems (ed W. R. Adey and A. F. Lawrence), Plenum Press, (1985).

Lawrence, A. F. and R. R. Birge, "Communication with Submicron Structures: Perspectives in the Application of Biomolecules to Computer Technology," in Nonlinear Electrodynamics in Biological Systems (ed W. R. Adey and A. F. Lawrence) Plenum Press, (1985).

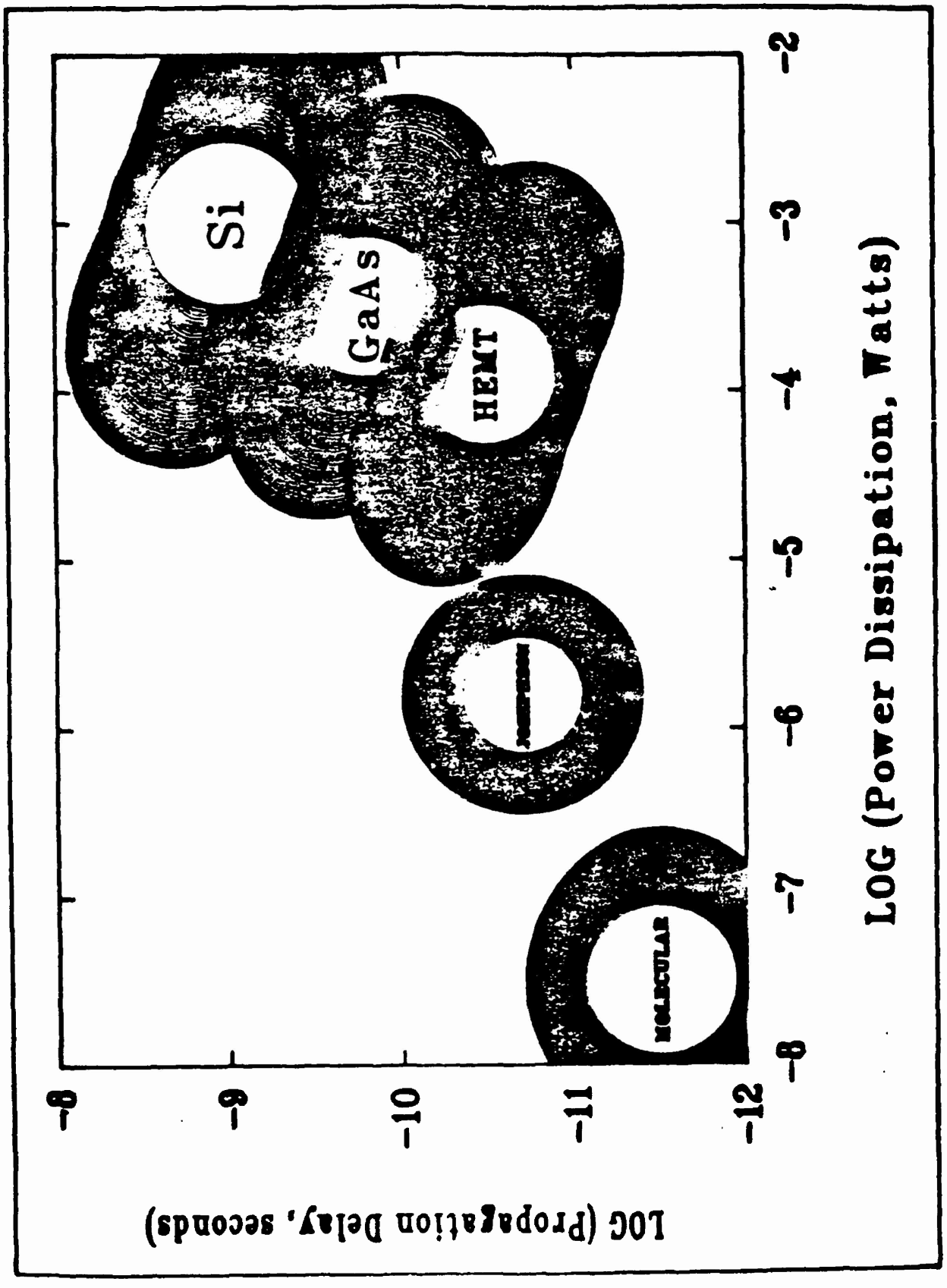

FIGURE 1. Comparisons between speed and power.
(from Lawrence and Birge)

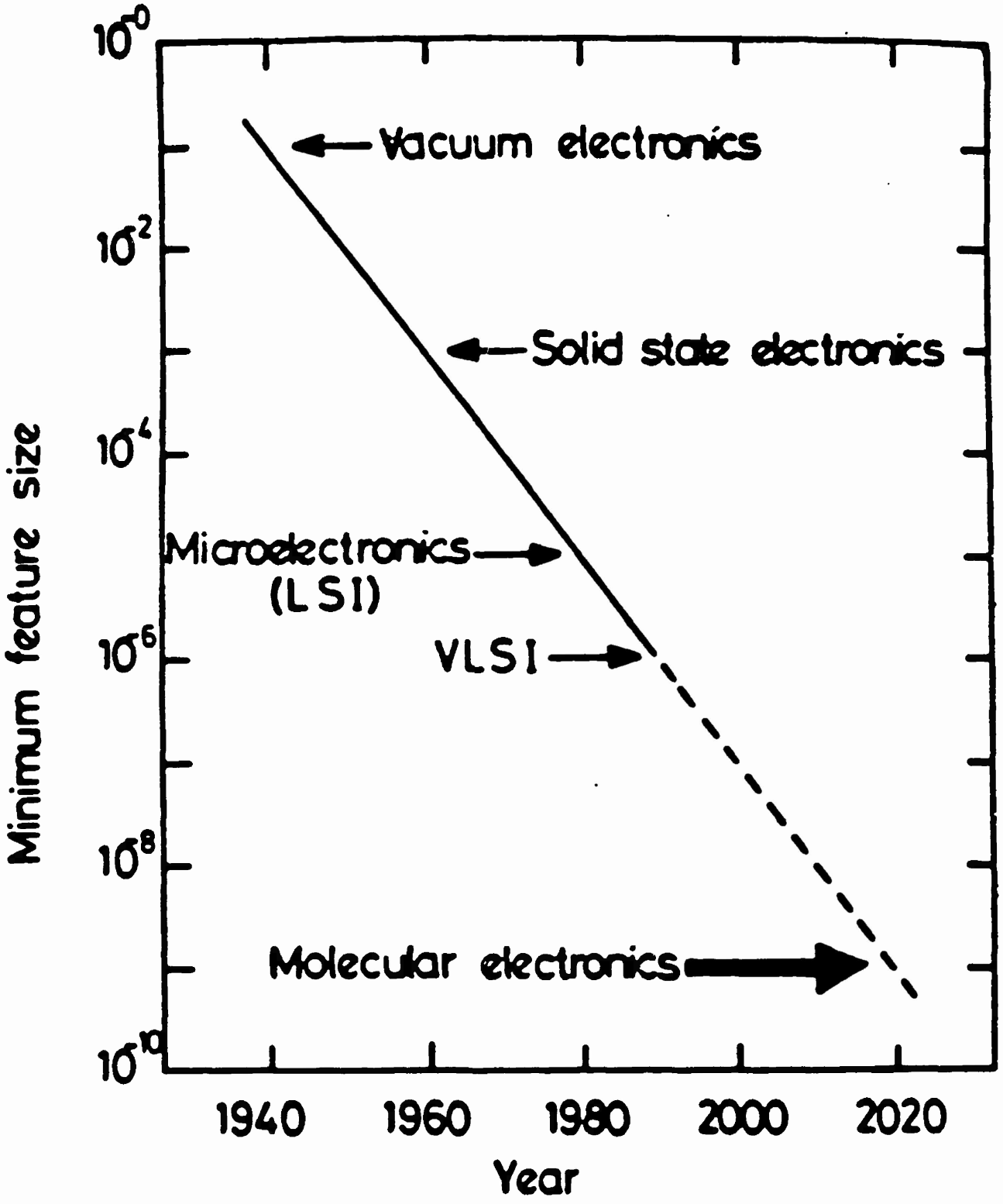

FIGURE 2. Minimum feature size for various types of past and projected electronic devices

(from G.D. Roberts, 1985)

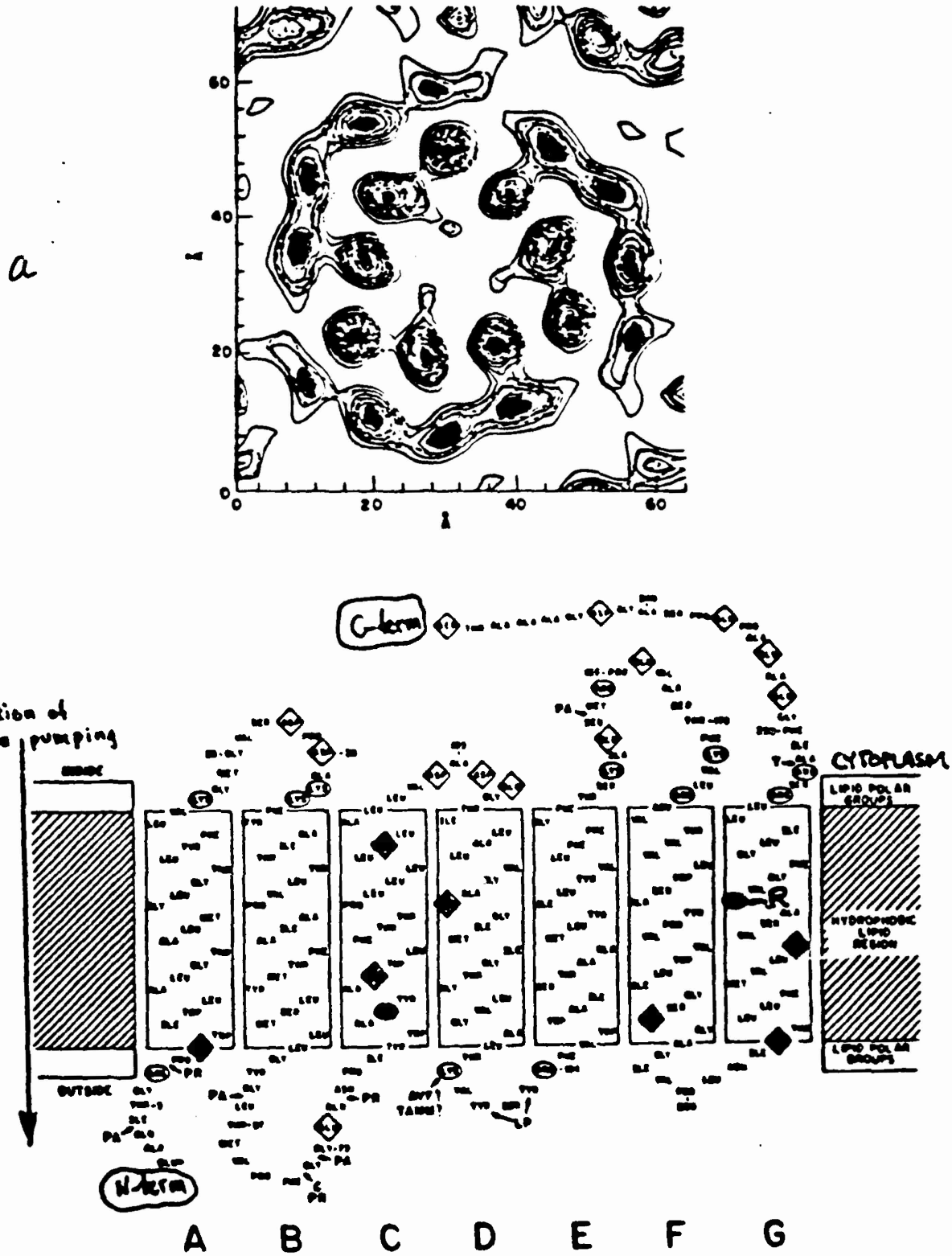

Figure 3. Bacteriorhodopsin.

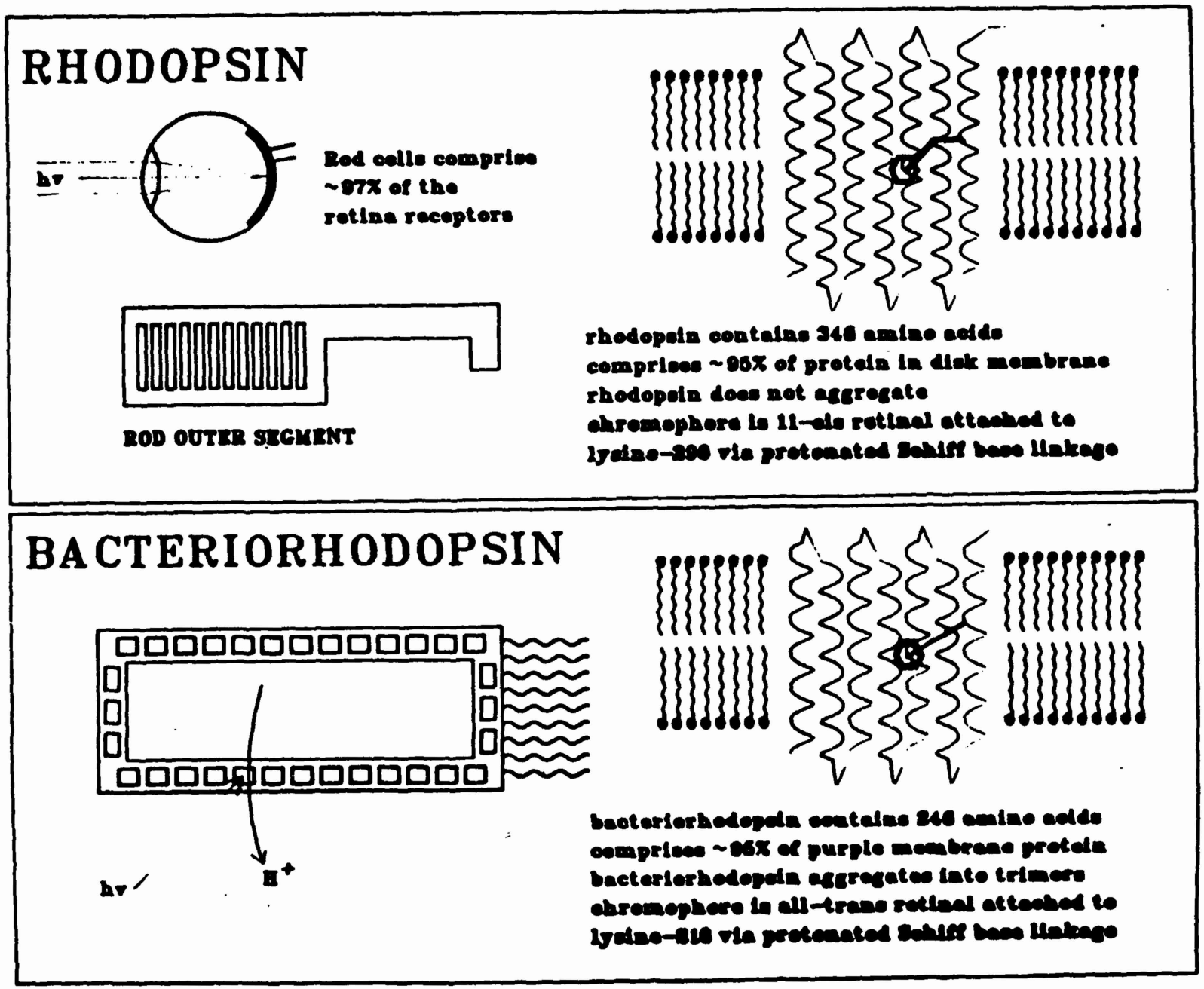

FIGURE 4. Rhodopsin and Bacteriorhodopsin.

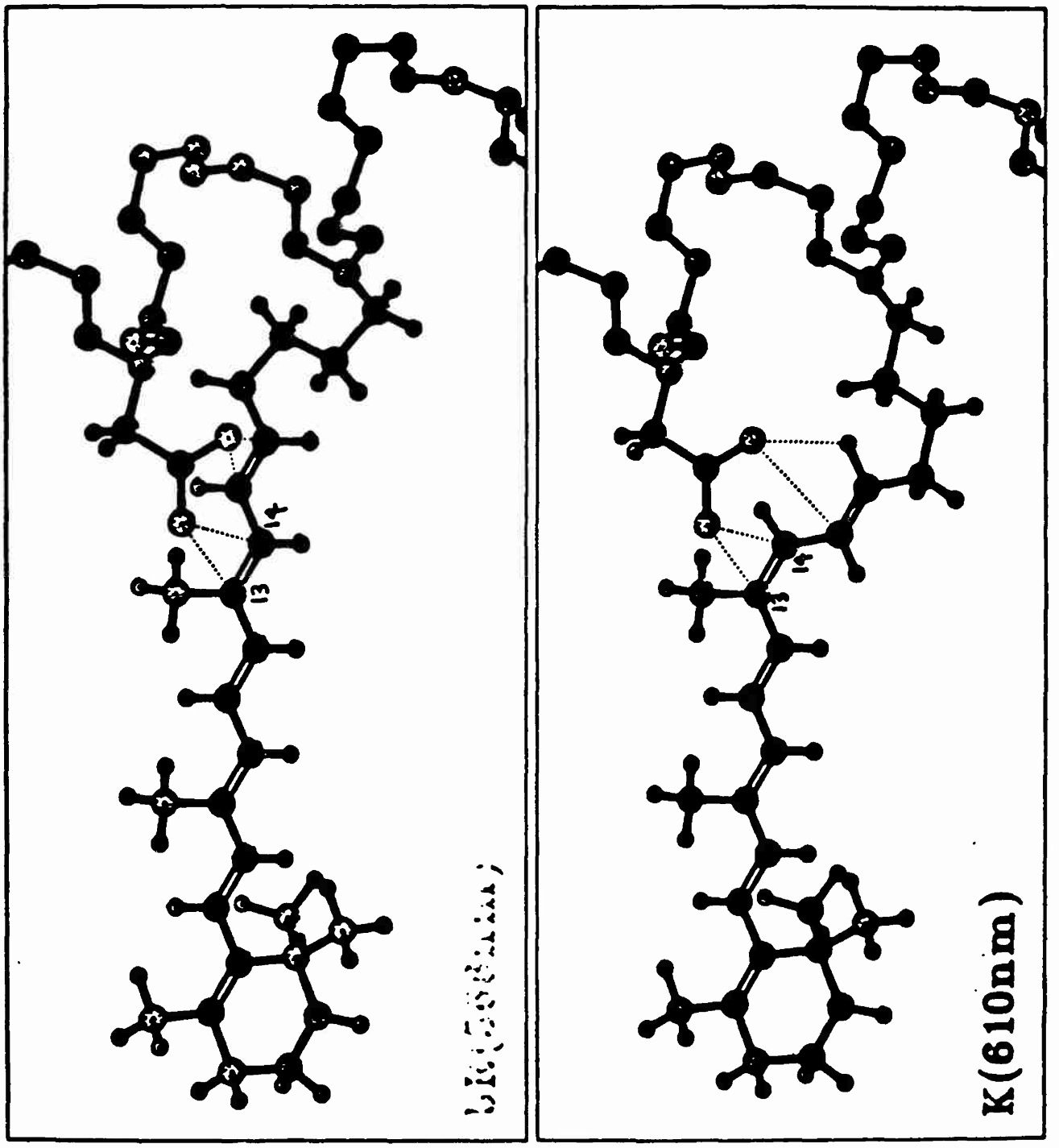

FIGURE 5. Conformational change in bacteriorhodopsin.

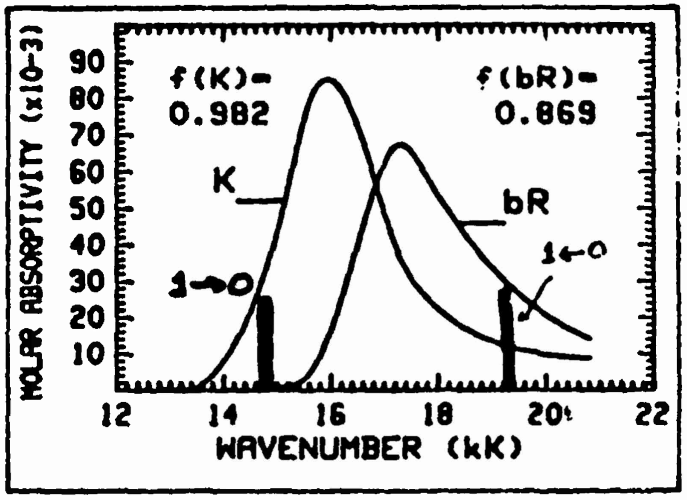

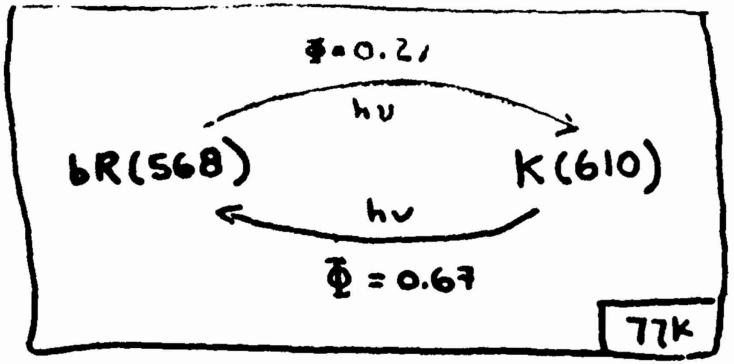

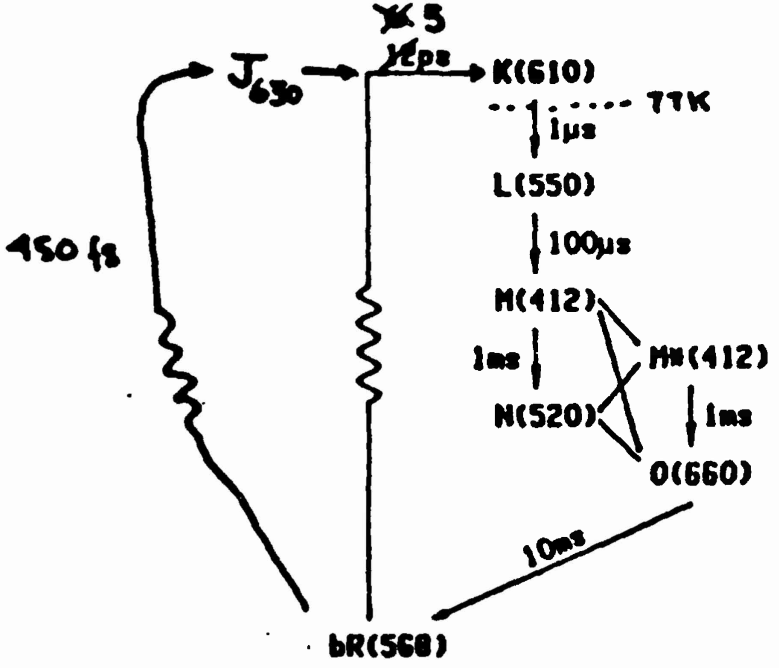

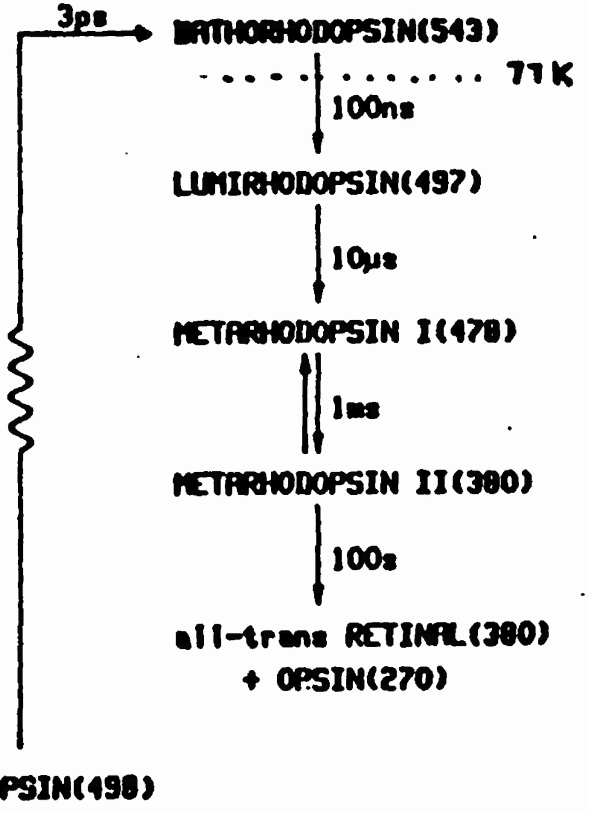

FIGURE 6. Photocycle for rhodopsin and bacteriorhodopsin.

CASE

BEST → 1 bit ≃ 300 Å × 900 Å × 900 Å (ultimate density ~ 99.99998 % reliability) (~4400 Mbytes/cm²)

WORST → 1 bit ≃ 300 Å × 1/2 × 1/2 (simple optical technology ~ 1 layer) (~100 Mbytes/cm²)

PROB. → 1 bit ≃ 300 Å × 0.8μ × 0.5μ (advanced optical technology) (~400 Mbytes/cm²)

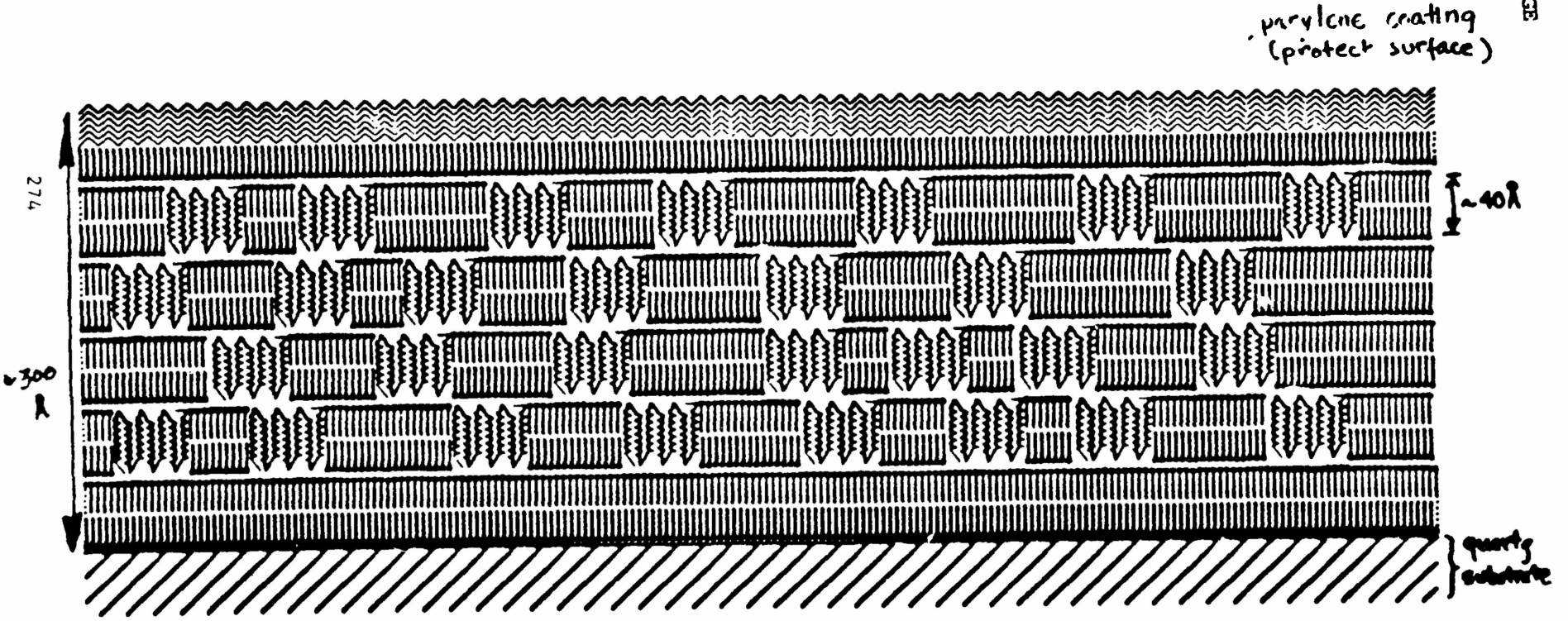

FIGURE 7. Bacteriorhodopsin film.

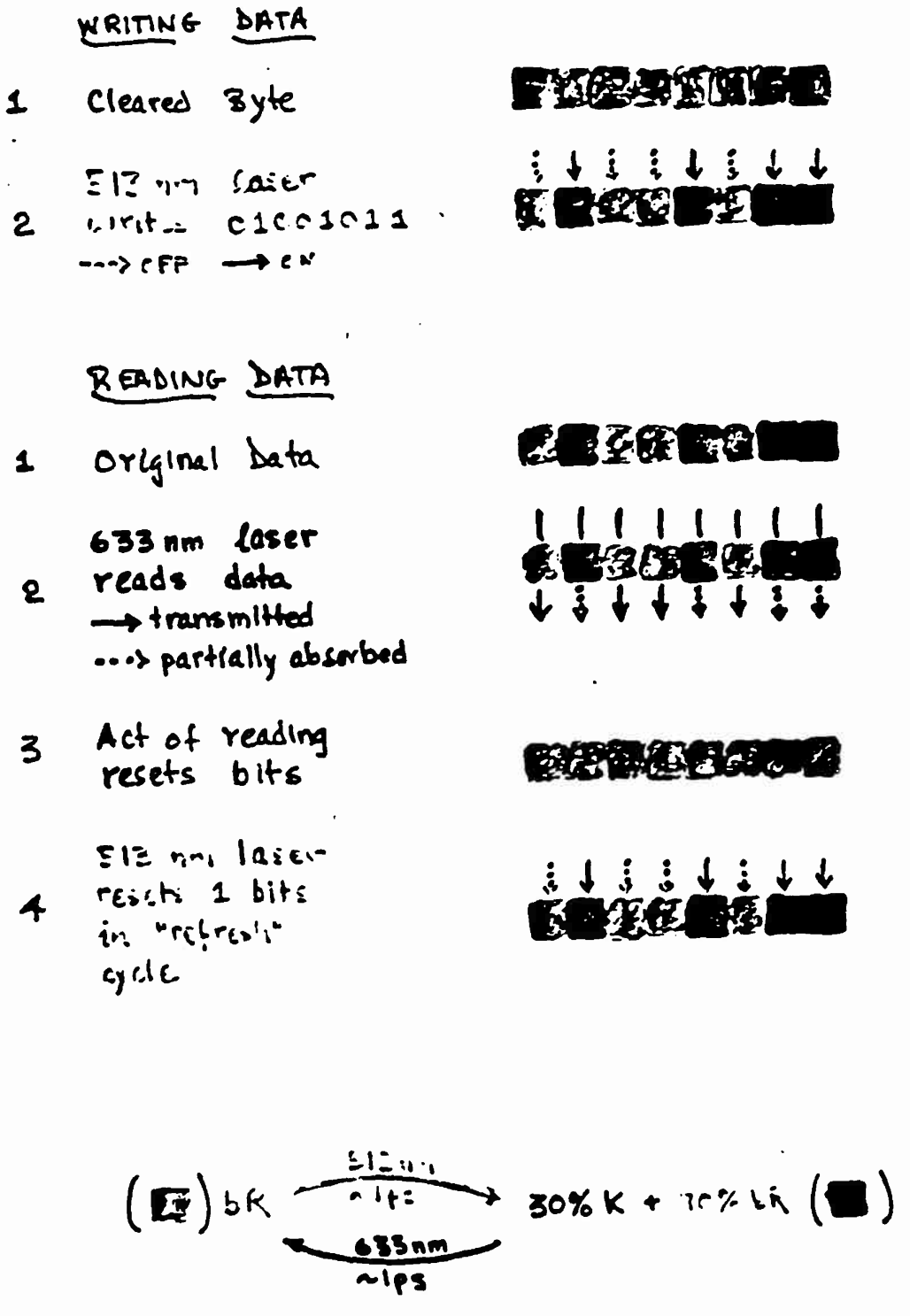

FIGURE 8. Bacteriorhodopsin as an optical memory.

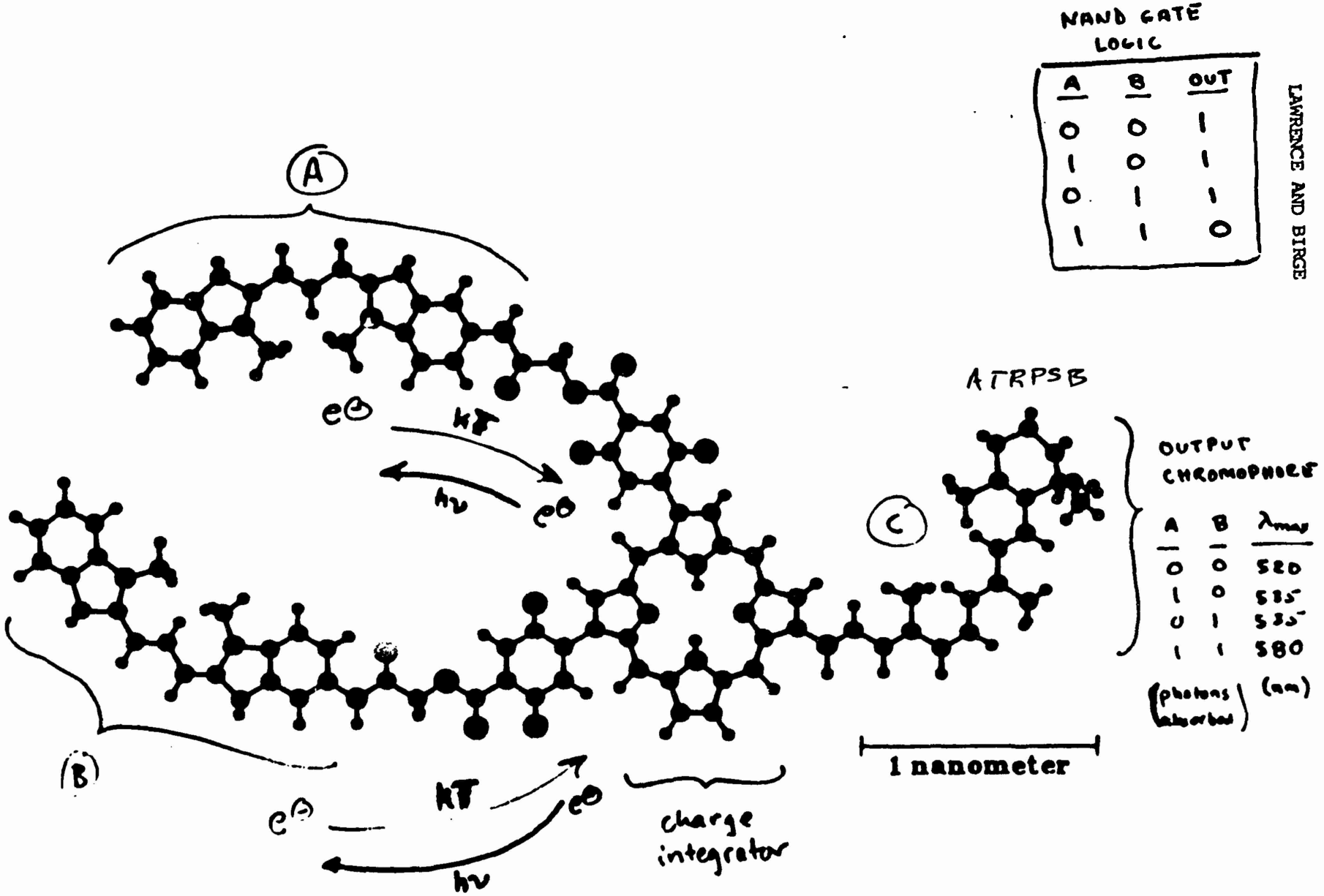

FIGURE 9. Optical gate.

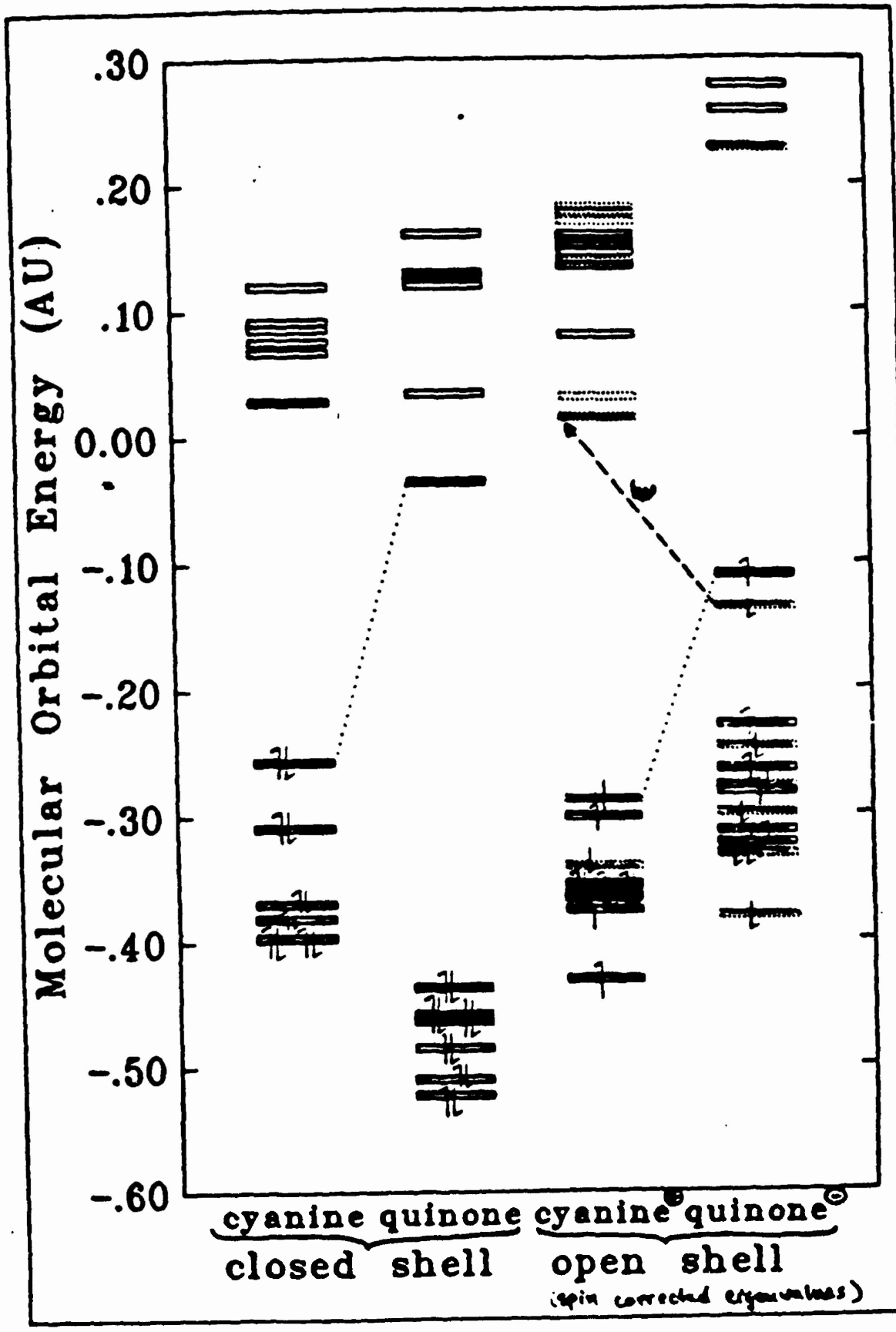

FIGURE 10. Molecular orbital calculations.

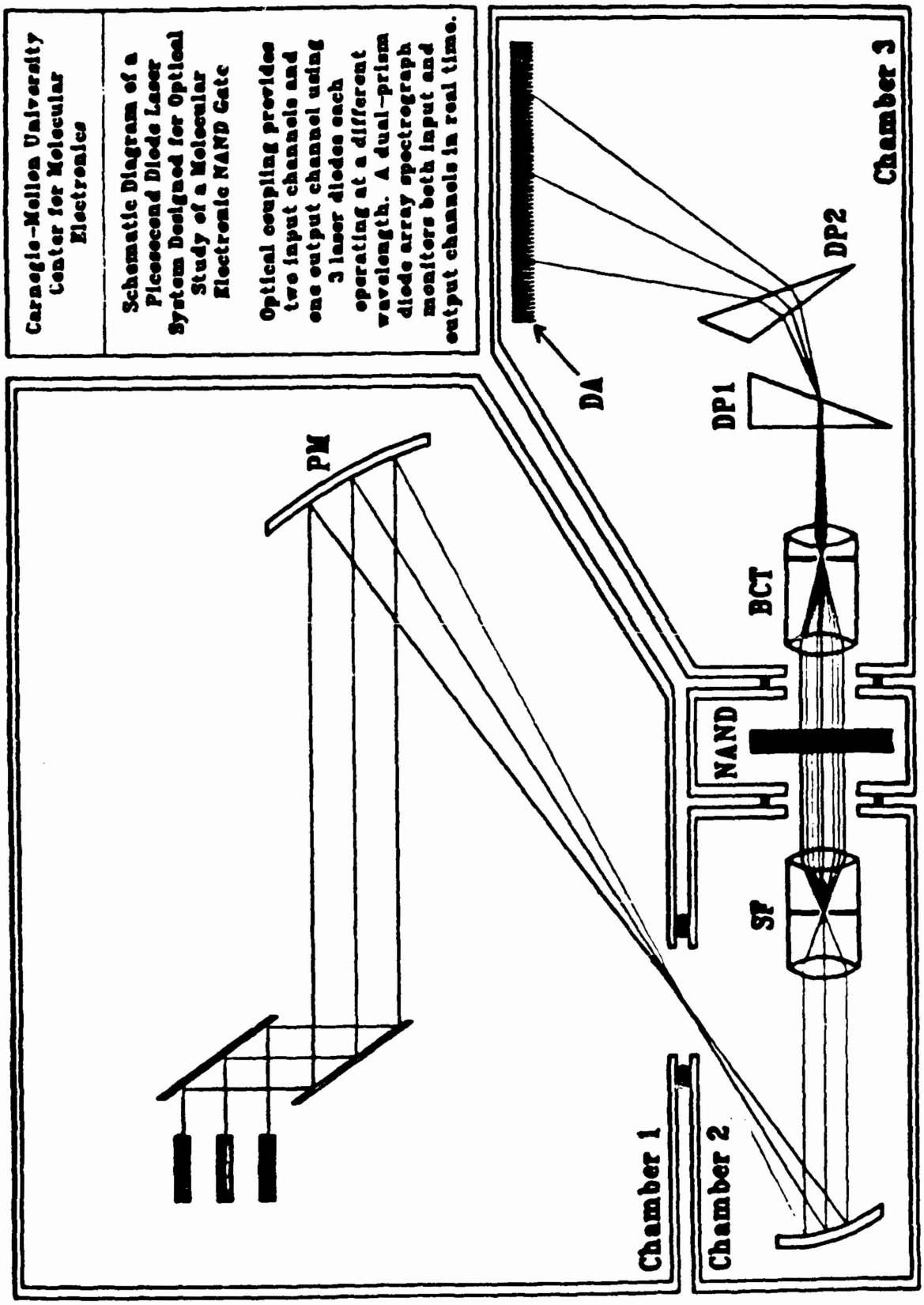

FIGURE 11. Schematic diagram.

A NOVEL CHITIN DEACETYLASE FROM THE DIMORPHIC FUNGI MUCOR ROUXII

Stephen Lombardi

Dartmouth College
Hanover, NH 03755

Numerous polysaccharides produced in microorganisms contain N-deacetylated amino sugar residues. Chitosan, an N-deacetylated glucosaminoglycan has been found in the cell walls of Phycomyces blakesleeanus and Mucor rouxii. chitin deacetylase, an enzyme which catalyzes hydrolysis of acetamido groups of chitin derivatives, was discovered in the supernatant fraction of cultures of the dimorphic fungi Mucor rouxii. Studies were performed, using the substrate 3,6-hydroxyethylated chitin (glycol chitin), with tritium labeled N-acetyl groups, to characterize the action of this enzyme.

A 300-fold purification of chitin deacetylase was obtained by ammonium sulfate precipitation followed by ion exchange chromatography. SDS-PAGE analysis showed a single band of approximately 20,000 molecular weight, presumably the chitin deacetylase. The chitin deacetylase shows a pH optimum of 4.5 and the Km for the enzyme was determined to be 2.4×10^{-4}M. The occurrence of the chitin deacetylase enzyme accounts for the formation of chitosan in Mucor rouxii and other fungi.

INDUCTION AND SELECTION OF FUNGAL HYPERPRODUCING MUTANTS OF EXTRACELLULAR BIOPOLYMERS

Benedict J. Gallo

Biotechnology Branch
Science and Advanced Technology Directorate
U.S. Army Natick Research, Development and Engineering Center
Natick, MA 01760-5021

A rapid, simple and effective method of inducing and isolating fungal strains with improved production of some extracellular biopolymers has been developed from existing protocols. The method uses the following simple steps: conidial mutagenesis, the growth of mutagenized spores into an anastomosing mycelial mat with subsequent conidial lawn development, random conidial transfer with velveteen to treatment kill plates containing the polyene antibiotic kabicidin, the isolation of surviving fungal colonies from the treatment plate and the primary testing of the isolates for the desired extracellular product. The process as described had an effective mutant yield of about 1.5%.

This methodology was used to obtain two hyperproducing cellulase mutant strains of Trichoderma reesei, TK041 and MCG80, and a cellulase hyperproducing mutant of Penicillium iriensis. Pearly, another mutant of Trichoderma reesei, was induced and selected using this protocol and shows an enhanced production of an extracellular pigment of an undetermined composition. Pearly was isolated because of its obviousness and produces two to three times more extracellular pigment than the parental strain.

BIOPOLYMER PROCESSING WITH MEMBRANE BIOREACTORS

S. Dean, N. Ahmad, E. De Bernardez and J. Rollings

Department of Chemical Engineering
Worcester Polytechnic Institute
Worcester, MA 01609

Biopolymeric materials, particularly polysaccharides, have the potential to supply low molecular weight stocks to the pharmaceutical, food, and petroleum industries. The current polysaccharide processing schemes involve an enzymatic depolymerization reaction operation followed by a separation step to remove undesirable high molecular weight species and the biocatalyst. We have developed a simultaneous depolymerization/separation scheme that combines these steps in a single operation.

In this operation an immobilized enzyme-membrane reactor is used to depolymerize water-soluble polysaccharides in a desirable and predictable manner. High molecular weight biopolymeric materials are fed through the shell side of an asymmetric ceramic filter at one end, and the low molecular weight products are collected from the lumen port at the other end. The enzyme is immobilized on the membrane. A mathematical model was developed to describe: a) the enzyme immobilization process, and b) the simultaneous depolymerization/separation process in the membrane bioreactor. The model predictions indicate that a nonhomogeneous enzyme distribution on the catalytic surface is obtained under typical immobilization conditions. The effects of enzyme distribution on the membrane, fluid phase physiochemical and transport properties, support physical properties, intrinsic kinetics and operating conditions on the simultaneous depolymerization/separation process have also been investigated.

CONFORMATIONAL STRUCTURE EFFECTS ON ENZYMATIC DEPOLYMERIZATION OF AMYLOSE

Juntae Park and James E. Rollings

Department of Chemical Engineering
Worcester Polytechnic Institute
Worcester, MA 01609

Amylose depolymerization kinetics catalyzed with -amylase has been studied in mixed aqueous-dimethyl sulfoxide (DMSO) solvents and mixed solvents containing butanol. It is determined that the observed kinetics are affected by the nature of the biopolymeric substrate conformation and that the enzymatic activity is affected by specific environmental conditions (temperature and solvent composition). It is found that substrate conformation (as demonstrated by its physical chemistry) strongly influences enzymatic activity. Soluble substrates exhibit rapid hydrolysis rates compared to precipitated substrates and, moreover, the specific structure of precipitated amylose also affects enzymatic activity. Highly structured biopolymeric substrates show less rapid hydrolysis rates than less structured biopolymeric substrates.